
THE UNIVERSITY
*of* EDINBURGH

# Investigating novel therapeutic approaches and targets to prevent synapse degeneration


Inês da Silva Amorim

Thesis submitted for the degree of PhD
The University of Edinburgh
2017

# Declaration

I declare that this thesis has been composed solely by myself and that it has not been submitted, in whole or in part, in any previous application for a degree. The work described in this thesis is my own, except where collaborative contributions were required. Any collaborations have been explicitly acknowledged in the text.

……..

Inês da Silva Amorim

# List of publications

Parts of this thesis have been published in peer-reviewed journals:

AMORIM, I. S., MITCHELL, N. L., PALMER, D. N., SAWIAK, S. J., MASON, R., WISHART, T. M. & GILLINGWATER, T. H. 2015. Molecular neuropathology of the synapse in sheep with CLN5 Batten disease. Brain and Behavior, 5, e00401.

AMORIM, I. S., GRAHAM, L. C., CARTER, R. N., MORTON, N. M., HAMMACHI, F., KUNATH, T., PENNETTA, G., CARPANINI, S. M., MANSON, J. C., LAMONT, D. J., WISHART, T. M. & GILLINGWATER, T. H. 2017. Sideroflexin 3 is a alpha-synuclein-dependent mitochondrial protein that regulates synaptic morphology. Journal of Cell Science, 130**,** 325-331.

# Acknowledgments

I would like to thank my supervisor Prof. Tom Gillingwater for making this PhD possible, for his support during the last four years and for always being so positive and help me work through the problems of the PhD. Another big thank you to all the members of the Gillingwater lab for their help and for making the days in the lab more enjoyable.

I would also like to thank everyone I have collaborated with during my PhD - without them this thesis would not have been possible. A special thanks to Prof. Jennifer Morton and Prof. David Palmer for the gift of tissue from sheep; to Maica, Laura and Tom Wishart for their help with proteomics and *Drosophila* experiments; to Dr. Gino Brunori, Dr. Jon Lyon and Ashley Broom, from GSK, for hosting me at Ware and teaching me to isolate mitochondria and run Seahorse assays; to Dr. Rod Carter and Prof. Nick Morton for their help running the Seahorse experiments in Edinburgh; to Dr. Tilo Kunath for the gift of SH-SY5Y cells; to Ann Wright for teaching me electron microscopy; to Dr. Jamie Marland for introducing me to pHluorin imaging; to Prof. Mike Cousin for supplies of vectors, antibodies and cells, for allowing me to use equipment from his lab and for discussions about calretinin; and to Derek Thomson for teaching me how to perform nerve lesions, for the company during the hours spent in surgery and for always being available to help with anything.

Finally, a special thank you to Antonio for being by my side, hearing about mitochondria and keeping me updated about the rest of the world; and to my family, who always supported my choices and who, in spite of the distance, never left my side.

# Abstract

Neurodegenerative diseases are associated with extensive physical and mental debilitation, significant costs to the healthcare system, as well as great emotional and financial burden to the patients, their families and care providers. Despite progress in our understanding of the mechanisms behind neurodegenerative diseases, the vast majority are still currently untreatable. Synapses are important pathological targets in a range of disorders, including Alzheimer's disease, Parkinson's disease, Huntington's disease and lysosomal storage disorders, such as Batten disease. Loss of synaptic connections and impairments in synaptic function are present in the initial stages of neurodegenerative conditions and throughout the course of disease progression. Therefore, synaptoprotective strategies are regarded as a potentially key factor in the development of effective therapies aimed at preventing or halting neurodegeneration. Despite the continuously growing body of research elucidating the molecular mechanisms that modulate synaptic function and vulnerability, the contribution of these pathways to neurodegenerative diseases is far from fully characterized. In addition, there are frequent issues regarding the applicability of the research performed using *in vitro* and small animal models of disease to develop therapeutic strategies for use in human patients. In the work described in this thesis, we initially validated the involvement of a selection of key synaptic targets, previously identified as regulators of synaptic degeneration in lower animal models, including mice and *Drosophila*, in a large animal model of neurodegenerative disease: CLN5 Batten sheep. Subsequently, we explored two of these individual synaptic protein targets in more detail (calretinin and α-synuclein), to further investigate their contribution to synaptic function and stability.

Calretinin is a poorly characterized protein, primarily known for its calcium buffering capacities and high levels of expression in a subpopulation of interneurons. In this work, we show calretinin is expressed in previously unreported cell populations, including motor axons and synapses from the peripheral nervous system, and that it is enriched in synapses in vitro. Furthermore, we show calretinin responds dynamically to synaptic activity and is directly involved in neurodegenerative pathways, as demonstrated by its ability to influence the course of Wallerian degeneration and apoptotic cell death.

α-synuclein plays a central role in the pathophysiology of Parkinson's disease and contributes to the maintenance of synaptic transmission and mitochondrial function. However, questions still remain about how to effectively manipulate α-synuclein to obtain therapeutic benefits. Therefore, we sought to explore downstream targets of α-synuclein in order to uncover new pathways through which this protein may influence synaptic stability. Using proteomics on mice lacking α-synuclein and *in vitro* cell systems we identified sideroflexin 3 (sfxn3). We show sfxn3 is localized at the inner mitochondrial membrane and that it functions outside the main canonical pathways of mitochondria energy production. In addition, overexpression of sfxn3 in *Drosophila* led to a significant loss of synaptic boutons at the level of the neuromuscular junction, suggesting regulated levels of sfxn3 are important for the maintenance of synaptic connections.

Altogether, the work developed in this thesis provides novel insights into pathways regulating synaptic stability and function. We not only provide evidence that the molecular targets studied are affected in a large animal model of neurodegenerative disease, and are therefore likely to be relevant to studies in human conditions, but we

also uncover two new molecular targets capable of independently regulating synaptic form and function.

## Lay Summary

Neurodegenerative diseases such as Alzheimer's and Parkinson's disease occur when neurons in specific regions of the brain start malfunctioning and, eventually, die. Although we have gained significant insight into important aspects of how and why neurodegenerative diseases develop, treating the dysfunction of neurons and preventing their degeneration is not straightforward. As a result, we lack efficient therapies to delay the progression of disease. One important factor in the instigation and progress of neurodegenerative conditions is the correct function of synapses, the terminal connections of neurons which are responsible for transmitting information. Synapses form extensive networks of interconnected nerve cells which are responsible for maintaining normal motor and cognitive functions. Therefore, maintaining a healthy cohort of synapses in the nervous system is of extreme importance to our well being. In my work, I have explored new molecular mechanisms that contribute to the health and stability of synapses. Translating research performed in some common models of disease, such as genetically modified mice, into humans has not always been successful, likely due to the more complex form and function of the human nervous system. Therefore, I started my work by confirming that a short list of synaptic proteins we had previously shown to influence how neurons degenerate in mice were similarly affected in a large animal (sheep) model of a childhood form of neurodegeneration, known as Batten disease. This confirmed that the molecular targets we were looking at in synapses were relevant to neurodegenerative pathways conserved from small rodents through to large animals, and presumably humans. I then looked at two individual synaptic candidates in more detail, two proteins known as calretinin and α-synuclein. The function of calretinin is currently very poorly understood. Here, I

demonstrated for the first time that calretinin is involved in synaptic function and directly contributes to instigate neurodegeneration in mice. α-synuclein is important for the development of Parkinson's disease but it is very difficult to target from a therapeutic point of view. Hence, I focused on trying to find proteins related to α-synuclein that could be used for therapeutic targets instead. I identified sfxn3 and showed that it can have a significant influence on the maintenance of synaptic connections. Taken together, my work provides novel insights into how to maintain healthy and functional synapses in the nervous system, which is important for understanding how neurons work and to aid in the development of new treatments for neurodegenerative conditions.

# Table of Contents

# List of Figures

# List of Tables

# List of Abbreviations

List of main abbreviations used throughout the text.

| | |
|---|---|
| 2H3 | Neurofilament (165 kDa) |
| α-BTX | α-bungarotoxin |
| AchR | Acetylcholine Receptor |
| AD | Alzheimer's disease |
| AMPA | α-amino-3-hydroxy-5-methyl-4-isoxazolepropionic acid |
| ALS | Amyotrophic Lateral Sclerosis |
| AU | Arbitrary units |
| Aβ | Amyloid β |
| BSA | Bovine Serum Albumin |
| CALB2 | Calretinin |
| CLN | Ceroid-lipofuscinosis, neuronal |
| CNP | 2',3'-cyclic nucleotide 3' phosphodiesterase |
| CNS | Central nervous system |
| CR | same as CALB2 |
| CSP-α | Cysteine-string protein α |
| DAVID | Database for Annotation, Visualization and Integrated Discovery |
| DIV | Day In Vitro |
| DOX | Doxycycline |
| dpi | days post injury |
| EEG | Electroencephalogram |
| ETC | Electron transport chain |
| GABA | γ-aminobutyric acid |
| GAPDH | Glyceraldehyde 3-phosphate dehydrogenase |
| GFAP | Glial fibrillary acidic protein |
| GFP | Green fluorescent protein |
| HD | Huntington's disease |
| HDAC2 | Histone deacetylase 2 |
| HET | Heterozygous |
| hpi | hours post injury |
| IPA | Ingenuity Pathway Analysis |
| iTRAQ | isobaric Tag for Relative and Absolute Quantitation |
| KD | Knock down |
| KEGG | Kyoto Encyclopedia of Genes and Genomes |
| KO | Knock out |
| LTD | Long term depression |

| | |
|---|---|
| LTP | Long term potentiation |
| mHtt | Mutant Huntingtin |
| MRI | Magnetic resonance imaging |
| NAC | non-amyloid component |
| NCL | Neuronal ceroid lipofuscinosis |
| NIH | National Institute of Health |
| NMDA | N-methyl-D-aspartate |
| NMJ | Neuromuscular Junction |
| OCR | Oxygen consumption rate |
| OE | Overexpression |
| OXPHOS | oxidative phosphorylation |
| PBS | Phosphate Buffered Saline |
| PFA | Paraformaldehyde |
| PD | Parkinson's disease |
| PNS | Peripheral nervous system |
| ROCK2 | Rho-associated, coiled-coil containing protein kinase 2 |
| ROS | Reactive oxygen species |
| RT | Room temperature |
| SEM | Standard error of the mean |
| Sfxn1 | Sideroflexin 1 |
| Sfxn2 | Sideroflexin 2 |
| Sfxn3 | Sideroflexin 3 |
| SIRT2 | Sirtuin 2 |
| SNAP-25 | Synaptosomal-associated protein 25 |
| SNARE | Soluble NSF (N-ethylmaleimide sensitive fusion proteins) attachment protein receptor |
| SV2 | Synaptic vesicle protein 2 |
| Syp | Synaptophysin |
| SypHy | Synaptophysin-pHluorin |
| UBR4 | Ubiquitin protein ligase E3 component n-recognin 4 |
| UPS | Ubiquitin-Proteasome System |
| VDAC2 | Vesicle-associated membrane protein 2 |
| vGAT | Vesicular γ-aminobutyric acid transporter |
| vGLUT1 | Vesicular glutamate transporter 1 |
| WT | Wild type |

# Chapter 1. General Introduction

## 1.1. The socioeconomic impact of neurodegenerative diseases

Neurodegenerative diseases are caused by the progressive dysfunction, and ultimately death, of neuronal populations. They can cause extensive physical and mental debilitation and yet the vast majority are currently untreatable. Some of the most prevalent neurodegenerative conditions include dementias (such as Alzheimer's disease (AD)), Parkinson's disease (PD), Multiple Sclerosis, and neuromuscular disorders such as Amyotrophic Lateral Sclerosis (ALS) (Gustavsson et al., 2011).

Dementias, in particular, are a growing concern due the current steady increase in life expectancy and demographic shift towards an aged population, which naturally increases the incidence of age-related disorders (Brookmeyer et al., 2007, Dorsey et al., 2007). It is estimated that over 6 million people suffer from dementia in Europe, and over 4 million in North America (ADI, 2010, Gustavsson et al., 2011), with these numbers expected to more than double by 2030 (ADI, 2010). The healthcare and indirect costs associated with dementia have been estimated to reach an annual sum of 100 billion euros and 200 billion US dollars in 2010, in Europe and North America respectively (ADI, 2010, Gustavsson et al., 2011). PD, another very prevalent neurodegenerative condition affects over 1% of the aged population in both Europe and the US, and costs the respective healthcare systems nearly 14 billion euros and 14 billion US dollars per year (Gustavsson et al., 2011, Kowal et al., 2013). In addition to the financial costs to the patients and healthcare system and the physical impairments often associated with neurodegenerative conditions, these disorders also impart a great

deal of emotional suffering to the patients, families and care providers (WHO). Therefore, it is of extreme importance we further our understanding of the mechanisms behind neurodegeneration and develop effective therapeutic strategies that can minimize the human and financial costs associated with neurodegenerative disorders.

**Table 1.1: Key prevalence and financial facts about Alzheimer's disease and Parkinson's disease.**

| Region | Parameter | Dementia | Parkinson's Disease | References |
|---|---|---|---|---|
| UK | Prevalence (population over 66) | 7.73% | 1.15% | [1] |
| UK | Number of people affected | 738,415 | 109,806 | [1] |
| UK | Cost per person (PPP EURO) | 30,016 | 21,500 | [1] |
| UK | Total cost (Million PPP EURO) | 22,164 | 2,361 | [1] |
| Europe | Prevalence (population over 66) | 1.23% | 0.24% | [1] |
| Europe | Number of people affected | 6,341,179 | 1,249,312 | [1] |
| Europe | Cost per person (PPP EURO) | 16,949 | 4,417 | [1] |
| Europe | Total cost (Million PPP EURO) | 105,163 | 13,933 | [1] |
| US | Prevalence (population over 60) | 6.50% * | 1-2% | [2, 3] |
| US | Number of people affected | 4,383,057 * | 630,000 | [2, 3] |
| US | Cost per person (USD) | 48,605 * | 22,851 | [2, 3] |
| US | Total cost (Million USD) | 213,040 * | 14,327 | [2, 3] |

* North America High Income Population.
PPP: purchasing power parity.
Statistics related to 2010.
Cost categories include direct health care costs, direct non-medical costs and indirect costs.
Dementia section includes CID10 codes F00-F03: Alzheimer's disease, vascular dementia, dementia in other diseases such as Huntington's and Parkinson's Diseases, and unspecified dementias.
[1] (Gustavsson et al., 2011); [2] (ADI, 2010); [3] (Kowal et al., 2013)

## 1.2. Therapies for neurodegenerative diseases

### 1.2.1. Current therapies and limitations

Current drug therapies for the management of neurodegenerative diseases, such as AD and PD, focus on the symptomatic treatment of the conditions and act mainly by controlling the levels of particular neurotransmitters in the brain. The effectiveness of these therapeutics is based on the principle that specific neuronal populations degenerate preferentially in AD and PD, leading to a reduction in the

available neurotransmitters and excitatory capacity of the affected neuronal populations, with consequent weakening of downstream neuronal circuits and ultimately loss of connectivity (AS, 2015).

In AD, the marked loss of cholinergic neurons in early stages of the disease led to the Cholinergic Hypothesis of Alzheimer's and to the development of drugs that could improve cholinergic signalling (Francis et al., 1999, Schliebs and Arendt, 2011). Currently, donepezil, rivastigmine and galantamine are amongst the medications used to treat patients with AD. These drugs act as cholinesterase inhibitors, resulting in reduced breakdown of acetylcholine in the brain and boosting the excitatory capacity of the degenerating cholinergic neurons. These lines of treatment have some small positive effects on cognition and are able to temporarily alleviate and stabilize symptoms of AD. However, they do not alter the underlying cause of pathology and do not prevent further degeneration from occurring (Becker and Greig, 2012, Bentham et al., 1999, Selkoe, 2013). A similar rationale underlies the available treatments for PD. In PD, however, the dopaminergic neurons of the substantia nigra are the most affected in early stages of the disease. Therefore, dopamine agonists, dopamine precursors (eg. Levodopa) and inhibitors of dopamine degradation (eg. MAO-B and COMT inhibitors) have been developed to manage the disease. Although able to temporarily ameliorate motor symptoms, these drugs do not show long-term benefits in effectively halting disease progression (Muzerengi and Clarke, 2015, Youdim, 2010b).

### 1.2.2. New therapeutic approaches

At present, treatment for most neurodegenerative diseases is delivered symptomatically. Consequently, when symptoms are reported by patients the degenerative process has already been active for a period of time. For instance, motor-symptoms in PD are perceived when over 50% of the dopaminergic neurons in the substantia nigra have already degenerated (Fearnley and Lees, 1991), and in Huntington's disease (HD) motor and cognitive impairments are detected in patients carrying the HD-causing mutation years before the onset of the characteristic motor symptoms (Paulsen et al., 2008, Stout et al., 2007). Strikingly, the pre-clinical period of AD has been estimated to be as long as 17 years, when deposition of amyloid-beta is predicted to start, while hippocampal atrophy and cognitive impairments are first detectable up to 5 years before the clinical diagnosis of AD (Villemagne et al., 2013). These facts highlight two major challenges that need to be addressed in neurodegeneration research: the early diagnosis of neurodegenerative diseases, which requires better screening tools and the improvement of biomarkers and diagnostic criteria for each condition; and the development of disease-modifying drugs that target the pathophysiology of the disease and halt disease progression (DeKosky et al., 2011, Hampel et al., 2010, Herrmann et al., 2011).

One strategy that has been widely explored is the clearance of protein aggregates, which are a hallmark of several neurodegenerative conditions. The deposition of Amyloid-beta (Aβ) plaques is a key feature found in the brain of patients with AD. As a result, research has focused, for many years, on attempting to clear Aβ plaques. However, this has not yet proven beneficial in clinical trials (Amtul, 2016, Selkoe and Hardy, 2016). A similar approach has been adopted for PD, where

strategies to clear α-synuclein and prevent its aggregation, a hallmark of the disease, are currently the focus of much attention (Dehay et al., 2015).

The use of antioxidants and neurotrophic factors are examples of other strategies that have been explored as possible therapeutic options for neurodegenerative diseases. Mitochondria are important modulators of neuronal function and survival, and play a crucial role in the control of reactive oxygen species (ROS). Elevated ROS levels and reduced capacity of mitochondria to neutralize ROS are important during the instigation and progress of neurodegeneration (Barnham et al., 2004, Lin and Beal, 2006). In agreement, antioxidants have been shown to ameliorate neuronal death in some models of disease (Nistico et al., 2012, Valera and Masliah, 2016). Neurotrophic factors, on the other hand, play an important role in the development, survival and repair of neurons, and there is increasing evidence indicating the loss of trophic support might contribute to the pathology of neurodegenerative diseases (Connor and Dragunow, 1998, Levy et al., 2005, Lu et al., 2013). Administration of neurotrophic factors has indeed been shown to promote neuronal survival and repair in animal models of PD, AD and HD (Decressac et al., 2012, Nagahara et al., 2013, Nagahara et al., 2009, Simmons et al., 2009).

Despite promising research regarding new therapeutic approaches, no drugs have yet passed clinical trials and the urgent requirement to develop novel disease-modifying drugs for the treatment of neurodegenerative conditions persists (Cummings et al., 2014, Lu et al., 2013). However, the lack of knowledge about the mechanisms contributing to the initiation and progression of neurodegeneration is hindering the drug-development progress. Neurons and neuronal compartments are

very dynamic and complex structures, with countless factors contributing not only to their function and stability but also to their vulnerability and degeneration. A variety of proteins and pathways cooperate to regulate these processes and, therefore, new therapeutic strategies aiming to ameliorate neurodegeneration will benefit from a multifactorial approach that targets multiple pathways simultaneously. One of the areas predicted to have a positive and broad impact is the maintenance of synaptic and axonal integrity (Coleman, 2005, Gillingwater and Wishart, 2013, Lu et al., 2013).

## 1.3. Synaptic pathology in neurodegenerative conditions

### 1.3.1. Synapses

Synapses are specialized structures that allow the transfer of information between individual neurons or between neurons and other cell types, such as muscle fibers (in this case, synaptic connections are termed neuromuscular junctions (NMJs)). Synapses can be electrical or chemical, with the latter subtype being the most well studied. Chemical synapses work by releasing neurotransmitters and are composed of a pre-synapse in the axonal terminal of a neuron, a synaptic cleft and a post-synaptic area in a dendritic spine of the receiving neuron (Figure 1.1). The correct functioning of the pre-synapse relies on the precise regulation of the synaptic vesicle cycle (Sudhof, 2004, Sudhof, 2012). When an action potential arrives at the pre-synapse, calcium channels open and allow the increase in intracellular calcium levels which activates the SNARE complex machinery at the active zone, leading to the fusion of vesicles with the pre-synaptic membrane and exocytosis of neurotransmitters into the

synaptic cleft. At the edge of the active zone, synaptic vesicles and their associated proteins are recycled through endocytic mechanisms. Simultaneously, at the post-synaptic density receptors such as glutamate (NMDAR and AMPAR) and acetylcholine receptors (AChR) are activated by the released neurotransmitters and prompt a response in the target neuron (Figure 1.1). Although the process of neurotransmission is tightly regulated, it is also incredibly plastic, which allows for the specialization of synapses to meet the particular requirements of the neuronal networks they are integrated in. Synaptic plasticity is referred to as the capacity of synapses to strengthen or weaken over time in response to their activity, and is believed to underlie processes such as learning and memory. Synaptic plasticity comes in the forms of short- or long-term depression or potentiation and is regulated by both pre and post-synaptic mechanisms (Citri and Malenka, 2008).

Given the requirement of synapses for neuronal function, it is essential to maintain synaptic form and function under homeostatic conditions. As outlined in the next sections, imbalances in the synaptic proteome, failure of pre- or post-synaptic mechanisms, and/or defects in synaptic plasticity can cause neurological and neurodegenerative conditions with devastating consequences.

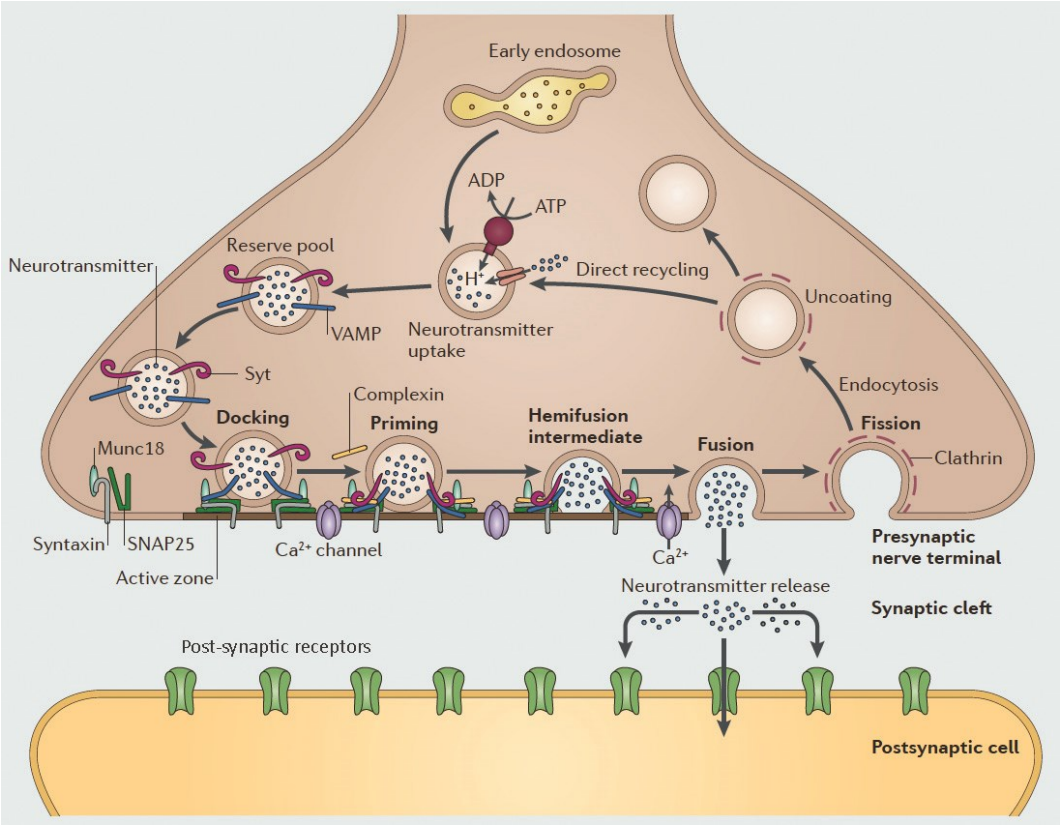


**Figure 1.1: Synapse and the synaptic vesicle cycle.** Synapses are the functional units of the nervous system responsible for the transmission of information between neurons. They are formed by a pre-synaptic nerve terminal, the synaptic cleft and a post-synaptic region. At the pre-synapse, synaptic vesicles undergo a cycle during which they are filled with neurotransmitters, docked to the active zone, primed for fusion and finally fused with the synaptic membrane upon a rise in calcium levels following an action potential. The exocytosis of synaptic vesicles releases neurotransmitters which activate receptors at the post-synaptic cell. To complete the synaptic vesicle cycle, vesicles are recovered by endocytosis and refilled with neurotransmitters. Figure adapted from (Rossetto et al., 2014).

### 1.3.2. Synapses are important pathological targets in diverse neurodegenerative conditions

Synapses have emerged as important sites of neuronal dysfunction in a wide range of neurodegenerative diseases (Gillingwater and Wishart, 2013, Henstridge et al., 2016). Loss of synapses and impairments in synaptic function are present in many

conditions, including AD (Sheng et al., 2012), PD (Picconi et al., 2012), HD (Milnerwood and Raymond, 2010) and lysosomal storage disorders, such as Batten disease (Kielar et al., 2009).

In AD degeneration is prominent in the hippocampus and association cortices. Early studies in human patients not only revealed that synapse loss was occurring in these areas during the course of disease progression, but also revealed a disproportionately large loss of synaptic connections, when compared to the loss of neuron cell bodies, indicating that synapse loss was likely occurring before neuronal death (Davies et al., 1987, Scheff and Price, 1993). In addition, the degree of synapse loss is often one of the best correlates of cognitive decline (DeKosky and Scheff, 1990, Ingelsson et al., 2004, Terry et al., 1991). Loss of hippocampal synapses and reduced levels of synaptic markers, such as the protein synaptophysin, haven been shown to correlate with cognitive function in patients suffering from AD and mild-cognitive impairment (Heinonen et al., 1995, Scheff et al., 2006, Sze et al., 1997). It is not yet fully understood why synapses degenerate in AD, although the accumulation of soluble forms of Aβ and hyperphosphorylated-tau are thought to play an important role (Spires-Jones and Hyman, 2014). These are believed to destabilize synapses and affect numerous downstream molecular mechanisms, such as AMPA and NMDA receptor mediated signalling (Hsieh et al., 2006, Shankar et al., 2007) and synaptic plasticity (Li et al., 2009, Shankar et al., 2008, Walsh et al., 2002).

In PD the corticostriatal and nigrostriatal pathways are particularly affected during the course of the disease. In agreement, impairments in synaptic function in these areas have been reported in various models of PD and found to precede neuronal loss (Day et al., 2006, Janezic et al., 2013, Stephens et al., 2005, Villalba et al., 2015).

Mice expressing mutations associated with familial forms of PD present defects in neurotransmission and synaptic plasticity (Sweet et al., 2015, Tong et al., 2009). Furthermore, increased levels and accumulation of α-synuclein, a protein central to the pathophysiology of PD, disrupt synaptic excitability and connectivity in models of the disease (Garcia-Reitbock et al., 2010, Nemani et al., 2010, Scott et al., 2010, Volpicelli-Daley et al., 2011).

Further evidence of how impairments in synaptic function underlie neuronal dysfunction in neurodegenerative conditions can be found in studies of HD. Although atrophy of the striatum, which precedes a generalized atrophy of the brain, is a key feature of the disease (Halliday et al., 1998), morphological defects in spines and synapses are evident before signs of neuronal death in both human post-mortem tissue and mouse models of the disease (Ferrante et al., 1991, Graveland et al., 1985, Spires et al., 2004). In addition, in HD patients cortical excitability is found to be altered before the onset of motor symptoms (Schippling et al., 2009), whereas animal models of the disease show early signs of deregulated synaptic plasticity and network activity (Cummings et al., 2006, Miller et al., 2008, Milnerwood et al., 2006, Walker et al., 2008).

### 1.3.3. Molecular mechanisms affecting synaptic stability

Neurodegenerative diseases display, early in the course of disease, impairments in synaptic function and structure. Although degeneration occurs in preferential neuronal populations and is initiated by different triggers, common pathways are disturbed in degenerating synaptic nerve terminals through the course of

disease. In the next subsections I will outline some of the major areas that affect synaptic stability and contribute to synaptic dysfunction.

#### *1.3.3.1. Synaptic function*

The correct functioning of the neurotransmission machinery is crucial to the maintenance of synaptic stability. Not only genetically modified animals that fail to express components of the SNARE machinery, such as SNAP-25 and VAMP2, are prenatally lethal (Schoch et al., 2001, Washbourne et al., 2002), but impaired SNARE function is also associated with extensive neurodegenerative phenotypes. Two proteins that have been shown to influence synaptic stability through this mechanism are CSP-α and α-synuclein. Deletion of CSP-α, a presynaptic chaperone, destabilizes SNAP-25 activity and compromises synaptic transmission (Fernandez-Chacon et al., 2004, Sharma et al., 2012). This results in widespread progressive neurodegeneration in CSP-α knock-out (KO) mice, which affects the neuromuscular system, GABAergic synapses and photoreceptor integrity, and leads to premature death before 4 months of age (Chandra et al., 2005, Fernandez-Chacon et al., 2004, Garcia-Junco-Clemente et al., 2010, Schmitz et al., 2006, Sharma et al., 2012). Interestingly, increasing α-synclein expression ameliorates degeneration and rescues lethality of the CSP-α KO mice (Chandra et al., 2005).

α-synclein itself has been repeatedly implicated in neurodegenerative mechanisms, initially due to its key contribution to the pathophysiology of PD (Stefanis, 2012). However, although aggregation of α-synclein is neurotoxic, deletion of proteins from the synuclein family in mice results in reduced dopamine levels in the brain and this family of proteins has been shown to contribute to the regulation of

neurotransmission during ageing (Burre et al., 2010, Chandra et al., 2004a). In fact, in its native conformation α-synclein acts as a chaperone for the assembly of SNARE-complexes and facilitates vesicle fusion (Burre et al., 2012, Burre et al., 2015).

Not only the pre-synapse but also the post-synapse contributes to the maintenance of neuronal function and stability. Defects in the function or abundance of post-synaptic receptors, such as AMPA and NMDA receptors, are associated with defects in synaptic plasticity in several neurodegenerative conditions, including PD, AD and HD (Henstridge et al., 2016). For instance, α-synuclein oligomers promote the internalisation of NMDA receptors and lead to reduced NMDA-dependent currents, resulting in impaired long-term potentiation (LTP) in hippocampal and dopaminergic cells (Chen et al., 2015, Cheng et al., 2011, Diogenes et al., 2012). Similarly, administration of oligomeric Aβ to hippocampal slices or *in vivo* microinjection into the hippocampal area results in disrupted LTP and enhanced long-term depression (LTD) (Li et al., 2009, Walsh et al., 2002). Impaired LTP and excessive LTD are associated with weakening and shrinking of synapses, which contribute to synapse elimination (Zhou et al., 2004). In addition, preferential loss of synaptic NMDA receptors, which occurs in AD models (Li et al., 2011), or an increase in extra-synaptic receptor signalling, as demonstrated for HD (Milnerwood et al., 2010), can have deleterious consequences for neuronal health. NMDA receptor signalling activates pro-survival pathways, including reduction of oxidative stress and induction of expression of survival genes, such as *bdnf*. On the other hand, extra-synaptic NMDA receptors mediate pro-death mechanisms, such as activation of calpains and apoptotic pathways (Hardingham and Bading, 2010). As a result, impaired synaptic plasticity

can have consequences not only for synaptic function and maintenance of neuronal networks, but may also shift the balance between pro-survival and pro-death pathways, leaving neurons more vulnerable to degeneration (Hardingham and Bading, 2010).

#### *1.3.3.2. Mitochondrial function*

Mitochondria are the main source of metabolic energy in cells. Nonetheless, in addition to producing ATP via oxidative phosphorylation (OXPHOS), mitochondria also play crucial roles in the maintenance of calcium homeostasis, control of reactive ROS and induction of apoptotic mechanisms. Moreover, mitochondria are extremely dynamic organelles. They constantly undergo fission and fusion and need to be transported between axons/synapses and the cell soma, where mitochondria biogenesis and degradation primarily occurs. As a result, many pathways contribute to the maintenance of mitochondrial homeostasis, including: adequate functioning of the OXPHOS chain and production of ATP; control of mitochondria DNA replication, transcription, translation and repair; maintenance of a low oxidative environment and control of ROS; mitochondrial quality control through fission and fusion mechanisms and removal of damaged mitochondria by mitophagy; and control of intracellular calcium levels. Failure of any of these pathways leads to pathology (DiMauro and Schon, 2008, Scheibye-Knudsen et al., 2015).

Synaptic mitochondria are particularly sensitive to insults and several factors have been proposed to account for their increased vulnerability. For instance, most mitochondria are produced in the cell soma and need to be transported along axons until they reach synapses (Sheng, 2014). Consequently, synaptic mitochondria may

have a longer life span than non-synaptic mitochondria and may accumulate more damage as a result. In addition, synapses are sites of high calcium fluctuations and energetic demand, and rely on mitochondria for sustaining synaptic activity (Marland et al., 2016, Pathak et al., 2015, Tong, 2007). Impaired mitochondrial function can therefore significantly affect synaptic function (Ly and Verstreken, 2006). Moreover, the demanding environment of synapses contributes to oxidative damage and $Ca^{2+}$ overload, to which synaptic mitochondria seem to be particularly vulnerable (Brown et al., 2006, Yarana et al., 2012).

Synaptic mitochondria form a subpopulation of mitochondria with distinct morphological, molecular and functional characteristics (Chang and Reynolds, 2006, Lai et al., 1977, Stauch et al., 2014b). Mitochondria at the synapse carry an adapted proteome, which may provide advantage towards the functional requirements of the synaptic environment but also contribute to the vulnerability of synapses to mitochondrial dysfunction. In fact, analysis of synaptic and non-synaptic mitochondria has shown synaptic mitochondria have lower basal OXPHOS activity and reduced levels of proteins responsible for $Ca^{2+}$ handling (Almeida et al., 1995, Stauch et al., 2014b). These changes may underlie the increased vulnerability of synaptic mitochondria to OXPHOS inhibition and $Ca^{2+}$ overload, with consequences for the vulnerability of synapses to neurodegeneration (Brown et al., 2006, Davey et al., 1997, Davey and Clark, 1996, Yarana et al., 2012). During aging, in contrast to what happens to most populations of non-synaptic mitochondria, which show decreased OXPHOS activity and energy production, mitochondria in synapses have been shown to maintain their bioenergetic capacity constant by increasing basal OXPHOS activity levels (Boffoli et al., 1994, Ferrandiz et al., 1994, Gomez et al., 2009, Stauch et al., 2014a).

Whereas synaptic proteins in aged mice show increased signs of oxidative damage, several antioxidant proteins are increased in aged synaptic mitochondria, which could represent an adaptive mechanism for dealing with increased ROS production due to cumulative damage or increased basal OXPHOS activity (Martinez et al., 1996, Stauch et al., 2014a).

Altered mitochondrial homeostasis is characteristic of several neurodegenerative disorders (DiMauro and Schon, 2008, Harris et al., 2012). For instance, mutations in genes encoding proteins from the mitochondria OXPHOS cause the childhood neurodegenerative disorder Leigh Syndrome (Lake et al., 2016), whereas mutations on the antioxidant protein SOD1 are associated with familial cases of ALS (Kiernan et al., 2011). In addition, mutations linked to PD, including in the *snca*, *pink1* and *dj-1* genes, have been shown to affect mitochondrial function and morphology (Haelterman et al., 2014), while toxins known to cause parkinsonian syndromes in humans, such as MPTP and rotenone, damage neurons by inhibiting mitochondria OXPHOS activity (Panov et al., 2005, Przedborski et al., 2004). In AD, the accumulation of Aβ and tau has been shown to disrupt mitochondrial trafficking and increase mitochondrial fragmentation (Rui et al., 2006, Wang et al., 2009, Wang et al., 2008b). Interestingly, synaptic mitochondria are affected by Aβ accumulation earlier than non-synaptic mitochondria, and exhibit decreased trafficking, impaired OXPHOS activity and increased oxidative stress (Du et al., 2010). $Ca^{2+}$ handling and mitochondrial trafficking are particularly affected in HD. In pre-symptomatic stages of the disease, mitochondria show disrupted $Ca^{2+}$ uptake and increased susceptibility to $Ca^{2+}$ overload (Choo et al., 2004, Milakovic and Johnson, 2005, Panov et al., 2002).

In addition, mutant huntingtin (mHtt) protein disrupts mitochondrial trafficking to synapses and promotes mitochondrial fragmentation (Kim et al., 2010, Shirendeb et al., 2012, Trushina et al., 2004).

Altogether, mitochondria play an important role in the maintenance of neuronal homeostasis but are also important sites of pathology in neurodegenerative diseases. In particular, a growing body of evidence indicates synaptic mitochondria have distinct functional features from non-synaptic mitochondria and are particularly vulnerable to some forms of mitochondrial dysfunction. Therefore, given their key contribution to both synaptic function and vulnerability, mitochondria are promising targets for neuroprotective therapies.

#### *1.3.3.3. Protein aggregates and protein clearance pathways*

Many neurodegenerative disorders are characterized by the presence of intracellular aggregates and inclusion bodies, which are often considered pathological hallmarks of the disease (Ross and Poirier, 2004). For instance, Aβ accumulates in plaques in the brain of patients with AD, α-synuclein inclusions are present in PD and Dementia with Lewy bodies, and the mHtt protein has a high propensity to aggregate (Ross and Poirier, 2004). Whereas large protein inclusions tend to be nuclear, cytoplasmic or secreted extracellularly, synapses can similarly be affected by the presence of insoluble protein aggregates. That is the case in AD, where Aβ and hyperphosphorylated-tau have been found in pre-synaptic compartments and dendritic spines (Hoover et al., 2010, Koffie et al., 2009, Takahashi et al., 2004), and in PD, in which aggregation of α-synuclein has been reported in synapses (Kramer and Schulz-Schaeffer, 2007, Spinelli et al., 2014).

The mechanisms behind the toxicity of protein aggregates are still controversial. On the one hand, it has been shown that the degree of inclusion bodies does not necessarily correlate with the severity of pathology in conditions such AD (Terry et al., 1991). In addition, several lines of evidence indicate that intermediate soluble oligomeric forms of aggregation-prone proteins, such as Aβ, α-synuclein and mHtt, are more damaging to cells than fibrils (Arrasate et al., 2004, Haass and Selkoe, 2007, Lue et al., 1999, Luth et al., 2014, Winner et al., 2011). The formation of neuronal inclusions has indeed been proposed to represent a protective mechanism which evolved to safeguard cells from the neurotoxic effects of misfolded proteins (Ross and Poirier, 2005). However, protein inclusions can affect synaptic function and interfere with protein quality control mechanisms (Bajic et al., 2012, Bence et al., 2001). As a result, it remains to be established what is the best strategy to deal with protein aggregation in neurodegenerative conditions, since not only protein inclusions but also the intermediate stages of misfolded protein monomers, soluble oligomeric species and proto-fibrils are associated with toxicity.

Clearance of protein aggregates and misfolded proteins is performed primarily by the ubiquitin-proteasome system (UPS) and autophagy mechanisms. The UPS degrades proteins that have been previously ubiquitinated, whereas autophagy is mediated by lysosomal degradation of proteins and has the capacity to deal with larger protein complexes than the UPS (Rubinsztein, 2006). Failure of any of these mechanisms results in neurodegenerative-like conditions. For instance, imbalances or mutations in components of the UPS, such as *Parkin*, *Uba1* and *Ufd2a*, have been

linked to PD, X-linked spinal muscular atrophy and spinocerebellar ataxia type 3, respectively (Lucking et al., 2000, Matsumoto et al., 2004, Ramser et al., 2008).

Degradation by the UPS is difficult for oligomeric and aggregated proteins, which tend to be degraded through autophagy (Berger et al., 2006, Iwata et al., 2005, Webb et al., 2003). However, ubiquitination of these proteins still occurs. Even though it may help prevent some of the toxic effects of misfolded proteins (Gray, 2001), excessive ubiquitination can also overload the UPS and interfere with its normal dynamics. Protein aggregates have been shown to directly inhibit UPS function, which has deleterious consequences for the normal homeostatic mechanisms controlling neuronal function (Bence et al., 2001). In agreement, inhibition of the UPS features in neurodegenerative conditions which present protein inclusions (Huang and Figueiredo-Pereira, 2010, Keller et al., 2000, Wang et al., 2008a). It is not clear why UPS inhibition occurs, but it could include overloading proteasomes with protein species that due to their conformation will not be degraded, sequestrating proteasome complexes into the protein aggregates themselves, and saturating the UPS system so that it is not able to cope with the regular cellular demands (Bence et al., 2001, Dantuma and Bott, 2014). In addition, mutant variants of proteins such as α-synuclein have the ability to directly bind the proteasome and impair its function (Snyder et al., 2003).

Whether protein aggregation is a cause or consequence of UPS failure, or vice-versa, is not clear, as the relationship between the two seems to function in a toxic loop (Bence et al., 2001, Dantuma and Bott, 2014). Misfolded proteins impair proteasome functions, which in turn prevents the efficient clearance of toxic species, aggravating protein aggregation and further inhibiting the UPS. On the other hand, impairments in

the UPS, due to normal ageing or genetic mutations, may promote the formation of protein aggregates responsible for neurodegenerative diseases such as AD and PD. Nonetheless, it is clear that protein aggregation and protein clearance mechanisms are a central theme in the field of neurodegeneration and can contribute to the impairment of neuronal function, and synaptic function in particular (Bingol and Schuman, 2005, Speese et al., 2003). Hence, strategies looking at stabilising non-toxic protein species, increasing the clearance or stabilisation of toxic protein aggregates and managing protein quality control mechanisms are attractive targets for the treatment of neurodegenerative conditions.

## 1.4. Synaptoprotective strategies for the treatment of neurodegenerative diseases

### 1.4.1. The importance of synaptoprotective strategies

Given the important role of synapses in neurodegenerative diseases it has been proposed that synaptoprotective therapies might be the key to preventing or halting neurodegeneration. In fact, this approach has several major advantages, as outlined by Lu and colleagues (Lu et al., 2013):

- Synapses are a common target of disease pathophysiology in a variety of conditions. Thus, synaptoprotective therapies have the advantage of being suitable to a wide range of neurodegenerative disorders, virtually regardless of the initial trigger of neuronal dysfunction;
- Synapses are essential for the maintenance of neuronal networks, which in turn underlie normal physiology and behaviour. Protecting neuronal

circuits is therefore expected to provide both functional and behavioural benefits;

- Synaptic dysfunction and loss are, to some extent, reversible. Therapies aiming to prevent synaptic dysfunction, to repair damaged synapses or to promote synaptogenesis and replace compromised networks are all expected to have therapeutic benefits;
- Synaptic dysfunction starts pre-symptomatically and is present throughout the progress of disease. Consequently, there is a wider therapeutic window for promoting the stability and repair of synapses than there is to address the pathogenesis of neurodegenerative disorders (Figure 1.2).

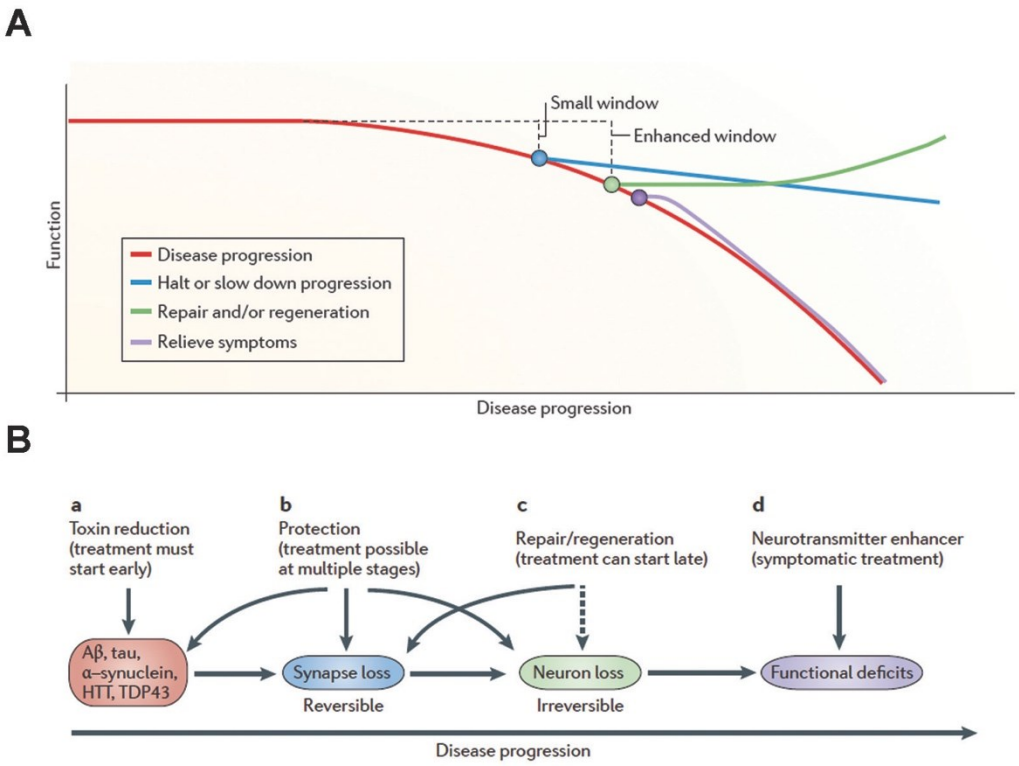


**Figure 1.2: Disease progression and therapeutic window for synaptoprotective interventions**. Graphical representation of disease progression (**A**) and examples of events in neurodegeneration (**B**).

During disease progression (A: red line) there is a small window of intervention when therapeutic strategies that target the pathogenic mechanisms of the disease may slow down disease progression (A: blue line; B: a). However, if the main pathophysiological mechanisms of the disease are targeted, there is an enhanced window of opportunities, with the possibility of repair or regeneration of the affected nervous tissue (A: green line; B: b, c). In particular, targeting synapse loss has the advantage of providing therapeutic benefits within a reasonable time frame during disease progression, and before reaching a potentially irreversible stage of neuronal loss. When the progression of disease reaches a critical symptomatic stage, therapies are aimed at ameliorating symptoms and do not halt disease progression (A: purple line; B: d). Figures obtained from (Lu et al., 2013).

### 1.4.2. Challenges

Studying synaptoprotective mechanisms is a promising route to the development of a new generation of drug treatments for neurodegenerative diseases. There are, however, important challenges that need to be considered. It is crucial that researchers continue to identify common pathways that affect synaptic stability and contribute to the pathophysiology of neurodegenerative diseases. In addition, we must acknowledge the complexity of the nervous system and the interdependency of the biological mechanisms that regulate neuronal function. It is, therefore, expected that multi-target approaches and combination therapies will be required to promote neuronal repair and homeostasis (Barabasi et al., 2011, Gillingwater and Wishart, 2013). Furthermore, in order to achieve effective translation of fundamental research into successful clinical trials we must not only be able to integrate the knowledge obtained from animal and *in vitro* models of disease with studies in human cohorts, but we also need to invest in research models that realistically recreate features of the human nervous system (Morton and Howland, 2013, Pouladi et al., 2013).

## 1.5. Aims

Given the established role of synapses as important targets of pathophysiology in many neurodegenerative conditions and the need to develop synaptoprotective therapies designed at halting disease progression, the aim of the work presented in this thesis was to explore novel mechanisms and molecular targets with the ability to modulate synaptic stability and degeneration *in vivo*. In order to achieve that goal, this thesis was divided into three main aims, resulting in three results chapters:

Aim 1 (Chapter 3): Promote translational research by validating the involvement of molecular targets, previously identified to influence synaptic degeneration in lower animal models (Wishart et al., 2012), in a large animal model of neurodegenerative disease, the CLN5 Batten sheep;

Aim 2 (Chapter 4): Study one of the candidates validated in Aim 1, calretinin, which has not been comprehensively explored in the published literature regarding its ability to modulate synaptic function and neurodegenerative mechanism;

Aim 3 (Chapter 5): Explore downstream targets of a well-known regulator of synaptic stability, α-synuclein, for which there are no validated therapeutic strategies currently available.

# Chapter 2. General Materials and Methods

## 2.1. Materials

Unless otherwise stated, reagents were obtained from Sigma-Aldrich and tissue culture specific reagents were obtained from Invitrogen. The list of primary and secondary antibodies used can be found in Table 2.1 and Table 2.2, respectively.

**Table 2.1: Primary antibodies.**

| Target | Species | Supplier | Cat No | ICC | IHC | WB |
|---|---|---|---|---|---|---|
| 2H3 | mouse | DSHB | 2H3 | | 1:100 | |
| α-synuclein | rabbit | Santa Ccruz | sc-7011-R | | | 1:5000 |
| ATP5A | rabbit | abcam | ab176569 | | | 1:5000 |
| β-actin | mouse | abcam | ab8226 | | | 1:1000 |
| β III tubulin | rabbit | abcam | ab18207 | 1:1000 | | |
| Calretinin | rabbit | Swant | 7697 | 1:200 | 1:100 | 1:5000 |
| CNPase | rabbit | abcam | ab27695 | | | 1:250 |
| NDUFB8 | mouse | Mitosciences | MS105 | | | 1:1000 |
| COX IV | mouse | abcam | ab14744 | | | 1:1000 |
| CSP | rabbit | abcam | ab79346 | | | 1:1000 |
| Dynamin 1 | goat | Santa Cruz | sc-6402 | | | 1:500 |
| GAPDH | mouse | abcam | ab9484 | | | 1:1000 |
| HDAC2 | mouse | active motif | 39533 | | | 1:500 |
| Horseradish Peroxidase | rabbit | Jackson ImmunoResearch | 323-005-021 | | 1:200 | |
| Neurofascin | rabbit | abcam | ab31457 | | | 1:5000 |
| ROCK2 | rabbit | abcam | ab125025 | | | 1:200 |
| sfxn3 | rabbit | sigma | HPA008028 | 1:10 | | 1:300 |
| SIRT2 | rabbit | abcam | ab75436 | | | 1:500 |
| SV2 | mouse | DSHB | SV2 | 1:200 | 1:50 | 1:5000 |
| Synapsin 1 | goat | Santa Cruz | sc-8295 | | | 1:300 |
| Ubr4 | goat | Santa Cruz | sc-162376 | | | |
| VDAC 2 | rabbit | abcam | ab47104 | | | 1:500 |
| vGAT | guinea-pig | Synaptic Systems | 131004 | | | 1:250 |
| vGLUT 1 | guinea-pig | Synaptic Systems | 135304 | | | 1:1000 |

ICC, IHC, WB: Dilutions used for immunocytochemistry (ICC), immunohistochemistry (IHC) and Western blotting (WB).

**Table 2.2: Secondary antibodies.**

| Target | Species | Supplier | Cat No | ICC | IHC | WB |
|---|---|---|---|---|---|---|
| anti-Guinea Pig IgG (H+L) Secondary Antibody, Alexa Fluor® 594 conjugate | Goat | Invitrogen | A-11076 | 1:500 | | |
| anti-Mouse IgG (H+L) Secondary Antibody, Alexa Fluor® 488 conjugate | Donkey | Invitrogen | A-21202 | 1:500 | 1:500 | |
| anti-Mouse IgG (H+L) Secondary Antibody, Alexa Fluor® 594 conjugate | Goat | Invitrogen | A-11032 | 1:500 | | |
| anti-Mouse IgG (H+L) Secondary Antibody, Alexa Fluor® 680 conjugate | Goat | Invitrogen | A-21058 | | 1:500 | |
| anti-Rabbit IgG (H+L) Secondary Antibody, Alexa Fluor® 488 conjugate | Donkey | Invitrogen | A-21206 | 1:500 | 1:500 | |
| anti-Rabbit IgG (H+L) Secondary Antibody, Alexa Fluor® 594 conjugate | Donkey | Invitrogen | A-21207 | 1:500 | | |
| Cy3 AffiniPure Goat Anti-Rabbit IgG (H+L) | Goat | Jackson Immuno Research | 111-165-003 | | 1:200 | |
| IRDye® 680RD Donkey anti-Rabbit IgG (H + L) | Donkey | LiCOR Biosciences | 926-68073 | | | 1:5000 |
| IRDye® 680RD Donkey anti-Goat IgG (H + L) | Donkey | LiCOR Biosciences | 926-68074 | | | 1:5000 |
| IRDye® 800CW Donkey anti-Mouse IgG (H + L) | Donkey | LiCOR Biosciences | 926-32212 | | | 1:5000 |

ICC, IHC, WB: Dilutions used for immunocytochemistry (ICC), immunohistochemistry (IHC) and Western blotting (WB).

## 2.2. Methods

This section contains a small selection of methods used across the various chapters of this thesis. For specific techniques used in individual chapters please refer to the Methods section included in Chapters 3 to 5.

### 2.2.1. Genotyping

Genomic DNA was extracted by digesting ear clips in 5 μg/mL Proteinase K in Lysis Buffer (100 mM Tris, 200 mM NaCl, 5 mM EDTA, 0.2% SDS, pH 8.0)

overnight at 55°C. The digestion samples were spun at 20,000g for 5 min, the supernatant collected and the DNA precipitated by addition of an equal volume of isopropanol. Following centrifugation at 20,000g for 5 min, the pellet was washed twice in 70% ethanol and spun at 20,000g for 5 min. The pellet was then allowed to air dry for at least 1 h and the DNA dissolved in 25 μL $H_2O$.

2 μL of genomic DNA were used for each PCR reaction. The amplified PCR products were separated by gel electrophoresis in 2% w/v agarose (SeaKem LE) gels in TAE buffer (40 mM Tris, 40 mM Glacial Acetic Acid, 1 mM EDTA, pH 8.0) and visualized in an UV chamber. The genotype of each mouse was determined according to the presence or absence of the WT or KO bands of appropriate size.

### 2.2.2. Isolation of crude synaptosomes

Crude synaptosomes were isolated as described in (Wishart et al., 2007, Wishart et al., 2012). Synaptosomes were prepared from fresh brain tissue whenever possible. For frozen sheep tissue, samples were incubated in a water bath at 37°C for up to 2 min to ensure they were completely thawed before proceeding.

Brain samples were homogenized in ice-cold sucrose buffer (320 mM sucrose, 1 mM EDTA, 5 mM Tris-HCl, pH 7.4) and centrifuged for 10 min at 900g and 4°C. The supernatant (S1) was collected and the pellet (P1) resuspended in sucrose buffer and centrifuged as before. The resulting pellet (P1') was kept as the non-synaptic fraction. The supernatant (S1') was combined with S1 and centrifuged at 20,000g for 15 min at 4°C to pellet out the synaptosomes (P2).

Synaptic and non-synaptic fractions were either directly used for subsequent experiments or stored at -80°C until required.

### 2.2.3. Western Blotting

Western blotting was performed essentially as described in (Eaton et al., 2013). Protein was extracted from cells or tissue by homogenization in RIPA buffer (ThermoScientific) with Halt Protease Inhibitor Cocktail (ThermoScientific), unless otherwise stated. The resulting homogenate was centrifuged for 20 min at 20,000g and 4°C and the supernatant, consisting of the soluble protein extract, was used for Western blotting. Protein concentration was determined by BCA assay (ThermoScientific).

5-100µg of protein per lane were prepared in NuPage® LDS Sample Buffer (Invitrogen), heated to 98°C for 5 min and loaded on pre-cast NuPage® Novex® 4-12% Bis Tris gradient gels (Invitrogen). Gels were run in XCell SureLock® Mini-Cell systems (Invitrogen) in Bolt® MES SDS Running Buffer (Invitrogen) for 15 min at 80 V and for 1 h at 150 V. Proteins were then transferred to PVDF membranes using the iBlot® or iBlot2® Dry Blotting System (Invitrogen). The membranes were blocked in Odyssey blocking buffer (Li-COR Biosciences) for at least 30 min, incubated in primary antibody overnight at 4°C and secondary antibody for 1 h at room temperature (RT). All antibodies were diluted in Odyssey blocking buffer with 0.1% Tween-20 and between incubations membranes were washed 3x in phosphate-buffered saline (PBS; in mM: 137 NaCl, 2.7 KCl, 10 $Na_2HPO_4$, 1.8 $KH_2PO_4$) for 10 min. Blots were imaged in an Odyssey Infrared Imaging System (Li-COR Biosciences) at a resolution of 169 µm and quantified using the ImageStudio Software (Li-COR Biosciences). The intensity of each fluorescent band was measured in triplicate, in order to minimize user variability.

For use with anti-α-synuclein and anti-calretinin antibodies, the membranes were fixed in 0.4% paraformaldehyde (PFA; Electron Microscopy Sciences) in PBS for 20 min and washed 3x for 5 min in PBS prior to blocking. This method has been shown to increase the sensitivity of α-synuclein detection (Lee and Kamitani, 2011) and we also found it improves the labelling of calretinin.

### 2.2.4. Statistical analysis

Quantitative data were collected and analysed in Microsoft Excel®. Statistical analysis was performed using GraphPad Prism® software. Details of individual statistical tests are outlined during the results sections or figure legends. Statistical significance was considered when p-value $< 0.05$.

# Chapter 3. Molecular neuropathology of the synapse in sheep with CLN5 Batten disease

## 3.1. Introduction

### 3.1.1. Translational studies in large animal models of neurodegenerative disease

Our growing understanding of the mechanisms regulating synaptic pathophysiology opens doors to the possibility of developing synaptoprotective therapies for the treatment of a variety of neurodegenerative disorders. However, one important issue concerning this type of translational research is the current predominance of studies using small animal models, such as mice, as these animals do not fully replicate crucial features of the human nervous system, including size and complexity (Aigner et al., 2010, Dolezalova et al., 2014, Morton and Howland, 2013, Pouladi et al., 2013). One solution to this problem might arise from the increasing availability of large animal models of neurodegeneration, such as sheep and pigs. Not only it is becoming more commonplace to use genetically-modified large animals in neurodegenerative research (Aigner et al., 2010, Morton and Howland, 2013), but there are also several human conditions where there is an equivalent endogenous disorder in a large animal species. One good example is the CLN5 New Zealand Borderdale model of Batten Disease (Frugier et al., 2008).

### 3.1.2. Neuronal Ceroid Lipofuscinosis; Batten Disease

Neuronal Ceroid Lipofuscinosis (NCLs), commonly referred to as Batten disease, is a group of autosomal-recessive progressive neurodegenerative disorders. NCLs are amongst the most common neurodegenerative diseases of childhood, with an incidence of up to 1:12500, and are currently untreatable (Santavuori et al., 2000). Mutations in several genes (*CLN1* to *CLN10*) have been identified to cause NCL variants which differ with regards to the age of onset of the disease, but that are characterized by a similar progression of clinical symptoms. Visual impairments and retinal degeneration, ultimately leading to blindness, are some of the earliest symptoms. Motor and cognitive dysfunction, seizures and an abnormal EEG rapidly follow and the disease invariably leads to premature death (Jalanko and Braulke, 2009, Santavuori et al., 2000).

Despite the fact that the genetic causes of NCLs have been identified, the molecular mechanisms underlying the pathophysiology of the disease remain unclear. A pathological hallmark of NCLs is the widespread accumulation of autofluorescent lysosome-derived storage material, most often composed of the subunit c of the mitochondrial ATP synthase (Palmer et al., 1992, Westlake et al., 1995). However, even though these inclusions are found in several neuronal and peripheral tissues of patients and animal models of the disease they are not the best correlate of disease severity, nor the main cause of pathology. In fact, the nervous system and subsets of neuronal populations, such as the thalamus in mice (Kielar et al., 2007, Partanen et al., 2008) and hypothalamus and cortical areas in human and ovine NCLs (Oswald et al., 2008, Tyynela et al., 2004), are preferentially affected. Glia activation most often precedes the onset of neurodegeneration and is, so far, the best cellular correlate of

disease progression in animal models of NCLs (Jalanko and Braulke, 2009, Mitchison et al., 2004, Palmer et al., 2013).

### 3.1.3. Animal models of NCLs: The CLN5 Batten sheep

Advances in the understanding of the pathogenesis and progression of NCLs have benefited from several animal models of the disease that are currently available. Various mouse models have been engineered (Jalanko and Braulke, 2009) and natural occurring mutations in *CLN* genes have been identified in a number of different species, including dogs, cows and sheep (Jolly et al., 1992, Jolly et al., 1997, Moroni-Rawson et al., 1995, UCL, 2015). When compared to rodent models of NCLs, large animal models, such as sheep, replicate better the human progression of the disease and are particularly useful to dissect region-specific pathophysiological features of the disease due to their brain size and CNS complexity (Jolly et al., 1989). In addition, their longer life span allows for a clinical progression that closely resembles the human disease and for better assessment of long-term effects of therapeutic strategies.

One specific Batten disease sheep model, the CLN5 Batten sheep, has been particularly well characterized. This model was initially identified in a flock of New Zealand Borderdale sheep which carry a nucleotide substitution at the consensus splice site c.571+1G>A of the *CLN5* gene (Jolly et al., 2002). The mutation leads to deletion of exon 3 of the *CLN5* transcript and, consequently, no transcripts of full-length *CLN5* and only a small amount of mutant *CLN5* transcripts are detectable in diseased animals, resulting in lack of a functional CLN5 protein (Frugier et al., 2008). By 21 months of age, the CLN5-deficient sheep show extensive degeneration of the cerebral cortex, positive GFAP staining and abundant cellular inclusions positive for the subunit-c of

mitochondrial ATP synthase. Such inclusions are also observed in cultured neurons from CLN5 fetal sheep brains and are reversed by lentiviral expression of full-length functional CLN5, indicating that CLN5 deficiency is key to the onset and progression of this NCL variant (Hughes et al., 2014, Hughes et al., 1999).

### 3.1.4. The function of the CLN5 protein

The function of the CLN5 protein is still poorly understood. CLN5 is expressed in a variety of peripheral tissues and in the brain, where it is found in both neurons and glia (Holmberg et al., 2004). Like many other CLN proteins, it is present in lysosomes and CLN5 deficiency leads to the accumulation of subunit-c of the mitochondrial ATP synthase in storage bodies (Frugier et al., 2008, Isosomppi et al., 2002, Tyynela et al., 1997). Although the function of the CLN5 protein remains unknown, it likely contributes to the production of the enzymatically active forms of TPP1/CLN2 and Cathepsin D/CLN10, two other lysosomal proteins involved in variants of NCL (Frugier et al., 2008). An interconnection between CLN5 and other CLN proteins has also been proposed by immunoprecipitation studies, where CLN5 was found to form complexes with CLN1, CLN2, CLN3, CLN6 and CLN8 (Schmiedt et al., 2010, Vesa et al., 2002). In addition, co-expression of CLN1 restores the detrimental effects caused by loss of functional CLN5 due to a common Y392X mutation in the protein (Lyly et al., 2009). CLN5 and CLN3 have further been implicated in endosome-Golgi trafficking through recruitment of Rab7 and gene expression profiling of knockout mice for both genes has suggested a common role in the stabilization of neuronal growth cones (Mamo et al., 2012, Uusi-Rauva et al., 2012).

### 3.1.5. Synaptic pathology in NCLs

Synaptic pathology is an established early feature of several neurodegenerative disorders and there is increasing evidence supporting an important role of synapses in NCLs. NCL rodent models present synaptic dysfunction, progressive synapse loss and alterations in the balance of the synaptic proteome (Kielar et al., 2009, Kim et al., 2008, Partanen et al., 2008), while the CLN6 ovine model of NCL shows synaptic dysfunction and loss with higher incidence in the brain regions affected earlier during the progression of disease (Kanninen et al., 2013). However, it has not been established whether equivalent molecular mechanisms are consistently affected across rodent and sheep models of Batten disease.

### 3.1.6. Aims

The aim of the work presented is this chapter was to establish whether known molecular regulators of synaptic pathophysiology, previously identified in rodent and *Drosophila* models of neurodegeneration (Wishart et al., 2012), were similarly present and modified in the brain of a large animal model of neurodegenerative disease, the CLN5 Batten sheep. This will allow us to identify whether molecular mechanisms of synaptic pathophysiology are conserved across species and if rodents can be used with confidence in translational studies aimed at developing synaptoprotective therapies for NCLs and other neurodegenerative conditions.

## 3.2. Materials and methods

### 3.2.1. Animals

Ovine tissue was obtained from Professor David Palmer (Lincoln University, New Zealand) and Professor Jennifer Morton (University of Cambridge, UK).

CLN5 homozygous (Batten sheep) and heterozygous controls were born, raised and diagnosed from a flock of Borderdale sheep at Lincoln University (New Zealand) (Frugier et al., 2008). All procedures were carried out in accordance with National Institute of Health (NIH) guidelines and the New Zealand Animal Welfare Act 1999 as approved by the Lincoln University Animal Ethics committee.

A cohort of heterozygous control and pre-symptomatic CLN5 sheep for Magnetic Ressonance Imaging (MRI) and molecular analyses were shipped by air from Lincoln University (New Zealand) to the University of Cambridge (UK). Animals were housed in a barn with windows and supplementary additional artificial light from 6am to 6pm. All animals had free access to hay feed and water, with additional pellet supplements provided every morning. Experimental procedures performed in Cambridge were conducted in accordance with the UK Animals (Scientific Procedures) Act 1986 and were approved by a University of Cambridge internal ethical review board.

### 3.2.2. Gross neuropathology

Sheep for gross neuropathological analyses were sacrificed at Lincoln University, in accordance with National Institute of Health guidelines and the New Zealand Animal Welfare Act 1999 and as approved by the Lincoln University Animal

Ethics committee. Sheep were stunned with a captive bolt, in a manner that did not damage the brain itself, and exsanguinated. Following confirmation of death, the head was perfused with saline (0.9% NaCl, 37 ºC) via one of the carotid arteries, to remove excess blood, and perfused-fixed with 10% formalin in saline, pH 7.4. The brain was removed and dissected at the sagittal midline, further fixed for 7 days in 10% formalin, equilibrated in cryoprotective solution (10% ethylene glycol, 20% sucrose in 0.9% NaCl) and stored at -80ºC until required.

Cryopreserved perfusion fixed frozen brain hemispheres were processed as described in (Oswald et al., 2005). Briefly, each hemisphere was serially sectioned at 50 µm on a sliding microtome (Microm, Germany), the sections were mounted on slides, stained with Nissl and then coverslipped. Images were captured using an upright microscope (Nikon Eclipse 50i) and analysed using NIS-Elements Software (Nikon Instruments Inc., Melville, NY, USA). To determine the cortical thickness, at least 25 measurements were made for each animal from the pial surface to the white matter (cortical layers I-VI) in the primary motor cortex and from the pial surface to the granular boundary with the white matter in the anterior lobe of the cerebellum.

The experiments described in this section were performed by Nadia Mitchell at the laboratory of Prof. David Palmer, Lincoln University.

### 3.2.3. Magnetic Resonance Imaging

Animals used for magnetic resonance imaging (MRI) were sacrificed at the University of Cambridge (UK) by an intravenous overdose of barbiturate-based anaesthetic and the brains perfuse-fixed in 4% PFA in saline. Heads were trimmed to remove the jaw and orbits but the brains were not removed from the cranium to

preserve the cortical surface. Brains were imaged in a 4.7T Bruker BioSpec 47/40 using a rapid acquisition with relaxation enhancement protocol with a field of view of 128×85.2×66.6 $mm^3$ and a matrix of 384×256×200 with two-fold anti-aliasing in all three directions to provide an isotropic resolution of 333 μm. The repetition time was 1.2 s with an affective echo time of 50 ms, an echo train length of 5 and a bandwidth of 50 KHz. Total scan time was 13.5 h per brain. For comparison, reconstructed images were rigidly-registered together using SPM12 (Wellcome Trust Centre for Neuroimaging, University College London) and the SPMMouse toolbox (Sawiak et al., 2013).

The experiments described in this section were performed by Stephen Sawiak and Roger Mason, in the laboratory of Prof. Jennifer Morton, University of Cambridge.

### 3.2.4. Quantitative western blotting

Tissue used for quantitative western blotting was obtained from Prof. Jennifer Morton (University of Cambridge, UK). Tissue was obtained from eight 20-24 month old CLN5 female sheep, and five heterozygous controls, four females and one castrated male, of comparable age.

Animals were sacrificed at the University of Cambridge (UK) by an intravenous overdose of barbiturate-based anaesthetic. Selected brain regions (motor cortex and cerebellum) were flash-frozen, within 15-20 min of time of death, by immersion in liquid nitrogen and stored at -80°C. At the University of Edinburgh, the tissue was used for the preparation of crude synaptosomes or whole brain lysates, and submitted to quantitative western blotting. Please see General Materials and Methods section for details about these techniques.

## 3.3. Results

### 3.3.1. Identification of brain regions affected by neurodegeneration in CLN5 sheep brain

To identify areas of the brain subject to substantial neurodegeneration at late stage disease, as well as an area that was relatively spared from neurodegeneration, gross neuropathological changes were analysed in complete sagittal sections of late stage CLN5 Batten sheep. While atrophy of all cortical regions was obvious macroscopically at 24 months, both subcortical nuclei and the cerebellum of CLN5 brains retained a normal appearance (Figure 3.1). Cortical atrophy appeared most severe, in descending order, in the primary visual, parieto-occipital and motor cortex regions of the CLN5 sheep brain. Cortical thickness was analysed in Nissl stained sections and revealed progressive thinning of the neuronal layers, particularly the upper layers (II-III). By 24 months of age few cortical neurons remained (Figure 3.2). At this age, the cortical thickness of the primary motor area of CLN5 animals was reduced by 44% from that observed in normal controls (Figure 3.2). In contrast, no cytoarchitectural differences were apparent in the cerebellum between control and CLN5 animals, and there was no detectable difference in cerebellar cortical thicknesses (Figure 3.1, Table 3.1).

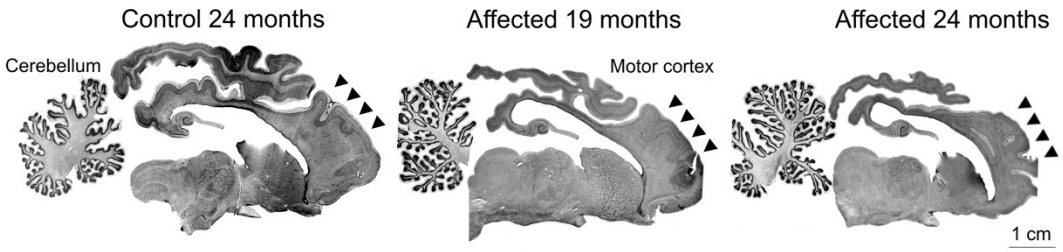


**Figure 3.1: Reduced cortical volume in CLN5 Batten sheep.** Nissl stained sections showed marked atrophy of the cortical mantle in affected sheep at 19 months of age, which was more pronounced by 24 months of age (see arrowheads). In contrast, the cerebellum and subcortical structures were relatively spared. Image produced in collaboration with NL Mitchell and DN Palmer.

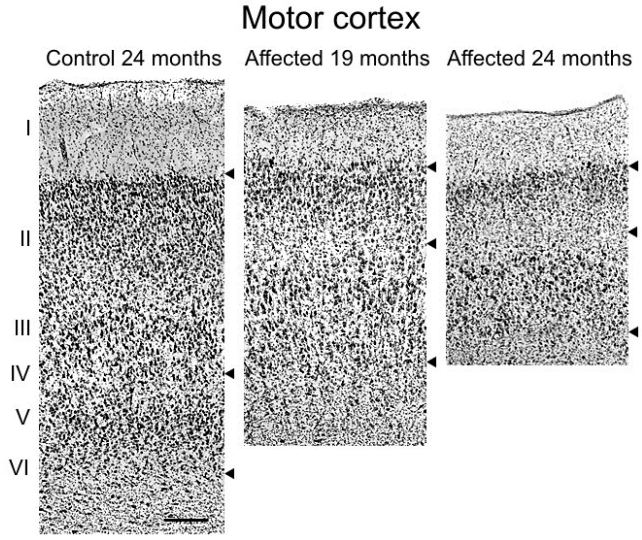


**Figure 3.2: Atrophy of motor cortex in CLN5 sheep brains.** Microscopic comparison of the motor cortex of Nissl stained sections (shown in Figure 3.1). Upper arrows mark the layer I/II boundary, the middle arrows indicate layer IV, and the lower arrow marks the layer VI/white matter boundary. Scale bar 200 µm. Image produced in collaboration with NL Mitchell and DN Palmer.

**Table 3.1: Cortical thickness measurements from 24 month old normal control and CLN5 Batten sheep brains.** Table produced in collaboration with NL Mitchell and DN Palmer.

| | Mean thickness (µm ± SEM)* | | |
|---|---|---|---|
| **Layers** | **Normal control** | **CLN5 affected** | **P value*** ** |
| **Cerebellar cortex** | 502 ± 10 | 493 ± 11 (98% ± 2.1)** | NS |
| **Motor cortex (I-VI)** | 1692 ± 45 | 940 ± 21 (56% ± 1.2)** | ≤ 0.001 |

* Measurements from 3 animals per group and >25 measurements per brain/region.

** % from control

*** Unpaired two-tailed t-test

To further validate these gross neuropathological findings, we used MRI techniques to extend our investigations of neuropathological changes in CLN5 sheep. Compared to brains of control sheep, brains from CLN5 affected Batten disease sheep at 22 months of age had a striking reduction of neocortical volume, with relative sparing of subcortical structures and the cerebellum (Figure 3.3).

Taken together, these studies confirmed that CLN5 deficiency in sheep affects brain areas in a differential manner, with the cerebellum being mostly spared from disease-related pathology and the cortex being severely affected.

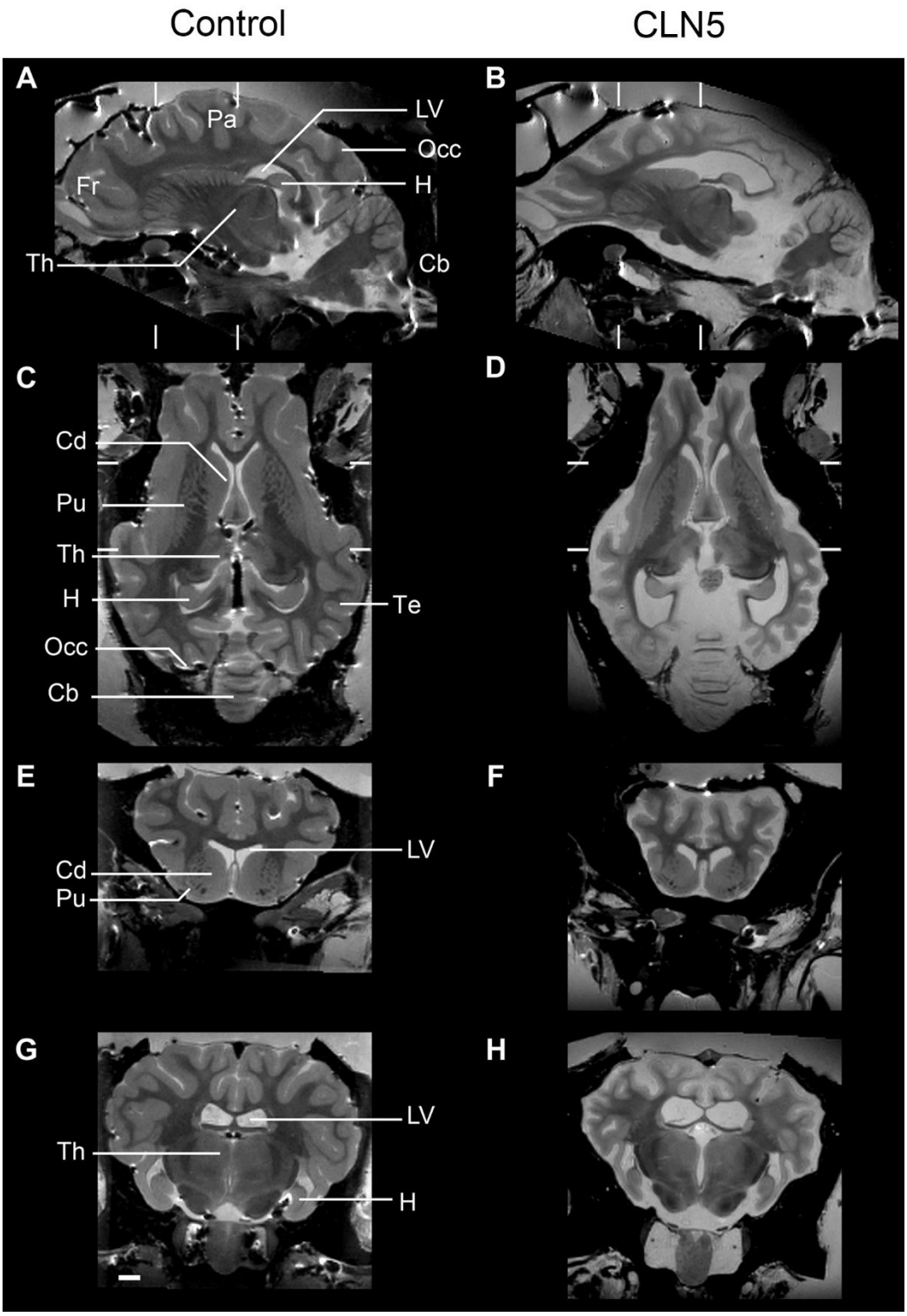


**Figure 3.3: MRI analyses of CLN5 Batten sheep brain confirms targeting of the cortex and sparing of the cerebellum.** Representative MR images of control (A, C, E, G) and CLN5 affected sheep (B, D, F, H). Sections are shown in sagittal (A-B), horizontal (C-D) and two coronal cuts (E-F

and G-H at the levels marked in A-D). The scale bar is 2 cm. Label abbreviations: Fr frontal lobe; Pa parietal lobe; Occ occipital lobe; Te temporal lobe; LV lateral ventricle, Th thalamus, H hippocampus; Cb cerebellum; Cd caudate; Pu putamen. Image produced in collaboration with J Morton, R Mason and SJ Sawiak.

### 3.3.2. Synapse loss in the motor cortex of CLN5 Batten sheep

Loss of synapses has been identified as a feature of CLN5 pathology in mouse models (von Schantz et al., 2009). We therefore wanted to verify whether synapses were also being targeted in the CLN5 Batten sheep.

In order to assess the relative density of synapses between CLN5 Batten sheep and control animals, we measured levels of the synaptic protein SV2 by quantitative fluorescent western blotting in whole brain tissue samples from the cerebellum and motor cortex. SV2 levels remained unchanged in the cerebellum of CLN5 sheep compared to controls, confirming the low vulnerability of synapses in this brain region (Figure 3.4). In contrast, SV2 levels were significantly reduced in the motor cortex, an affected region of CLN5 Batten sheep, indicating a substantial loss of synapses (Figure 3.4).

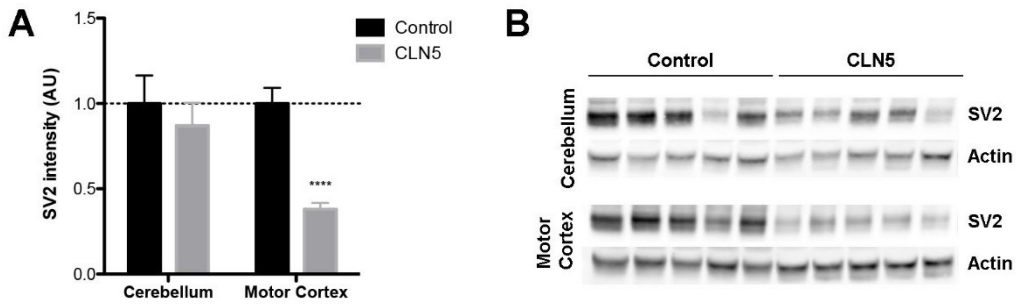


**Figure 3.4: Loss of synapses in affected brain regions from CLN5 Batten sheep. A)** Quantitative fluorescent western blotting in preparations of whole tissue revealed relatively stable levels of SV2, a core synaptic protein, in the cerebellum of control and CLN5 sheep. In contrast, in the motor cortex of CLN5 Batten disease affected sheep the levels of SV2 are reduced by 60%, indicating there is severe synapse loss restricted to this brain area of the Batten affected sheep. (N=5 animals, n=10 distinct tissue samples from control sheep; N=8, n=16 from CLN5 sheep; ****P<0.0001, unpaired two-tailed t-test). **B)** Representative fluorescent western blots (N=5 animals per genotype) showing a consistent decrease in SV2 levels in the motor cortex of CLN5 Batten disease affected sheep when compared to controls. Note the relatively stable levels of SV2 in the cerebellum of CLN5 sheep. Actin was used as loading control.

### 3.3.3. Preparation of synapse-enriched fractions from sheep brain tissue

In order to perform a reliable analysis focused on synaptic pathology of CLN5 Batten sheep, we wanted to establish whether we could generate tissue samples enriched with synaptic material (synaptosomes) from frozen brain tissue samples from sheep with a similar efficiency and reproducibility to that obtained when using fresh mouse tissue (Wishart et al., 2012). We adapted the sub-cellular fractionation protocol previously used for fresh mouse brain for application with frozen brain samples from sheep. Although larger volumes of buffer and a higher number of passages were required to completely homogenize the sheep tissue when compared to the mouse

whole brain, we were able to successfully isolate synaptic enriched fractions from various regions of the brain of sheep. Using fluorescent western blotting, we confirmed a robust enrichment of the synaptic protein SV2 and almost complete exclusion of the nuclear protein HDAC2 on synaptosome preparations from control and CLN5 sheep brains, in both the cerebellum and motor cortex (Figure 3.5).

We thus concluded it is possible to use standard synaptosome protocols to generate preparations of synaptically-enriched tissue from sheep brains, even using samples that had been frozen and stored rather than freshly-harvested brain tissue.

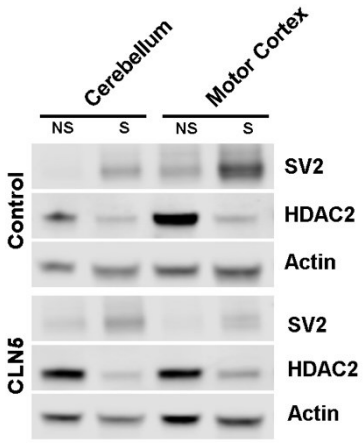


**Figure 3.5: Characterization of synaptosome preparations from control and CLN5 Batten disease affected sheep brains.** Representative western blots from synaptic (S) and non-synaptic (NS) fractions generated from the cerebellum and motor cortex of control and CLN5 Batten disease affected sheep brains. Immunoblotting with SV2 and HDAC2 demonstrates, respectively, the synaptic enrichment of the synaptic fractions and their low contamination with nuclear components. Actin was used as a loading control. All lanes were loaded with 20µg of protein.

### 3.3.4. Identification of synaptic proteins in mouse and sheep synaptosomes

The ability to isolate synaptosome preparations from the cerebellum and motor cortex of sheep brains offered us the possibility to examine whether known molecular regulators of synaptic pathophysiology, previously identified in *Drosophila* and mouse models (Wishart et al., 2012), were also expressed in and localized to synapses in the sheep brain.

We chose to compare the levels of eight individual proteins previously shown to be present in mouse synapses, and whose expression levels were found to be robustly modified in synapses undergoing degeneration: α-synuclein, Calretinin; 2',3'-cyclic nucleotide 3' phosphodiesterase (CNP); Cysteine-string protein alpha (CSP-α; DNAJC5); Neurofascin; Rho-associated, coiled-coil containing protein kinase 2 (ROCK2); Sirtuin 2 (SIRT2); and Ubiquitin protein ligase E3 component n-recognin 4 (UBR4) (Wishart et al., 2012). Direct comparison of these proteins in synaptosome preparations from wild-type mice and sheep using fluorescent western blotting confirmed that all eight proteins were conserved between the two species and that all were detectable using the same primary antibodies as used in mouse studies (Figure 3.6).

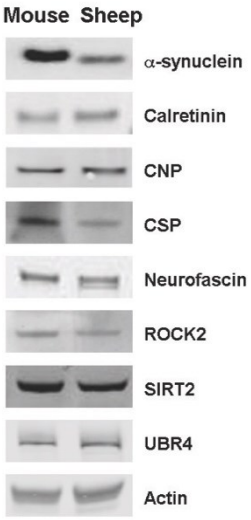


**Figure 3.6: Identification of synaptic proteins in synaptosome preparations from mice and sheep.** Representative fluorescent western blots confirming the expression and detection, in both mouse and sheep synaptosomes, of eight synaptic proteins implicated in the regulation of synaptic stability and degeneration, as well as a loading control (actin). Note that all synaptic proteins previously identified in mouse synapses were similarly present, and detectable using the same primary antibodies, in sheep synapses. 20μg of protein were loaded per lane. Mouse synaptosomes were prepared from whole brain, whereas sheep synaptosomes were prepared from cerebellum or motor cortex.

### 3.3.5. Region-specific modifications in known regulators of synaptic stability in CLN5 Batten sheep

The ability to detect and measure levels of individual proteins implicated in the regulation of synaptic degeneration (Figure 3.6) allowed us to directly assess whether molecular pathways being instigated in degenerating synapses from the sheep brain are the same as those previously reported in the mouse (Wishart et al., 2012). Therefore, we generated region-specific synaptosome preparations from the brains of 5 control and 8 CLN5 Batten disease affected sheep. Due to the large volume of the sheep brain, and to ensure a representative fraction of it was studied, for each brain

region from each individual sheep two synaptosomes fractions were prepared and assayed independently.

Quantitative fluorescent western blotting revealed that the levels of the eight proteins studied were not significantly altered in the cerebellum of CLN5 sheep when compared to unaffected controls (Figure 3.7). This analysis not only confirmed we could repeatedly detect and measure all eight synaptic proteins across samples from multiple animals, but also demonstrated that levels of these proteins are relatively stable in healthy areas of the brain from CLN5 Batten sheep. In striking contrast, a comparison of protein levels in the severely affected brain region (motor cortex) revealed significant changes for seven out of the eight proteins examined (Figure 3.8). Most proteins showed a reduction of over 50% in CLN5 synaptosomes when compared to controls (α-synuclein, CSP-α, Neurofascin, ROCK2, and SIRT2). In contrast, levels of Calretinin were almost twice those observed in synapses from control sheep.

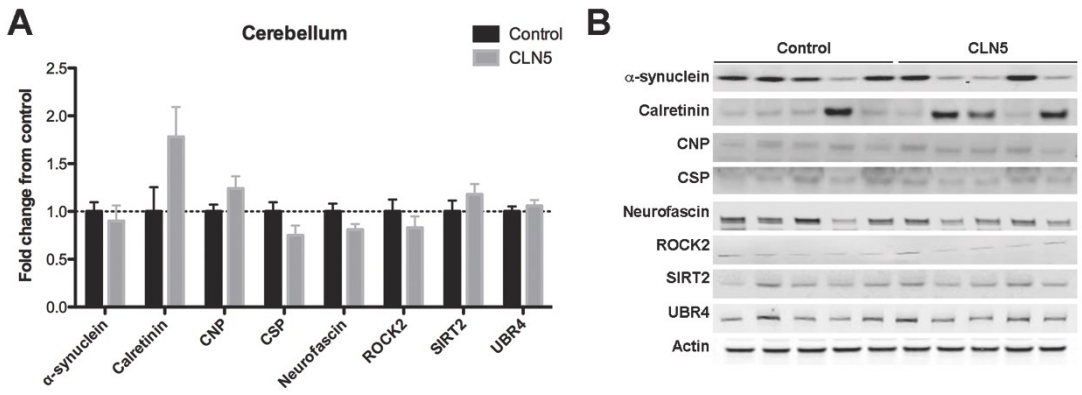


**Figure 3.7: Stable expression of synaptic proteins in the cerebellum of CLN5 sheep. A)** Levels of the eight synaptic proteins in synaptosome preparations generated from the unaffected cerebellum of control and CLN5 Batten disease affected sheep were measured by quantitative fluorescent western blotting. Actin was used as loading control. Quantitative data shown as mean ± SEM (N=5, n=10 control; N=8, n=16 CLN5). Statistical analyses revealed no significant differences (P>0.05 in unpaired

two-tailed t-test) in the level of any protein between control and CLN5 samples. **B)** Representative western blots.

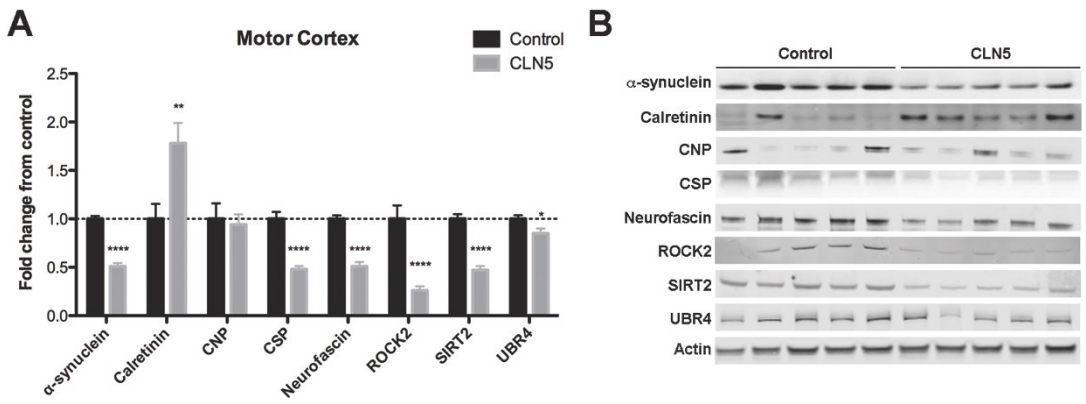


**Figure 3.8: Modified expression levels of synaptic proteins in motor cortex from CLN5 Batten disease affected sheep. A)** Levels of the eight synaptic proteins in synaptosome preparations generated from the unaffected cerebellum of control and CLN5 Batten disease affected sheep were measured by quantitative fluorescent western blotting. Actin was used as loading control. Quantitative data shown as mean ± SEM (N=5, n=10 control; N=8, n=16 CLN5). * $p<0.05$, ** $p<0.01$, **** $p<0.0001$ in unpaired two-tailed t-test. **B)** Representative western blots.

Altogether, these results confirm that synaptic proteins previously implicated in synaptic degeneration pathways in mice and *Drosophila* show dynamic alterations to their expression levels in a large animal model of neurodegenerative disease, the CLN5 Batten sheep, and that synaptic pathology in this model is selectively found in synapses from affected brain regions.

## 3.4. Discussion

### 3.4.1. Overview of results

We investigated whether molecular aspects of synaptic pathophysiology previously identified in *Drosophila* and mouse models of a range of neurodegenerative diseases (Wishart et al., 2012) are recapitulated in a large animal model of neurodegenerative disease, the CLN5 Batten sheep. We observed a regionally specific atrophy of the brain with pronounced degeneration of the motor cortex and sparing of the cerebellum. In agreement, we have shown there is an equivalent disruption of synaptic integrity, as assessed by the levels of SV2 protein in whole brain lysates, in the motor cortex, with the cerebellum being relatively spared from synapse loss. In addition, we demonstrated the ability to generate synaptosome preparations from frozen samples of sheep brain, and used this technique to confirm the conserved expression of synaptic proteins between sheep and mouse tissues. Finally, we found that molecular pathways previously shown to regulate synaptic pathophysiology in *Drosophila* and mice were similarly perturbed in synapses from affected regions of CLN5 sheep brain. Taken together, these findings suggest that molecular mechanisms underlying synaptic pathophysiology are conserved in an established sheep model of Batten disease.

### 3.4.2. Synaptic pathology is a feature of Batten Disease

Our initial findings confirmed the regionally-restricted nature of disruption to synaptic integrity in areas of the brain of CLN5 sheep undergoing significant neurodegeneration (e.g. loss of SV2 was observed in the affected motor cortex but not

in the spared cerebellum). Previous studies using mouse models of Batten disease have revealed that synaptic disruption is intimately linked to the regional onset of neurodegeneration (Kielar et al., 2009, Koch et al., 2011, Luiro et al., 2006), with our findings demonstrating that the relationship between synaptic pathology and neurodegeneration is likely to be similarly conserved in CLN5 sheep, and conceivably as well in human patients. However, given the symptomatic nature of the sheep investigated in this study, further studies addressing synaptic changes at pre and early-symptomatic time points will be required to establish whether synaptic loss precedes or occurs concurrently with gross neuropathological changes.

### 3.4.3. Molecular mechanisms of synaptic pathology are conserved across disease models

A second aim of this study was to investigate whether the same molecular regulators we had previously found to be involved in synaptic and axonal stability in *Drosophila* and mouse models (Wishart et al., 2012) were similarly altered in synapses from CLN5 Batten sheep. Whereas the levels of the proteins analysed were relatively stable in the cerebellum (Figure 3.7), a region not affected by gross morphological changes, 7 out the 8 proteins analysed showed significantly altered expression restricted to the motor cortex (Figure 3.8). Thus, the results indicate that there are molecular features of synaptic pathology preserved across various animal models of neurodegenerative disease. Moreover, these features are specific to synapses undergoing degeneration and are not widespread consequences of the disease process.

The proteins analysed in this study are involved in diverse cellular mechanisms, including synaptic transmission (eg. α-synuclein, CSP-α), calcium

buffering (Calretinin) and axonal growth (ROCK2) (Donnelier and Braun, 2014, Lashuel et al., 2013, Riento and Ridley, 2003, Schwaller, 2014). This illustrates the complexity of processes affecting synapse stability and supports the hypothesis that therapeutic strategies for neurodegenerative diseases are likely to require targeting of multiple molecular processes in order to obtain therapeutic benefit (Van der Schyf and Geldenhuys, 2011, Youdim, 2010a). Nonetheless, our findings points toward the existence of common pathways involved not only in variants of NCLs but also common to other neurodegenerative conditions.

Of particular interest, α-synuclein is a known regulator of synaptic function which has been highly implicated in the pathophysiology of Parkinson's disease (Stefanis, 2012). We found the levels of the α-synuclein protein to be downregulated by 50% in the motor cortex of CLN5 sheep. Interestingly, changes in α-synuclein have also been reported in several other studies of Batten disease, particularly in CLN1 and CLN10 (cathepsin D) deficient mice (Blom et al., 2013, Cullen et al., 2009), and recently in Atp13a2-deficient (CLN12) mice (Schultheis et al., 2013). In addition, α-synuclein is known to modulate synaptic pathology in mice, at least in part through interactions with another synaptic protein, CSP-α (Chandra et al., 2005). Levels of CSP-α were also significantly modified in synapses from affected regions of CLN5 sheep brain. Deletion of CSP-α causes extensive neuromuscular degeneration in mice, due to defects in the assembly of SNARE complexes at the synapse (Fernandez-Chacon et al., 2004, Sharma et al., 2012, Sharma et al., 2011) and mutations in CSP-α lead to a dominant adult form of NCL, Kuf's disease (CLN4; (Benitez et al., 2011, Noskova et al., 2011)).

Other proteins analysed in this study, such as ROCK2 and SIRT2, have not previously been directly implicated in the pathophysiology of NCLs. They have, nonetheless, been studied regarding their contribution to other neurodegenerative conditions. Modulating the activity of SIRT2, which belongs to a family of protein deacetylases, has proven beneficial in attenuating neurodegeneration in disorders such as Parkinson's and Huntington's diseases (Donmez and Outeiro, 2013, Luthi-Carter et al., 2010, Outeiro et al., 2007). Whereas ROCK2, which is involved in the regulation of actin dynamics and cytoskeleton stability, is also regarded as a promising target for neuroprotective therapies (Kubo et al., 2008, Tonges et al., 2011). ROCK inhibitors have indeed shown promising results in animal models of various neurodegenerative conditions, including spinal muscular atrophy, Alzheimer's disease, Huntington's disease and Parkinson's disease (Bowerman et al., 2012, Shao et al., 2008, Song et al., 2013, Tönges et al., 2012).

Altogether, these results indicate that molecular features of synaptic pathology are conserved across various animal models of neurodegenerative disease. The recognition that common pathways are affected in etiologically diverse neurodegenerative conditions is central to the development of broad-range synaptoprotective strategies. Moreover, the fact that these pathways are conserved across species is key to the translation of research from lower animal models to human patients.

### 3.4.4. Use of large animal models in neurodegenerative research

The considerable overlap in the molecular characteristics of synaptic pathology between sheep and small animal models supports the notion that therapies designed to target these pathways resulting from rodent studies could be taken forward into sheep models, better placed to replicate the size and age-related aspects of the human nervous system (Aigner et al., 2010, Dolezalova et al., 2014, Morton and Howland, 2013, Pouladi et al., 2013). The ability to demonstrate the therapeutic effectiveness of a treatment in a large animal model would provide a strong basis for subsequent translation to clinical trials with human patients. This approach is likely to reduce the financial waste associated with failed clinical trials based on studies in small animal models (Perrin, 2014), and accelerate the identification of the best candidate therapies for human patients.

# Chapter 4. Novel role for calretinin in synaptic function and stability

## 4.1. Introduction

### 4.1.1. Calretinin interneurons

Calretinin (CR) is a calcium-binding protein, encoded by the *Calb2* gene, best known as a marker of a subpopulation of inhibitory interneurons in the CNS. CR-immunoreactive cells (CR-IR) represent a subpopulation of around 20% of GABAergic interneurons, depending on the species and brain regions analysed. For example, while CR-IR neurons in the cortex account for 15-25% of the GABAergic population in rodents, this fraction rises to 20-45% in primates (Dzaja et al., 2014). CR-IR cells have been identified not only in various areas of the cerebral cortex and hippocampus, but also in the cerebellum, substantia nigra compacta, ventral tegmental area, thalamus, olfactory and optic tracts, and other regions (Jacobowitz and Winsky, 1991, Schiffmann et al., 1999). Their morphological features are varied, ranging from bipolar to multipolar cells and, in the hippocampus, presenting dendrites either densely populated with spines or spine free (Cauli et al., 2014, Gulyas et al., 1992, Miettinen et al., 1992). Although most CR-IR neurons are thought to be GABAergic, not all co-express GABA (Meinrenken et al., 2003). In addition, the neurochemical properties of CR-IR neurons are not unique, as CR-IR cells may co-express a variety of neuropeptides, including somatostatin, vasoactive intestinal polypeptide and neuropeptide Y (Cauli et al., 2014). The electrophysiological properties of CR-IR neurons are similarly not uniform, but seem to be associated with their morphology. For instance, whereas multipolar neurons display a regular firing pattern, bipolar

neurons tend to show bursting firing patterns (Caputi et al., 2009). Taken together, the existing literature points towards the existence of a heterogeneous population of CR-IR neurons for which characteristic morphological and functional features have yet to be fully defined.

### 4.1.2. Calretinin is a $Ca^{2+}$-binding protein with dynamic $Ca^{2+}$ properties

CR belongs to the calbindin sub-family of calcium binding proteins, which are characterized by the presence of 6 structural motifs, known as EF-hand $Ca^{2+}$-binding domains, and are recognized for their $Ca^{2+}$ binding properties and buffer capacity (Camp and Wijesinghe, 2009, Schwaller, 2014). In CR, the $6^{th}$ of these domains is inactive while the $5^{th}$ has a low $Ca^{2+}$ affinity, acting mainly as a binding site for other proteins and thus conferring CR properties of a $Ca^{2+}$ sensor (Arendt et al., 2013). The first 4 motifs, however, are responsible for CR's $Ca^{2+}$ buffering capabilities and bind $Ca^{2+}$ ions in a cooperative manner (Faas et al., 2007). This results in a non-linear kinetics of $Ca^{2+}$ regulation in which, upon an increase in intracellular calcium $[Ca^{2+}]_i$, CR behaves like a slow buffer when the initial $[Ca^{2+}]_i$ is at a basal level of ~100nM but acts as a fast-buffer when $[Ca^{2+}]_i$ is elevated to the order of ~1μM. This property has been shown to have functional consequences at sites of neurotransmitter release (Schmidt et al., 2013), where $[Ca^{2+}]_i$ is elevated during action potentials, and suggests that CR may play differential roles within subcellular regions according to the local $[Ca^{2+}]_i$.

Further evidence for a dynamic role for CR comes from studies addressing its $Ca^{2+}$-dependent localization and conformational changes (Table 4.1). At low $[Ca^{2+}]_i$

CR is predominantly cytosolic. However, Winsky and Kuznicki found that, in rat brain preparations, when $[Ca^{2+}]_i$ is increased CR translocates to synaptic vesicles and the synaptic membrane (Winsky and Kuznicki, 1995). In another study using chick embryonic cultures, CR was shown to increase its membrane localization at a developmental stage coincidental with the onset of spontaneous synaptic activity, and hence with the onset of frequent $Ca^{2+}$ currents through the plasma membrane (Hack et al., 2000). CR's translocation within cell compartments might be attributed to its potential recruitment by different proteins in response to changes in $[Ca^{2+}]_i$ levels. CR undergoes significant conformational changes according to the local $[Ca^{2+}]_i$ and its mobility is decreased in the presence of high $Ca^{2+}$ levels, potentially reflecting the establishment of interactions at high $[Ca^{2+}]_i$ (Arendt et al., 2013, Kuznicki et al., 1995). These interactions might lead to the recruitment of CR to membrane sites and result in a specialization of CR function to meet the demands of a high $Ca^{2+}$ environment.

**Table 4.1: Properties of CR according to the intracellular $Ca^{2+}$ levels.**

| Parameter | Low $[Ca^{2+}]_i$ | High $[Ca^{2+}]_i$ | Reference |
|---|---|---|---|
| $Ca^{2+}$ buffering | Slow | Fast | (Faas et al., 2007) |
| Mobility | Slow | Very slow | (Arendt et al., 2013) |
| Subcellular localization | Mainly cytosolic | Enriched in membranes | (Hack et al., 2000, Winsky and Kuznicki, 1995) |

### 4.1.3. Calretinin modulates neuronal excitability

From a fundamental neuroscience research perspective, CR has mainly been used a marker for a subpopulation of interneurons, with few studies addressing its functional role in the nervous system. It has been shown, nonetheless, that CR might be an important modulator of neuronal excitability and synaptic plasticity.

The first indication that CR might be implicated in modulating synaptic function came from studies in CR knock-out ($CR^{-/-}$) mice. Schurmans and colleagues developed the $CR^{-/-}$ mice in 1997 and showed that these mice have impaired long-term potentiation in the dentate gyrus, likely due to excessive release of GABA in the region (Schurmans et al., 1997). In addition, the lack of CR expression in these mice was later shown to lead to increased excitability of cerebellar granule cells with consequences for motor coordination, which can be restored by rescue of CR expression exclusively in this cell type (Bearzatto et al., 2006, Gall et al., 2003, Schiffmann et al., 1999). Further evidence for a role of CR in synaptic function is exemplified by its interaction with the calcium channel $Ca_v2.1$, preferentially in the presence of $Ca^{2+}$, which contributes to modulate the activity of $Ca_v2.1$ and, consequently, of $Ca^{2+}$ signals (Christel et al., 2012). Moreover, triple knock-out of calretinin, calbindin and parvalbumin, three $Ca^{2+}$-binding proteins of the same family, results in excessive exocytosis in Inner Hair Cells, presumably due to poor spatial restriction of $Ca^{2+}$ signals to the active zone (Pangrsic et al., 2015).

Altogether, several lines of evidence indicate CR may play an important role in modulating $Ca^{2+}$ signals and neuronal excitability, via $Ca^{2+}$ buffering and/or by establishing $Ca^{2+}$-dependent interactions. The consequences of CR's function to synaptic function and stability are still, nevertheless, a field poorly explored.

### 4.1.4. The role of calretinin in neurodegeneration

It has previously been shown in this thesis (Chapter 3) that CR expression is altered in synaptic terminals of a sheep model of Batten disease, specifically in the brain regions most affected by the disease. In addition, our group has previously

demonstrated that altered expression of CR is characteristic of other neurodegenerative scenarios (Table 4.2), suggesting this protein might play an important role in modulating synaptic stability across a range of diseases and model systems.

**Table 4.2: Changes in CR expression in animal models of neurodegenerative disease.**

| Condition | Tissue | Expression | Reference |
|---|---|---|---|
| Cortical injury | Synaptosomes (Mouse) | down | (Wishart et al., 2012) |
| Batten disease | Synaptosomes (Sheep) | up | Chapter 3 |
| Axonal injury | Olfactory Receptor Neurons (Drosophila) | detrimental | (Wishart et al., 2012) |

The available literature, however, provides conflicting evidence as to whether the expression of CR is preferentially protective or detrimental to neuronal stability. Some studies report CR positive interneurons to be spared in patients or experimental models of Alzheimer's, Parkinson's or Huntington's disease (Cicchetti and Parent, 1996, Fonseca and Soriano, 1995, Pike and Cotman, 1995), while others show the opposite effect, with significant loss of CR interneurons in Alzheimer's disease, amyotrophic lateral sclerosis or following ischemic injury (Baglietto-Vargas et al., 2010, Freund and Magloczky, 1993, Hsu et al., 1994, Morrison et al., 1996, Morrison et al., 1998). Most importantly, the majority of these studies focused on the subpopulation of CR immunoreactive interneurons and did not address the remaining neuronal subtypes nor the molecular mechanisms that might underlie CR's role in neuronal stability. This gap in the literature has just begun to be filled by two recent studies: Wishart and colleagues (Wishart et al., 2012) demonstrated that CR plays a role in synaptic degeneration in the mouse corticostriatal system and in axonal degeneration in *Drosophila*, extending the level of influence of CR outside the interneuron subpopulation; whereas Dong and colleagues (Dong et al., 2012) revealed

that CR plays a protective role during oxidative stress in a Huntington's disease *in vitro* model.

### 4.1.5. Aims

Research is slowly revealing an important role for CR in synaptic function and neurodegenerative pathways. Given the current evidence suggesting CR may contribute to modulate synaptic stability across various models of neurodegenerative disorders, including our large animal of model of Batten disease, we wanted to further explore the poorly understood function of CR and its contribution to the modulation of neurodegenerative mechanisms and synaptic function. Therefore, we set two main aims:

- Confirm the ability of CR to modulate neurodegeneration in a mouse model of *in vivo* peripheral nerve degeneration;
- Explore the function of CR in central synapses and how it may contribute to synaptic stability.

## 4.2. Materials and methods

### 4.2.1. Animals

Wild-type (WT) CD1 and C57Bl/6J mice were obtained directly from the University of Edinburgh managed rodent colonies. $CR^{-/-}$ mice were imported from the laboratory of Prof. Serge Schiffmann (University of Brussels, Belgium) and maintained on a C57Bl/6J background (Schurmans et al., 1997).

All rodents were kept under standard husbandry conditions in animal facilities at the University of Edinburgh. All procedures were performed under license from the UK Home Office and approved by the University of Edinburgh Veterinary Services. All animals were sacrificed by Schedule 1 methods, either by cervical dislocation or overdose of anaesthetic by inhalation of isoflurane (Abbot).

### 4.2.2. Genotyping

Genotyping was performed as described in the General Materials and Methods section. Details of the primers, reaction mixes and PCR programs used can be found in Table 4.3, Table 4.4 and Table 4.5, respectively.

**Table 4.3: Primers used for genotyping of $CR^{-/-}$ mice.**

| Primer | Sequence 5' - 3' | Size bp |
|---|---|---|
| WT forward (cr-ex2) | GTTCTCTAGCTCTTTACCTTCAATGTACCCA | |
| WT Reverse (cr-it1) | GCTGGCTGAGTACTCCAAGGGTACACATT | 243 |
| KO forward (cr-it1) | GTTCTCCGTGGAGGTGGTGACTTCCTAGTC | |
| KO reverse (neo-pv) | GCTAAAGCGCATGCTCCAGACTGCCTTGG | 150 |

**Table 4.4: PCR reagent mix for 1 reaction.**

| Reagent | µl per 1 reaction |
|---|---|
| $ddH_20$ | 9.6 |
| 5x Green GoTaq Flexi Buffer (Promega) | 3.5 |
| MgCl2 25mM (Promega) | 0.9 |
| dNTP mix 10mM (Invitrogen) | 0.4 |
| Forward Primer 10µM | 0.7 |
| Reverse Primer 10µM | 0.7 |
| GoTaq Flexi DNA polymerase (Promega) | 0.2 |
| DNA | 2 |
| Total | 18 |

**Table 4.5: PCR program used for genotyping of $CR^{-/-}$ mice.**

| Step | Temperature (°C) | Time |
|---|---|---|
| 1. Separation | 94 | 5 min |
| 2. Denaturation | 94 | 30 sec |
| 3. Annealing | 61 | 45 sec |
| 4. Polymerization | 72 | 45 sec |
| Repeat 2-4 34x | | |
| 5. Final | 72 | 5 min |
| | 12 | ∞ |

### 4.2.3. Peripheral nerve lesions

Peripheral nerve lesions were performed in mice 4-5 months old, as described previously (Gillingwater et al., 2002). Mice were initially anaesthetized in an induction chamber with 5% of isoflurane and maintained thereafter with 2-3% of isoflurane delivered via a face mask, or anaesthetised via intra-peritoneal injection of 240 mg/kg Tribromoethanol. A small skin incision was made at the level of the sciatic notch and

a 1-2mm section of the sciatic nerve was removed, ensuring complete transection. The wound was sutured and immediately following surgery all mice received an intramuscular injection of 4 mg/kg of the analgesic Rimadyl®. Mice were allowed free access to food and water and kept under standard husbandry conditions until sacrifice 15 to 22 hours post-injury (hpi). To ensure comparability of results extra care was taken regarding the precision of the time point of analysis, anatomical location of the lesion and age of the mice.

### 4.2.4. Immunohistochemistry of lumbrical muscles

Lumbrical muscles were dissected in PBS and fixed in 4% PFA in PBS for 20 min. Fixed muscles were permeabilised in 4% Triton X-100 in PBS for 90 min and blocked in 2% Triton X-100 with 4% w/v Bovine Serum Albumin (BSA) in PBS for 30 min. Immunolabelling was performed by serial incubation with primary antibodies in block for 72 h at 4°C and secondary antibodies in PBS for 12 h at 4°C. Post-synaptic acetylcholine receptors (AchR) were labelled with α-bungarotoxin conjugated to tetramethylrhodamine (α-BTX; Molecular Probes) 1.25 µg/ml in PBS for 10 min. Muscles were extensively washed in PBS between the staining steps. Finally, muscles were whole-mounted in Mowiol (Calbiochem) on glass slides and cover-slipped.

### 4.2.5. Quantification of synaptic integrity

Following sacrifice between 15 and 22hpi, lumbrical muscles from injured and contralateral non-injured hind limbs were rapidly dissected and processed for immunohistochemistry as described above, using antibodies against 2H3 and SV2

proteins. Synaptic integrity was manually assessed by using an integrity score adapted from (Murray et al., 2008), as follows: 0: no presence of any intact axons or fragments; 1: no fully intact axons but fragmented debris or presence of a portion of the incoming nerve; 2: overall denervated muscle with presence of a few nerve ramifications in <25% of the muscle area but no visible occupied endplates; 3: overall denervated muscle with presence of a few nerve ramifications in <25% of the muscle area and a few visibly occupied endplates; 4: presence of nerve ramifications in 25%-50% of the muscle area and visibly occupied endplates; 5: presence of nerve ramifications in 50%-75% of the muscle area and visibly occupied endplates; 6: apparently intact muscle or presence of nerve ramifications in >75% of the muscle area and visibly occupied endplates. Muscle area corresponds to the area of the muscle covered with post-synaptic endplates.

Quantification was performed at 40x magnification on a Nikon eclipse 50i microscope with double filter, on at least 3 muscles of each of 3 mice per condition and with the operator blind to the identity of each muscle. Representative images were captured in a Zeiss LSM 710 laser scanning confocal microscope.

### 4.2.6. Immunohistochemistry of spinal cord sections

Adult C57Bl/6J mice were deeply anaesthetized via an intraperitoneal injection of 300 mg/kg Sodium Pentobarbital and perfused-fixed with 4% PFA in PBS. The whole spinal cord was dissected, post-fixed in 4% PFA in PBS overnight and cryopreserved in 30% sucrose in PBS for 24 h before being embedded in 100% OCT. 30 μm sections were cut in a freezing microtome and mounted in charged glass slides (Fisher Scientific).

Tissue sections were incubated in blocking solution (1% Triton X-100, 4% BSA in PBS) for 30 min prior to incubation with primary antibodies overnight at 4°C and in secondary antibodies for 90 min at RT. The antibodies were diluted in blocking solution and the sections were thoroughly washed in PBS between incubations. Section were covered in Mowiol, protected with a glass coverslip and imaged in a Zeiss LSM 710 confocal microscope.

### 4.2.7. Primary neuronal cultures

Primary neurons were prepared from E17.5 C57Bl6/J mouse embryos as described previously (Gordon et al., 2011). Embryos were sacrificed by decapitation, the hippocampus rapidly dissected in ice-cold HBSS and the resulting tissue was incubated in a solution of 20 units/ml of Papain (Worthington Biochemicals) in HBSS (Invitrogen) for 20 min at 37°C. After removal of excess papain, the tissue was resuspended in DMEM/F12 media supplemented with 100 U/mL penicillin/streptomycin and 10% v/v foetal bovine serum (Sigma) and disaggregated. The cell suspension was centrifuged at 200g for 5 min at RT and the pellet resuspended in Neurobasal media supplemented with 2% v/v B-27, 0.5 mM L-Glutamine and 100 U/mL penicillin/streptomycin.

$40x10^3$ cells were plated on sterile glass coverslips coated with Poly-D-Lysine and laminin. To prepared coverslips, 50 µg/ml Poly-D-Lysine in 0.1 M Sodium Borate buffer pH 8.5 was applied for 2 h and thoroughly washed in $H_2O$ before addition of a 50 uL drop of 10 µg/ml of laminin (Invitrogen) in supplemented Neurobasal media. Cells were platted in laminin spots, allowed to settled for 1 h in a 37°C, 5% $CO_2$ incubator, and thereafter grown in supplemented Neurobasal media. At day-in-vitro

(DIV) 3 the media was further supplemented with 1 μM cytosine β-D-arabinofuranoside to prevent glial proliferation. At DIV 7 50% of culture media was replaced with fresh media.

### 4.2.8. Immunocytochemistry

Cells plated in glass coverslips were fixed for 10 min in warm 4% PFA in PBS, permeabilized for 5 min in 0.1% Triton-X100 in PBS and blocked for 30 min in 2.5% BSA in PBS. Cells were incubated in spots of primary antibody for 2 h at RT and in secondary antibody for 1 h at RT. All antibodies were diluted in 2.5% BSA in PBS. Coverslips were washed in PBS between incubations, mounted on Mowiol spots in glass slides and imaged in a Zeiss LSM 710 confocal microscope.

### 4.2.9. Calretinin intensity distribution

WT hippocampal neurons at DIV 14-16 immunolabelled with CR and β-III-tubulin were imaged in a Zeiss 710 Confocal Microscope at constant laser settings. The intensity of CR staining was measured in regions of interests of identical area in the cell body of all individual neurons in each image. For each coverslip, the intensity of CR was normalized to the mean value of all the neurons imaged in the same experiment. Neurons were imaged at 40x magnification from each of 3 images per coverslip from a total of 4 coverslips from 2 independent cultures.

### 4.2.10. Puncta colocalisation analysis

Colocalisation between SV2 and CR puncta was performed using the "spots colocalisation" tool on the IMARIS software. WT hippocampal neurons at DIV 14-16 were immunolabelled for SV2 and CR and z-stacks were acquired at 63x magnification, on a Zeiss LSM 710 Confocal Microscope. Using the IMARIS "spots" tool, spots were created so as to colocalise with the CR or SV2 puncta. The "spots colocalisation" tool was then used to calculate the total number of spots and the number of spots colocalising between the two channels. Data was acquired from at least 15 fields of view from 2 coverslips per independent culture.

### 4.2.11. Synaptic enrichment analysis

WT hippocampal neurons at DIV 14-16 were stained for SV2 and CR and z-stacks imaged at 63x magnification on a Zeiss LSM 710 Confocal Microscope. The enrichment of CR in synaptic sites was calculated as the ratio between the fluorescence of CR in SV2 puncta and in adjacent axonal regions. At least 100 synaptic sites from each of 2 images per coverslip were obtained and analysed for a total of 6 coverslips from 3 independent cultures.

### 4.2.12. Calretinin $K^+$-dependent distribution

For analysis of $K^+$ dependent distribution of CR, WT hippocampal neurons at DIV 14-16 were incubated with low or high levels of KCl in order to depolarize neurons and simulate an action potential. This method has been shown to depolarize

cells and lead to activity-dependent changes in cultured neurons and synaptosome preparations (Kohansal-Nodehi et al., 2016, Macias et al., 2001, Smillie et al., 2013).

For stimulation experiments, the culture media was removed and neurons were washed once in warm PBS, incubated for 30 s with Low $K^+$ (136 mM NaCl, 2.5 mM KCl, 2 mM $CaCl_2$, 1.3 mM $MgCl_2$, 10 mM Glucose, 10 mM HEPES, pH 7.4, 37°C) or High $K^+$ (88.5 mM NaCl, 50 mM KCl, 2 mM $CaCl_2$, 1.3 mM $MgCl_2$, 10 mM Glucose, 10 mM HEPES, pH 7.4, 37°C) buffer and immediately fixed in warm 4% PFA in PBS. For recovery experiments, neurons were similarly incubated for 30 s in Low or High $K^+$ buffer but further incubated 2x for 30 s in Low $K^+$ prior to being fixed. Fixed neurons were immunolabeled with CR and SV2 antibodies and imaged at 63x magnification in a Zeiss LSM 710 confocal microscope. Images were analysed using the IMARIS software. Colocalisation of puncta was performed as described above. Data was acquired from at least 15 fields of view from 2 coverslips per independent culture.

### 4.2.13. Transfection procedures

Knockdown (KD) DsiRNA constructs were obtained from IDT (Integrate DNA Technologies) and transfected using Lipofectamine RNAiMAX reagent (Invitrogen) according to the manufacturers instructions. Briefly, 10 nM DsiRNA was incubated with 2 µl/ml of Lipofectamine RNAiMAX in MEM media at RT for 5 min before being added to the cells. Cy3 fluorescent control was used to label transfected cells and universal control NCI DsiRNA was used as negative control. Cells were incubated with the knock-down constructs (see Table 4.6) for 48 h before analysis.

Overexpression constructs were obtained from various sources (see Table 4.6) and transfected using Lipofectamine 2000 reagent (Invitrogen), as described in (Gordon et al., 2011). 0.2-1 µg of constructs were incubated, at the desired concentration, with 2 µl/ml of Lipofectamine 2000 in MEM media at RT for 20 min. The cell culture media was replaced with MEM and the cells incubated with the desired construct/Lipofectamine mix for 2 h. MEM was then removed and the cells allowed to grow in their own pre-conditioned culture media until required.

**Table 4.6: Constructs used for transfection of cultured neurons.**

| Vector | Type | Supplier | Cat No |
|---|---|---|---|
| SypHy | Plasmid | Addgene. Gift from Prof. Mike Cousin | 24478 |
| GCaMP6f | Plasmid | Addgene. Gift from Prof. Mike Cousin | 40755 |
| GFP-Sypnaptophysin | Plasmid | Gift from Prof. Mike Cousin | |
| N1-mCer | Plasmid | Gift from Prof. Mike Cousin | |
| N1-mCer-Calb2 | Plasmid | Cloning from pCMV6-Calb2 into N1-mCer | |
| pCMV6-Calb2 | Plasmid | Origene | MR203611 |
| pCMV6-empty | Plasmid | Origene | PS100001 |
| Calb2 | DsiRNA | IDT DNA | MMC.RNA1.N007586.12.1 |
| Calb2 | DsiRNA | IDT DNA | MMC.RNA1.N007586.12.3 |
| Cy3 | DsiRNA | IDT DNA | Cy3 DS Transfection Control |
| NC1 | DsiRNA | IDT DNA | Negative Control (DS NC1) |

### 4.2.14. $H_2O_2$ treatment

WT hippocampal neurons at DIV 13 were transfected with CR KD constructs. 48 h after transfection cells were exposed to 0 µM or 100 µM $H_2O_2$ for 2 h. $H_2O_2$ 100x dilutions were made fresh in Neurobasal media and further diluted directly into the culture media, as described in (Whittemore et al., 1995). After the 2 h treatment cells were fixed in 4% PFA, stained with DAPI for 5 min and mounted in glass slides in Mowiol. Slides were imaged in an epifluorescent microscope and live/dead cells were

identified according to the morphology of the nuclei, as described in (Whittemore et al., 1995): live cells have round nuclei, whereas dead cells have shrunken or collapsed nuclei, with condensed staining. At least 10 fields of view were analysed per individual slide.

### 4.2.15. Synaptophysin-pHluorin imaging

Synaptophysin-pHluorin experiments were performed as described in (Gordon et al., 2016, Gordon et al., 2011). Primary WT hippocampal neurons were transfected, at DIV 7, with 1 μg of synaptophysin-pHluorin (SypHy) and 1 μg of pCMV6-Calb2 or pCMV6-empty. At DIV 12-15, cultures were mounted in an imaging chamber with embedded parallel platinum wires (RC-21BRFS, Warner Instruments) and positioned on the stage of a Zeiss Axio Observer D1 epifluorescence microscope. Neurons were visualized with a 40x oil-immersion objective at 500/530nm excitation/emission (ex/em). Cells were continuously perfused with Imaging buffer (119 mM NaCl, 2.5 mM KCl, 2 mM $CaCl_2$, 2 mM $MgCl_2$, 30 mM glucose, 25 mM HEPES, 10 uM CNQX, 50 uM APV, pH 7.4) and fluorescent images were captured every 4 s using a Hamamatsu Orca-ER digital camera. Neurons were imaged at rest for at least 60 s, stimulated with a train of 300 action potentials at a frequency of 10 Hz (100 mA, 1 ms pulse width), allowed to recover for 3 min and perfused with $NH_4Cl$ buffer (69 mM NaCl, 2.5 mM KCl, 2 mM $CaCl_2$, 2 mM $MgCl_2$, 30 mM glucose, 25 mM HEPES, 50 mM $NH_4Cl$, pH 7.4) to reveal the maximum fluorescence of the pHluorin probes.

Images were analysed using ImageJ software. Frames were aligned using the StackReg plugin (http://bigwww.epfl.ch/thevenaz/stackreg/) with rigid body algorithm. Nerve terminals were selected using regions of interest (ROIs) of identical

size (oval 5x5 pixels) and the total fluorescence intensity of each ROI was measured over time using the Time Series Analyzer plugin (https://imagej.nih.gov/ij/plugins/time-series.html). Changes in fluorescence (ΔF / F0) were calculated as $((F - F_0) / F_0)$, ($F_0$: fluorescence of terminal at rest; F: fluorescence at a given time). The stimulation peak was calculated as the maximum fluorescence in data normalized to the maximum fluorescence during $NH_4Cl$ perfusion, to account for variations in pHluorin expression between cells. Endocytosis rate constants (τ) were determined from data normalized to the peak fluorescence using GraphPad Prism software. Traces between 100 s and 200 s were fitted to a non-linear one phase decay function of the type $y = (y_i - y_f).e^{(-x/\tau)}$ . Only curves fitted with $R^2 > 0.80$ were accepted for further analysis.

### 4.2.16. Real-time imaging

Primary hippocampal neurons were transfected, 3 days prior to imaging, with a combination of one or more of the following constructs: 1 μg of SypHy, 0.2 μg N1-mCer-Calb2, 1 μg of GCaMP6f or 1 μg GFP-synaptophysin. At DIV13-15, coverslips were mounted in an imaging chamber and imaged as described for Synaptophysin-pHluorin imaging. Wavelength settings used were 500/530nm ex/em for SypHy, GCaMP6f and GFP-Synaptophysin, and 430/530nm ex/em for N1-mCer-Calb2.

Analysis of CR intensity in boutons and axons was performed as described in (Chi et al., 2001). An oval ROI of 5x5 pixels was placed on nerve terminals (synapses) and adjacent regions (axons). The fluorescence was tracked over time and the change in fluorescence calculated as $F / F_0$ ($F_0$: fluorescence of terminal at rest; F: fluorescence at a given time). Dispersion rate constants (τ) were determined from data normalized

to the peak fluorescence using GraphPad Prism software. Traces between 100 s and 200 s were fitted to a non-linear one phase association function of the type $y = y_0 + (plateau - y_0).(1-e^{(-x/\tau)})$. Only curves fitted with $R^2 > 0.80$ were accepted for further analysis. GCaMP6f intensity was tracked on nerve terminals in ROIs colocalising with N1-mCer-Calb2.

### 4.2.17. Co-Immunoprecipitation

Experiments for co-immunoprecipitation (co-ip) of CR and its synaptic binding partners were adapted from (Christel et al., 2012). Freshly prepared synaptosomes from adult CD1 mice were resuspended in IP Lysis buffer (50 mM Tris-HCl, 150 mM NaCl, 1% Triton-X, pH 7.6) with either 1 mM EGTA (Low $Ca^{2+}$) or 1 mM $CaCl_2$ (High $Ca^{2+}$) containing protease inhibitors. These $Ca^{2+}$ and EGTA concentrations were chosen as they have previously been shown to alter the conformation of CR and its ability to form specific interactions (Christel et al., 2012, Schwaller et al., 1997). Samples were incubated on ice for 15 min, vortexing every 5 min, and centrifuged for 20 min at 20,000g and 4°C.

50 µl of Recombinant Protein G Sepharose (Generon), from a 50% slurry in Low/High $Ca^{2+}$ Lysis buffer, were incubated with 3 µl of anti-calretinin antibody for 1 h at 4°C on a roller and further incubated with synaptosomes for 2 h at 4°C. Control experiments for non-specific binding were performed without the addition of CR antibody. The beads were washed 2x in Low/High $Ca^{2+}$ Lysis buffer and further 2x in Low/High $Ca^{2+}$ buffer prepared without Triton-X 100 or protease inhibitors. At this point, the beads were either resuspended 1:1 in Low/High $Ca^{2+}$ buffer (without Triton-X 100 or protease inhibitors) and frozen, or the co-IP proteins were eluted by boiling

the beads in 2x NuPAGE® LDS Sample Buffer. Elution samples were readily used for western blotting and frozen beads were sent for mass spectrometry (MS) analysis at the Roslin Institute (University of Edinburgh). For each $Ca^{2+}$/EGTA condition, samples were prepared in duplicates and processed independently for MS.

The protein G agarose beads containing bait and interacting proteins were washed twice with 500µl of TBS. Washed beads were resuspended in 50 mM ammonium bicarbonate and digested with sequencing grade modified trypsin (Promega), following reduction with 5 mM dithiothreitol and alkylation with 10 mM iodoacetamide. The resulting peptide mixture was spun at 800g and the supernatant was collected. The digested peptides were cleaned up using Stagetips by following the standard protocol from (Rappsilber et al., 2007).

Nanoflow LC-MS/MS was performed on a micrOTOF-II mass spectrometer (Bruker, Germany) coupled to a RSLCnano LC system (Thermo). A tryptic digest of each sample was delivered to a trap column (Acclaim PepMap100, 5 µm, 100 Å, 100 µm i.d. × 2cm) at a flow rate of 20 µL/min in 100% solvent A (0.1% formic acid in LCMS grade water). After 4 min of loading and washing, peptides were transferred to an analytical column (Acclaim PepMap100, 3 µm, 100 Å, 75 µm i.d. × 25 cm) and separated at a flow rate of 300 nL/min using a 60-min gradient from 7% to 35% solvent B (solvent B, 0.1% FA in acetonitrile). The eluent from LC was passed onto the nano electrospray source of the micrOTOF-II, which was operated in data-dependent mode, automatically switching between MS and MS2 mode. The m/z values of tryptic peptides were measured using a MS scan (300-2000 m/z), followed by MS/MS scans of the six most intense peaks. Rolling collision energy for fragmentation was selected based on the precursor ion mass and a dynamic exclusion was applied for 30 sec.

Raw spectral data were processed with DataAnalysis (Bruker) software and the resulting peak lists were searched using Mascot 2.4 server (Matrix Science) against IPI Mouse sequence database containing 59,534 entries. Mass tolerance on peptide precursor ions was fixed at 25 ppm and on fragment ions at 0.05 Da. The peptide charge was set to 2+ and 3+. Carbamidomethylation of cysteine was selected as a fixed modification and oxidation of methionine and de-amidation were chosen as variable modifications. False discovery rate was limited to < 1% for peptide IDs after searching decoy databases.

### 4.2.18. Label-free proteomics

Synaptosomes were prepared as described in General Materials and Methods, from whole brain of $CR^{+/+}$ and $CR^{-/-}$ adult mice. Synaptosomes were lysed in Label-free buffer (100 mM Tris pH 7.4, 4% SDS, protease inhibitors), incubated on ice for 20 min and centrifuged at 20,000g for 20 min to remove insoluble proteins. Protein concentration was calculated using BCA assay and a combination of 3 pooled samples per genotype were sent for Label-free proteomics at Dundee Fingerprints Proteomics (University of Dundee, UK).

An equivalent of 300 µg of protein from each sample were reduced with 100 mM DTT at RT for 10 min and samples were then processed using a filter-aided sample preparation (FASP) protocol adapted from (Wisniewski et al., 2009). After removal of SDS with 8 M urea, filters were washed twice with 200 µl 40 mM ammonium bicarbonate and the proteins captured on the filters were digested twice with trypsin (2x2 µg), first overnight and then for another 6 h in 200 µl, in ammonium bicarbonate at 40 mM at 30$^{o}$C. Analysis of the resulting peptides was performed on an

LTQ Velos-Pro orbitrap (Thermo Scientific) mass spectrometer coupled with a Dionex Ultimate 3000 RS (Thermo Scientific). LC buffers were the following: buffer A (2% acetonitrile and 0.1% formic acid in Milli-Q water (v/v)) and buffer B (80% acetonitrile and 0.08% formic acid in Milli-Q water (v/v). In addition to the $CR^{+/+}$ and $CR^{-/-}$ samples, a pooled sample made from an equal amount of $CR^{+/+}$ and $CR^{-/-}$ was generated to run as a quality control for the mass spectrometer and to increase the number of proteins identified and quantified. Samples were diluted 1/50 in 1% formic acid and aliquots of 10 µl of each sample was loaded at 5 µl/min onto a trap column (100 µm × 2 cm, PepMap nanoViper C18 column, 5 µm, 100 Å, Thermo Scientific) equilibrated in 98% buffer A. The trap column was washed for 3 min at the same flow rate and then the trap column was switched in-line with a Thermo Scientific, resolving C18 column (75 µm × 50 cm, PepMap RSLC C18 column, 2 µm, 100 Å). The peptides were eluted from the column at a constant flow rate of 300 nl/min with a linear gradient from 95% buffer A to 40% buffer B in 130 min, and then to 98% buffer B by 152 min. The column was then washed with 98% buffer B for 20 min and re-equilibrated in 98% buffer A for 17 min. Each of the three samples ($CR^{+/+}$, $CR^{-/-}$ and pool of both samples) were run in triplicate using LTQ-Orbitap Velos in data dependent mode. A scan cycle comprised MS1 scan (m/z range from 335-1800) in the velos orbitrap followed by 15 sequential dependant MS2 scans (the threshold value was set at 5000 and the minimum injection time was set at 200 ms) in LTQ with collision induced dissociation. The resolution of the Orbitrap Velos was set at to 60,000. To ensure mass accuracy, the mass spectrometer was calibrated on the first day that the runs are performed.

The resulting raw mass spectrometry data was imported into *Progenesis QI for proteomics* (v2.0.5387.52102; Non Linear Dynamics, UK). Data sets were aligned to

the pooled control samples (alignment scores between 81.0% and 98.8%) and filtered to exclude peptides with power <0.8 and ANOVA p-value>0.05. Retention time was limited to 12-130 min and only the 3 most intense reads for each peptide were included. Data was exported as an mgf file and sent back to Dundee Fingerprints Proteomics for identification of individual peptide sequences using Mascot Search Engine (Swiss Prot database, with mouse species filter). Mascot generated data was re-imported into Progenesis and filtered to include only proteins identified by more than 1 unique peptide, with ANOVA p-value < 0.05 and expression levels altered by ≥10% in $CR^{-/-}$ synaptosomes when compared to control (KO/WT ratio -1.10≤ and ≥1.10).

*In silico* analysis was performed using two tools: Ingenuity Pathway Analysis (IPA; QIAGEN); and Database for Annotation, Visualization and Integrated Discovery (DAVID; National Institutes of Health, USA). More information on these tools can be found at http://www.ingenuity.com and http://david.abcc.ncifcrf.gov, respectively.

The proteomics results were submitted to the IPA software (v27821452). Amongst other functions, IPA uses hand-curated experimental data to generate networks of proteins according to their involvement in known molecular mechanisms and calculates their statistical significance using the Exact Fisher's Test. In order to get results as accurate as possible, we restricted the IPA mapping tools to only include data derived from experimental evidence and narrowed down the networks of proteins to contain a maximum of 35 proteins. We used the IPA software to determine the molecular pathways (Top Canonical Pathways) and disorders (Top Diseases and Disorders) most affected by loss of CR.

DAVID bioinformatics tools (v6.6) were used to complement the IPA results. Proteins that meet our filtering criteria were used to determine the Functional Annotation Clusters of the samples. Each cluster consists of at least 3 subcategories containing proteins functionally related. For each subcategory the DAVID software calculates a p-value using the Exact Fisher's Test, and the mean value of the –log() of these is used to calculate an enrichment score for each cluster, so that a cluster enriched in a sample will have a low p-value and a high enrichment score. For ease of comparison between IPA and DAVID results, enrichment scores from Functional Annotation Clusters were converted back to p-values. In addition, DAVID was used to map the proteomics data to KEGG (Kyoto Encyclopedia of Genes and Genomes) pathways, similarly to what had been done in the Canonical Pathways tools from IPA.

## 4.3. Results

### 4.3.1. Calretinin is expressed throughout the nervous system

To date, the vast majority of studies addressing CR's role in the nervous system have been carried out either in cell lines or restricted to the subpopulation of interneurons expressing high levels of CR. However, there are hints in the literature that CR may be more widely expressed in the nervous system. For example, CR is relatively abundant in the retina, in cerebellar granule cells and hippocampal neurons (Camp and Wijesinghe, 2009, Schurmans et al., 1997). Furthermore, studies have shown expression of CR in brain synapses (Winsky and Kuznicki, 1995, Wishart et al., 2012) and the presence of CR immunoreactive neurons in the spinal cord (Fahandejsaadi et al., 2004, Ren et al., 1993). However, the extent of CR's expression in the nervous system has not been fully characterized. Therefore, we further explored the expression of CR in the central and peripheral nervous system of the mouse.

*In vivo*, CR is widely expressed in both the CNS and PNS, with CR being found in synaptic and non-synaptic fractions of the brain, in the spinal cord and in the sciatic nerve. In contrast, CR was not detected in skeletal muscle (Figure 4.1). We further investigated the expression of CR in the spinal cord and demonstrated it is expressed in motor and sensory neurons, and that it is particularly abundant in neuronal projections of the ventral root (Figure 4.2). In addition, CR is found at the neuromuscular junction, both at the level of the axons and the nerve terminals (Figure 4.3).

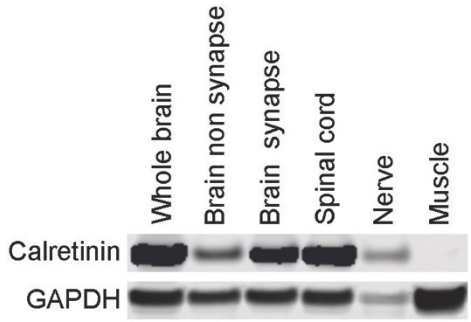


**Figure 4.1: CR is expressed in tissues from the central and peripheral nervous system.** Western blotting of tissues from the mouse central nervous system and neuromuscular system. CR is highly expressed in the central and peripheral nervous system, and is absent from skeletal muscle. All lanes were loaded with 30 µg of protein. GAPDH was used as a loading control.

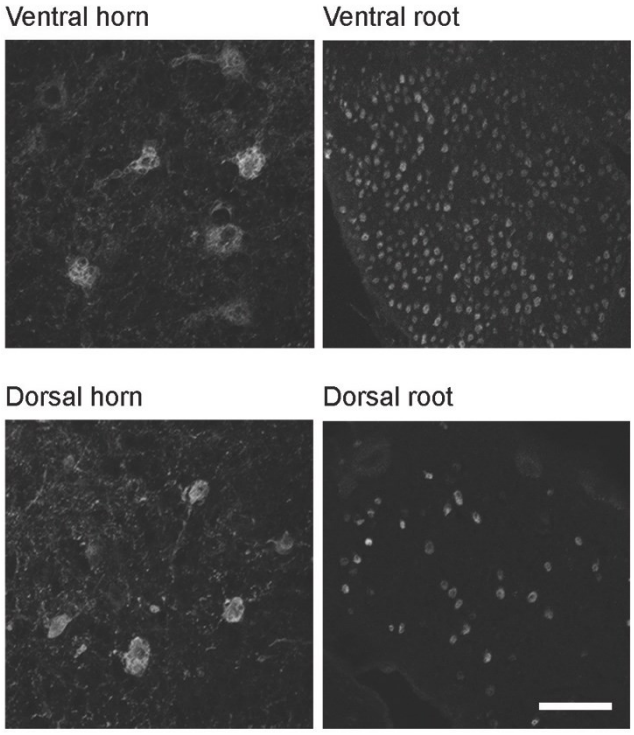


**Figure 4.2: CR is expressed in the spinal cord.** CR immunofluorescence in spinal cord sections of an adult mouse. Note the presence of CR positive neurons in the ventral and dorsal horns, as well as staining of axonal projections in the ventral and dorsal roots. Scale bar = 50 µm.

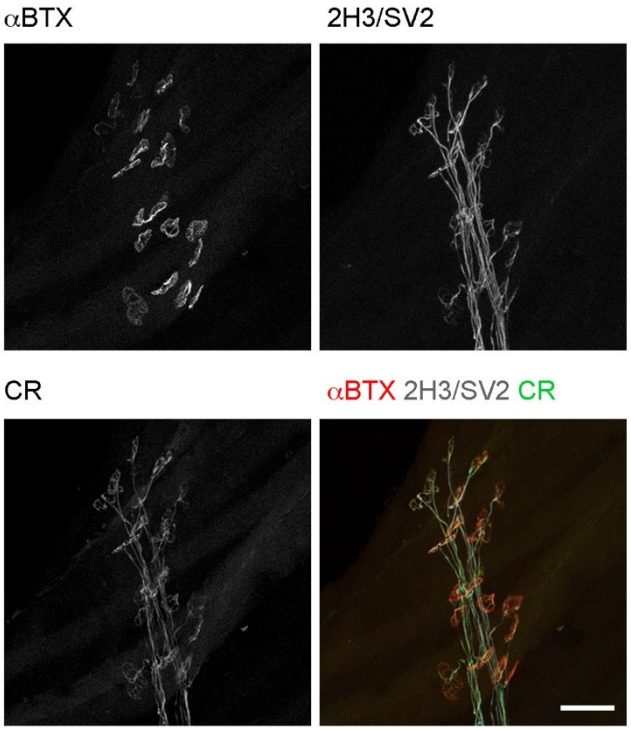


**Figure 4.3: CR is expressed in motor axons and neuromuscular nerve terminals.** Post-synaptic acetylcholine receptors, motor axons and nerve terminals from hind limb lumbrical muscles were immunolabeled with αBTX and 2H3/SV2 antibodies, respectively. Note the CR staining resembling the pattern of 2H3/SV2 staining, indicating it is expressed in motor axons and nerve terminals. Scale bar = 50 μm.

### 4.3.2. Loss of calretinin delays Wallerian degeneration

We have identified CR as an interesting target for further study in (Wishart et al., 2012), where it was found that levels of CR were altered in mouse striatal synapses undergoing degeneration and that CR *Drosophila* mutants presented delayed Wallerian degeneration in olfactory receptor neurons. In addition, we have shown elevated levels of CR are characteristic of synapses from affected brains areas of sheep suffering from Batten disease, suggesting that excessive CR might contribute to the

neuropathology of the disease. Therefore, we wanted to further explore the contribution of CR to neurodegeneration pathways.

To determine whether, similar to what was reported in *Drosophila*, loss of CR delayed Wallerian degeneration in mice, we performed peripheral nerve lesions in $CR^{+/+}$ and $CR^{-/-}$ mice. We instigated Wallerian degeneration by transecting the sciatic nerve and assessed the preservation of axonal and synaptic structures in hind limb lumbrical muscles, which are innervated by branches of the sciatic nerve, at defined time-points following injury. Loss of CR did not block Wallerian degeneration from ultimately occurring, but significantly delayed the onset of axonal degradation (Figure 4.4). Morphological characteristics of degeneration were first detected in $CR^{+/+}$ mice after 15 hpi and by 20 hpi there were no traces of innervated neuromuscular junctions. In contrast, significant loss of innervation was only identified in $CR^{-/-}$ mice after 18 hpi, indicating a ~3 h delay in the instigation of axonal breakdown in the absence of CR. Loss of axonal connections didn't reach completion in $CR^{-/-}$ mice until 22 hpi.

Overall, these results suggest that instigation of degeneration, as assessed by the loss of immunolabelled axonal connections, was delayed by around 3 h in $CR^{-/-}$ mice. CR did not, nonetheless, significantly affect the rate of Wallerian degeneration in the PNS, which was completed within 5 h in both $CR^{+/+}$ and $CR^{-/-}$ mice. Thus, CR seems to play a role in the initial stages of Wallerian degeneration in the PNS.

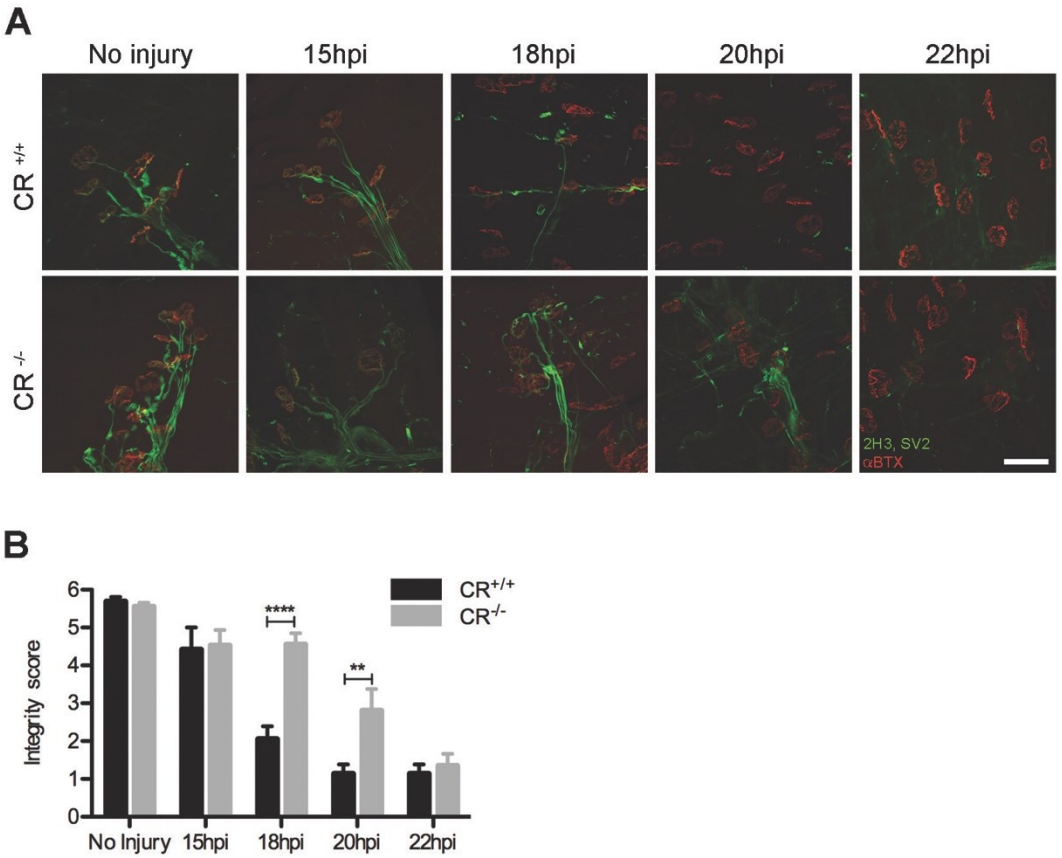


**Figure 4.4: Loss of CR expression delays Wallerian degeneration in the PNS. A)** Representative confocal micrographs of NMJs in lumbrical muscles at different time-points following sciatic nerve lesion. Green: axons/nerve terminals; red: acetylcholine receptors. Scale bar = 50 µm. **B)** Time course of integrity of the NMJ following sciatic nerve lesion. Note the moderate delay in instigation of degeneration in $CR^{-/-}$ mice. Data represented as mean ± SEM, N≥3, **p<0.01, ****p<0.001 two-Way ANOVA with Bonferroni post-test.

### 4.3.3. Calretinin is enriched in nerve terminals

The previous results show CR is more widely expressed than previously believed and that it may play an active role in neurodegenerative pathways. However, the properties of CR and its function besides $Ca^{2+}$ buffering are poorly understood.

Therefore, we wanted to further explore the function of CR in neurons so as to be able to understand how it may play a role in neurodegeneration.

In order to study CR's role in more detail, we used dissociated hippocampal neurons from wild-type mice. In contrast to the common belief that CR is essentially only expressed in a subpopulation of interneurons, in our *in vitro* system CR was ubiquitously expressed in the vast majority of hippocampal neurons (Figure 4.5 A). Nonetheless, a subpopulation of cells could be identified by its higher expression of CR, which accounted for ~3% of the overall neuronal population (Figure 4.5 B). This proportion in agreement with the previous knowledge (Cauli et al., 2014) about CR and we believe these cells constitute the population of CR-immunoreactive interneurons. However, as we are interested in the function of CR across all neuron types, we decided to focus our subsequent experiments on the population of hippocampal neurons expressing basal levels of CR, rather than just CR-immunoreactive interneurons.

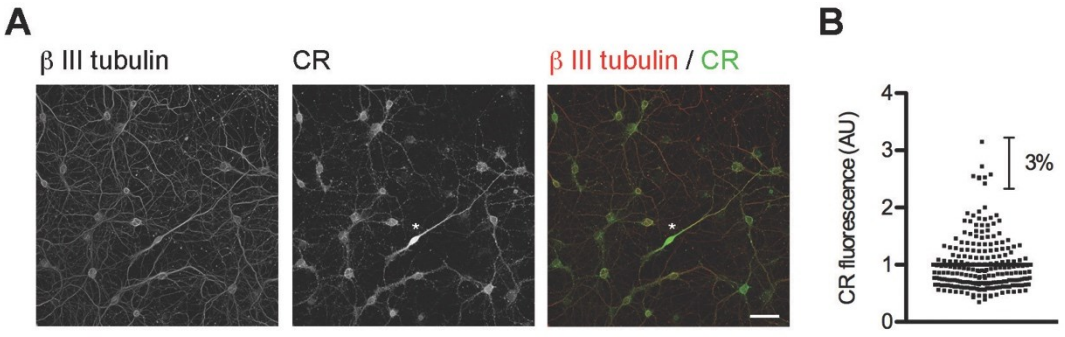


**Figure 4.5: CR is widely expressed in hippocampal neurons. A)** Hippocampal neurons from WT mice cultured to DIV16. Immunolabelling of CR and β-III-tubulin shows CR is present at detectable levels in the soma and projections of all neurons in culture. A small population of cells

expressed very high levels of CR compared to the remaining neurons (asterisk). Scale bar = 50 µm. **B)** Quantification of the intensity of CR in the soma of individual neurons highlights two populations of neurons: one expressing basal levels of CR and a second population expressing high levels of CR, presumably CR-immunoreactive interneurons, which accounted for 3% of the hippocampal neurons in our culture system.

The pattern of CR expression evolved during the culture of hippocampal neurons, with puncta expressing relatively high levels of CR becoming more abundant as cells matured (Figure 4.6). Double immunolabelling of DIV 16 neurons with CR and the synaptic vesicle protein SV2 showed CR puncta colocalise with sites of SV2 expression (Figure 4.7 A), where CR is expressed over 4 fold in comparison with neighbouring axonal areas (Figure 4.8).

Colocalisation analysis between CR and SV2 puncta showed 90% of CR puncta are positive for SV2, confirming CR accumulates at synapses. On the other hand, only 30% of SV2 puncta were simultaneously positive for CR (Figure 4.7 B), suggesting CR is either expressed transiently at synapses or does not accumulate equally in all types of nerve terminals. Co-labelling of CR with anti vGAT and vGLUT antibodies, to identify inhibitory and excitatory synapses, respectively, showed CR puncta are preferentially found in excitatory nerve terminals (Figure 4.7 C).

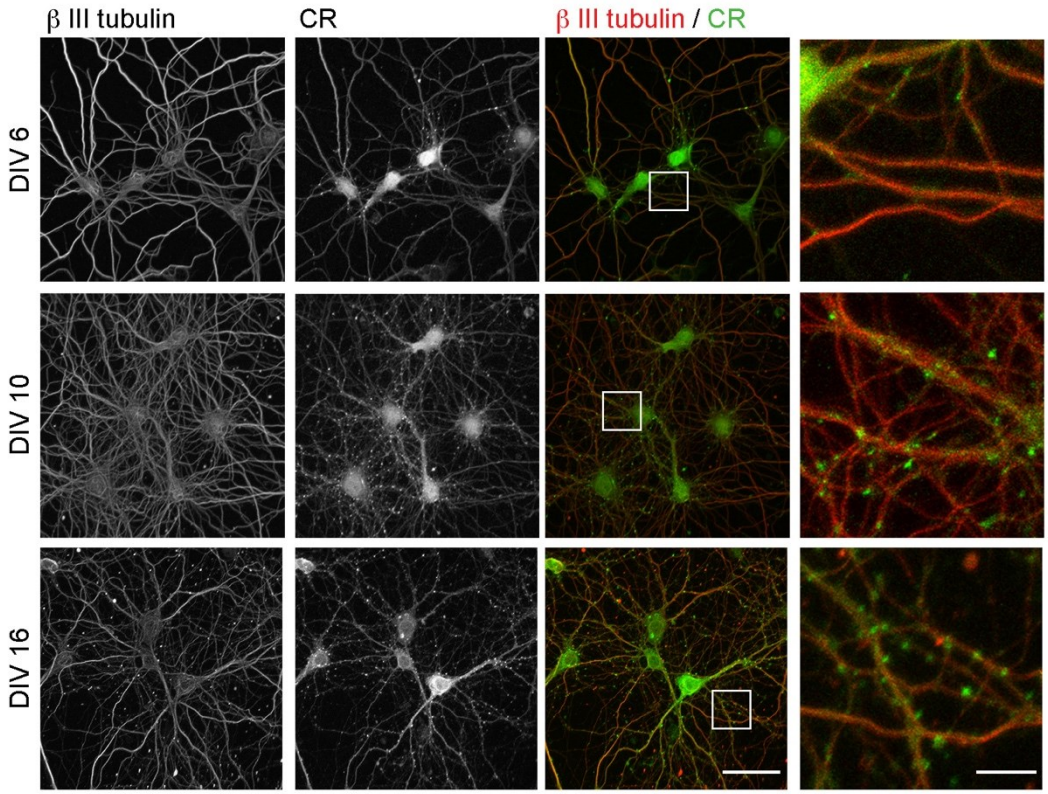


**Figure 4.6: The pattern of CR expression evolves as neurons mature.** Hippocampal neurons cultured to DIV 6, DIV 10 and DIV 16 were immunolabelled for CR and β-III-tubulin. Note the appearance of a punctate staining of CR as neurons mature. Right panel contains higher magnification images from highlighted regions on the 3rd panel. Scale bar = 50 μm (panels on the left), 10 μm (panel on the right).

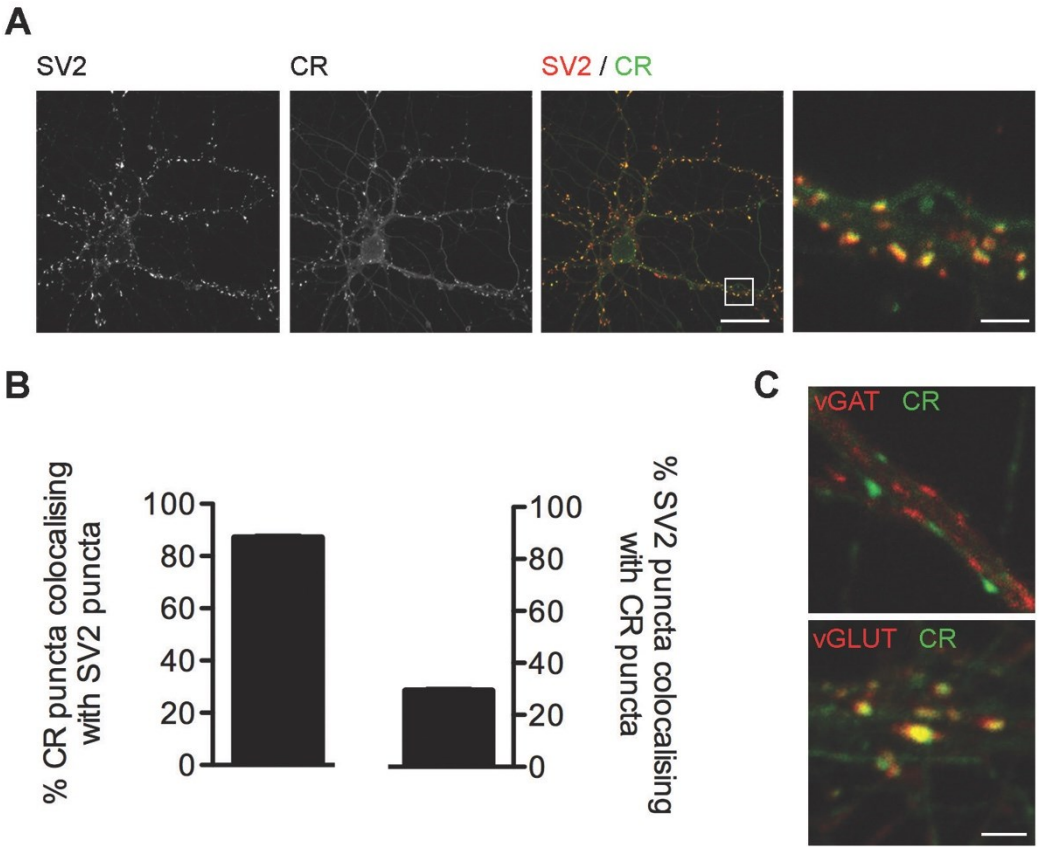


**Figure 4.7: CR is present in excitatory nerve terminals. A)** CR and SV2 immunolabelling of DIV 16 hippocampal neurons shows CR puncta colocalise with SV2. Scale bar = 20 µm (panels on the left), 2 µm (panel on the right). **B)** Quantification of colocalisation between CR and SV2 puncta indicates 90% of CR puncta colocalise with SV2, whereas only 30% of SV2 puncta are positive for CR. Data represented as mean ± SEM, N=3. **C)** Hippocampal neurons at DIV 16 immunolabelled for CR and vGAT or vGLUT demonstrate CR puncta colocalise with vGLUT but not vGAT, suggesting CR is preferentially enriched in excitatory nerve terminals. Scale bar = 2 µm.

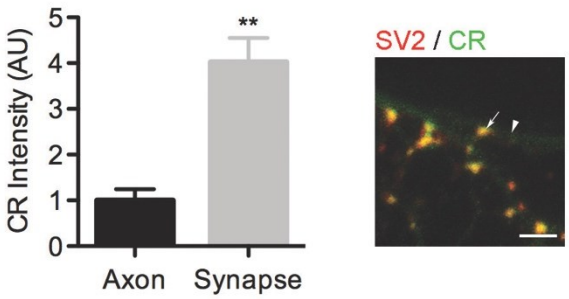


**Figure 4.8: CR is enriched in synaptic terminals.** Quantification of CR intensity in puncta colocalising with SV2 (arrows) and in adjacent axonal areas (arrow heads) confirms CR is enriched in synaptic terminals. N=3, **p<0.01 unpaired two-tailed t-test. Scale bar = 2 µm.

### 4.3.4. Calretinin responds dynamically to synaptic activity

After establishing that CR is enriched in nerve terminals we wanted to determine how it responded to synaptic activity. Therefore, we incubated hippocampal neurons in physiological media containing 2.5 or 50 mM KCl, as incubation with 50 mM KCl leads to depolarization of neurons and activates activity-dependent pathways (Macias et al., 2001, Smillie et al., 2013). In low levels of $K^+$ (2.5 mM KCl; Low $K^+$), CR staining presented the punctate staining described above. However, when neurons where stimulated with High $K^+$ (50 mM KCl; Stimulation), there was a striking reduction in the punctate appearance of CR (Figure 4.9 B). The number of CR puncta and the colocalisation between SV2 and CR puncta were reduced by 70% upon stimulation (Figure 4.9 C, D). Reapplying low $K^+$ levels to cells (Recovery) reverted the dispersion of CR and restored its colocalisation with SV2 (Figure 4.9). Altogether, these results suggest CR responds dynamically to synaptic activity, by dispersing and reclustering from nerve terminals in an activity-dependent manner.

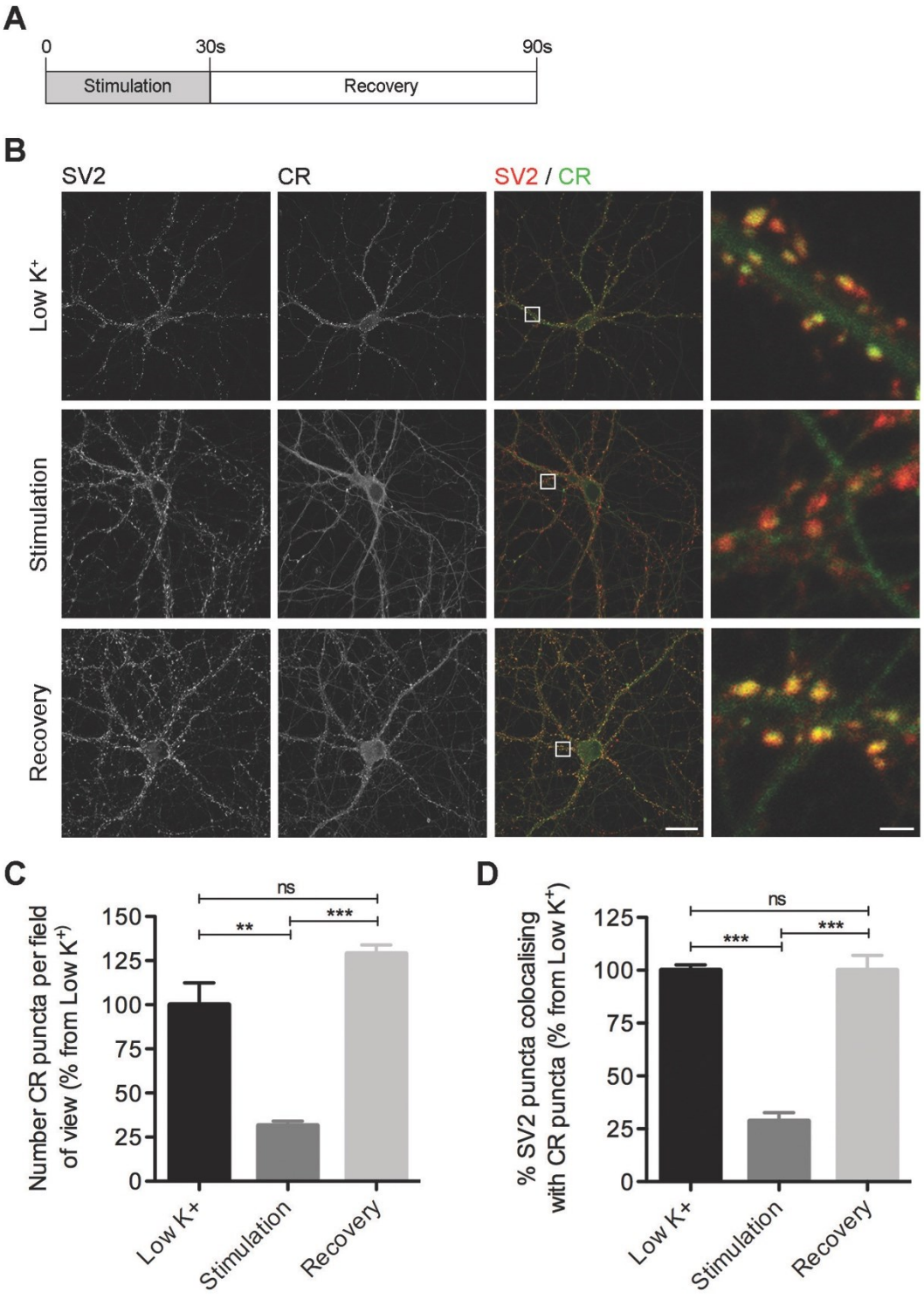


**Figure 4.9: CR disperses from nerve terminals during synaptic activity. A)** Schematic of the protocol applied for assessing the response of CR to a potassium ($K^+$) depolarisation stimulus. Hippocampal neurons at DIV 16 were stimulated for 30 s in Low or High $K^+$ buffer and either readily fixed (Stimulation) or allowed to recover in Low $K^+$ buffer for 60 s (Recovery). **B)** Representative

pictures from neurons incubated with low $K^+$ (low $K^+$) and from neurons exposed to high $K^+$ immediately after depolarisation (Stimulation) or after recovery in low $K^+$ (Recovery). The subcellular localization of CR changed dramatically upon depolarization in High $K^+$, with CR redistributing away from nerve terminals. Recovery in Low $K^+$ restored CR's high degree of co-localization with the synaptic marker SV2. Panels on the right are close-ups from the highlight regions of the images on the left. Scale bar = 20 μm (panels on the left), 2 μm (panel on the right). **C)** Number of CR puncta are greatly reduced upon stimulation of neurons. Recovery in Low $K^+$ restores the number of CR puncta to control Low $K^+$ levels. N=3, **p<0.01, ***p<0.001 in one-Way ANOVA with Tukey post-test. **D)** Colocalisation analysis between SV2 and CR puncta confirms the specific reduction in the number of CR puncta upon stimulation. N=3, ***p<0.001 in one-Way ANOVA with Tukey post-test.

To confirm that dispersion of CR was indeed due to synaptic activity we performed real-time imaging of fluorescently tagged CR during stimulation with a train of action potentials. Transfecting low levels of CR lead to its colocalization with synaptophysin (syp), confirming the synaptic localisation of CR (Figure 4.10 A). After a train of 300 action potentials, at 10Hz, CR dispersed from nerve terminals (Figure 4.10 B). Measuring the fluorescence intensity of the protein in synaptic puncta (synapses) and in adjacent axonal regions (axons) demonstrated an increase in axonal intensity and reduction of the fluorescence in synaptic areas, concomitant with the administration of the action potential stimulus (Figure 4.10 C). Recording of $Ca^{2+}$ signals using the fluorescent $Ca^{2+}$ indicator GCaMP6f showed the typical sharp rise in $Ca^{2+}$ immediately after an action potential, and fast recovery of $Ca^{2+}$ levels to basal levels during the post-stimulation period (Figure 4.10 D). The curve of CR fluorescence, however, is indicative of much slower kinetics of CR's return to nerve terminals than that of the recovery of $Ca^{2+}$ levels, suggesting CR may remain in the peri-active zone to buffer excessive $Ca^{2+}$ after synaptic activity. Comparing the

activity-dependent behaviour of CR with that of a typical synaptic protein, synaptophysin, revealed the kinetics of dispersion of the two proteins from nerve terminals, following a train of action potentials, are very similar (Figure 4.10 E). However, the post-stimulation recovery of CR tended to be slightly slower that Syp, although it did not reach statistical significance (Figure 4.10 E, F).

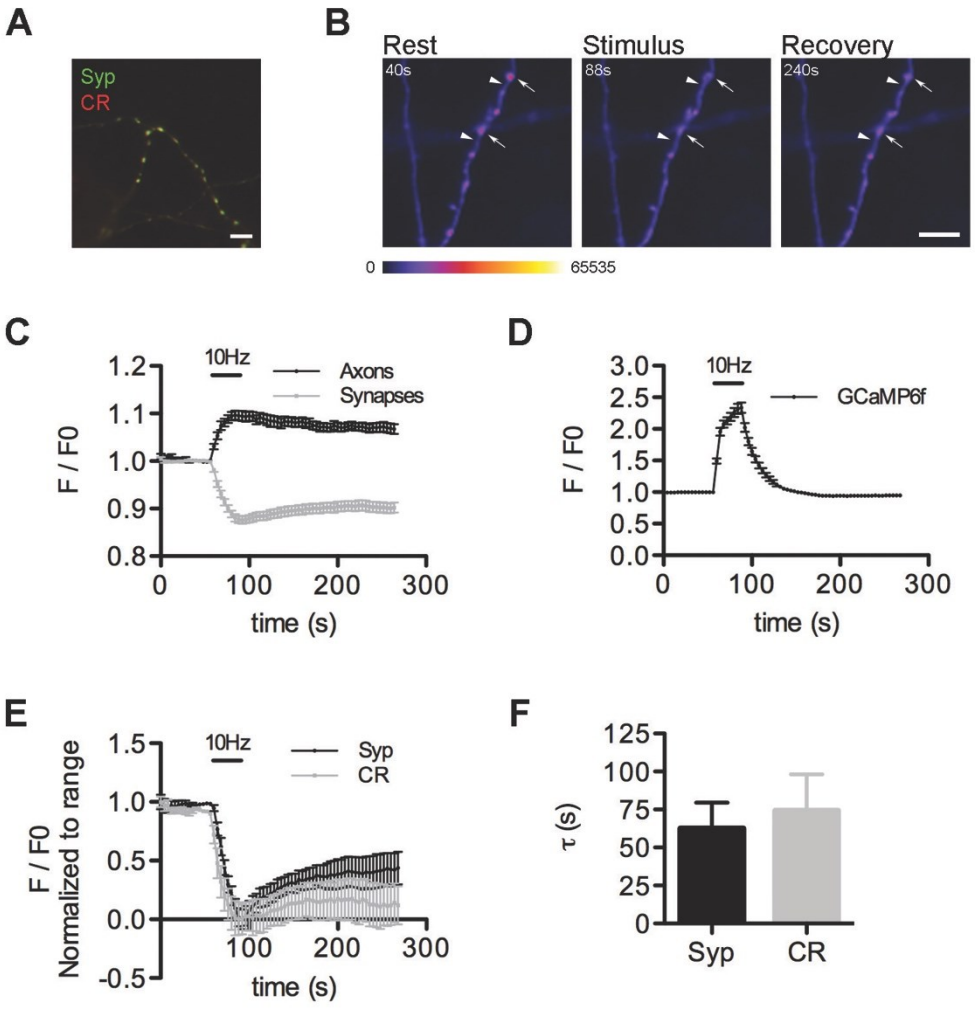


**Figure 4.10: CR responds dynamically to synaptic activity. A)** Hippocampal neurons transfected with Synaptophysin (Syp, green) and CR (CR, red). Note the colocalisation between Syp and CR. Scale bar = 5 μm. **B)** False colour images from neurons transfected with CR before (Rest) and after (Stimulation) stimulation with 300 action potentials, and over 2 min after stimulation (Recovery).

Arrows indicate nerve terminals and arrow heads indicate axonal areas. Scale bar = 5 μm. **C)** Mean fluorescent traces (F/F0) of CR in synapses and axons. Note the change in fluorescence during the action potential (10Hz). The opposite direction in the change of fluorescence for axons and synapses suggests CR disperses from nerve terminals to the adjacent axonal regions. Traces are represented as mean ± SEM, n≥28. **D)** $Ca^{2+}$ imaging using GCaMP6f showing the fast kinetics of $Ca^{2+}$ signals. Traces represent F/F0 mean ± SEM, n=90. **E)** F/F0 fluorescence, normalized to the range of fluorescence, in hippocampal nerve terminals expressing CR or Syp. Traces represent F/F0 mean ± SEM, N=6, n=59 (CR), n=89 (Syp), p>0.05 two-way ANOVA with Holm-Šídák post-test. **F)** Mean time constant (τ) for post-stimulation recovery of CR and Syp. Bars represent mean ± SEM, N=5, unpaired two-tailed t-test, p>0.05.

### 4.3.5. $Ca^{2+}$-dependent interactions of calretinin in nerve terminals

We have shown thus far that CR is expressed in nerve terminals and responds dynamically to synaptic activity. The nature of this behaviour could be due to the ability of CR to act as a $Ca^{2+}$ buffer during neurotransmission. However, it has been suggested CR also acts as a $Ca^{2+}$ sensor and interactions have been published between CR and the $Ca^{2+}$ channel $Ca_V2.1$ and the huntingtin protein (Christel et al., 2012, Dong et al., 2012). $Ca^{2+}$ levels have, in addition, been shown to alter the conformation of the protein and have been proposed to influence the capacity of CR to form interactions (Arendt et al., 2013, Kuznicki et al., 1995, Schwaller et al., 1997). Therefore, we sought to explore $Ca^{2+}$-dependent interactions of CR as an attempt to clarify its behaviour during synaptic activity.

We isolated crude synaptosomes from WT mouse whole brain and performed co-immunoprecipitation experiments in the presence of $Ca^{2+}$ or EGTA. Mass spectrometry identification of the interacting proteins revealed CR is present in

complexes with synaptic proteins, cytoskeletal proteins and proteins involved in immune response (Table 4.7).

**Table 4.7: CR interactions at the synapse.**

| Protein | Gene | Accession | Unique Peptides |
|---|---|---|---|
| Actin, cytoplasmic 1 | Actb | IPI00110850 | 6 |
| Sodium/potassium-transporting ATPase subunitalpha-3 | Atp1a3 | IPI00122048 | 10 |
| complement C1q subcomponent subunit C precursor | C1qc | IPI00788462 | 3 |
| Clathrin heavy chain 1 | Cltc | IPI00169916 | 5 |
| Cathepsin B | Ctsb | IPI00113517 | 2 |
| Isoform 3 of Dynamin-1 | Dnm1 | IPI00465648 | 2 |
| Dihydropyrimidinase-related protein 2 | Dpysl 2 | IPI00114375 | 5 |
| Glyceraldehyde-3-phosphate dehydrogenase (Fragment) | Gm2606 | IPI00989722 | 5 |
| Isoform Alpha-2 of Guanine nucleotide-binding protein G(o) subunit alpha | Gnao1 | IPI00115546 | 2 |
| LOC100503273 Hemoglobin subunit epsilon-Y2 | Hbb-y | IPI00555131 | 2 |
| Heat shock cognate 71 kDa protein | Hspa8 | IPI00323357 | 6 |
| Inter-alpha-trypsin inhibitor heavy chain H2 | Itih2 | IPI00227834 | 2 |
| Isoform 5 of Myelin basic protein | Mbp | IPI00223378 | 3 |
| Microtubule-associated protein 1B | Mtap1b | IPI00130920 | 2 |
| Isoform Ib of Synapsin-1 | Syn1 | IPI00136372 | 7 |
| Isoform Ia of Synapsin-1 | Syn1 | IPI00649886 | 10 |
| Thrombospondin-1 | Thbs1 | IPI00118413 | 2 |
| Tubulin beta-2A chain | Tubb2a | IPI00338039 | 11 |
| Tubulin beta-2C chain | Tubb2c | IPI00169463 | 12 |

Description: Protein description;
Gene: Gene coding the identified protein;
Accession: IPI Accession number;
Unique peptides: Number of unique peptides used to identify the protein.

Using Western blotting, we confirmed the interaction of CR with the synaptic proteins synapsin 1 and dynamin 1 (Figure 4.11 A), which are important regulators of synaptic vesicle dynamics (Hilfiker et al., 1999, Smillie and Cousin, 2005). Interestingly, the interactions were stronger in the presence of EGTA (Figure 4.11 B). This suggests $Ca^{2+}$ may compete with existing interactions or alter the ability of CR to

bind other proteins, possibly by altering its conformation or recruiting CR to areas other than the pre-synaptic active zone, as suggested by previous results (see Figure 4.9 and Figure 4.10).

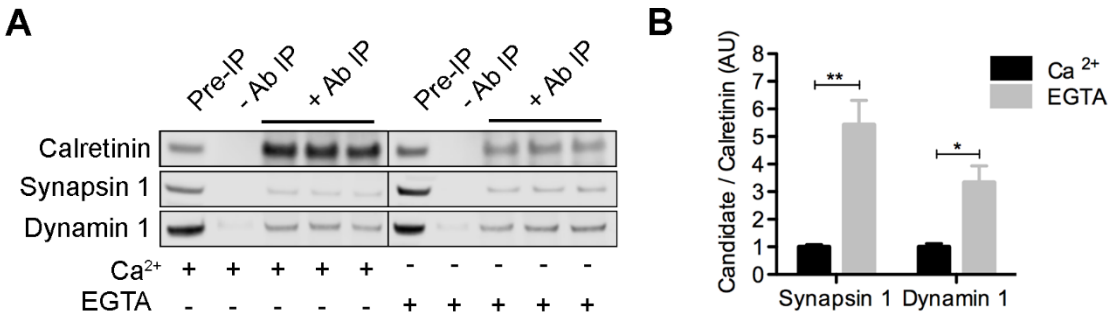


**Figure 4.11: CR co-immunoprecipitates with synaptic proteins. A)** Co-immunoprecipitation of CR in synaptosomal protein extracts in the presence or either $Ca^{2+}$ or EGTA, confirms the interactions between CR and the synaptic proteins synapsin 1 and dynamin 1. Representative Western blots include lanes loaded with a fraction of the original protein extract (Pre-IP), a control experiment performed without the addition of CR anti-body (-Ab IP) and three replicates of co-ip experiments (+ Ab IP). **B)** Quantification of fluorescence signals from blots in A revealed that a higher fraction of synapsin 1 and dynamin 1, relative to CR levels, co-immunoprecipitated with CR in the presence of EGTA. Bars represent mean ± SEM, N=3, *p<0.05, **p<0.01 in unpaired two-tailed t-test.

### 4.3.6. Label-free proteomics in $CR^{-/-}$ synaptosomes

To further characterize the role of CR in synaptic function and gain clues about how it might contribute to synaptic function and stability, we performed Label-free proteomics on synaptosomal fractions isolated from $CR^{-/-}$ and $CR^{+/+}$ mice. Of the 718 proteins identified by mass spectrometry, 263 were identified by more than 1 unique

peptide and 141 had expression levels altered by more than 10% in $CR^{-/-}$ synaptosomes when compared to $CR^{+/+}$ (Figure 4.12). The list of 141 proteins considered for further analysis can be found in Table 4.8.

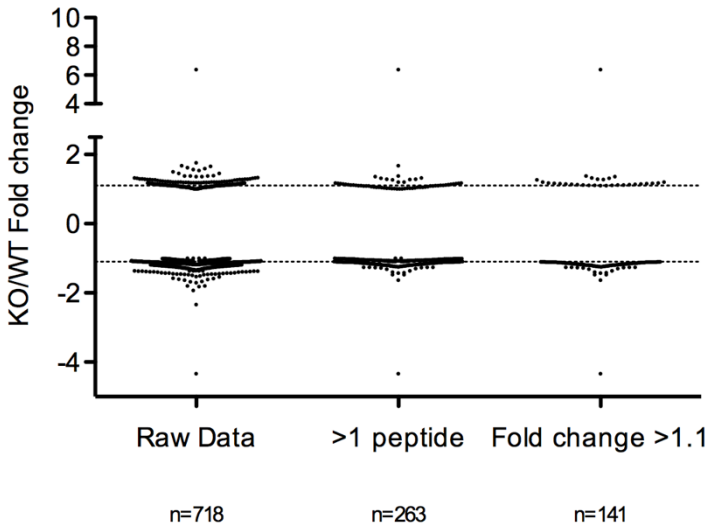


**Figure 4.12: Label-free proteomics filtering steps.** Y-axis represents the fold change in the levels of proteins between $CR^{-/-}$ (KO) and $CR^{+/+}$ (WT) synaptosomes. X-axis columns contain all proteins included in the various stages of data analysis. 718 proteins were identified by label-free proteomics (Raw data column) and the data-set was filtered to include only proteins identified by more than 1 unique peptide (>1 peptide column, 263 proteins). Of these, 141 proteins had expression levels altered by more than 10% in the KO synaptosomes compared to WT (fold change >1.1 column).

**Table 4.8: Proteins altered by more than 10% in $CR^{-/-}$ mice, as identified by label-free proteomics.**

| KO/WT ratio | Description | Gene | UniProt Accession | Unique peptides | Score |
|---|---|---|---|---|---|
| -4.340 | Calretinin | Calb2 | Q08331 | 8 | 460.97 |
| -1.630 | ATP synthase subunit delta, mitochondrial | Atp5d | Q9D3D9 | 2 | 100.39 |
| -1.473 | Neurocalcin-delta | Ncald | Q91X97 | 3 | 155.52 |
| -1.469 | Fatty acid synthase | Fasn | P19096 | 2 | 79.33 |
| -1.429 | Calcium-binding mitochondrial carrier protein Aralar1 | Slc25a12 | Q8BH59 | 6 | 398.36 |

| | | | | | |
|---|---|---|---|---|---|
| -1.415 | Vesicle-associated membrane protein-associated protein A | Vapa | Q9WV55 | 2 | 79.75 |
| -1.400 | Electrogenic sodium bicarbonate cotransporter 1 | Slc4a4 | O88343 | 2 | 77.97 |
| -1.365 | Tubulin beta-2A chain | Tubb2a | Q7TMM9 | 3 | 185.54 |
| -1.316 | Reticulon-3 | Rtn3 | Q9ES97 | 2 | 151.45 |
| -1.299 | Glucose-6-phosphate isomerase | Gpi | P06745 | 2 | 81.23 |
| -1.281 | AP-2 complex subunit mu | Ap2m1 | P84091 | 2 | 91.01 |
| -1.271 | Vacuolar protein sorting-associated protein 35 | Vps35 | Q9EQH3 | 2 | 198.66 |
| -1.269 | NADH dehydrogenase [ubiquinone] iron-sulfur protein 2, mitochondrial | Ndufs2 | Q91WD5 | 4 | 250.22 |
| -1.264 | Glutathione S-transferase Mu 1 | Gstm1 | P10649 | 3 | 238.22 |
| -1.262 | AP-2 complex subunit alpha-2 | Ap2a2 | P17427 | 3 | 228.46 |
| -1.260 | Calcium/calmodulin-dependent protein kinase type II subunit alpha | Camk2a | P11798 | 6 | 383.51 |
| -1.255 | Synaptic vesicle glycoprotein 2A | Sv2a | Q9JIS5 | 2 | 77.06 |
| -1.253 | Dynamin-1-like protein | Dnm1l | Q8K1M6 | 3 | 232.21 |
| -1.238 | 14-3-3 protein gamma | Ywhag | P61982 | 2 | 83.87 |
| -1.238 | Rab GDP dissociation inhibitor alpha | Gdi1 | P50396 | 5 | 352.86 |
| -1.237 | Heat shock 70 kDa protein 1B | Hspa1b | P17879 | 2 | 123.07 |
| -1.236 | Immunoglobulin superfamily member 8 | Igsf8 | Q8R366 | 2 | 117.71 |
| -1.231 | Plexin-A4 | Plxna4 | Q80UG2 | 2 | 104.62 |
| -1.228 | Succinate dehydrogenase [ubiquinone] iron-sulfur subunit, mitochondrial | Sdhb | Q9CQA3 | 2 | 120.12 |
| -1.228 | Trafficking protein particle complex subunit 4 | Trappc4 | Q9ES56 | 2 | 92.79 |
| -1.225 | Protein piccolo | Pclo | Q9QYX7 | 2 | 114.48 |
| -1.225 | Glutamate receptor ionotropic, NMDA 2B | Grin2b | Q01097 | 2 | 91.95 |
| -1.224 | Citrate synthase, mitochondrial | Cs | Q9CZU6 | 7 | 389.69 |
| -1.221 | Cytochrome c oxidase subunit 5A, mitochondrial | Cox5a | P12787 | 3 | 173.32 |
| -1.212 | Neurofilament heavy polypeptide | Nefh | P19246 | 2 | 91.97 |
| -1.208 | 1-phosphatidylinositol 4,5-bisphosphate phosphodiesterase beta-1 | Plcb1 | Q9Z1B3 | 3 | 148.66 |
| -1.207 | Calcineurin subunit B type 1 | Ppp3r1 | Q63810 | 2 | 125.78 |
| -1.206 | Nucleosome assembly protein 1-like 1 | Nap1l1 | P28656 | 2 | 137.95 |
| -1.206 | Glutathione S-transferase P 1 | Gstp1 | P19157 | 2 | 110.25 |
| -1.199 | Cytoplasmic FMR1-interacting protein 2 | Cyfip2 | Q5SQX6 | 5 | 254.56 |

| | | | | | |
|---|---|---|---|---|---|
| -1.198 | Mitochondrial 2-oxoglutarate/malate carrier protein | Slc25a11 | Q9CR62 | 3 | 137.11 |
| -1.197 | Neuroplastin | Nptn | P97300 | 2 | 79.2 |
| -1.196 | Heat shock protein 105 kDa | Hsph1 | Q61699 | 5 | 362.31 |
| -1.195 | Ubiquitin carboxyl-terminal hydrolase isozyme L3 | Uchl3 | Q9JKB1 | 2 | 109.08 |
| -1.194 | Leucine-rich PPR motif-containing protein, mitochondrial | Lrpprc | Q6PB66 | 4 | 191.93 |
| -1.190 | 4-aminobutyrate aminotransferase, mitochondrial | Abat | P61922 | 6 | 306.77 |
| -1.189 | MICOS complex subunit Mic60 | Immt | Q8CAQ8 | 3 | 150.01 |
| -1.187 | Neurofilament medium polypeptide | Nefm | P08553 | 5 | 347.7 |
| -1.183 | 4F2 cell-surface antigen heavy chain | Slc3a2 | P10852 | 4 | 202.53 |
| -1.178 | Endoplasmic reticulum resident protein 29 | Erp29 | P57759 | 2 | 75.33 |
| -1.177 | NADH dehydrogenase [ubiquinone] iron-sulfur protein 3, mitochondrial | Ndufs3 | Q9DCT2 | 3 | 199.52 |
| -1.176 | Macrophage migration inhibitory factor | Mif | P34884 | 2 | 131.29 |
| -1.176 | V-type proton ATPase 116 kDa subunit a isoform 1 | Atp6v0a1 | Q9Z1G4 | 3 | 196.52 |
| -1.175 | T-complex protein 1 subunit alpha | Tcp1 | P11983 | 2 | 97.54 |
| -1.172 | Heat shock 70 kDa protein 12A | Hspa12a | Q8K0U4 | 2 | 97.7 |
| -1.172 | V-type proton ATPase subunit d 1 | Atp6v0d1 | P51863 | 2 | 152.99 |
| -1.166 | Serine/threonine-protein kinase PAK 3 | Pak3 | Q61036 | 2 | 108.76 |
| -1.166 | T-complex protein 1 subunit delta | Cct4 | P80315 | 2 | 148.57 |
| -1.165 | Protein NDRG2 | Ndrg2 | Q9QYG0 | 2 | 89.11 |
| -1.164 | Dihydropyrimidinase-related protein 5 | Dpysl5 | Q9EQF6 | 2 | 83.05 |
| -1.162 | Ubiquitin-like modifier-activating enzyme 1 | Uba1 | Q02053 | 3 | 189.85 |
| -1.159 | Casein kinase II subunit alpha | Csnk2a1 | Q60737 | 3 | 167.86 |
| -1.159 | Actin, cytoplasmic 1 | Actb | P60710 | 5 | 320.23 |
| -1.156 | Nucleoside diphosphate kinase B | Nme2 | Q01768 | 2 | 177.17 |
| -1.155 | Cytoplasmic dynein 1 heavy chain 1 | Dync1h1 | Q9JHU4 | 8 | 414.44 |
| -1.155 | Sodium/calcium exchanger 1 | Slc8a1 | P70414 | 2 | 125.14 |
| -1.152 | Glial fibrillary acidic protein | Gfap | P03995 | 2 | 104.87 |
| -1.150 | Stress-induced-phosphoprotein 1 | Stip1 | Q60864 | 7 | 401.04 |
| -1.148 | Endoplasmin | Hsp90b1 | P08113 | 2 | 158.22 |
| -1.147 | Alpha-adducin | Add1 | Q9QYC0 | 2 | 102.22 |

| | | | | | |
|---|---|---|---|---|---|
| -1.144 | Protein kinase C and casein kinase substrate in neurons protein 1 | Pacsin1 | Q61644 | 2 | 75.17 |
| -1.143 | Synaptopodin | Synpo | Q8CC35 | 2 | 93.14 |
| -1.141 | Heat shock protein HSP 90-alpha | Hsp90aa1 | P07901 | 10 | 496.68 |
| -1.141 | Catenin delta-2 | Ctnnd2 | O35927 | 2 | 105.36 |
| -1.140 | ATP-citrate synthase | Acly | Q91V92 | 3 | 160.48 |
| -1.138 | Neurofilament light polypeptide | Nefl | P08551 | 11 | 693.1 |
| -1.137 | 78 kDa glucose-regulated protein | Hspa5 | P20029 | 7 | 488.49 |
| -1.135 | Catenin alpha-2 | Ctnna2 | Q61301 | 4 | 258.12 |
| -1.135 | Tumor protein p63-regulated gene 1-like protein | Tprg1l | Q9DBS2 | 2 | 81.76 |
| -1.133 | Serine/threonine-protein phosphatase 2A 65 kDa regulatory subunit A alpha isoform | Ppp2r1a | Q76MZ3 | 4 | 170.65 |
| -1.133 | NADH dehydrogenase [ubiquinone] 1 alpha subcomplex subunit 12 | Ndufa12 | Q7TMF3 | 2 | 123.94 |
| -1.129 | ATP synthase subunit O, mitochondrial | Atp5o | Q9DB20 | 4 | 276.74 |
| -1.125 | Protein disulfide-isomerase A3 | Pdia3 | P27773 | 2 | 94.75 |
| -1.123 | Calnexin | Canx | P35564 | 2 | 151.84 |
| -1.120 | ADP-ribosylation factor 5 | Arf5 | P84084 | 3 | 202.89 |
| -1.120 | Glutamate receptor 2 | Gria2 | P23819 | 2 | 147.75 |
| -1.119 | Alpha-actinin-1 | Actn1 | Q7TPR4 | 3 | 214.65 |
| -1.119 | Alpha-internexin | Ina | P46660 | 7 | 488.54 |
| -1.118 | Stress-70 protein, mitochondrial | Hspa9 | P38647 | 4 | 391.5 |
| -1.116 | Septin-9 | Sept9 | Q80UG5 | 2 | 118.68 |
| -1.116 | Spectrin beta chain, non-erythrocytic 1 | Sptbn1 | Q62261 | 15 | 806.7 |
| -1.115 | 14-3-3 protein eta | Ywhah | P68510 | 2 | 142.17 |
| -1.114 | Dynamin-1 | Dnm1 | P39053 | 3 | 164.25 |
| -1.114 | Plectin | Plec | Q9QXS1 | 5 | 294.42 |
| -1.114 | Reticulon-1 | Rtn1 | Q8K0T0 | 2 | 124.29 |
| -1.113 | Syntaxin-binding protein 1 | Stxbp1 | O08599 | 9 | 670.3 |
| -1.112 | Beta-centractin | Actr1b | Q8R5C5 | 3 | 220.12 |
| -1.112 | Ras/Rap GTPase-activating protein SynGAP | Syngap1 | F6SEU4 | 3 | 162.33 |
| -1.112 | Ganglioside-induced differentiation-associated protein 1 | Gdap1 | O88741 | 2 | 81.87 |
| -1.111 | Guanine nucleotide-binding protein G(o) subunit alpha | Gnao1 | P18872 | 2 | 145.14 |
| -1.111 | Microtubule-associated protein 2 | Map2 | P20357 | 6 | 390.1 |
| -1.110 | Adenylate kinase isoenzyme 1 | Ak1 | Q9R0Y5 | 2 | 122.56 |

| | | | | | |
|---|---|---|---|---|---|
| -1.110 | F-actin-capping protein subunit beta | Capzb | P47757 | 2 | 105.56 |
| -1.108 | Succinyl-CoA ligase [ADP-forming] subunit beta, mitochondrial | Sucla2 | Q9Z2I9 | 4 | 241.99 |
| -1.108 | Creatine kinase B-type | Ckb | Q04447 | 4 | 281.26 |
| -1.107 | Syntaxin-1B | Stx1b | P61264 | 5 | 401.63 |
| -1.106 | Sarcoplasmic/endoplasmic reticulum calcium ATPase 2 | Atp2a2 | O55143 | 4 | 260 |
| -1.105 | Myosin-10 | Myh10 | Q61879 | 4 | 289.79 |
| -1.104 | Sorting and assembly machinery component 50 homolog | Samm50 | Q8BGH2 | 3 | 156.87 |
| -1.104 | Pyruvate kinase PKM | Pkm | P52480 | 5 | 361.44 |
| -1.103 | Sodium/potassium-transporting ATPase subunit alpha-3 | Atp1a3 | Q6PIC6 | 8 | 474.95 |
| -1.102 | ADP/ATP translocase 1 | Slc25a4 | P48962 | 6 | 470.75 |
| -1.102 | Tubulin beta-3 chain | Tubb3 | Q9ERD7 | 5 | 350.43 |
| -1.102 | Leucine-rich glioma-inactivated protein 1 | Lgi1 | Q9JIA1 | 2 | 88.53 |
| 1.105 | NADH dehydrogenase [ubiquinone] 1 beta subcomplex subunit 7 | Ndufb7 | Q9CR61 | 2 | 108.21 |
| 1.105 | Microtubule-associated protein tau | Mapt | P10637 | 2 | 77.15 |
| 1.106 | Pyruvate dehydrogenase E1 component subunit alpha, somatic form, mitochondrial | Pdha1 | P35486 | 4 | 173.63 |
| 1.107 | 2',3'-cyclic-nucleotide 3'-phosphodiesterase | Cnp | P16330 | 7 | 404.16 |
| 1.111 | Trifunctional enzyme subunit alpha, mitochondrial | Hadha | Q8BMS1 | 5 | 282.91 |
| 1.116 | Fatty acid-binding protein, epidermal | Fabp5 | Q05816 | 2 | 93.82 |
| 1.122 | Stathmin | Stmn1 | P54227 | 2 | 119.28 |
| 1.123 | Ubiquitin-40S ribosomal protein S27a | Rps27a | P62983 | 2 | 73.51 |
| 1.125 | Alpha-enolase | Eno1 | P17182 | 2 | 120.49 |
| 1.126 | Carbonic anhydrase 2 | Ca2 | P00920 | 3 | 150.22 |
| 1.137 | Cytochrome b-c1 complex subunit 1, mitochondrial | Uqcrc1 | Q9CZ13 | 2 | 118.94 |
| 1.138 | Peptidyl-prolyl cis-trans isomerase A | Ppia | P17742 | 3 | 198.99 |
| 1.145 | Monofunctional C1-tetrahydrofolate synthase, mitochondrial | Mthfd1l | Q3V3R1 | 3 | 255.65 |
| 1.152 | Very long-chain specific acyl-CoA dehydrogenase, mitochondrial | Acadvl | P50544 | 3 | 140.23 |
| 1.155 | Breast carcinoma-amplified sequence 1 homolog | Bcas1 | Q80YN3 | 3 | 140.93 |
| 1.161 | Acyl-CoA synthetase family member 2, mitochondrial | Acsf2 | Q8VCW8 | 2 | 105.98 |
| 1.165 | Tetraspanin-2 | Tspan2 | Q922J6 | 2 | 110.77 |

| | | | | | |
|---|---|---|---|---|---|
| 1.170 | D-beta-hydroxybutyrate dehydrogenase, mitochondrial | Bdh1 | Q80XN0 | 2 | 90.24 |
| 1.172 | Secretogranin-2 | Scg2 | Q03517 | 2 | 110.02 |
| 1.172 | Long-chain-fatty-acid--CoA ligase ACSBG1 | Acsbg1 | Q99PU5 | 2 | 118.99 |
| 1.200 | ATPase inhibitor, mitochondrial | Atpif1 | O35143 | 4 | 174.75 |
| 1.205 | Ectonucleotide pyrophosphatase/phosphodiesterase family member 6 | Enpp6 | Q8BGN3 | 2 | 99.38 |
| 1.266 | Myelin basic protein | Mbp | P04370 | 2 | 72.78 |
| 1.281 | ATP synthase-coupling factor 6, mitochondrial | Atp5j | P97450 | 4 | 166.86 |
| 1.288 | Acetyl-CoA acetyltransferase, mitochondrial | Acat1 | Q8QZT1 | 3 | 154.92 |
| 1.290 | Keratin, type II cytoskeletal 1b | Krt77 | Q6IFZ6 | 2 | 118.92 |
| 1.320 | Histone H4 | Hist1h4a | P62806 | 4 | 196.54 |
| 1.324 | Endophilin-A1 | Sh3gl2 | Q62420 | 2 | 108.28 |
| 1.362 | NADH dehydrogenase [ubiquinone] iron-sulfur protein 6, mitochondrial | Ndufs6 | P52503 | 6 | 458.14 |
| 1.384 | cAMP-dependent protein kinase catalytic subunit alpha | Prkaca | P05132 | 2 | 102.6 |
| 1.673 | Keratin, type I cytoskeletal 10 | Krt10 | P02535 | 3 | 155.88 |
| 6.383 | Somatotropin | Gh1 | P06880 | 2 | 156.85 |

KO/WT Ratio: Ratio between the expression levels of a given protein in $CR^{-/-}$ mice compared to $CR^{+/+}$;
Description: Protein description;
Gene: Gene coding the identified protein;
UniProt Accession: UniProt Accession number;
Unique peptides: Number of unique peptides used to identify the protein;
Score: Confidence score.

To highlight the pathways and functional categories associated with loss of CR, we performed pathway analysis using the IPA software on the filtered proteomics data-set. IPA identified alterations in the $CR^{-/-}$ proteome relevant to several neurological and neuromuscular disorders, including Huntington's disease, Alzheimer's disease and motor neuron diseases (Table 4.9). Cellular functions affected by loss of CR included cell death, microtubule dynamics and synaptic transmission (Table 4.9). The full list of functions and diseases identified by IPA, including the list of proteins identified for each category, can be found in Appendix 1.

In order to identify established molecular pathways affected in $CR^{-/-}$ mice, we used the IPA Canonical Pathways tool. Interestingly, the top pathways identified included mitochondrial dysfunction, Huntington's disease, long-term potentiation and clathrin-mediated endocytosis (Table 4.10).

**Table 4.9: Selection of top diseases and cellular functions associated with the proteomic changes in $CR^{-/-}$ mice, as identified by IPA.**

| IPA Diseases Annotation | p-Value | IPA Functions Annotation | p-Value |
|---|---|---|---|
| Disorder of basal ganglia | 1.20E-23 | organization of cytoskeleton | 3.26E-18 |
| Neuromuscular disease | 5.70E-22 | cell death | 6.20E-16 |
| Movement Disorders | 7.03E-22 | microtubule dynamics | 4.02E-15 |
| Dyskinesia | 1.98E-15 | morphology of cells | 7.46E-14 |
| Neurological signs | 2.21E-15 | transport of molecule | 2.76E-12 |
| Huntington's Disease | 1.33E-14 | neurotransmission | 1.43E-11 |
| Tauopathy | 4.64E-11 | proliferation of cells | 2.58E-09 |
| Progressive motor neuropathy | 2.93E-10 | synaptic transmission | 6.38E-09 |
| Alzheimer's disease | 6.65E-10 | differentiation of cells | 8.07E-09 |
| Hereditary myopathy | 1.98E-09 | dendritic growth/branching | 9.99E-09 |
| Autosomal dominant disease | 3.30E-09 | accumulation of filaments | 1.22E-08 |
| Sporadic motor neuron disease | 9.45E-09 | long-term potentiation of synapse | 2.04E-08 |

**Table 4.10: Top canonical pathways associated with the proteomic changes in $CR^{-/-}$ mice, as identified by IPA.**

| IPA Canonical Pathways | p-value | Molecules |
|---|---|---|
| Oxidative Phosphorylation | 2.7E-10 | ATP5J,SDHB,ATP5D,NDUFB7,ATP5O,COX5A,NDUFS6,NDUFA12,NDUFS2,UQCRC1,NDUFS3 |
| Mitochondrial Dysfunction | 3.0E-09 | ATP5J,PDHA1,SDHB,ATP5D,NDUFB7,ATP5O,COX5A,NDUFS6,NDUFA12,NDUFS2,UQCRC1,NDUFS3 |
| Remodeling of Epithelial Adherent Junctions | 2.5E-07 | DNM1,CTNNA2,TUBB3,ACTB,TUBB2A,DNM1L,ACTN1 |
| Huntington's Disease Signaling | 5.4E-07 | ATP5J,DNM1,GRIN2B,SDHB,PACSIN1,HSPA1B,HSPA9,PLCB1,DNM1L,HSPA5,AP2A2 |
| Unfolded protein response | 1.2E-06 | HSP90B1,HSPH1,HSPA1B,HSPA9,CANX,HSPA5 |
| 14-3-3-mediated Signaling | 2.0E-06 | TUBB3,YWHAG,YWHAH,PDIA3,MAPT,TUBB2A,PLCB1,GFAP |
| Aldosterone Signaling in Epithelial Cells | 1.7E-05 | HSP90B1,PDIA3,HSPH1,HSPA9,HSP90AA1,PLCB1,HSPA5,HSPA12A |
| Synaptic Long Term Potentiation | 1.8E-05 | GRIN2B,CAMK2A,PDIA3,PPP3R1,GRIA2,PRKACA,PLCB1 |
| Lipid Antigen Presentation by CD1 | 2.1E-05 | AP2M1,PDIA3,CANX,AP2A2 |
| Calcium Signaling | 2.1E-05 | GRIN2B,MYH10,CAMK2A,PPP3R1,GRIA2,PRKACA,SLC8A1,ATP2A2 |
| Clathrin-mediated Endocytosis Signaling | 2.1E-05 | DNM1,AP2M1,CSNK2A1,ACTB,PPP3R1,SH3GL2,DNM1L,AP2A2 |

To complement the IPA analysis and help narrow down the most relevant pathways affected by loss of CR in synapses, we performed a second in silico analysis using the DAVID web tool. Functional Annotation Cluster analysis revealed an enrichment in proteins associated with structures such as vesicles, mitochondria and cytoskeleton (

Table 4.11). Pathways involved in stress response, synaptic transmission and mitochondria oxidative phosphorylation were also found to be enriched in the data-set. Mapping of the data to established KEGG pathways (Table 4.12) revealed proteomic alterations relevant to neurodegenerative diseases such as Parkinson's disease, Alzheimer's disease, Huntington's disease and Amyotrophic Lateral Sclerosis. In addition, mitochondrial and synaptic pathways, such as those involved in oxidative phosphorylation and long-term potentiation, were similarly detected during analysis.

**Table 4.11: Top functional clusters associated with the proteomic changes in CR$^{-/-}$ mice, as identified by DAVID analysis.**

| DAVID Functional Annotation Cluster | p-value |
|---|---|
| Vesicle | 2.57E-10 |
| Mitochondria | 1.38E-08 |
| Nucleotide binding | 1.00E-05 |
| Cytoskeletal part | 4.47E-05 |
| Stress response | 6.92E-05 |
| Synaptic transmission | 7.24E-05 |
| Oxidative phosphorylation | 1.41E-04 |
| Neurofilament | 1.70E-04 |
| Chaperone | 3.02E-04 |
| ATP metabolic process | 7.08E-04 |

**Table 4.12: Top KEGG pathways associated with the proteomic changes in CR$^{-/-}$ mice, as identified by DAVID analysis.**

| DAVID KEGG Pathways | p-value | Molecules |
|---|---|---|
| Parkinson's disease | 6.4E-08 | ATP5J COX5A NDUFB7 UQCRC1 ATP5O SLC25A4 RPS27A SDHB UBA1 ATP5D NDUFS3 NDUFS2 SEPT5 NDUFS6 |
| Alzheimer's disease | 3.9E-07 | MAPT ATP5J GRIN2B COX5A NDUFB7 UQCRC1 ATP5O PLCB1 ATP2A2 SDHB PPP3R1 ATP5D NDUFS3 NDUFS2 |
| Huntington's disease | 4.2E-07 | ATP5J GRIN2B AP2M1 COX5A NDUFB7 UQCRC1 ATP5O SLC25A4 PLCB1 AP2A2 SDHB ATP5D NDUFS3 NDUFS2 |
| Oxidative phosphorylation | 3.0E-06 | ATP6V0D1 ATP5J SDHB NDUFB7 COX5A ATP5D ATP6V0A1 NDUFS2 NDUFS3 UQCRC1 NDUFS6 ATP5O |
| Citrate cycle (TCA cycle) | 1.1E-03 | SDHB ACLY CS SUCLA2 PDHA1 |
| Amyotrophic lateral sclerosis (ALS) | 1.5E-03 | GRIA2 NEFM NEFL GRIN2B NEFH PPP3R1 |
| Butanoate metabolism | 2.1E-03 | BDH1 ACAT1 ABAT HADHA PDHA1 |
| Long-term potentiation | 3.8E-03 | GRIA2 CAMK2A PRKACA PLCB1 GRIN2B PPP3R1 |
| Tight junction | 3.9E-03 | ACTB PPP2R1A CSNK2A1 VAPA SPTBN1 ACTN1 CTNNA2 MYH10 |
| Propanoate metabolism | 9.9E-03 | ACAT1 ABAT HADHA SUCLA2 |
| Prion diseases | 1.5E-02 | STIP1 PRKACA HSPA5 HSPA1B |

Altogether, IPA and DAVID analysis confirmed the involvement of CR in synaptic function and highlighted a role for the protein in mitochondria function and in neurodegenerative conditions, particularly Huntington's disease and neuromuscular disorders. In this thesis, we have previously shown CR is important for the neuromuscular system, in particular to Wallerian degeneration (see Figure 4.4), and

there is published evidence linking CR to Huntington's disease (Dong et al., 2012). Therefore, we decided to focus on the validation of the proteomics results associated with other relevant cellular functions, including how CR may influence synaptic transmission and mitochondria dysfunction.

### 4.3.7. Loss of calretinin increases cell death by oxidative stress

Pathway analysis using IPA indicated the canonical pathway of mitochondrial dysfunction was significantly affected in $CR^{-/-}$ mice (Table 4.10). A prediction analysis, performed on IPA, revealed that $CR^{-/-}$ mice are likely to be more sensitive to oxidative stress than $CR^{+/+}$ mice (Appendix II). To test this hypothesis, we knocked-down (KD) CR in cultured hippocampal neurons and applied an oxidative stress insult. In agreement with the proteomics results, a 20-30% KD of CR resulted in increased cell death caused by acute exposure to $H_2O_2$ (Figure 4.13 B-D). These results indicate that CR plays an important role in the control of oxidative stress and that even a small reduction in CR levels can have significant consequences for cell death pathways.

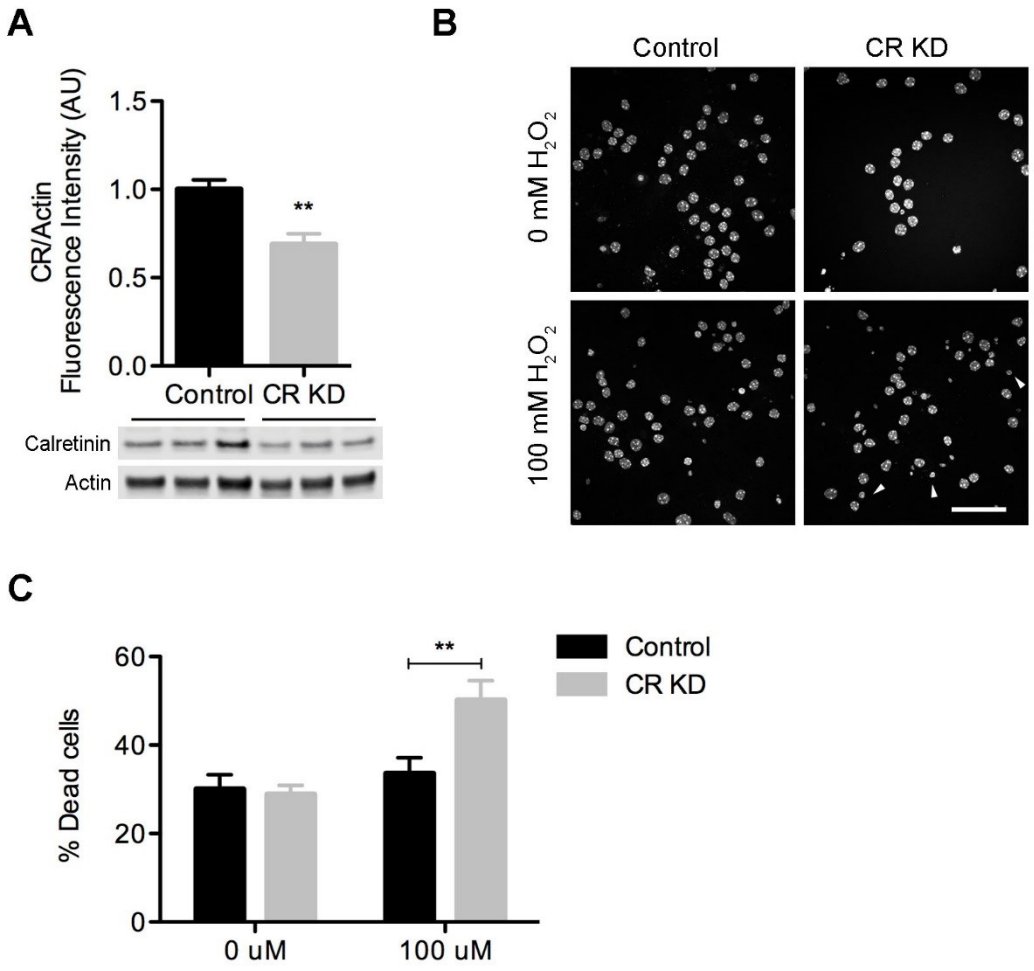


**Figure 4.13: Loss of CR causes mitochondria dysfunction and oxidative stress. A)** Quantification and representative western blots from cell lysates from control and CR KD cultures. 48h KD of CR in hippocampal neurons resulted in a ~25% decrease in the expression of CR. Bars represent mean ± SEM, N=6 across two independent cultures, **p<0.01 unpaired two-tailed t-test. **B)** Representative images from control and CR KD hippocampal neurons exposed to $H_2O_2$. DAPI staining (blue) reveals that CR KD cells are more sensitive to $H_2O_2$ treatment. Note the increase in the fraction of dead cells (collapsed nuclei, indicated by arrow heads) when CR KD cells are exposed to 100 µM $H_2O_2$, but not when control cells are subjected to the same treatment. Scale bar = 50 µM. **C)** Quantification of % dead cells from experiments in C. Bars represent mean ± SEM, N=6 across two independent cultures, **p<0.01 in two-way ANOVA with Bonferroni post-test.

### 4.3.8. Exploring the effect of calretinin on synaptic function

Given the dynamic behaviour of CR during synaptic activity and the strong indication that synaptic functions are affected in $CR^{-/-}$ mice, we wanted to investigate whether manipulating intracellular levels of CR would lead to changes in the dynamics of synaptic vesicle release and recycling. Therefore, we performed Synaptophysin-pHluorin (SypHy; Figure 4.14) experiments in hippocampal cultures where CR had been overexpressed (OE) or knocked-down (KD).

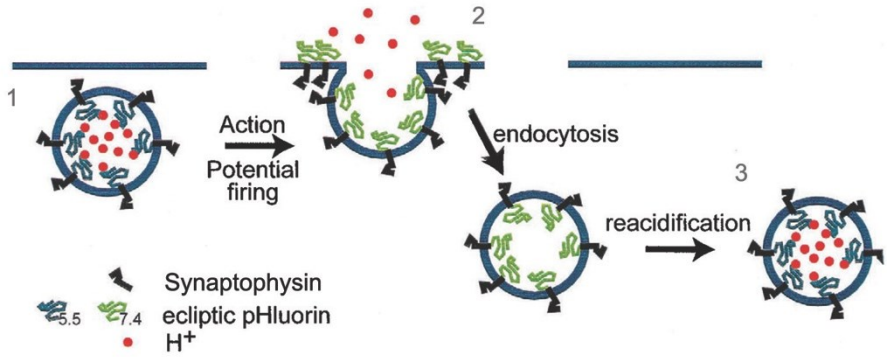


**Figure 4.14: Use of pHluorins for the study of synaptic function.** pHluorins are genetically encoded fluorescent probes that facilitate the study of neurotransmission in live neurons (Burrone et al., 2006, Sankaranarayanan et al., 2000). pHluorins consist of a synaptic vesicle protein, such as synaptophysin, modified to express an intra-luminal pH-sensitive GFP tag. Due to the difference in pH between the lumen of synaptic vesicles and the extracellular medium, pHluorins are used to infer the location of the synaptic protein they encode from fluorescent signals. When in synaptic vesicles, which have an acidic lumen (pH 5.5), pHluorins are quenched (1). However, during the fusion of synaptic vesicles with the plasma membrane after an action potential, pHluorins are exposed to extracellular medium (pH 7.4) and fluoresce (2). Upon vesicle retrieval and reacidification, pHluorins are once more quenched (3). The kinetics of increase and decrease in pHluorin fluorescent signals thus correlates with the kinetics of exo and endocytosis of synaptic vesicles, respectively. Figure adapted from (Sankaranarayanan et al., 2000).

48h KD of CR lead to a 20-30% decrease in the expression levels of CR, consistently across cultures (Figure 4.13 B). SypHy experiments performed in KD and control treated cultures resulted in identical ΔF/F0 traces during a stimulation with 300 action potentials, at 10Hz (Figure 4.15). In addition, the peak fluorescence was comparable between the two conditions (Figure 4.15 C), indicating KD of CR did not produce an observable effect on the extent of exocytosis. When traces were normalized to the peak fluorescence for each condition, which allows us to look at the kinetics of SypHy retrieval, the traces and time constants (τ) of vesicle retrieval following stimulation were identical between CR KD and control neurons (Figure 4.15 D, E). This suggests that modest KD of CR did not affect the kinetics of endocytosis. A similar experiment performed in cultures in which CR was OE, revealed the characteristic pattern of SypHy fluorescence during and following stimulation (Figure 4.16 A, B). The peak fluorescence was similar between cultures treated with CR OE or an empty vector (Figure 4.16 C), as was the kinetics of vesicle retrieval (Figure 4.16 D, E).

Overall, these results indicate that OE and modest KD of CR was not sufficient to induce overt effects on the kinetics of exocytosis or endocytosis in hippocampal nerve terminals during a single stimulation of the readily releasable pool of synaptic vesicles. Nevertheless, these results should be interpreted with care as they don't comprehensively cover the range of synaptic activity patterns characteristic of hippocampal terminals.

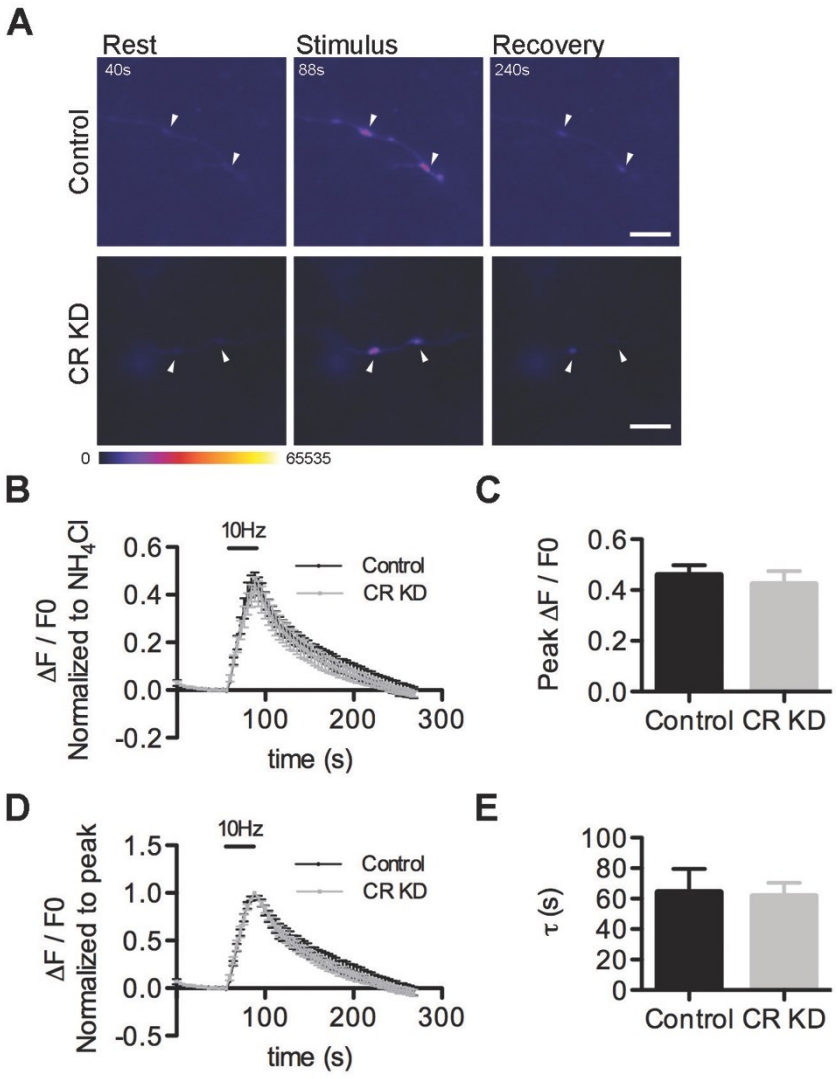


**Figure 4.15: Reduced levels of CR do not affect synaptic vesicle exocytosis or endocytosis. A)** False colour images from SypHy fluorescence in control and CR KD neurons before (Rest) and after (Stimulation) stimulation with 300 action potentials, and over 2 min after stimulation (Recovery). Arrow heads indicate nerve terminals. Scale bar = 5 µm **B)** SypHy traces normalised to the maximum fluorescence obtained with $NH_4Cl$. Traces represent ΔF/F0 mean ± SEM, N=4, p>0.05 two-way ANOVA with Holm-Šídák post-test. **C)** Peak fluorescence during stimulation. ΔF/F0 mean ± SEM, N=4, p>0.05 unpaired two-tailed t-test. **D)** ΔF/F0 traces normalized to peak fluorescence. Traces represent mean ± SEM, N=4, p>0.05 two-way ANOVA with Holm-Šídák post-test. **E)** Time constant (τ) for post-stimulation recovery of fluorescence. Mean ± SEM, N=4, p>0.05 unpaired two-tailed t-test.

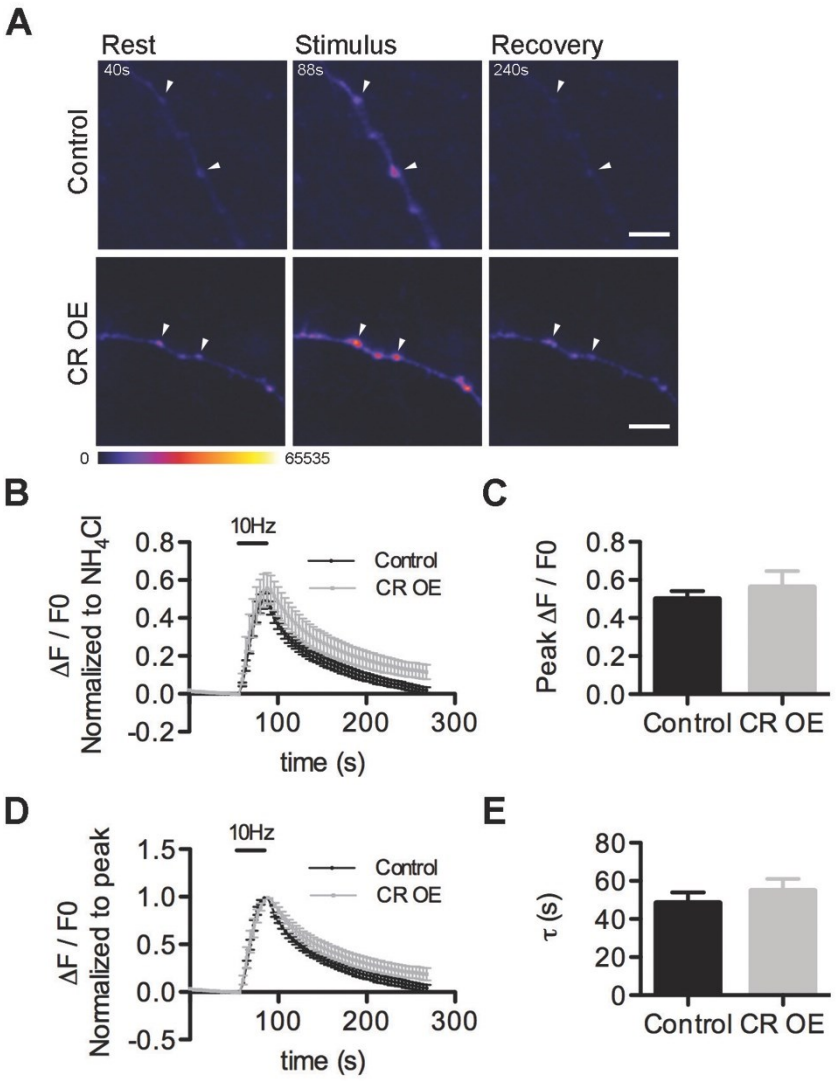


**Figure 4.16: Increased levels of CR do not overtly affect synaptic vesicle exocytosis or endocytosis.** **A)** False colour images from SypHy fluorescence in control and CR OE neurons before (Rest) and after (Stimulation) stimulation with 300 action potentials, and over 2 min after stimulation (Recovery). Arrow heads indicate nerve terminals. Scale bar = 5 µm. **B)** SypHy traces normalised to the maximum fluorescence obtained with $NH_4Cl$. Traces represent ΔF/F0 mean ± SEM, N=5, p>0.05 two-way ANOVA with Holm-Šídák post-test. **C)** Peak fluorescence during stimulation. ΔF/F0 mean ± SEM, N=5, p>0.05 unpaired two-tailed t-test. **D)** ΔF/F0 traces normalized to peak fluorescence. Traces represent mean ± SEM, N=5, p>0.05 two-way ANOVA with Holm-Šídák post-test. **E)** Time constant (τ) for post-stimulation recovery of fluorescence. Mean ± SEM, N=5, p>0.05 unpaired two-tailed t-test.

## 4.4. Discussion

### 4.4.1. Overview of results

CR is a poorly characterized $Ca^{2+}$ binding protein, primarily known for its high levels of expression in a subpopulation of interneurons. However, there have been indications in the literature pointing towards a broader role for CR in the nervous system and, in particular, in neurodegenerative pathways and synaptic stability. In this thesis, we had already shown that calretinin is upregulated in synapses from areas of the brain from CLN5 Batten sheep that are undergoing degeneration (Chapter 3). Here, we extended the influence of CR to the peripheral nervous system and demonstrated that deletion of CR in mice delays the onset of Wallerian degeneration in the peripheral nervous system. In addition, we extended the body of knowledge regarding CR's expression and function in the mouse nervous system. In particular, we have shown CR is not exclusively found in interneurons but that it is also expressed at lower levels in hippocampal neurons and motor axons and synapses from the peripheral nervous system. In addition, in cultured mouse hippocampal neurons, CR is enriched in synaptic terminals, where it has a dynamic role and responds to activity-dependent stimulus. In agreement with our experimental findings throughout the chapter, proteomics analysis of synaptosomes from $CR^{-/-}$ mice revealed a significant role of CR in synaptic and mitochondrial function, in neurodegenerative conditions, such as Huntington's disease, and in neuromuscular disorders. Altogether, we have established that CR is involved in neurodegenerative pathways at the synapse and that it plays an active role during synaptic transmission.

### 4.4.2. CR beyond the interneuron

CR has so far been regarded as merely a protein enriched in a subpopulation of interneurons. However, a recent study has demonstrated the presence of CR in synapses from the mouse corticostriatal system and in *Drosophila* olfactory receptor neurons (Wishart et al., 2012). In this chapter, we have shown CR is highly expressed in tissues from the central and peripheral nervous systems of the mouse (Figure 4.1). In particular, CR is enriched in synaptic sites and is present in motor axons and neuromuscular synapses (Figure 4.3 and Figure 4.8). These findings have important consequences for the study of CR, as they demonstrate that CR is not expressed only in central interneurons and highlight the importance of regarding CR as a potential modulator of neuronal function throughout the CNS and PNS.

### 4.4.3. CR and Wallerian degeneration

The fact that CR is present in motor axons and neuromuscular synapses (Figure 4.3) and the previous findings from (Wishart et al., 2012) indicating loss of CR delayed axonal degeneration in *Drosophila*, prompted us to explore the consequences of CR deletion to Wallerian degeneration in the mouse PNS. We found that $CR^{-/-}$ mice presented a delay in the initial phase of axonal degeneration, as assessed by the preservation of neurofilament structures (Figure 4.4). The initial breakdown of axonal connections was delayed by approximately 3 h, compared to $CR^{+/+}$ mice. From then on Wallerian degeneration progressed along a similar, albeit delayed, time-course independently of the presence or absence of CR. Thus, CR seems to be particularly important in the initial stages of Wallerian degeneration in the PNS. The mechanisms

leading to the delay in Wallerian degeneration in $CR^{-/-}$ mice are not straightforward. Proteomics on CNS synaptosomes indicated loss of CR leads to changes in several cytoskeletal components and protein quality control mechanisms, including proteins of the ubiquitin proteasome system (eg. UCHL3 and UBA1). The combined functional effects of these changes are difficult to predict and to extrapolate to the PNS, although it is conceivable they could culminate in a delay of microtubule disassembly in $CR^{-/-}$ motor axons.

Further experiments are needed to fully understand in which capacity CR influences Wallerian degeneration in the PNS. Nonetheless, these early results are encouraging and confirm that CR plays an active role in neurodegenerative pathways. In addition, IPA analysis was consistent with loss of CR being associated with several neuromuscular and movement disorders (Table 4.9), highlighting the importance of further exploring the role of CR in the PNS.

### 4.4.4. CR and synaptic function

The finding that CR is enriched at hippocampal synapses is of particular interest. It not only provides, for the first time, clear experimental evidence that CR is present in synaptic compartments of neurons, but it also shows that CR is particularly enriched in glutamatergic terminals (Figure 4.7). In addition, using label-free proteomics we identified glutamate receptors as being downregulated in $CR^{-/-}$ synaptosomes (Table 4.8). These facts offer clues towards a possible specialization of CR to meet the demands of excitatory synapses.

Triggering synaptic activity in cultured hippocampal neurons, either via $K^+$ or electrical stimulation, induced the temporary dispersion of CR from synaptic terminals

(Figure 4.9 and Figure 4.10). The reason why this happens in not clear, but it indicates that CR is enriched at synaptic sites during rest periods, where it may help maintain stable low free $Ca^{2+}$ levels and interact with synaptic proteins, such as synapsin 1 and dynamin 1. The functional consequences of these interactions have yet to be explored. The mechanisms leading to the dispersion of CR from synaptic terminals could be directly related to $Ca^{2+}$, since CR changes its conformation and $Ca^{2+}$-binding properties according to the intracellular $Ca^{2+}$ levels (Arendt et al., 2013, Kuznicki et al., 1995). Thus, it is possible that during periods of rest CR acts mainly as $Ca^{2+}$-sensor and is preferentially localised to synaptic sites, where its localisation is possibly maintained by interactions with synaptic or cytoskeletal proteins. Upon arrival of an action potential, and consequent increase in $Ca^{2+}$, CR's conformation may change, altering protein-protein interactions, and CR is allowed to diffuse to areas outside the active zone, where it may buffer excessive $Ca^{2+}$.

Proteomics results revealed an involvement of CR in several steps of pathways involved in neurotransmission. There were changes in proteins associated with exocytosis (eg. syntaxin 1 and syntaxin binding protein 1), endocytosis (eg. AP2 complex and dynamin 1), vesicle reacidification (eg. V-ATPase) and post-synaptic structures (eg. NMDA and AMPA receptors), which illustrate the broad range of influence of CR at the synapse. In addition, signalling proteins, including calcineurin and CaMKIIa, which help regulate synaptic function (Colbran and Brown, 2004, Marks and McMahon, 1998), were downregulated in $CR^{-/-}$ mice. We performed synaptopHluorin experiments in order to try clarify the contribution of CR to synaptic transmission (Figure 4.15 and Figure 4.16). However, the experiments were inconclusive. Although it was clear that CR is not required for synaptic transmission,

as expected from previous publications (Schurmans et al., 1997), we tested only a very specific stimulation paradigm, which is meant to stimulate the release of vesicles from the readily releasable pool. In addition, our levels of KD and OE might not have been sufficient to trigger a phenotype. To fully address possible effects of CR in the synaptic vesicle cycle, a more thorough study is therefore needed. Unfortunately, due to time constraints and low availability of animals, further synaptoHluorin experiments, including experiments in $CR^{-/-}$ mice, were not possible.

Altogether, the work in this chapter presents novel exciting evidence highlighting the enrichment of CR in synaptic terminals, its dynamic behaviour during synaptic activity and its contribution to synaptic function pathways.

### 4.4.5. Further insights into CR's function from label-free proteomics

The function of CR, besides its calcium buffering capabilities, is very poorly understood. Using label-free proteomics we were able to uncover some of the key cellular pathways CR might be involved in. Whether these are a direct consequence of loss of CR functional interactions or a result of impaired $Ca^{2+}$ handling, remains to be addressed. Nonetheless, our results indicate CR participates, directly or indirectly, in important pathways for maintaining neuronal homeostasis.

As expected, one consequence of the loss of CR would be poorer intracellular $Ca^{2+}$ handling, with consequent increases in the vulnerability of cells to $Ca^{2+}$ overload, poorer $Ca^{2+}$ buffering by the ER and mitochondria, possibly leading to dysfunction in these organelles, and impairments in $Ca^{2+}$-dependent signalling pathways. Indeed, we

found several such signalling molecules with altered expression in $CR^{-/-}$ mice, including calnexin, calcineurin and CaMKIIa (Table 4.8), as well as impairments in mitochondria function (Table 4.10 and Table 4.12). We were particularly interested in the proteomic changes in $CR^{-/-}$ mice which were consistent with impairments seen in neurodegenerative conditions, including Huntington's disease, Parkinson's disease and Alzheimer's disease. Interestingly, the changes associated with these conditions were related with alterations in mitochondrial proteins, structural and cytoskeletal components and protein quality control mechanisms (Table 4.9 and Table 4.12). As previously discussed (see General Introduction), these cellular pathways are important for maintaining neuronal and synaptic homeostasis.

We have shown that reduced levels of CR increased the sensitivity of cells to oxidative stress (Figure 4.13). This property of CR is likely to have practical consequences for neurodegenerative conditions where mitochondria dysfunction and oxidative stress are part of the pathophysiology of the disease (Lin and Beal, 2006). In fact, it has previously been shown that overexpression of CR was protective against oxidative stress in a cell model of Huntington's disease (Dong et al., 2012). The pathways of ubiquitin-proteasome system and the unfolded protein response are also likely to be important for the influence of CR in neurodegeneration. Proteins involved in ER function and the unfolded protein response (eg. calnexin and HSPA5/Grp78) are down-regulated in $CR^{-/-}$ mice, suggesting an inhibition of the ER unfolded protein response responsible for the correct folding of newly secreted proteins (Walter and Ron, 2011). On the other hand, components of the ubiquitin proteasome system (eg. UBA1 and UCHL3) are similarly down-regulated. A combination of impaired protein folding and reduced protein degradation could promote the accumulation of misfolded

proteins in $CR^{-/-}$ mice and the formation of intracellular aggregates, with consequences for neurodegenerative conditions such as Parkinson's disease and Huntington's disease (Scheper and Hoozemans, 2015). Similarly, an increase in CR expression, as has been shown in CLN5 Batten sheep, could aggravate ER stress and potentiate the activation of apoptotic mechanisms (Merksamer and Papa, 2010).

Altogether, the proteomics results highlight the importance of CR across several cellular pathways, including synaptic, mitochondria and ER function, as well as the regulation of cytoskeletal components. In addition, the overall results in this chapter demonstrate that CR is important beyond the interneuron and open several routes to better investigate the function of CR and how it contributes to neuronal homeostasis and neurodegeneration.

# Chapter 5. Identification of sfxn3 as a novel α-synuclein-dependent mitochondrial protein involved in the maintenance of synaptic stability

## 5.1. Introduction

### 5.1.1. α-synuclein in neurodegenerative disorders

α-synuclein belongs to a family of proteins primarily expressed in nervous tissue, which includes α-, β- and γ-synucleins (Clayton et al., 2007, Pears et al., 2007). Due to its involvement in neurodegenerative diseases α-synuclein is the most studied protein of the synuclein family. α-synuclein was identified as the non amyloid-β component of amyloid plaques in Alzheimer's disease (Iwai et al., 1995, Ueda et al., 1993) and is the main component of Lewy bodies and Lewy neurites (Baba et al., 1998, Mezey et al., 1998). Lewy bodies are abnormal protein inclusions characteristic of a group of disorders collectively known as Lewy body diseases or synucleinopathies, which include dementia with Lewy bodies, PD and Multiple System Atrophy (Pollanen et al., 1993). Moreover, α-synuclein has been implicated as a genetic cause of Parkinson's disease, with mutations and multiplications of the *SNCA* gene that encodes α-synuclein being associated with familial cases of the disease (Chartier-Harlin et al., 2004, Krüger et al., 1998, Polymeropoulos et al., 1997, Singleton et al., 2003, Zarranz et al., 2004).

### 5.1.2. Structure of α-synuclein

α-synuclein is a 140 amino acid protein encoded by the *SNCA* gene. It presents a dynamic conformational structure which is believed to contribute to its pathological features (Burre et al., 2013, Mor et al., 2016). There are three well defined domains in the sequence of α-synuclein (Figure 5.1 A): 1) an N-terminal region with membrane-binding properties responsible for α-synuclein binding to synaptic vesicles and mitochondrial membranes; 2) a central domain which includes the non-amyloid-β-component (NAC) sequence required for protein aggregation; 3) and a soluble acidic C-terminal region through which α-synuclein interacts with other proteins (Mor et al., 2016).

Due to its conformational plasticity, α-synuclein has been shown to adopt several conformations and to assemble in multimeric and fibril-like structures (Figure 5.1 B). α-synuclein is natively unfolded but has the ability to bind lipid membranes and other proteins. These interactions, required for the physiological functions of the protein, alter its structure and stabilize it in monomeric or functional multimeric forms (Bartels et al., 2011, Burre et al., 2014, Davidson et al., 1998, Wang et al., 2011). However, when α-synuclein is predominantly unbound in solution, it readily forms oligomers and aggregates over time (Burre et al., 2013). In addition, point mutations and post-translation modifications, such as phosphorylation and ubiquitination, affect the stability of the protein and potentiate the formation of aggregation-competent species (Burre et al., 2012, Lee et al., 2008a, Ono et al., 2011, Paleologou et al., 2010). α-synuclein oligomers act as seeds for the aggregation process and have the ability to spread between cells in a prion-like manner (Luk et al., 2012, Luk et al., 2009, Nonaka et al., 2010). As oligomers increase in size, they eventually form amyloid-like fibril

structures and aggregate into large protein inclusions, giving rise to Lewy Bodies (Mor et al., 2016).

The high conformational flexibility of α-synuclein makes it prone to being structurally unstable, with devastating consequences for cell homeostasis (see below). As a result, it is believed that the levels of α-synuclein need to be tightly regulated, through control of protein synthesis and degradation, so as to avoid instigating the formation of toxic species (Lashuel et al., 2013, Mor et al., 2016).

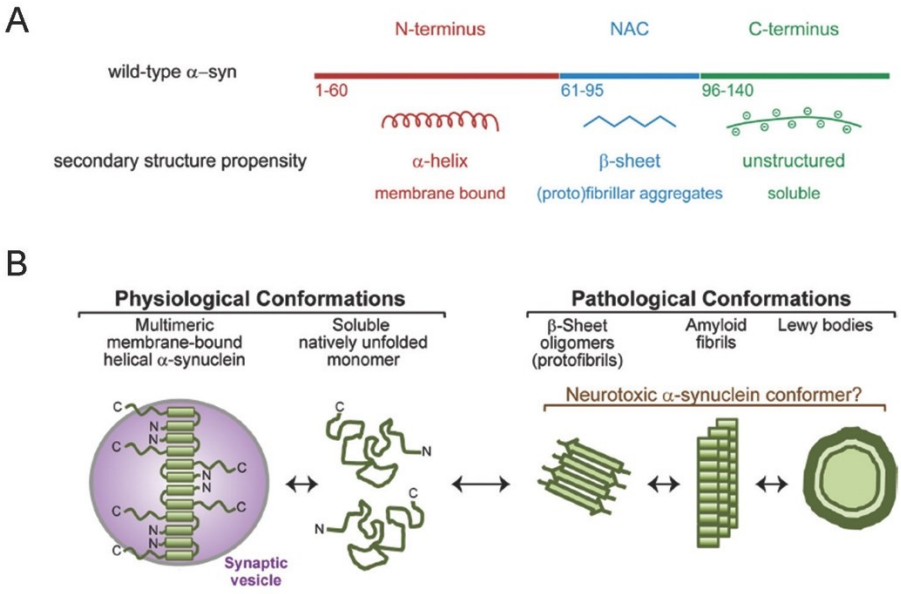


**Figure 5.1: Conformation of α-synuclein. A)** There are three main regions in the α-synuclein protein: i) the N-terminus of α-synuclein adopts an α-helix conformation upon binding to lipid membranes; ii) the NAC region can adopt a β–sheet structure and is required and sufficient for the formation of protein aggregates; iii) the C-terminal region is unstructured and participates in protein-protein interactions. Image adapted from (Vamvaca et al., 2009). **B)** α-synuclein can adopt physiological and pathological conformations. Unfolded monomers and membrane-bound multimers are associated with the physiological functions of the protein. β–sheet oligomers, amyloid fibrils and Lewy bodies are considered pathological species as they are associated with the neurotoxic effects of α-synuclein. Image adapted from (Burre et al., 2015).

### 5.1.3. Mechanisms of α-synuclein toxicity

The strong evidence indicative of a detrimental effect of α-synuclein inclusions *in vivo* lead to the study of the toxicity of its overexpression and aggregation. It has been demonstrated that accumulation of α-synuclein aggregates is neurotoxic both *in vivo* and *in vitro*, with misfolded α-synuclein interfering with various cellular mechanisms, such as mitochondrial function, proteasomal activity, vesicle trafficking and synaptic transmission (Burre, 2015, Haelterman et al., 2014, Lashuel et al., 2013, Stefanis, 2012).

Although a hallmark of the neurodegenerative processes in synucleinopathies, the presence of α-synuclein inclusions in neurons is not the only cause of pathology. In fact, several studies indicate that soluble oligomers of α-synuclein are more toxic than insoluble aggregates. For instance, stereotaxic lentiviral injection of α-synuclein variants prone to the formation of oligomers, rather than fibrils, results in more severe loss of dopaminergic neurons in rat models (Winner et al., 2011), modest overexpression of α-synuclein without formation of inclusions impairs synaptic functions (Nemani et al., 2010, Scott et al., 2010), and soluble α-synuclein oligomers, but not fibrils, promote dysfunction of mitochondrial complex I (Luth et al., 2014). From a disease-related perspective, it has been proposed that Lewy bodies may develop as a protective mechanism from the damaging effects of misfolded α-synuclein. However, not only fibrils but also monomeric α-synuclein is sequestered into Lewy bodies, which may in turn aggravate neuronal dysfunction by loss of physiological pools of the protein (Kollmann et al., 2013, Qiao et al., 2008). Thus, it is important we clarify not only the mechanisms associated with the pathological

features of α-synuclein, but also how, in its functional form, this protein might contribute to neuronal homeostasis.

### 5.1.4. α-synuclein contributes to synaptic function and stability

Knockout studies in mice revealed that α-synuclein is not essential for the structural development of the CNS nor required for synaptic transmission (Abeliovich et al., 2000, Cabin et al., 2002). Instead, it seems to play a more long-term modulatory role, being involved in the regulation and maintenance of synaptic function. In nerve terminals, α-synuclein contributes to the regulation of synaptic vesicle recycling and mobility. Deletion or ablation of α-synuclein expression in mice has been shown to impair neurotransmitter release during prolonged repetitive stimulation and to reduce the availability of synaptic vesicles from the reserve pool (Cabin et al., 2002, Murphy et al., 2000). On the other hand, overexpression of α-synuclein inhibits neurotransmission and intersynaptic trafficking of vesicles (Nemani et al., 2010, Scott and Roy, 2012). In addition, α-synuclein affects dopamine metabolism. It interacts with tyrosine-hydroxylase and acts as a negative regulator of dopamine biosynthesis, so that increased levels of α-synuclein result in decreased production of this neurotransmitter (Liu et al., 2008, Perez et al., 2002). Moreover, α-synuclein is believed to modulate the function of the dopamine transporter DAT, although through unknown mechanisms, and to affect the density and activity of the vesicular dopamine transporter VMAT2 (Butler et al., 2015, Guo et al., 2008).

The best characterized synaptic function of α-synuclein is, however, associated with its role in the regulation of neurotransmission by promoting SNARE-complex assembly (Burre et al., 2010, Chandra et al., 2004b). The chaperone activity of α-

synuclein seems to be particularly important for neuronal homeostasis, as it rescues the extensive neurodegenerative phenotype caused by deletion of CSP-α (Chandra et al., 2005), which is mediated by SNAP-25 activity (Sharma et al., 2012). In addition, triple knockout of all the proteins from the synuclein family leads to an age-dependent neurodegenerative phenotype due to the destabilization of SNARE complexes (Burre et al., 2010).

Further evidence for a neuroprotective role of α-synuclein comes from various studies not restricted to its chaperone function. For instance, deficit of α-synuclein expression was found to induce nigrostriatal degeneration *in vivo* (Al-Wandi et al., 2010, Gorbatyuk et al., 2010), to reduce cell viability in cultured cerebellar granule neurons (Monti et al., 2007) and to lead to age-dependent deficits in dopamine metabolism (Al-Wandi et al., 2010). In addition, knock-down or loss of α-synuclein aggravates the neurodegeneration caused by various stimuli, such as oxidative stress (Quilty et al., 2006), 6-hydroxydopamine toxicity (Monti et al., 2007) and even transgenic expression of mutant A53T α-synuclein (Cabin et al., 2005).

The evidence supporting the toxicity of α-synuclein overexpression and aggregation contrasts with the reports of its neuroprotective action. The dual function of α-synuclein suggests a distinct nature of its pathological and physiological functions, which is supported by the fact that the amino acid sequences responsible for α-synuclein toxicity and chaperone function have been mapped to different regions of the protein (Burre et al., 2012). Given the current efforts to develop therapeutic strategies that reduce α-synuclein aggregation and/or expression for the treatment of

Parkinson's disease and related disorders it is essential we clarify the physiological role of this critical protein at the synapse.

### 5.1.5. Aim

α-synuclein is a well known regulator of synaptic stability and its contribution not only to the neuropathology of disorders such as Parkinson's disease, but also to global mechanisms impacting on synaptic stability, makes it an extremely significant field to study. Importantly, α-synuclein itself is difficult to target therapeutically due to its conformational flexibility and to our current poor understanding concerning how to achieve a compromise between the physiological and neurotoxic effects of the protein (Lashuel et al., 2013). By improving our fundamental understanding about α-synuclein one might expect to reveal pathways downstream of this protein that contribute to the maintenance of synaptic stability. These pathways could, in theory, be more attractive targets for developing synaptoprotective therapies. Thus, the aim of this chapter was to:

- Identify new targets of α-synuclein function at the synapse;
- Explore one downstream target of α-synuclein, sideroflexin 3, and validate its ability to independently regulate synaptic morphology and stability.

## 5.2. Materials and Methods

### 5.2.1. Animals

C57Bl/6J (α-syn$^{+/+}$) and C57Bl/6JOlaHsd mice (α-syn$^{-/-}$), which carry a natural α-synuclein deletion (Specht and Schoepfer, 2001), were obtained directly from the University of Edinburgh managed rodent colonies. Sfxn3$^{tm1b(KOMP)Wtsi}$ mice (sfxn3$^{-/-}$ mice; http://www.mousephenotype.org/data/genes/MGI:2137679) were obtained from the Wellcome Trust Sanger Institute Mouse Genetics Project as part of the nPad MRC Mouse Consortium, and maintained on a C57Bl/6N background. All rodents were kept under standard husbandry conditions in animal facilities at the University of Edinburgh. Mice used for experiments were of mixed gender and 2 to 4 months old. All animal work was covered by appropriate licenses from the UK Home Office and approved by the University of Edinburgh Veterinary Services. All animals were sacrificed by Schedule 1 methods, either by cervical dislocation or overdose of anaesthetic by inhalation of isoflurane.

### 5.2.2. Genotyping

Genomic DNA was extracted as described in the General Materials and Methods. Details of the primers, reaction mixes and PCR programs used can be found in Table 5.1, Table 5.2 and Table 5.3, respectively.

**Table 5.1: Primers used for genotyping of sfxn3 mice.**

| Primer | Sequence 5' - 3' | Size bp |
|---|---|---|
| Common Forward | GGATCTGAGGACATTTGGGC | |
| WT Reverse | CTGGGCAAAGGATCAGGAAG | 344 |
| KO Reverse | TCGTGGTATCGTTATGCGCC | 133 |

**Table 5.2: PCR reagent mix.**

| Reagent | µl per 1 reaction |
|---|---|
| $ddH_20$ | 8.9 |
| 5x Green GoTaq Flexi Buffer (Promega) | 3.5 |
| MgCl2 25mM (Promega) | 0.9 |
| dNTP mix 10mM (Invitrogen) | 0.4 |
| Forward Primer 10µM | 0.7 |
| Reverse Primer 1 10µM | 0.7 |
| Reverse Primer 2 10µM | 0.7 |
| GoTaq Flexi DNA polymerase (Promega) | 0.2 |
| DNA | 2 |
| Total | 18 |

**Table 5.3: PCR program for genotyping of $Sfxn3^{-/-}$ mice.**

| Step | Temperature (°C) | Time |
|---|---|---|
| 1. Separation | 94 | 5 min |
| 2. Denaturation | 94 | 30 sec |
| 3. Annealing | 58 | 45 sec |
| 4. Polymerization | 72 | 45 sec |
| Repeat 2-4 34x | | |
| 5. Final | 72 | 5 min |
| | 12 | ∞ |

### 5.2.3. Peripheral nerve lesions

Peripheral nerve lesions were performed as described in Chapter 4, in mice 2-3 month old. Briefly, mice were kept under anaesthesia by delivery of isoflurane via a face mask. A small incision was made at the level of the sciatic notch and a 1-2mm section of the sciatic nerve was removed. Following surgery all mice received an intramuscular injection of 4 mg/kg of the analgesic Rimadyl® and were allowed free access to food and water. Mice were sacrificed 12 hours to 6 days post-injury (12hpi to 6dpi). To ensure comparability of results extra care was taken regarding the

precision of the time point of analysis, anatomical location of the lesion and age of the mice.

### 5.2.4. Immunohistochemistry of neuromuscular junctions in lumbrical muscles

Immunostaining of lumbrical muscles was performed as described in Chapter 4, with minor modifications to account for the fact that younger mice were used. Lumbrical muscles were dissected in PBS, fixed in 4% PFA in PBS for 20 min, permeabilised in 4% Triton X-100 in PBS for 90 min and blocked in 2% Triton X-100 with 4% w/v BSA in PBS for 30 min. 2H3 and SV2 primary antibodies were incubated in block for 48 h at 4°C and secondary antibodies were applied for 2 h at RT, in PBS. Muscles were then exposed to 1.25 μg/ml α-BTX in PBS for 10 min and mounted in Mowiol on glass slides.

### 5.2.5. Electron microscopy

Electron microscopy on sciatic nerves was performed as described in (Hunter et al., 2014). Immediately after sacrifice at 6dpi, sciatic nerves distal from the site of lesion and equivalent nerve portion from the contralateral uninjured limb were dissected in PBS and fixed in 4% PFA and 2.5% glutaraldehyde in phosphate buffer (0.1 M $Na_2HPO_4$, pH 7.4) for 48 h at 4°C. Nerve preparations were post-fixed in 1% osmium tetroxide (Electron Microscopy Sciences) for 30 min and dehydrated in an ascending alcohol series which included a 40 min treatment with 1% uranyl acetate in 70% ethanol. The nerves were incubated in propylene oxide for 1 h and embedded in

Durcupan resin. Ultra-thin transverse sections (~90 nm) were cut, collected in formvar-coated grids (Agar Scientific, UK) and stained with lead citrate (68 mM lead nitrate, 137 mM tri-sodium citrate, 160 mM NaOH) before imaging in a Philips CM12 transmission electron microscope.

### 5.2.6. Axonal and neuromuscular junction measurements

For quantitative measurements of axonal parameters all electron micrographs were taken at 1150x magnification. A minimum of 100 myelinated axons per mouse from 5 images of randomly selected areas were analysed manually using ImageJ software, as described in (Sherman et al., 2012). Axon calibre and g-ratio were measured by manually drawing a line along the inner and outer borders of the myelin sheath of an axon. The perimeter of the lines drawn was measured and the axon calibre calculated as the diameter of a circular object with the same perimeter as the inner border. g-ratio was calculated as the fraction between the perimeters of the outer and inner borders.

Neuromuscular measurements were obtained from individual endplates and muscle fibres from lumbrical muscles imaged at 40x magnification on an Olympus IX71 microscope. Images were captured by a chilled CCD camera (Hammamatsu C4742–96–12G04) and used for manual measurements on ImageJ, as described in (Murray et al., 2008). Measurements were taken from at least 50 endplates and 50 individual muscle fibres from each of 4 lumbrical muscles per mouse.

### 5.2.7. Quantification of axonal and synaptic degeneration

Axonal degeneration was assessed in electron micrographs by quantifying the percentage of axons from injured sciatic nerves at 6dpi that fell into each of one of five degeneration categories: 1 *No degeneration*: axon and myelin sheath appear intact; 2 *Early degeneration*: myelin sheath is intact but the cytoplasm of the axon is becoming electron dense or its neurofilament distribution looks disorganized; 3 *Intermediate degeneration*: myelin sheath is mostly intact but the axon is clearly affected; 4 *Advanced degeneration*: myelin sheath is becoming loose and the axon is clearly affected; 5 *Complete degeneration*: myelin sheath is completely degraded and it is not possible to distinguish the frontiers of the axon and myelin sheath. Degeneration categories were defined based on the observations from (Beirowski et al., 2004). For each individual mouse, a minimum of 100 axons were analysed and the percentage of each category was calculated from the pooled counts from 10 images from randomly selected areas of a section.

Synaptic degeneration at the NMJ following sciatic nerve transection was manually assessed by quantifying the percentage of intact and degenerated NMJs in deep lumbrical muscles, as described in (Murray et al., 2008). The criteria used to quantify synaptic degeneration was as follows: intact NMJs had endplates fully occupied by pre-synaptic structures and were connected to intact axons; degenerated NMJs included fragmented NMJs, which showed occupied endplates but were not connected to an axon or the latter was fragmented, and vacant NMJs, which had no connected axons and did not colocalize with pre-synaptic structures. Over 100 NMJs from each of 4 lumbrical muscles per mouse were quantified. Quantification was

performed at 40x magnification on a Nikon eclipse 50i microscope with double filter. Representative images were captured in a Zeiss LSM 710 confocal microscope.

For quantification of both axonal and synaptic degeneration at least 3 mice were used per genotype and the analysis was performed with the operator blind to the identity of each image.

### 5.2.8. Proteomics by isobaric Tag for Relative and Absolute Quantitation (iTRAQ)

iTRAQ proteomics and data analysis were performed as previously described (Roche et al., 2014, Wishart et al., 2012). Crude synaptosomes (see General Materials and Methods) from α-syn$^{+/+}$ and α-syn$^{-/-}$ mice were homogenized in iTRAQ extraction buffer (6 M Urea, 2 M thio-urea, 2% CHAPS, 0.5% SDS, 10% protease inhibitors) and centrifuged for 25 min at 20,000g, 4°C. The supernatants from extracts from 4 mice per genotype were pooled together and 100 µg of protein, as determined by BCA assay, were sent for isobaric tag for relative and absolute quantitation (iTRAQ) analysis at Dundee Fingerprints Proteomics (University of Dundee, UK). 100 µg of protein was labelled with tags: 114 and 116 α-syn$^{+/+}$; 115 and 117 α-syn$^{-/-}$ and following processing were injected onto an Ultimate RSLC nano UHPLC system coupled to a LTQ Orbitrap Velos Pro (Thermo Scientific). Results were filtered to only include those proteins that were identified by at least 2 unique peptides and demonstrated a ≥15% change in protein levels in both α-syn$^{+/+}$ vs α-syn$^{-/-}$ comparisons.

iTRAQ proteomics results were examined using three software packages for *in silico* analysis: Database for Annotation, Visualization and Integrated Discovery (DAVID; National Institutes of Health, USA); Ingenuity Pathway Analysis (IPA;

QIAGEN) and VarElect (LifeMap Sciences, USA). More information on these tools can be found on Chapter 4 and at *http://www.ingenuity.com*, *http://david.abcc.ncifcrf.gov* and *https://ve.genecards.org*, respectively.

The iTRAQ results of the proteins with altered expression in α-syn$^{-/-}$ synapses were submitted to the IPA and DAVID software. We used the IPA software to determine the molecular pathways (Top Canonical Pathways) and disorders (Top Diseases and Disorders) most affected by loss of α-synuclein, as described in Chapter 4. DAVID gene ontology (GO) analysis was used to assess the enrichment of GO terms in the samples analysed. Statistical analysis was performed by the software using the Exact Fisher's Test. The VarElect web tool uses information from the GeneCard and MalaCards databases to relate genes to phenotypes and disease terms. This tool was used to select the fraction of the proteomics data that included proteins associated with the terms "mitochondria" and the group of terms "Parkinson's", "Parkinson", "PD", "synuclein" and "SNCA".

### 5.2.9. Culture of SH-SY5Y cells

SH-SY5Y cells stably transfected with WT human α-synuclein were obtained from Dr. Tilo Kunath (University of Edinburgh). Briefly, SH-SY5Y cells were electroporated with a Tet-OneTM plasmid (Clontech) encoding full-length human α-synuclein and a DOX-responsive clonal line was selected and maintained in complete culture media consisting of high-glucose DMEM media supplemented with 10% v/v FBS, 10 U/ml Penicillin/Streptomycin, 2 mM L-Glutamine, 1 mM Sodium Pyruvate and 2 μg/μl puromycin to select for stably transfect cells. Cells were maintained in an undifferentiated state and split every 3-5 days. Cells plated at a density of $10^4$ cells/cm$^2$

in uncoated plates or glass coverslips were differentiated in culture media with 10 µM Retinoic Acid for 5 days, with 50% of media changed at day 3. Following differentiation cells were washed twice with warm DMEM media and cultured thereafter in DMEM media supplemented with 1% Penicillin/Streptomycin and 2 µg/µl puromycin. For induction of α-synuclein expression, culture media was supplemented with 10 µg/ml of Doxycycline.

### 5.2.10. Isolation of mitochondria

Crude mitochondria were purified from fresh mouse brain tissue using the Mitochondria Isolation Kit for Tissue (ab110169, abcam) following the manufacturer's instructions.

### 5.2.11. Fractionation of mitochondria

Fractionation of mitochondria was performed as described in (Nishimura et al., 2014). Undifferentiated SH-SY5Y cells cultured to 80-90% confluency on a T175 flask were harvested and washed in ice-cold PBS. The cell pellet was resuspended in 5 ml of Mitochondria Isolation Buffer (210 mM Mannitol, 70 mM Sucrose, 3 mM HEPES-KOH pH 7.4, 0.2 mM EGTA, protease inhibitors) and the cells disrupted by homogenization with 50-60 up-and-down strokes on a pre-chilled glass Dounce homogeniser. The homogenate was layered on an equal volume of 340 mM sucrose and centrifuged at 500g for 10 min at 4°C. The supernatant, now free of unbroken cells and nuclei, was centrifuged at 10,000g for 10 min at 4°C to recover mitochondria as a pellet. The mitochondria were resuspended in approximately 10 volumes of 0.15

mg/ml digitonin in Mitochondria Isolation Buffer, incubated on ice for 15 min, vortexing sporadically, and centrifuged at 10,000g for 10 min at 4°C. The solubilized outer mitochondrial membrane was recovered in the supernatant. The pellet, which contains mitoplasts (mitochondrial matrix encapsulated by the inner mitochondrial membrane) was resuspended in RIPA buffer, incubated on ice for 20 min and centrifuged at 20,000g for 20 min at 4°C to solubilize the inner mitochondrial membrane and matrix proteins.

### 5.2.12. Isolation of purified synaptosomes

For use in mitochondria respiration assays, purified synaptosomes were isolated from fresh brain tissue, using a protocol adapted from (Choi et al., 2009, Dunkley et al., 2008). A freshly dissected whole brain from an adult mouse was homogenized in 20 ml of ice-cold Isolation buffer (225 mM Sucrose, 74 mM Mannitol, 1 mM EGTA, 5 mM HEPES, pH 7.4) using a PTFE dounce homogenizer, divided in two centrifuge tubes and centrifuged at 1,000g for 10 min at 4°C. For each tube, the supernatant was transferred to a new tube and the pellet resuspended in 10 ml of Isolation buffer and centrifuged as before. The supernatants were combined and centrifuged at 21,000g for 10 min at 4°C. The pellet was resuspended in 5 ml of 3% Percoll (GE Healthcare) in Isolation Media and carefully layered on top of a discontinuous Percoll gradient (layers of 24% and 10% Percoll in Isolation Media) in 50 ml open top centrifuge tubes. The gradients were centrifuged at 30,750g for 9 min at 4°C, with minimum acceleration and no deceleration on JA-25.50 fixed angle rotor in a Beckman Avanti JA-25 centrifuge. Following the centrifugation in Percoll gradients, synaptosomes were recovered from the band between 10% and 24% Percoll,

washed in 10 ml of ice-cold Ionic Media (140 mM NaCl, 20 mM HEPES, 1.2 mM Na2HPO4, 1 mM MgCl2, 5 mM NaHCO3, 5 mM KCl, 10 mM Glucose, pH 7.4) and centrifuged at 20,000g for 15 min at 4°C. The pellets from the duplicate preparations from the same animal were combined and resuspended in 2 ml Ionic Media. The protein concentration of the samples was determined using BCA assay.

### 5.2.13. Mitochondrial Respiration Assays

Measurements of mitochondria respiration rates were performed as described in (Choi et al., 2009, Subramaniam et al., 2014). 10 μg of synaptosomes per well (≥5 technical replicas per sample) were loaded into wells of XF$^e$24 V7 (Seahorse Biosciences) uncoated plates. The plate was centrifuged at 2,000g for 20 min at 4°C and 500 μl of Incubation Media (120 mM NaCl, 3.5 mM KCl, 1.3 mM CaCl2, 0.4 mM KH2PO4, 1.2 mM Na2SO4, 2 mM MgSO4, 4 mg/ml fatty-acid free bovine serum albumin, 15 mM Glucose, 10 mM pyruvate, 37°C) were added to each well prior to loading the cartridge into the XF$^e$24 Seahorse Analyzer (Seahorse Biosciences), according to the manufacturer's instructions. Oxygen consumption rates (OCR) were measured in groups of 2 cycles of 1 min wait, 1 min mix, 3 min measurements, with sequential injections between each 2 cycles. The pattern of injections followed protocols for two different assays. In the coupling assay, samples were sequentially exposed to 4 μg/ml oligomycin (Oligo), 4 μM FCCP (FCCP) and 4 μg/ml antimycin A (AA); in the electron flow assay, sequential injection of 2 μM rotenone (Rot), 10 mM succinate (Succ), 4 μg/ml antimycin A (AA) and 0.1 mM TMPD with 10 mM Ascorbate (TMPD), all in the presence of 4 μM FCCP. Immediately before and after the Seahorse runs, all wells were screened under a light microscope for signs of

detached synaptosomes. Any wells with areas of detachment were discarded from further analyses.

For data analysis, OCR values for each injection step were calculated as the mean of the measurements of 2 cycles. Parameters for the coupling assay were calculated as follows: *Basal*: respiration before addition of any compound; *ATP linked respiration*: Basal– Oligo; *Spare capacity*: FCCP – Basal; *Maximum capacity*: FCCP – AA; *Leak respiration*: Oligo – AA; *Non-mitochondrial respiration*: AA. Respiration driven by individual mitochondrial complexes was inferred for the OCR values from the Electron Flow Assay as follows: *Basal*: uncoupled respiration before addition of any compound; *Complex I*: Basal respiration – Rot; *Complex II/III*: Succ – Rot; *Complex IV*: TMPD – AA.

### 5.2.14. Mitochondrial enzymatic activity assays

The enzymatic activity of the mitochondrial Complex I and Complex IV was determined using the Complex I Enzyme Activity Microplate assay kit (ab109721, abcam) and Complex IV Rodent Enzyme Activity Microplate Assay Kit (ab109911, abcam), respectively. Frozen purified synaptosomes were thawed on ice, centrifuged at 20,000g for 5 min at 4°C and processed according to the manufacturer's instructions for each kit. Briefly, synaptosomes were lysed with 1% Lauryl Maltoside in the specific buffer of each assay, 25 µg (Complex I) or 75 µg (Complex IV) of protein was loaded onto the microplate wells and incubated for 3 h at RT (Complex I) or overnight at 4°C (Complex IV). Following two washes, the wells were loaded with assay solution and the absorbance read at 450 nm (Complex I) or 550 nm (Complex IV) on a GloMax (Complex I) or BioTek (Complex IV) microplate reader. All samples

were run in duplicates. The rate of change in optic density (OD) was calculated for each sample and normalized to the amount of protein in each well, as determined by BCA assay at the end of the experiment.

### 5.2.15. Drosophila

*Drosophila melanogaster* flies were raised on standard cornmeal food at room temperature. The elav-Gal4 and GMR-Gal4 driver strains were used with stocks obtained from the Bloomington Drosophila stock centre (IDs: Canton-S; $y^{1}$ $w^{67c23}$; P(EPgy2)CG6812$^{EY02703}$; CG6812$^{KK102815}$). Crosses were maintained at 22°C for 24 h before removal of adults and embryos were incubated in a water bath to increase levels and activity of the Gal4 proteins. Incubation temperatures were 25 or 30°C for low dose Tg(-OE/KD) or high dose Tg(+OE/KD), respectively.

For immunohistochemistry analysis of NMJs, third instar larvae were dissected and fixed in Bouin's fixative (15:5:1 of saturated picric acid, 37% formaldehyde and glacial acetic acid) for 10 min. Fixed larvae were extensively washed in PBST (PBS with 0.1% TritonX-100) and blocked in 10% normal goat serum (Jackson ImmunoResearch) in PBST for 2 h at RT. Anti-HRP antibody was incubated overnight at 4°C and Cy3 secondary antibody was applied for 2 h at RT. Between incubations larvae were extensively washed in PBST. Fully stained preparations were mounted on glass slides in Vectashield antifade medium (Vector Laboratories). The NMJs on muscle 12 and on muscle 6/7 on segment 3 of both hemisegments of each larvae were imaged on Zeiss LSM 710 confocal microscope. Z-stacks were acquired at 0.5 μm steps at 40X magnification. IMARIS was used to determine the number and transverse diameter of the boutons on each NMJ. Individual NMJs were excluded from analysis

only if they had been damaged during dissection of the larvae or if they were obstructed by other fluorescently labelled structures.

Experiments involving *Drosophila* were performed in conjunction with Laura Graham and Dr. Guiseppa Pennetta. Imaging and data analysis was performed by Ines Amorim.

## 5.3. Results

### 5.3.1. Assessing the feasibility of using the peripheral nervous system to study α-synuclein at the synapse

The peripheral nervous system (PNS) provides an ideal system to study degeneration of axons and synapses in close detail. The neuromuscular junction (NMJ) synapse is an easily accessible and well characterized synaptic structure, which can be manipulated *in vivo* to instigate neurodegeneration without causing a major systemic response to neuronal injury (Beirowski et al., 2004, Gillingwater et al., 2002). In addition, peripheral nerve lesions have been widely used in the study of Wallerian degeneration and have proved very useful in finding new modulators of synaptic stability, such as the $Wld^s$ mutation (Gillingwater and Ribchester, 2001). We therefore set out to assess whether we could use the PNS as a model system to study mechanisms downstream of α-synuclein which could be involved in the maintenance of synaptic and axonal stability.

α-synuclein has been regarded as a critical protein in several neurodegenerative scenarios and its effect in the degeneration of the CNS has been extensively studied. The most well-established function for α-synuclein is its role in synaptic activity and facilitation of neurotransmitter storage and release in central synapses (Bellucci et al., 2012, Lashuel et al., 2013). To the best of our knowledge, no studies have been carried out to access these properties of α-synuclein in the PNS. However, it has been suggested that α-synuclein may help regulate acetylcholine compartmentalization in motor neurons (Pelkonen and Yavich, 2011) and might contribute to modulate

Wallerian degeneration in the PNS (Siebert et al., 2010). In order to establish if Wallerian degeneration in the PNS is indeed affected by loss of α-synuclein we first wanted to validate and extend the findings from Siebert and colleagues (Siebert et al., 2010), who proposed mice that lacking α-synuclein showed trends towards better preservation of axonal morphology following a sciatic nerve lesion.

#### *5.3.1.1. C57Bl/6JOlaHsd mice do not express α-synuclein*

To study the consequences of losing endogenous expression of α-synuclein on synaptic stability in the PNS we used C57Bl/6JOlaHsd mice (α-syn$^{-/-}$). This mouse strain carries a natural deletion of the α-synuclein locus (Specht and Schoepfer, 2001) and has been used, in conjunction with the C57Bl/6J strain (α-syn$^{+/+}$), to study the function of α-synuclein by several groups (Cabin et al., 2005, Siebert et al., 2010, Yavich et al., 2006, Yavich et al., 2004).

Loss of α-synuclein expression from the CNS and PNS in α–syn$^{-/-}$ mice was confirmed by immunoblotting of protein extracts from brain and sciatic nerve. As expected, immunodetection of α-synuclein revealed the presence of a single 14kDa band in the tissues from α-syn$^{+/+}$ mice but not from α-syn$^{-/-}$ mice (Figure 5.2).

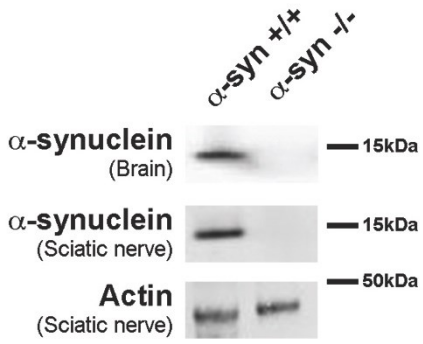


**Figure 5.2 Deletion of α-synuclein in the CNS and PNS of α-syn$^{-/-}$ mice.** Representative western blots showing α-synuclein protein levels in whole brain and sciatic nerve from α-syn$^{+/+}$ and α-syn$^{-/-}$ mice, confirming the absence of α-synuclein in the α-syn$^{-/-}$ mice. Actin was used as a loading control. Each lane was loaded with 20 µg of protein.

#### *5.3.1.2. Absence of α-synuclein does not influence axonal and synaptic morphology in the PNS*

To establish if loss of α-synuclein leads to gross morphological alterations in axons and NMJs from adult mice, we performed electron and confocal microscopy studies of sciatic nerves and NMJs from hind limb lumbrical muscles, respectively.

The ultrastructure of axons in the sciatic nerve was indistinguishable between α-syn$^{+/+}$ and α-syn$^{-/-}$ mice (Figure 5.3 A). Qualitative assessment revealed the presence of unmyelinated and myelinated axons across a range of different calibres. In all myelinated axons, the myelin sheath was tightly wrapped around the axon, which in turn showed a clear cytoplasm with an even distribution of neurofilaments and the presence of intact mitochondria. Quantitatively, the density of myelinated axons did not differ between α-syn$^{+/+}$ and α-syn$^{-/-}$ mice (Figure 5.3 B). In addition, the mean axonal diameter and myelin g-ratio, as well as the correlation between g-ratio and axon diameter, were identical in α-syn$^{+/+}$ and α-syn$^{-/-}$ mice (Figure 5.3 C-E).

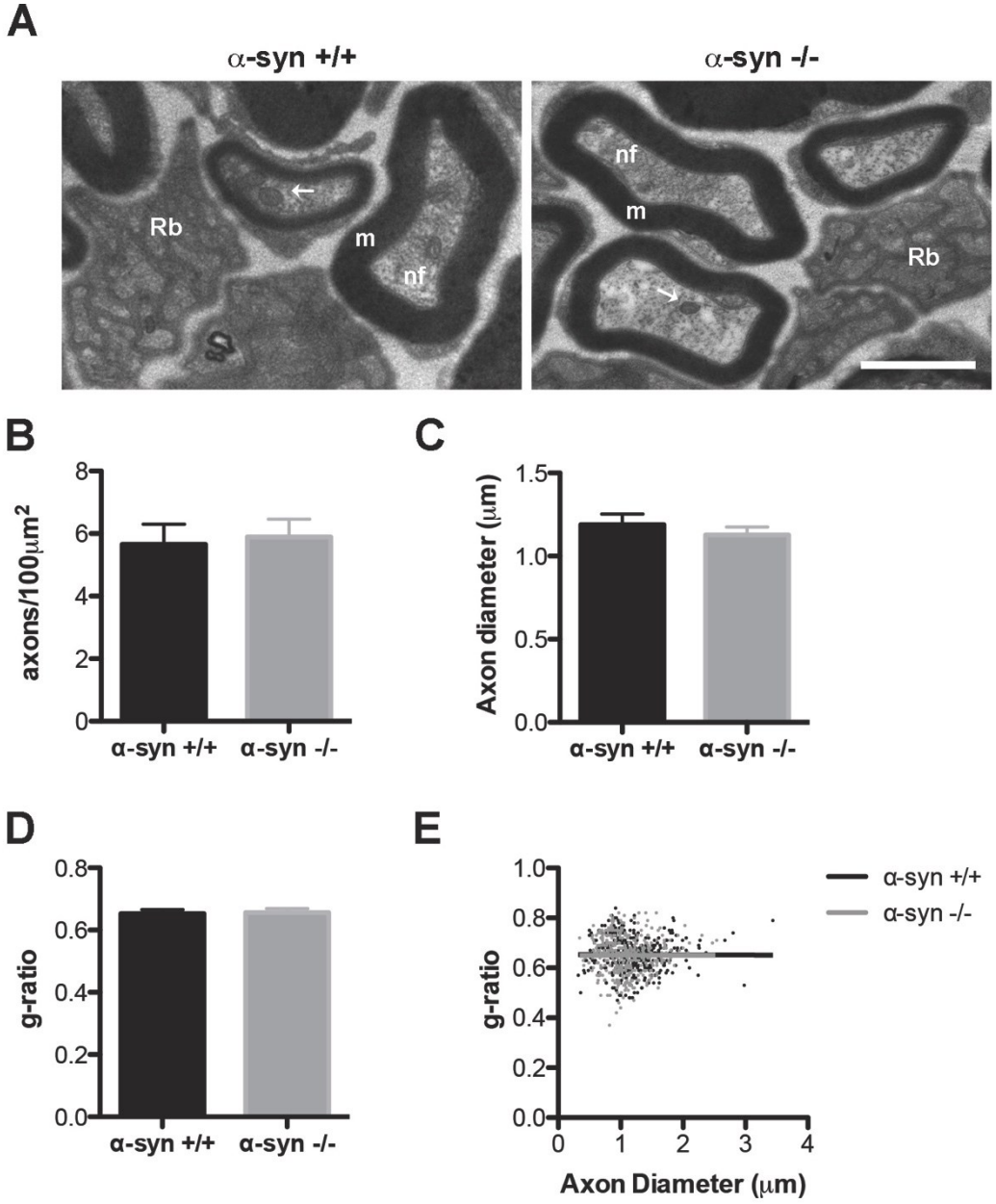


**Figure 5.3: Loss of α-synuclein does not influence the morphology and myelination of axons in the sciatic nerve. A)** Example electron micrographs from sections of the sciatic nerve. Individual axons showed intact neurofilament bundles (nf) and mitochondria (arrows). Myelin (m) was found to be tightly wrapped around all myelinated axons and Remak bundles (Rb) of small unmyelinated axons were also present in both mouse strains. Scale bar = 1 μm. **B)** Density of myelinated axons is identical in α-syn$^{+/+}$ and α-syn$^{-/-}$ mice. Data represented as mean ± SEM, N=3, $p>0.05$, unpaired two-tailed t-test. **C-D)** Axon

diameter (C) and myelin g-ratio (D) were not influenced by the loss of α-synuclein. Data represented as mean ± SEM, N=3, $p>0.05$, unpaired two-tailed t-test. **E)** Axon diameter plotted versus g-ratio showed identical distribution between genotypes.

The morphological characteristics of NMJs were analysed in immunohistochemical preparations of lumbrical muscles. In both α-syn$^{+/+}$ and α-syn$^{-/-}$ mice no major axonal abnormalities were observed and all motor endplates were fully innervated and occupied by pre-synaptic motor nerve terminals (Figure 5.4 A). Endplates had a pretzel-like appearance, characteristic of fully mature post-synaptic structures, and their approximate area was identical in the two genotypes (Figure 5.4 B). In addition, the diameter of muscle fibres was not influenced by the loss of α-synuclein expression (Figure 5.4 C).

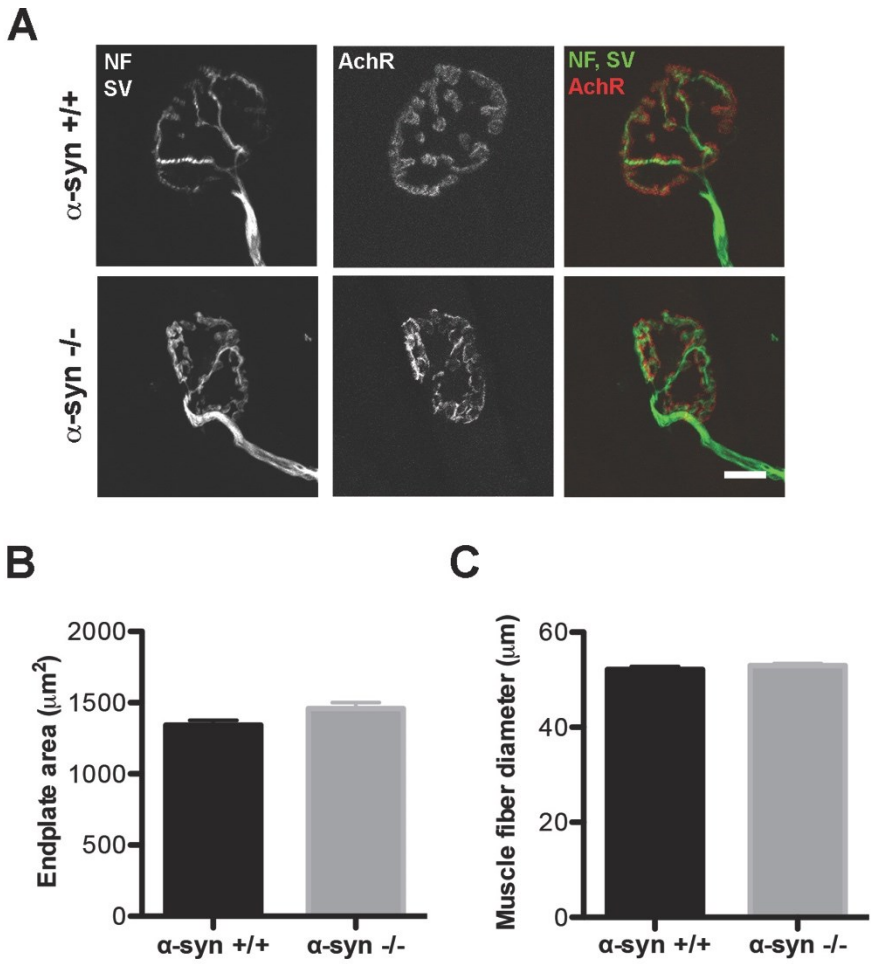


**Figure 5.4: Morphology of the neuromuscular junctions in conserved despite absence of α-synuclein. A)** Confocal micrographs of example NMJs from lumbrical muscles of the hind limb. Note that in both genotypes endplates (AchR) were fully occupied by overlying motor nerve terminals (labelled with antibodies against neurofilaments (NF) and synaptic vesicles (SV)). Scale bar = 10 μm. **B, C)** Quantification of endplate area (B) and muscle fibre diameter (C) showed no difference between α-syn$^{+/+}$ and α-syn$^{-/-}$ mice. Data represented as mean ± SEM, N=3, $p>0.05$, unpaired two-tailed t-test.

#### *5.3.1.3. Wallerian degeneration in the PNS occurs normally in the absence of α-synuclein*

To determine the influence of α-synuclein expression on the progression of axonal and synaptic degeneration we induced Wallerian degeneration of motor

terminals by transecting the sciatic nerve. Following axotomy, the nerve distal to site of injury, including its nerve terminals, degenerate in a progressive and well-characterized manner that allows us to follow the course of both axonal and synaptic degeneration (Beirowski et al., 2004, Gillingwater et al., 2002).

Axonal degeneration was assessed by electron microscopy of the distal sciatic nerve at 6dpi, a time point at which most axons will be undergoing degeneration (Beirowski et al., 2004, Gillingwater et al., 2002). Axons were classified according to their ultrastructural appearance into one of five categories representative of their state of degeneration. Analysis of electron micrographs showed a similar morphological appearance of axonal degeneration in the two mouse strains (Figure 5.5 A) with the distribution of degenerative axonal morphologies not differing between α-syn$^{+/+}$ and α-syn$^{-/-}$ mice (Figure 5.5 B-C).

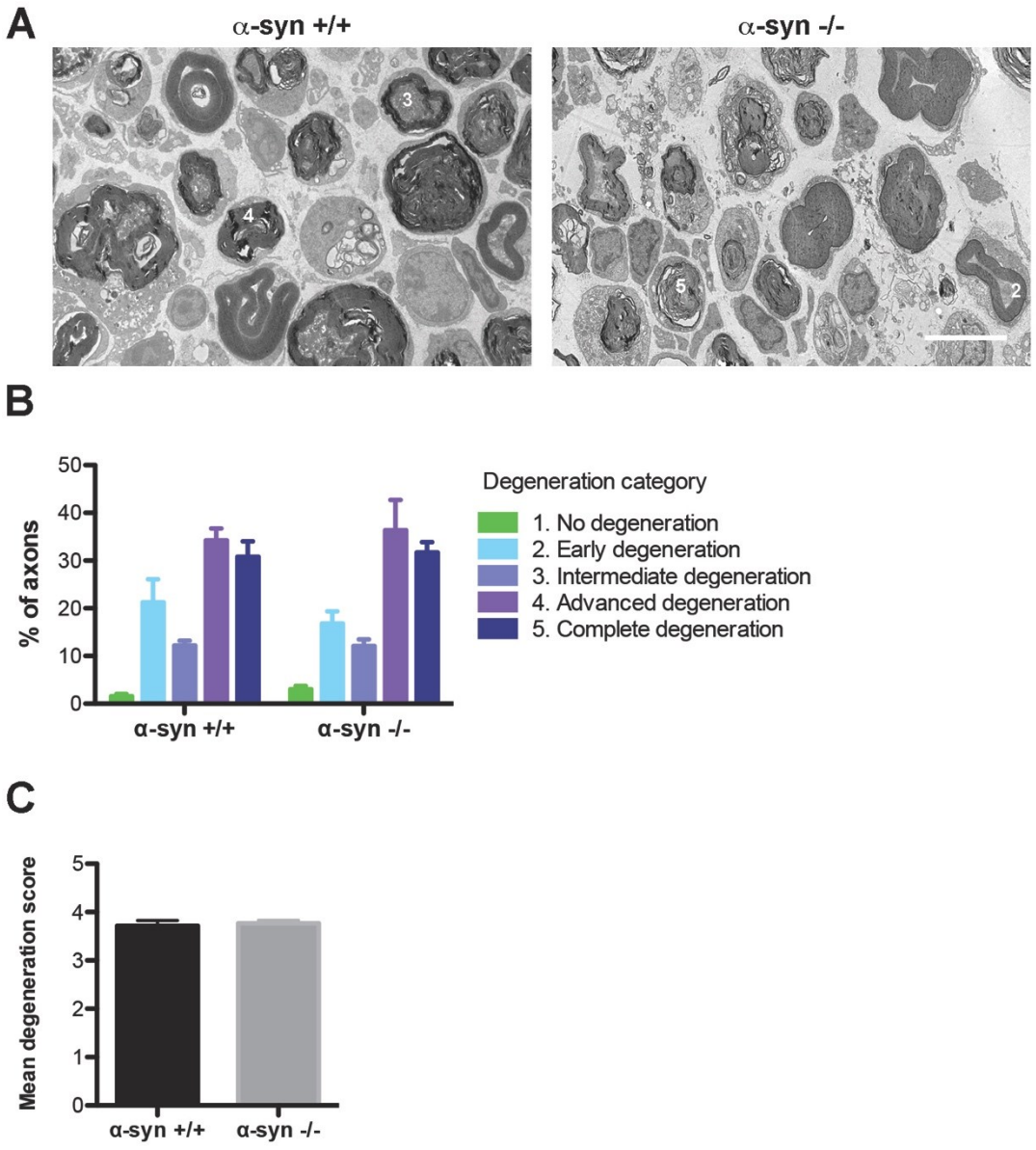


**Figure 5.5: Degeneration of the sciatic nerve is not influenced by the absence of α-synuclein. A)** Representative electron micrographs of degenerating axons in the sciatic nerve at 6dpi. The morphological appearance of axonal degeneration was similar between α-syn$^{+/+}$ and α-syn$^{-/-}$ mice. Numbers 1 to 5 indicate examples of axons belonging to the degeneration categories used to analyse different morphologies for quantitative analysis (see methods). Scale bar = 5 µm. **B)** Bar chart showing a similar distribution of degenerating axon morphologies in the sciatic nerve 6dpi in both genotypes. Data represented as mean ± SEM, N=3, $p>0.05$, unpaired two-tailed t-test within each category. **C)** Loss of α-synuclein did not influence the mean axon degeneration score in the sciatic nerve 6dpi. Data represented as mean ± SEM, N=3, $p>0.05$, unpaired two-tailed t-test.

As branches from the sciatic nerve provide axonal innervation to NMJs in the deep lumbrical muscles from the hindpaw, immunohistochemistry and confocal microscopy were used to assess synaptic degeneration in these muscles. Wallerian degeneration after nerve injury is instigated much earlier in distal motor nerve terminals than in the corresponding axons located in peripheral nerves leading to the majority of Wallerian degeneration being complete at NMJs within around 24hpi, depending on the distance of the nerve terminals to the site of lesion (Gillingwater and Ribchester, 2001, Miledi and Slater, 1970). The morphological characteristics of degenerating NMJs were identical between α-syn$^{+/+}$ and α-syn$^{-/-}$ mice: pre-synaptic structures became progressively fragmented before being lost from the NMJ, with degeneration proceeding in a retrograde manner. Vacant endplates were first seen at 12hpi and there was a gradual loss of NMJ innervation until 18hpi, when the vast majority of NMJs analysed were completely vacant (Figure 5.6 A). Quantification of the percentage of degenerated NMJs at several time-points following nerve injury revealed that the time-course of Wallerian degeneration was not influenced by the loss of α-synuclein (Figure 5.6 B).

Overall, the results in this section argue against a significant influence of α-synuclein on synaptic stability and/or degeneration in the PNS. Therefore, we decided to focus our research in the rest of this chapter on the CNS, where the importance of α-synuclein for synaptic stability has previously been well established (Burre, 2015, Stefanis, 2012).

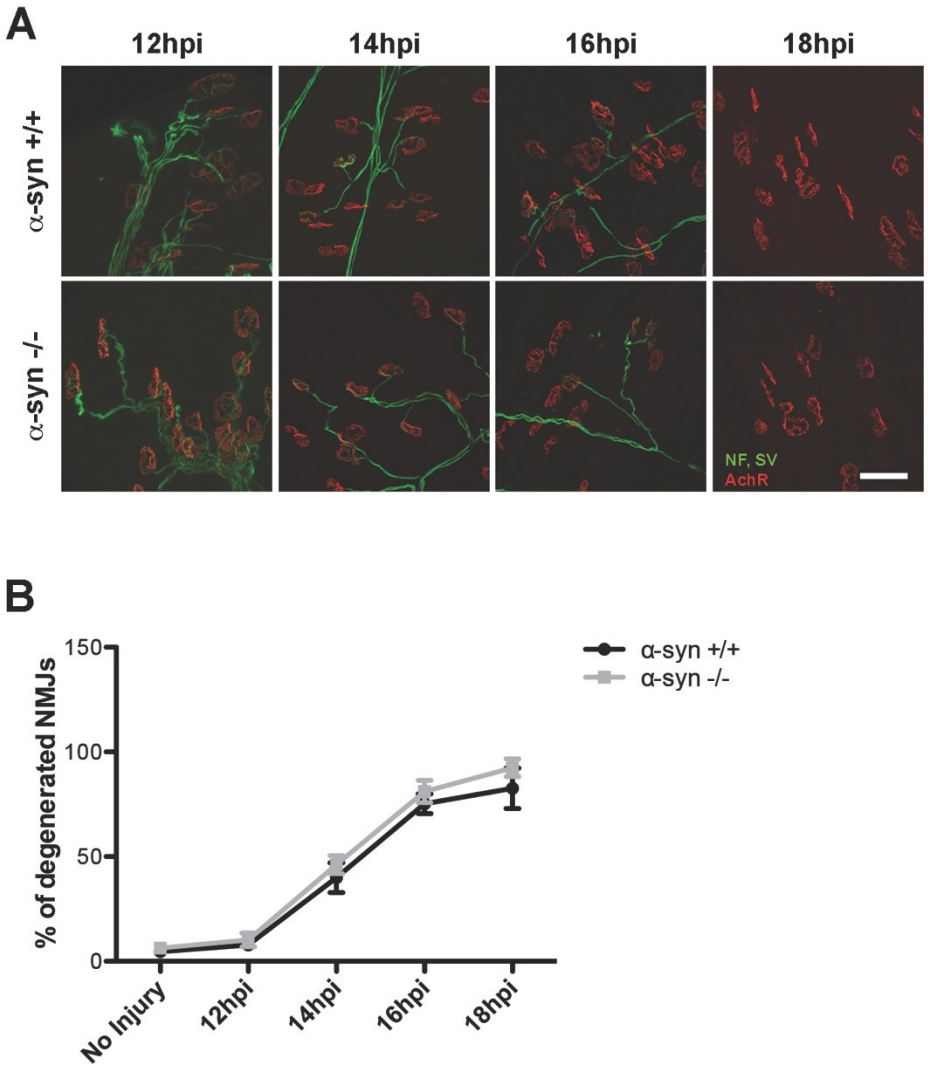


**Figure 5.6: Rate of neuromuscular degeneration was not affected by loss of α-synuclein. A)** Representative confocal micrographs of NMJs in lumbrical muscles at different time-points following sciatic nerve lesion (axons/nerve terminals, green; motor endplates, red). Note the progressive degeneration and loss of motor nerve terminals in both α-syn$^{+/+}$ and α-syn$^{-/-}$ mice. Scale bar = 50 μm. **B)** Time course of nerve terminal degeneration at the NMJ following sciatic nerve lesion was identical in the two genotypes analysed. Data represented as mean ± SEM, N=12 for "no injury", N=3 for all other time-points, $p>0.05$, two-Way ANOVA with Bonferroni post-test.

### 5.3.2. Identification of novel α-synuclein targets at the synapse

In order to uncover molecular mechanisms downstream of α-synuclein with the potential to mediate maintenance of synaptic function and stability, we quantified changes in the synaptic proteome of mice lacking α-synuclein. iTRAQ proteomics on crude synaptosomes isolated from the brain of α-syn$^{+/+}$ and α-syn$^{-/-}$ mice identified 2,615 individual proteins. Raw mass spectrometry data was filtered to leave only those proteins identified by at least two unique peptides and with expression levels consistently altered by more than 15% across two independent technical replicates. The 200 remaining filtered proteins (Table 5.4) were submitted to bioinformatics pathway analysis using IPA, DAVID and VarElect.

**Table 5.4: Filtered proteomics data-set.**

| KO/WT Ratio | Description | Gene | UniProt Accession | Unique Peptides | Score | Mitochondria Evidence | Novel | Reference |
|---|---|---|---|---|---|---|---|---|
| 0.53 | Solute carrier family 2, facilitated glucose transporter member 1 | Slc2a1 | P17809 | 2 | 51.09 | Y | Y | N / A |
| 0.55 | NADH dehydrogenase [ubiquinone] 1 beta subcomplex subunit 11, mitochondrial | Ndufb11 | O09111 | 3 | 198.87 | Y | N | (Panelli et al., 2013) |
| 0.57 | Syndecan (Fragment) | SDC4 | I3PMU3 | 3 | 113.33 | N | N / A | N / A |
| 0.63 | Solute carrier family 39 (Zinc transporter), member 7 | Slc39a7 | Q14C53 | 2 | 96.01 | N | N / A | N / A |
| 0.63 | Bcl-2-like protein 1 (Fragment) | Bcl2l1 | A2AHX9 | 2 | 59.07 | Y | N | (Akhtar et al., 2004) |
| 0.65 | Zinc transporter ZIP6 (Fragment) | Slc39a6 | D3Z7N4 | 2 | 48.40 | N | N / A | N / A |
| 0.65 | Glia maturation factor beta | Gmfb | A7VJ98 | 3 | 184.00 | N | N / A | N / A |
| 0.65 | Eukaryotic translation initiation factor 5A-1 | Eif5a | P63242 | 5 | 139.47 | Y | Y | N / A |
| 0.67 | Immunoglobulin-binding protein 1 | Igbp1 | Q61249 | 2 | 155.33 | N | N / A | N / A |
| 0.68 | RWD domain containing 4A, isoform CRA_b | Rwdd4a | H3BJI4 | 2 | 61.28 | N | N / A | N / A |
| 0.68 | Microtubule-associated protein tau | Mapt | P10637 | 20 | 1309.97 | Y | N | (Spires-Jones et al., 2009) |
| 0.69 | Centrin-2 (Fragment) | Cetn2 | B1AUQ7 | 2 | 50.06 | N | N / A | N / A |
| 0.69 | Sodium-dependent phosphate transporter 2 | Slc20a2 | Q80UP8 | 3 | 159.55 | N | N / A | N / A |
| 0.70 | S100 calcium binding protein A1 (Fragment) | S100A1 | Q9JL08 | 2 | 22.94 | Y | Y | N / A |
| 0.71 | ARP3 Actin-Related Protein 3 Homolog | Actr3 | Q3TGE1 | 11 | 765.22 | N | N / A | N / A |
| 0.72 | DnaJ homolog subfamily C member 8 | Dnajc8 | A2ALF0 | 2 | 60.57 | N | N / A | N / A |
| 0.72 | Metallo-beta-lactamase domain-containing protein 2 | | G3X997 | 2 | 107.58 | N | N / A | N / A |
| 0.72 | mRNA, clone:2-63 (Fragment) | Gprc5b | Q9JMF0 | 2 | 177.90 | N | N / A | N / A |
| 0.72 | Tropomodulin-2 | Tmod2 | Q9JKK7 | 4 | 181.60 | N | N / A | N / A |
| 0.73 | Sodium-dependent neutral amino acid transporter SLC6A17 | Slc6a17 | Q8BJI1 | 2 | 62.77 | N | N / A | N / A |
| 0.73 | ATP synthase subunit e, mitochondrial | Atp5i | Q06185 | 2 | 145.42 | Y | Y | N / A |
| 0.73 | Charged multivesicular body protein 3 | Chmp3 | Q9CQ10 | 2 | 59.10 | N | N / A | N / A |
| 0.74 | Solute carrier family 13 member 5 | Slc13a5 | Q67BT3 | 2 | 84.38 | N | N / A | N / A |

| | | | | | | | | |
|---|---|---|---|---|---|---|---|---|
| 0.74 | Sodium-dependent phosphate transporter 1 | Slc20a1 | Q61609 | 2 | 67.87 | N | N / A | N / A |
| 0.74 | Amyloid beta A4 precursor protein-binding family A member 1 | Apba1 | B2RUJ5 | 5 | 137.31 | N | N / A | N / A |
| 0.74 | Calmodulin | Calm1 | P62204 | 9 | 2240.54 | N | N / A | N / A |
| 0.74 | RNA-binding protein | Tsn | Q545E6 | 3 | 149.58 | N | N / A | N / A |
| 0.74 | Acyl-Coenzyme A binding domain containing 6 | Acbd6 | Q14BV7 | 2 | 150.05 | N | N / A | N / A |
| 0.74 | Nucleobindin 2 | Nucb2 | Q3TV28 | 2 | 91.59 | N | N / A | N / A |
| 0.75 | Protein FAM49A | Fam49a | Q8BHZ0 | 3 | 173.38 | N | N / A | N / A |
| 0.75 | Transcription elongation factor A protein-like 3 (Fragment) | Tceal3 | A2AEC2 | 7 | 155.13 | N | N / A | N / A |
| 0.75 | Uncharacterized protein | | F2Z452 | 2 | 133.15 | N | N / A | N / A |
| 0.75 | Glutamate--cysteine ligase regulatory subunit (Fragment) | Gclm | F6VNW5 | 2 | 54.43 | N | N / A | N / A |
| 0.76 | Calcineurin B homologous protein 1 | Chp1 | P61022 | 4 | 235.87 | N | N / A | N / A |
| 0.76 | Tax1-binding protein 1 homolog | Tax1bp1 | Q3UKC1 | 3 | 48.04 | N | N / A | N / A |
| 0.76 | Ectonucleotide pyrophosphatase/phosphodiesterase family member 5 | Enpp5 | Q9EQG7 | 2 | 34.04 | N | N / A | N / A |
| 0.76 | Synaptosomal-associated protein 29 | Snap29 | Q9ERB0 | 3 | 112.44 | N | N / A | N / A |
| 0.76 | Translation initiation factor eIF-2B subunit epsilon | Eif2b5 | Q8CHW4 | 2 | 50.65 | N | N / A | N / A |
| 0.77 | Charged multivesicular body protein 4b | Chmp4b | Q9D8B3 | 7 | 221.39 | N | N / A | N / A |
| 0.77 | Solute Carrier Family 16 (Monocarboxylate Transporter), Member 1 | Slc16a1 | Q8BPS5 | 4 | 74.44 | Y | Y | N / A |
| 0.77 | MCG124812 | Taok1 | B2RX66 | 9 | 115.23 | N | N / A | N / A |
| 0.77 | Gamma-aminobutyric acid receptor subunit alpha-3 | Gabra3 | P26049 | 4 | 177.85 | N | N / A | N / A |
| 0.77 | Neurabin-2 | Ppp1r9b | Q6R891 | 13 | 642.86 | N | N / A | N / A |
| 0.77 | MCG68069 | Npm1 | Q5SQB7 | 7 | 199.91 | N | N / A | N / A |
| 0.77 | Coiled-coil domain-containing protein 104 (Fragment) | Cfap36 | Q5SNY8 | 2 | 79.71 | N | N / A | N / A |
| 0.77 | SERPINE1 MRNA Binding Protein 1 | Serbp1 | Q3UEI6 | 7 | 123.76 | N | N / A | N / A |

| | | | | | | | | |
|---|---|---|---|---|---|---|---|---|
| 0.77 | von Willebrand factor A domain-containing protein 5A | Vwa5a | Q99KC8 | 2 | 33.87 | N | N / A | N / A |
| 0.77 | Isoform Testis-specific of Angiotensin-converting enzyme | Ace | P09470 | 3 | 78.17 | Y | N | (Sonsalla et al., 2013) |
| 0.77 | Dynactin 2 | Dctn2 | Q3TPZ5 | 17 | 1040.32 | Y | N | (LaMonte et al., 2002) |
| 0.77 | Solute Carrier Family 1 (Glutamate/Neutral Amino Acid Transporter), Member 4 | Slc1a4 | Q3US35 | 3 | 105.64 | N | N / A | N / A |
| 0.77 | Coatomer subunit epsilon | Cope | O89079 | 3 | 77.74 | N | N / A | N / A |
| 0.77 | Myosin regulatory light chain 12B | Myl12b | Q3THE2 | 3 | 106.53 | N | N / A | N / A |
| 0.78 | Syntaxin-4 | Stx4 | P70452 | 2 | 80.91 | N | N / A | N / A |
| 0.78 | Ran-specific GTPase-activating protein | Ranbp1 | P34022 | 4 | 103.76 | N | N / A | N / A |
| 0.78 | Band 4.1-like protein 1 | Epb41l1 | A2AUK5 | 16 | 656.89 | N | N / A | N / A |
| 0.78 | EWS RNA-Binding Protein 1 | Ewsr1 | Q9CRS5 | 2 | 67.18 | N | N / A | N / A |
| 0.78 | Sodium/hydrogen exchanger (Fragment) | Slc9a6 | Q80U52 | 3 | 172.47 | Y | Y | N / A |
| 0.78 | Neuromodulin | Gap43 | P06837 | 17 | 1888.99 | N | N / A | N / A |
| 0.78 | Protein 1110004F10Rik | 1110004F10Rik | D6RI64 | 2 | 74.56 | N | N / A | N / A |
| 0.79 | E3 ubiquitin-protein ligase RBX1 | Rbx1 | P62878 | 3 | 106.92 | N | N / A | N / A |
| 0.79 | Eif3j protein (Fragment) | Eif3j | Q2YDW1 | 4 | 79.93 | N | N / A | N / A |
| 0.79 | Endoplasmic reticulum resident protein 29 | Erp29 | P57759 | 5 | 194.18 | N | N / A | N / A |
| 0.79 | Glial fibrillary acidic protein | Gfap | P03995 | 21 | 759.21 | Y | N | (Maragakis and Rothstein, 2006) |
| 0.79 | Eukaryotic Translation Initiation Factor 4B | Eif4b | Q3TDD8 | 12 | 508.52 | N | N / A | N / A |
| 0.79 | Endoplasmic Reticulum Protein 44 | Erp44 | Q3URM4 | 5 | 304.43 | N | N / A | N / A |
| 0.80 | Translationally-controlled tumor protein | Tpt1 | P63028 | 6 | 466.43 | Y | N | (Kim et al., 2001) |
| 0.80 | Cytoplasmic dynein 1 intermediate chain 1 | Dync1i1 | O88485 | 13 | 413.11 | N | N / A | N / A |
| 0.80 | RNA-binding protein FUS (Fragment) | Fus | G3UXT7 | 2 | 71.27 | N | N / A | N / A |
| 0.80 | Isoform 2 of Apoptosis-inducing factor 3 | Aifm3 | Q3TY86 | 6 | 169.04 | Y | N | (Kohda et al., 2016) |
| 0.80 | GDP-D-Glucose Phosphorylase 1 | Gdpgp1 | Q8C3E3 | 2 | 91.64 | N | N / A | N / A |
| 0.80 | Homer protein homolog 1 | Homer1 | Q9Z2Y3 | 16 | 689.18 | N | N / A | N / A |
| 0.80 | Solute carrier family 1 (Glial high affinity glutamate transporter), member 2 | Slc1a2 | Q3UYK6 | 14 | 2942.59 | N | N / A | N / A |

| | | | | | | | | |
|---|---|---|---|---|---|---|---|---|
| 0.80 | Ubiquitin-protein ligase E3A | Ube3a | O08759 | 6 | 143.36 | N | N / A | N / A |
| 0.81 | Serine/threonine kinase receptor associated protein | Strap | B2RUC7 | 8 | 293.12 | N | N / A | N / A |
| 0.81 | E3 ubiquitin-protein ligase RNF34 | Rnf34 | Q99KR6 | 2 | 49.04 | N | N / A | N / A |
| 0.81 | Peflin | Pef1 | Q8BFY6 | 2 | 45.46 | N | N / A | N / A |
| 0.81 | Sorbin and SH3 domain-containing protein 1 | Sorbs1 | Q62417 | 3 | 70.23 | N | N / A | N / A |
| 0.81 | Protein Ppp1r9a | Ppp1r9a | H3BKQ7 | 16 | 580.30 | N | N / A | N / A |
| 0.81 | Lisch-like isoform 7 | Ildr2 | B5TVM9 | 2 | 110.49 | N | N / A | N / A |
| 0.81 | Ribosome maturation protein SBDS | Sbds | P70122 | 3 | 60.65 | N | N / A | N / A |
| 0.82 | Secretogranin V, isoform CRA_b | Scg5 | Q3TT51 | 4 | 113.06 | N | N / A | N / A |
| 0.82 | Proteasome subunit beta type (Fragment) | Psmb7 | Q5D098 | 2 | 48.71 | N | N / A | N / A |
| 0.82 | Semaphorin-4A | Sema4a | D3YWV5 | 2 | 57.35 | N | N / A | N / A |
| 0.82 | GRIP1-associated protein 1 | Gripap1 | Q8VD04 | 12 | 379.05 | N | N / A | N / A |
| 0.82 | WD repeat-containing protein 26 | Wdr26 | E0CYH4 | 2 | 61.42 | N | N / A | N / A |
| 0.82 | Cldn10 protein (Fragment) | Cldn10 | Q921J6 | 2 | 96.17 | N | N / A | N / A |
| 0.83 | GTPase Activating Protein (SH3 Domain) Binding Protein 2 | G3bp2 | Q3U931 | 4 | 109.58 | N | N / A | N / A |
| 0.83 | Isoform 2 of FXYD domain-containing ion transport regulator 6 | Fxyd6 | Q9D164 | 2 | 144.70 | N | N / A | N / A |
| 0.83 | Sodium/potassium-transporting ATPase subunit alpha-2 | Atp1a2 | D3YYN7 | 46 | 6589.88 | N | N / A | N / A |
| 0.83 | Apoptosis repressor interacting with CARD | Nol3 | Q53YU5 | 2 | 56.36 | Y | Y | N / A |
| 0.83 | Coiled-coil domain-containing protein 177 | Ccdc177 | Q3UHB8 | 7 | 208.58 | N | N / A | N / A |
| 0.83 | Heterogeneous Nuclear Ribonucleoprotein U (Scaffold Attachment Factor A) | Hnrnpu | Q3TGN5 | 6 | 245.04 | N | N / A | N / A |
| 0.84 | Deubiquitinating protein VCIP135 | Vcpip1 | Q8CDG3 | 4 | 110.13 | N | N / A | N / A |
| 0.84 | Protein Hook homolog 3 | Hook3 | Q8BUK6 | 5 | 128.20 | N | N / A | N / A |
| 0.84 | Isoform 2 of Voltage-dependent L-type calcium channel subunit beta-4 | Cacnb4 | Q8R0S4 | 8 | 182.02 | N | N / A | N / A |
| 1.16 | 60 kDa heat shock protein, mitochondrial | Hspd1 | P63038 | 29 | 2122.06 | Y | N | (Magnoni et al., 2013) |
| 1.16 | Cofilin 1, non-muscle | Cfl1 | Q544Y7 | 17 | 760.20 | Y | N | (Schonhofen et al., 2014) |
| 1.16 | Niemann-Pick Disease, Type C2 | Npc2 | Q3U3C2 | 2 | 113.09 | N | N / A | N / A |

| | | | | | | | | |
|---|---|---|---|---|---|---|---|---|
| 1.16 | Tyrosine 3-monooxygenase | Th | P24529 | 6 | 156.95 | Y | N | (Zhu et al., 2012) |
| 1.16 | Apolipoprotein, MICOS complex subunit Mic27 | Apool | B1AV14 | 2 | 140.85 | Y | Y | N / A |
| 1.16 | Saccharopine Dehydrogenase (Putative) | Sccpdh | Q3ULN6 | 4 | 181.62 | Y | Y | N / A |
| 1.16 | Mitochondrial import receptor subunit T | Tomm40 | Q9QYA2 | 3 | 166.67 | Y | N | (Bender et al., 2013) |
| 1.16 | Nucleosome Assembly Protein 1-Like 5 | Nap1l5 | Q9CTE1 | 2 | 62.79 | N | N / A | N / A |
| 1.16 | Dynactin subunit 3 | Dctn3 | Q9Z0Y1 | 3 | 72.24 | N | N / A | N / A |
| 1.16 | Mitochondrial pyruvate carrier 1 | Mpc1 | D3YWY6 | 2 | 130.20 | Y | Y | N / A |
| 1.16 | Sideroflexin-3 | Sfxn3 | Q3U4F0 | 9 | 567.75 | Y | Y | N / A |
| 1.16 | Thymidylate kinase | Dtymk | P97930 | 5 | 103.94 | Y | Y | N / A |
| 1.16 | Aldo-Keto Reductase Family 1, Member A1 (Aldehyde Reductase) | Akr1a1 | Q3UJW9 | 5 | 209.70 | Y | N | (Tseveleki et al., 2010) |
| 1.17 | Albumin 1 (Precursor) | Alb | Q546G4 | 26 | 1290.23 | Y | N | (Pisani et al., 2012) |
| 1.17 | Translation elongation factor (Fragment) | Tsfm | Q8VDE3 | 4 | 285.49 | Y | Y | N / A |
| 1.17 | RIKEN cDNA 2900041A09, isoform CRA_a | Tppp | Q3URG1 | 4 | 188.15 | Y | N | (Olah and Ovadi, 2014) |
| 1.17 | Protein LSM12 homolog | Lsm12 | Q9D0R8 | 4 | 188.03 | N | N / A | N / A |
| 1.17 | Acetyl-CoA Acetyltransferase 1 | Acat1 | Q3TQP7 | 19 | 1100.06 | Y | Y | N / A |
| 1.17 | 39S ribosomal protein L12, mitochondrial | Mrpl12 | Q9DB15 | 5 | 159.63 | Y | Y | N / A |
| 1.17 | Isocitrate dehydrogenase [NAD] subunit alpha, mitochondrial | Idh3a | Q9D6R2 | 13 | 978.55 | Y | Y | N / A |
| 1.17 | Glutamate decarboxylase | Gad1 | Q548L6 | 7 | 246.00 | Y | N | (Trifonov et al., 2012) |
| 1.18 | Succinyl-CoA ligase [ADP/GDP-forming] subunit alpha, mitochondrial | Suclg1 | Q9WUM5 | 5 | 159.11 | Y | Y | N / A |
| 1.18 | Glutamate decarboxylase | Gad2 | Q548L4 | 4 | 163.52 | N | N / A | N / A |
| 1.18 | Biliverdin reductase B (Flavin reductase (NADPH)) | Blvrb | Q3U6G1 | 2 | 93.97 | N | N / A | N / A |
| 1.18 | Reticulocalbin-1 | Rcn1 | Q05186 | 2 | 115.90 | N | N / A | N / A |
| 1.18 | Nucleoside diphosphate kinase | Nme1 | Q5NC81 | 9 | 601.42 | Y | Y | N / A |
| 1.18 | Tumor protein D53 | Tpd52l1 | O54818 | 2 | 56.45 | N | N / A | N / A |
| 1.18 | Cdc42 effector protein 4 | Cdc42ep4 | Q9JM96 | 3 | 115.19 | N | N / A | N / A |

| | | | | | | | | |
|---|---|---|---|---|---|---|---|---|
| 1.19 | ATP-dependent Clp protease proteolytic subunit | Clpp | Q8CF81 | 3 | 134.37 | Y | Y | N / A |
| 1.19 | MCG122050 | Tbca | Q5I0U7 | 3 | 82.03 | N | N / A | N / A |
| 1.19 | Prostamide/prostaglandin F synthase | Fam213b | Q9DB60 | 3 | 134.93 | N | N / A | N / A |
| 1.19 | Guanine nucleotide-binding protein subunit gamma | Gng5 | Q3UKC8 | 2 | 78.00 | N | N / A | N / A |
| 1.19 | Lysosomal alpha-glucosidase | Gaa | P70699 | 3 | 132.10 | Y | N | (Lim et al., 2015) |
| 1.19 | Delta(3,5)-Delta(2,4)-dienoyl-CoA isomerase, mitochondrial | Ech1 | O35459 | 2 | 81.25 | Y | N | (Long et al., 2016) |
| 1.19 | Protein lin-7 homolog A | Lin7a | Q8JZS0 | 7 | 273.46 | N | N / A | N / A |
| 1.19 | Estradiol 17-beta-dehydrogenase 8 (Fragment) | H2-Ke6 | G3UX44 | 3 | 223.52 | N | N / A | N / A |
| 1.19 | MC3T3-E1 calcyclin | S100a6 | Q545I9 | 2 | 71.27 | N | N / A | N / A |
| 1.20 | Isoform 3 of Synapsin-1 | Syn1 | O88935 | 18 | 1764.65 | N | N / A | N / A |
| 1.20 | NAD(P)H-hydrate epimerase | Apoa1bp | Q8K4Z3 | 3 | 163.45 | Y | Y | N / A |
| 1.20 | NADH dehydrogenase [ubiquinone] 1 beta subcomplex subunit 4 | Ndufb4 | Q9CQC7 | 6 | 183.48 | Y | N | (McFarland et al., 2008) |
| 1.21 | Enoyl-CoA hydratase, mitochondrial | Echs1 | Q8BH95 | 8 | 346.60 | Y | Y | N / A |
| 1.21 | Isobutyryl-CoA dehydrogenase, mitochondrial | Acad8 | D3YTT4 | 3 | 199.17 | Y | Y | N / A |
| 1.21 | Peroxiredoxin-1 (Fragment) | Prdx1 | B1AXW5 | 10 | 362.02 | Y | N | (Lee et al., 2008b) |
| 1.21 | Succinyl-CoA ligase [ADP-forming] subunit beta, mitochondrial | Sucla2 | Q9Z2I9 | 17 | 1068.72 | Y | Y | N / A |
| 1.21 | Pyruvate dehydrogenase E1 alpha 1 | Pdha1 | Q3UFJ3 | 20 | 1534.48 | Y | Y | N / A |
| 1.21 | Ermin | Ermn | Q5EBJ4 | 3 | 134.80 | N | N / A | N / A |
| 1.22 | Superoxide dismutase | Sod2 | Q3U8W4 | 6 | 130.01 | Y | N | N / A |
| 1.22 | Cofilin 2 | Cfl2 | Q3UHW9 | 7 | 352.99 | N | N / A | N / A |
| 1.22 | Microtubule-associated proteins 1A/1B light chain 3A | Map1lc3a | Q91VR7 | 3 | 95.67 | Y | N | (McFarland et al., 2008) |
| 1.22 | Aldehyde dehydrogenase X, mitochondrial | Aldh1b1 | Q9CZS1 | 4 | 105.96 | Y | Y | N / A |
| 1.22 | Dynamin 2 | Dnm2 | Q3TBU6 | 15 | 958.66 | N | N / A | N / A |
| 1.22 | Succinyl-CoA:3-ketoacid-coenzyme A transferase | Oxct1 | Q3UK61 | 9 | 666.20 | Y | Y | N / A |

| | | | | | | | | |
|---|---|---|---|---|---|---|---|---|
| 1.23 | Synapsin-2 | Syn2 | Q64332 | 16 | 2141.85 | N | N / A | N / A |
| 1.23 | Electron transfer flavoprotein subunit alpha, mitochondrial | Etfa | Q99LC5 | 11 | 873.14 | Y | Y | N / A |
| 1.23 | GrpE protein homolog 1, mitochondrial | Grpel1 | Q99LP6 | 6 | 133.16 | Y | Y | N / A |
| 1.23 | Casein kinase II subunit beta | Csnk2b | G3UXG7 | 2 | 60.49 | N | N / A | N / A |
| 1.23 | Transcription elongation factor B polypeptide 2 | Tceb2 | P62869 | 4 | 138.39 | N | N / A | N / A |
| 1.23 | Isocitrate dehydrogenase 3 (NAD+), gamma (Fragment) | Idh3g | Q684I8 | 6 | 331.74 | Y | Y | N / A |
| 1.23 | Isoform 2 of Vesicle-associated membrane protein 1 | Vamp1 | Q62442 | 6 | 435.09 | Y | N | (Sevlever et al., 2015) |
| 1.23 | Protein ETHE1, mitochondrial | Ethe1 | Q9DCM0 | 3 | 125.61 | Y | N | (Tiranti et al., 2004) |
| 1.24 | Malate dehydrogenase, mitochondrial | Mdh2 | P08249 | 16 | 3361.24 | Y | Y | N / A |
| 1.24 | Isoform 2 of Plakophilin-4 n | Pkp4 | Q68FH0 | 5 | 126.42 | N | N / A | N / A |
| 1.24 | Solute Carrier Family 25, Member 27 | Slc25a27 | Q9CX10 | 3 | 128.37 | Y | Y | N / A |
| 1.25 | Methylmalonate-semialdehyde dehydrogenase [acylating], mitochondrial | Aldh6a1 | Q9EQ20 | 11 | 375.66 | Y | Y | N / A |
| 1.25 | Clathrin, Light Chain B | Cltb | Q3TJ95 | 13 | 497.83 | N | N / A | N / A |
| 1.25 | NADH dehydrogenase [ubiquinone] 1 alpha subcomplex subunit 3 | Ndufa3 | Q9CQ91 | 2 | 79.46 | Y | N | (Poche et al., 2016) |
| 1.25 | Ubiquilin 1 | Ubqln1 | Q3T992 | 6 | 191.51 | N | N / A | N / A |
| 1.26 | Destrin (Fragment) | Dstn | A8QKB4 | 10 | 389.49 | N | N / A | N / A |
| 1.26 | Rho GTPase-activating protein 1 | Arhgap1 | Q5FWK3 | 5 | 134.35 | N | N / A | N / A |
| 1.26 | Aromatic-L-amino-acid decarboxylase (Fragment) | Ddc | Q5SUV9 | 3 | 212.30 | N | N / A | N / A |
| 1.27 | Isovaleryl-CoA dehydrogenase, mitochondrial | Ivd | Q9JHI5 | 10 | 291.17 | Y | Y | N / A |
| 1.27 | NADH dehydrogenase [ubiquinone] 1 alpha subcomplex subunit 10, mitochondrial | Ndufa10 | Q99LC3 | 7 | 335.89 | Y | N | (Lake et al., 2016) |
| 1.27 | Ester hydrolase C11orf54 homolog | | CK054 | 3 | 58.86 | N | N / A | N / A |
| 1.27 | GTP:AMP phosphotransferase AK4, mitochondrial (Fragment) | Ak4 | A2ARF6 | 2 | 138.36 | Y | N | (Liu et al., 2009b) |
| 1.27 | Fatty acid-binding protein, brain | Fabp7 | P51880 | 2 | 152.26 | N | N / A | N / A |

| | | | | | | | | |
|---|---|---|---|---|---|---|---|---|
| 1.27 | Histone H3 (Fragment) | H3f3a | E0CZ27 | 2 | 54.78 | N | N / A | N / A |
| 1.28 | Endophilin-B2 | Sh3glb2 | A2AWI7 | 14 | 492.69 | N | N / A | N / A |
| 1.28 | Superoxide dismutase [Cu-Zn] | Sod1 | P08228 | 7 | 954.48 | Y | N | (Kaur et al., 2016) |
| 1.29 | ES1 protein homolog, mitochondrial | D10Jhu81e | Q9D172 | 6 | 225.28 | N | N / A | N / A |
| 1.29 | NADH dehydrogenase [ubiquinone] 1 alpha subcomplex subunit 6 | Ndufa6 | Q9CQZ5 | 4 | 141.05 | Y | N | (McFarland et al., 2008) |
| 1.29 | Ubiquitin-Conjugating Enzyme E2N | Ube2n | A2RTT4 | 6 | 196.19 | N | N / A | N / A |
| 1.30 | Mitochondrial ATP synthase epsilon subunit (Fragment) | Atp5e | G8DXN9 | 2 | 46.14 | Y | N | (Alves et al., 2015) |
| 1.30 | Mitochondrial import inner membrane translocase subunit TIM16 | Pam16 | Q9CQV1 | 2 | 56.43 | Y | Y | N / A |
| 1.31 | Sorting nexin-3 | Snx3 | D3Z789 | 4 | 63.94 | N | N / A | N / A |
| 1.32 | ATP synthase subunit | Atp5o | Q9DB20 | 8 | 543.69 | Y | N | Lacovelli 2016 |
| 1.32 | S100 calcium binding protein A13 | S100a13 | Q545H7 | 3 | 106.20 | N | N / A | N / A |
| 1.32 | Iron-sulfur cluster assembly enzyme ISCU, mitochondrial | Iscu | Q9D7P6 | 3 | 95.44 | Y | Y | N / A |
| 1.33 | Peptidyl-prolyl cis-trans isomerase F, mitochondrial | Ppif | Q99KR7 | 3 | 127.97 | Y | N | (Warne et al., 2016) |
| 1.34 | Lin-7 Homolog C | Lin7c | Q3TTY6 | 5 | 141.42 | N | N / A | N / A |
| 1.35 | Mitochondrial import inner membrane translocase subunit Tim10 B | Timm10b | D3YVK5 | 2 | 110.87 | Y | Y | N / A |
| 1.36 | Mitochondrial intermembrane space import and assembly protein 40 | Chchd4 | Q8VEA4 | 3 | 93.65 | Y | Y | N / A |
| 1.36 | Desmoplakin | Dsp | E9Q557 | 21 | 351.44 | N | N / A | N / A |
| 1.37 | Cytochrome c oxidase subunit 5B, mitochondrial | Cox5b | P19536 | 8 | 653.00 | Y | N | (Chung et al., 2013) |
| 1.37 | Histone H4 (Fragment) | | Q6B822 | 2 | 69.41 | N | N / A | N / A |
| 1.39 | Cryab protein | Cryab | Q52L78 | 2 | 95.40 | Y | N | (Liu et al., 2015) |
| 1.39 | Profilin-2 | Pfn2 | Q9JJV2 | 2 | 205.71 | N | N / A | N / A |
| 1.40 | UPF0598 protein C8orf82 homolog | | Q8VE95 | 2 | 63.79 | N | N / A | N / A |
| 1.41 | Histone H2B (Fragment) | Hist1h2bj | A0JLV3 | 3 | 199.21 | N | N / A | N / A |
| 1.42 | Histidine triad nucleotide-binding protein 1 | Hint1 | P70349 | 3 | 62.50 | N | N / A | N / A |
| 1.43 | Peptidyl-prolyl cis-trans isomerase | Ppia | Q3TE63 | 7 | 327.00 | Y | N | (Kaur et al., 2016) |

| | | | | | | | | |
|---|---|---|---|---|---|---|---|---|
| 1.44 | Beta-synuclein | Sncb | Q91ZZ3 | 9 | 966.78 | Y | N | (Chandra et al., 2004a) |
| 1.46 | Fatty acid binding protein 5, epidermal | Fabp5 | Q497I3 | 6 | 173.10 | N | N / A | N / A |
| 1.47 | Fatty acid binding protein 3, muscle and heart | Fabp3 | Q5EBJ0 | 4 | 168.23 | N | N / A | N / A |
| 1.50 | Heme-binding protein 1 | Hebp1 | Q9R257 | 2 | 73.66 | N | N / A | N / A |
| 1.99 | Peroxiredoxin 5 | Prdx5 | Q3UWS9 | 5 | 330.85 | Y | N | (Davey and Bolanos, 2013) |

KO/WT Ratio: Ratio between the expression levels of a given protein in α-syn$^{-/-}$ mice compared to α-syn$^{+/+}$. Average of two technical replicas;
Description: Protein description;
Gene: Gene coding the identified protein;
UniProt Accession: UniProt Accession number;
Unique peptides: Number of unique peptides used to identify the protein;
Score: Confidence score;
Mitochondria Evidence: N: No. Y: Yes. Evidence that a given protein is localises in mitochondria; or that it influences or is influenced by mitochondrial function;
Novel: N: No; Y: Yes; N/A: Not Applicable. Evidence that a given protein has previously been associated with α-synuclein, Parkinson's Disease or Neurodegeneration in general.
Reference: Example references demonstrating the previous association of a protein with α-synuclein, Parkinson's Disease or Neurodegeneration in general.

IPA analysis revealed an extensive involvement of α-synuclein in neurodegenerative scenarios (Table 5.5), ranging from neuromuscular disorders and dementia to particular diseases such as Parkinson's, Alzheimer's and Huntington's diseases. Remarkably, all of these conditions have previously been associated with synaptic dysfunction (see General Introduction). Performing a more focused analysis to identify individual cellular pathways affected by loss of α-synuclein revealed a very strong involvement of mitochondrial canonical pathways, including mitochondria dysfunction, oxidative phosphorylation and tricarboxylic acid (TCA; Krebs) cycle (Table 5.6). Gene ontology (GO) annotation analysis using DAVID confirmed the enrichment in terms associated with mitochondrial functions (Table 5.7) and filtering the data using the VarElect engine revealed a striking enrichment of proteins (74 out of 200) belonging to mitochondrial pathways (Table 5.4). This finding provides significant experimental support for the hypothesis that α-synuclein has important physical and/or functional interactions with mitochondria (Haelterman et al., 2014, Nakamura, 2013). Further bioinformatics analysis of these 200 mitochondrial proteins identified 37 proteins not previously associated with α-synuclein or neurodegeneration (Table 5.8, Figure 5.7). These proteins were therefore considered to represent potential novel α-synuclein-dependent regulators of synaptic stability.

**Table 5.5: Top diseases and disorders affected in α-syn$^{-/-}$ mice.**

| Diseases and Disorders | P-value |
|---|---|
| Movement Disorders | 4.06E-15 |
| Neuromuscular disease | 5.00E-13 |
| Huntington's Disease | 4.15E-09 |
| Schizophrenia | 2.41E-09 |
| Dementia | 2.33E-05 |
| Alzheimer's disease | 4.60E-05 |
| Parkinson's disease | 9.16E-08 |
| Amyotrophic lateral sclerosis | 6.34E-06 |
| Neurodegeneration | 5.09E-05 |

**Table 5.6: Top canonical pathways affected in α-syn$^{-/-}$ mice.**

| Canonical pathways | P-value |
|---|---|
| Mitochondrial Dysfunction | 9.36E-08 |
| TCA Cycle II (Eukaryotic) | 2.01E-06 |
| Glutamate Dependent Acid Resistance | 9.64E-05 |
| Oxidative Phosphorylation | 1.15E-05 |
| RhoA Signaling | 1.68E-04 |

**Table 5.7: Gene Ontology annotation enrichment.**

| DAVID GO annotation | P-value |
|---|---|
| Generation of precursor metabolites and energy | 2.30E-09 |
| Transmission of nerve impulses | 8.13E-07 |
| Oxidation reduction | 2.23E-06 |
| Synaptic transmission | 2.96E-06 |
| Regulation of neurotransmitter levels | 3.92E-06 |
| Electron transport chain | 2.46E-05 |

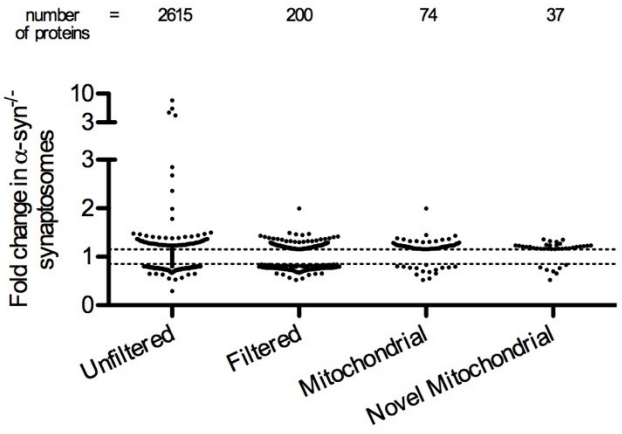


**Figure 5.7: Graphical representation of the filtering steps taken during the analysis of iTRAQ proteomics data.** Y-axis represents the mean fold change, from two technical replicates, of each protein in $\alpha$-syn$^{-/-}$ synaptosomes when compared to control $\alpha$-syn$^{+/+}$ synaptosomes. "Unfiltered" column includes all 2,615 proteins identified by iTRAQ. "Filtered" column contains the subset of identified proteins which met the selection criteria of being identified by more than 1 unique peptide and being altered by more than 15% in two technical replicates. Since mitochondrial pathways were shown to be some of the most affected in $\alpha$-syn$^{-/-}$ mice, the 200 filtered proteins were further selected to include only mitochondrial proteins ("Mitochondrial" column, 74 proteins). Mitochondrial proteins were further filtered to include proteins not previously associated with $\alpha$-synuclein or neurodegeneration. These group of 37 proteins, here referred to as "novel mitochondrial", was prioritized for further study.

**Table 5.8**: **Novel proteins identified to belong to α-synuclein dependent pathways.**

| UniProt | Description |
|---|---|
| Q9DB15 | 39S ribosomal protein L12, mitochondrial |
| Q3TQP7 | Acetyl-CoA Acetyltransferase 1 |
| Q9CZS1 | Aldehyde dehydrogenase X, mitochondrial |
| B1AV14 | Apolipoprotein, MICOS complex subunit Mic27 |
| Q53YU5 | Apoptosis repressor interacting with CARD |
| Q06185 | ATP synthase subunit e, mitochondrial |
| Q8CF81 | ATP-dependent Clp protease proteolytic subunit |
| Q99LC5 | Electron transfer flavoprotein subunit alpha, mitochondrial |
| Q8BH95 | Enoyl-CoA hydratase, mitochondrial |
| P63242 | Eukaryotic translation initiation factor 5A-1 |
| Q99LP6 | GrpE protein homolog 1, mitochondrial |
| Q9D7P6 | Iron-sulfur cluster assembly enzyme ISCU, mitochondrial |
| D3YTT4 | Isobutyryl-CoA dehydrogenase, mitochondrial |
| Q9D6R2 | Isocitrate dehydrogenase [NAD] subunit alpha, mitochondrial |
| Q684I8 | Isocitrate dehydrogenase 3 (NAD+), gamma (Fragment) |
| Q9JHI5 | Isovaleryl-CoA dehydrogenase, mitochondrial |
| P08249 | Malate dehydrogenase, mitochondrial |
| Q9EQ20 | Methylmalonate-semialdehyde dehydrogenase [acylating], mitochondrial |
| D3YVK5 | Mitochondrial import inner membrane translocase subunit Tim10 B |
| Q9CQV1 | Mitochondrial import inner membrane translocase subunit TIM16 |
| Q8VEA4 | Mitochondrial intermembrane space import and assembly protein 40 |
| D3YWY6 | Mitochondrial pyruvate carrier 1 |
| Q8K4Z3 | NAD(P)H-hydrate epimerase |
| Q5NC81 | Nucleoside diphosphate kinase |
| Q3UFJ3 | Pyruvate dehydrogenase E1 alpha 1 |
| Q9JL08 | S100 calcium binding protein A1 (Fragment) |
| Q3ULN6 | Saccharopine Dehydrogenase (Putative) |
| Q3U4F0 | Sideroflexin-3 |
| Q80U52 | Sodium/hydrogen exchanger (Fragment) |
| Q8BPS5 | Solute Carrier Family 16 (Monocarboxylate Transporter), Member 1 |
| P17809 | Solute carrier family 2, facilitated glucose transporter member 1 |
| Q9CX10 | Solute Carrier Family 25, Member 27 |
| Q9Z2I9 | Succinyl-CoA ligase [ADP-forming] subunit beta, mitochondrial |
| Q9WUM5 | Succinyl-CoA ligase [ADP/GDP-forming] subunit alpha, mitochondrial |
| Q3UK61 | Succinyl-CoA:3-ketoacid-coenzyme A transferase |
| P97930 | Thymidylate kinase |
| Q8VDE3 | Translation elongation factor (Fragment) |

To select individual proteins from the short-list of 37 to be prioritised for further analyses, we performed extensive literature searches to uncover those with potential links with PD and/or related forms of neurodegeneration. Using this approach, Sideroflexin 3 (sfxn3) was identified as a protein of particular interest (Figure 5.8). Microarray studies

reported that levels of sfxn3 transcripts or protein were altered in the substantia nigra of PD patients and in rodents subjected to a 6-hydroxydopamine lesion (Charbonnier-Beaupel et al., 2015, Fuller et al., 2014, Simunovic et al., 2009). In addition, a related protein (sfxn1) interacts with connexin 32, mutations in which cause a variant of Charcot-Marie-Tooth disease (Bergoffen et al., 1993, Fowler et al., 2013), reduced levels of the sfxn1 protein have been reported in patients with Alzheimer's Disease (Minjarez et al., 2016), and sfxn2 is deregulated in dopaminergic cells in response to rotenone treatment (Jin et al., 2007). Sfxn3 belongs to a family of proteins (sideroflexins 1-5) that are putative iron transporters, with predicted transmembrane domains and mitochondrial localization (Fleming et al., 2001, Li et al., 2010). The functional role of these proteins, however, remains unexplored.

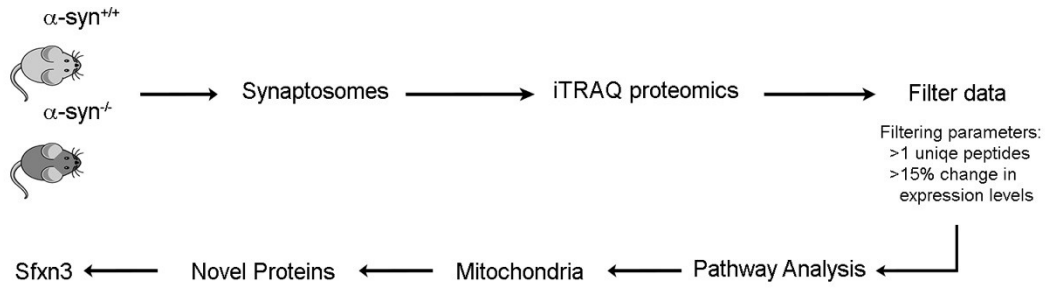


**Figure 5.8: Schematic overview of experimental design and workflow.** Crude synaptosomes were isolated from α-syn$^{-/-}$ and α-syn$^{+/+}$ and submitted to iTRAQ proteomics. Filtering of the raw data and bioinformatics pathway analysis revealed an enrichment in proteins belonging to mitochondrial pathways. Further analysis of data to include only proteins not previously associated with neurodegeneration or α-synuclein function allowed us to reach a small list of novel proteins with potential to cooperate with α-synuceiln to regulate synaptic function and stability. A search of the published literature indicated sfxn3 was a protein with good potential to modulate neurodegenerative pathways.

Levels of sfxn3 protein were increased in synapses from α-syn$^{-/-}$ mice (Table 5.4 and Figure 5.9), suggesting that sfxn3 expression is inversely correlated with α-synuclein. To confirm this, we over-expressed α-synuclein in stably transfected SH-SY5Y cells. Exposure of SH-SY5Y cells to Doxycycline (DOX) for 24h led to a robust increase in the expression of α-synuclein (), which was accompanied by a significant decrease in the levels of sfxn3 protein (Figure 5.10). Thus, sfxn3 levels are bi-directionally regulated by α-synuclein.

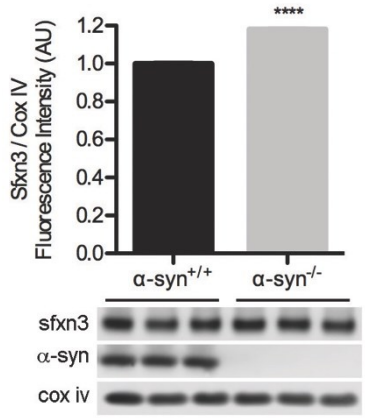


**Figure 5.9: Validation of sfxn3 upregulation in α-syn$^{-/-}$ mice.** Sfxn3 protein levels were significantly upregulated in synaptosomes from α-syn$^{-/-}$ compared to α-syn$^{+/+}$ controls. Bars represent mean ± SEM, N=3, ****p<0.0001, unpaired t-test. Cox IV was used as a loading control.

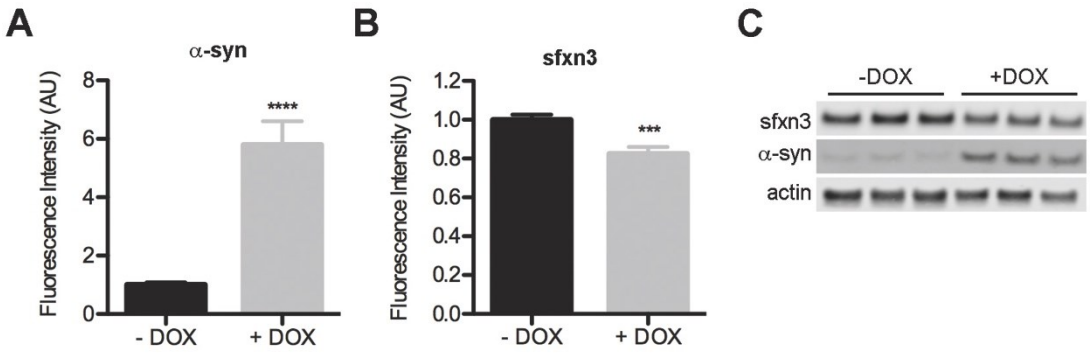


**Figure 5.10: α-synuclein regulates the levels of sfxn3. A)** α-synuclein levels are increased in the presence of Doxycycline (+DOX). Actin was used as loading control. Bars represent mean ± SEM, n≥9 across three different cultures, ****p<0.0001, unpaired two-tailed t-test. **B)** Levels of sfxn3 protein were significantly reduced in SH-SY5Y cells overexpressing WT α-synuclein induced by Doxycycline (+DOX). Actin was used as loading control. Bars represent mean ± SEM, n≥9 across three different cultures, ***p<0.001, unpaired two-tailed t-test. **C)** Representative western blots from A and B are shown for n=3 per treatment.

### 5.3.3. Sfxn3 is a mitochondrial protein enriched in the inner mitochondrial membrane

Sfxn3 is predicted to be a mitochondrial protein (Pagliarini et al., 2008), but direct experimental evidence for its tissue/cellular expression and subcellular localisation is currently lacking. We used western blotting to analyse expression levels of sfxn3 protein in the mouse nervous system and peripheral tissues (Figure 5.11). Sfxn3 was highly expressed in the brain, both in synaptic and non-synaptic fractions, in spinal cord and in peripheral nerve. It was also present in liver and kidney, but was not detectable in skeletal muscle or cardiac muscle. Thus, sfxn3 is not a ubiquitously expressed protein, being particularly enriched in the nervous system.

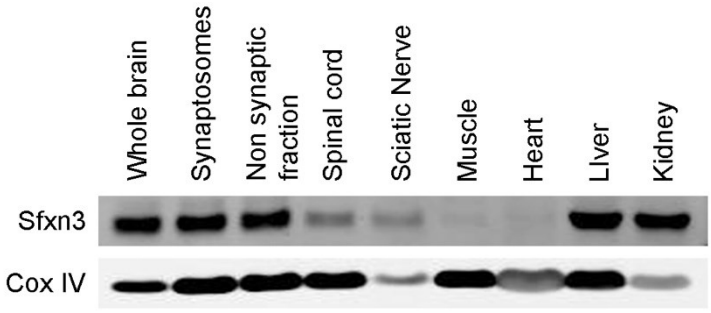


**Figure 5.11: Sfxn3 is not ubiquitously expressed.** Representative western blot showing sfxn3 expression across several tissues from an adult wild-type mouse. Cox IV was used as a mitochondrial marker. All lanes were loaded with 30 μg of protein.

Isolation of mitochondrial and cytosolic fractions from mouse brain indicated that sfxn3 was expressed exclusively in mitochondria (Figure 5.12 A). Furthermore, differential extraction of mitochondrial outer membrane and mitoplasts, using a mild digitonin solubilisation of isolated mitochondria from SH-SY5Y cells, revealed that sfxn3 was localised to the mitoplast fraction (Figure 5.12 B). Given the presence of transmembrane domains in the sfxn3 protein (Li et al., 2010), we conclude that sfxn3 is preferentially localised to the inner mitochondrial membrane.

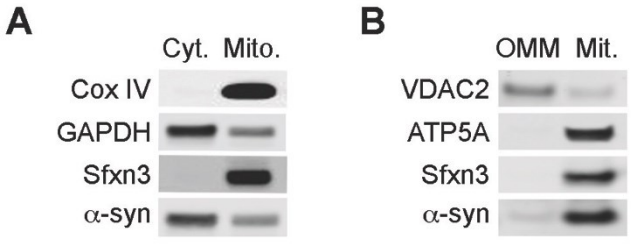


**Figure 5.12: Sfxn3 is a protein of the inner mitochondrial membrane. A)** Sfxn3 was exclusively localised to mitochondrial, but not cytosolic, fractions isolated from mouse brain. As expected, α-synuclein (α-syn) was found in both fractions. Cox IV was used as a mitochondrial marker and GAPDH as a cytosolic marker. Both lanes were loaded with 5 μg of protein. **B)** Sfxn3 was exclusively localised to the inner

mitochondrial membrane. Outer mitochondrial membrane (OMM) and mitoplasts (Mit.) were isolated from undifferentiated SH-SY5Y cells. VDAC2 was used as a marker for the OMM and ATP5A as a marker for the inner mitochondrial membrane and mitoplasts.

### 5.3.4. Sfxn3 is not required for basal mitochondrial bioenergetics functions

The presence of sfxn3 in the inner mitochondrial membrane prompted us to ask whether sfxn3 plays a role in canonical bioenergetic pathways, including oxidative phosphorylation. To test this, we isolated purified synaptosomes from WT ($sfxn3^{+/+}$), HET ($sfxn3^{+/-}$) and sfxn3-KO ($sfxn3^{-/-}$) mice and performed mitochondrial respiration assays using a Seahorse $XF^e24$ Analyzer. Mitochondria bioenergetic functions can be comprehensively investigated by performing two assays: the coupling assay and the electron flow assay (see Materials and Methods, Figure 5.13 A). The coupling assay tests the ability of mitochondria to cope with basal energetic requirements and short bursts of high energetic demand. The electron flow assay assesses the individual activity of complexes I, II/III and IV of the electron transport chain (ETC).

During the coupling assay, oxygen consumption rates (OCR) during basal respiration were similar between WT, HET and KO mice (Figure 5.13 B, C). Accordingly, the fraction of ATP-linked respiration was comparable between mice of all genotypes (Figure 5.13 D). Uncoupling of mitochondria using FCCP induced a similar increase in OCR in WT, HET and KO mice (Figure 5.13 B, C), with equivalent respiration rates associated with spare and maximum respiratory capacity (Figure 5.13 D). This indicates synapses from both sfxn3 HET and KO mice are able to cope with basal energy requirements and to sustain high levels of ETC activity during acute stress (such as acute

administration of FCCP). In the electron flow assay, the activity of each mitochondrial complex was tested under the sustained influence of FCCP, to stimulate maximum strain of the ETC. Sfxn3 KO mice showed a trend towards reduced activity of mitochondrial complexes I-IV, which achieved statistical significance for complex I and complex II/III (Figure 5.13 E-G). The performance of HET mice was comparable with WT, suggesting that a very significant reduction in sfxn3 levels is likely required to impact on ETC function.

Altogether, these results suggest sfxn3 is not required for mitochondrial bioenergetics pathways at the synapse, as basal mitochondrial respiration was unaffected by the absence of sfxn3. However, prolonged exposure to the mitochondria uncoupler FCCP unmasked subtle impairments in the function of individual ETC complexes, suggesting that loss of sfxn3 might impact on the capacity of mitochondria to cope with long-term high energetic burden.

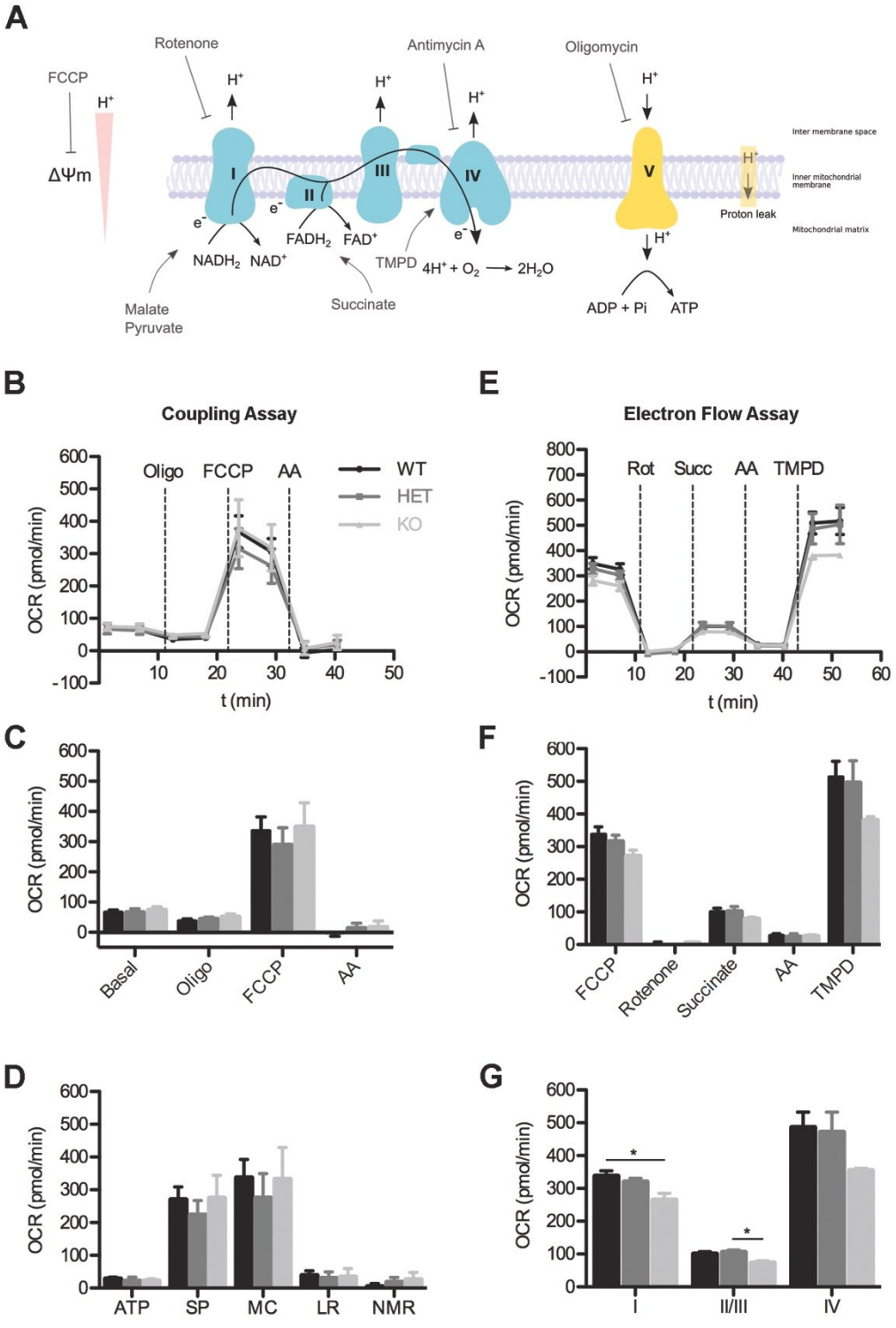


**Figure 5.13: Sfxn3 is not required for oxidative phosphorylation. A)** Schematic of the mitochondria respiratory chain. Mitochondria complexes I-V form an integral part of the mitochondrial inner membrane. Substrates such as malate and pyruvate stimulate the production of $NADH_2$ via the Krebs cycle, whereas

succinate preferentially boosts the production of $FADH_2$. The reduction of the nucleotides $NADH_2$ and $FADH_2$ at complex I and II, respectively, provides electrons to be used in the process of oxidative phosphorylation. Electrons ($e^-$) travel from complex I and/or II to complex IV, where they are combined with $O_2$ to produce $H_2O$. Oxygen consumption rates can thus be used to infer the activity of the ETC. As electrons are fed into the ETC, protons ($H^+$) are transferred through the inner membrane, creating a differential of potential between the mitochondrial matrix and inter membrane space, known as the mitochondrial membrane potential ($\Delta\Psi m$). It is the driving force of the $H^+$ gradient that stimulates the ATPsynthase, also known as complex V, to produce ATP. The activity of the ETC can be manipulated by the addition of substrates or inhibitors. Providing malate/pyruvate or succinate to mitochondria will instigate the activity of complexes I and II, respectively, whereas TMPD acts as an artificial electron donor which feeds complex IV directly. On the other hand, complexes I, IV and V can be inhibited in the presence of rotenone, antimycin A and oligomycin, respectively. The $\Delta\Psi m$ is abolished by FCCP and, as there is no proton driving force for the ATPsynthase to function, this results in the induction of maximum activity by complexes I-IV, in order to attempt to restore $\Delta\Psi m$. ETC activity can be monitored using a Seahorse Analyzer. A Seahorse Analyzer provides a plate based assay in which the levels of oxygen are measured over time and different compounds and substrates can be added to wells containing mitochondria, organelles or cell preparations. It thus provides an ideal platform to study mitochondria bioenergetics in detail in real time. **B-D)** Coupling assay showed no differences in oxygen consumption rates in synaptosomes isolated from WT, HET and sfxn3-KO mice (B, C). Dashed vertical lines in A indicate the time of injection of Oligomycin (Oligo), FCCP (FCCP), and Antimycin A (AA). Traces and bars represent mean ± SEM, N=3-5, $p>0.05$ in One-Way ANOVA with Tukey post-test. D) Bioenergetics parameters derived from C. ATP: ATP-sensitive respiration, SP: spare respiratory capacity, MC: maximum respiratory capacity, LR: leak-respiration, NMR: non-mitochondrial respiration. Data are represented as mean ± SEM, N=3-5, $p>0.05$ in One-Way ANOVA with Tukey post-test. **E-G)** Electron flow assay revealed a trend towards reduction of ETC activity driven by individual mitochondrial complexes (E, F). Dashed vertical lines in E indicate the time of injection of rotenone (Rot), succinate (Succ), Antimycin A (AA) and TMPD. Traces represent mean ± SEM, N=3-5. Bars represent mean ± SEM, n=3-5, $p>0.05$ in One-Way ANOVA with Tukey post-test. G) Calculation of respiration driven by complex I, complex II/II and complex IV

indicates a specific reduction in complex I and complex II/III activity in KO mice compared to WT and HET. Data are represented as mean ± SEM, N=3-5, *p<0.05 in One-Way ANOVA with Tukey post-test.

To evaluate if the subtle effects in mitochondria respiration prompted by reduced levels of sfxn3 were due to the enzymatic activity or abundance of key ETC proteins, we performed enzymatic assays on immunocaptured Complex I and Complex IV. The rates of NADH and cytochrome c oxidation revealed identical enzymatic activities of Complex I and Complex IV, respectively, in synaptosomes from WT and sfxn3 KO mice (Figure 5.14). Quantitative western blotting for ATP5A (a component of ATPsynthase), and the Complex I and Complex IV proteins NDUFB8 and cox IV indicated that no compensatory changes were occurring in these ETC proteins in sfxn3 KO mice compared to WT controls (Figure 5.15).

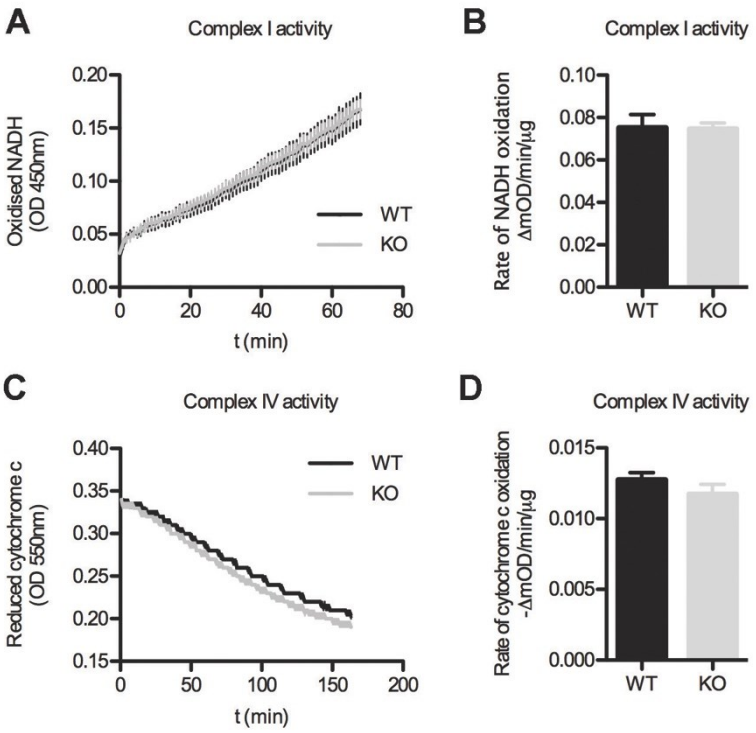


**Figure 5.14: Enzymatic activities of mitochondrial Complex I and Complex IV are not affected by loss of sfxn3. A)** Complex I activity measured by tracking the absorbance of oxidised NADH. For each time point traces represent mean ± SEM, N=3. **B)** Rate of Complex I activity derived from A shows the enzymatic activity of Complex I is not compromised in sfxn3 KO mice. Data are represented as mean ± SEM, N=3, $p>0.05$ in unpaired two-tailed t-test. **C)** Complex IV activity measured by tracking the absorbance of reduced cytochrome c. For each time point traces represent mean ± SEM, N=3. **D)** Rate of Complex IV activity derived from C show the oxidation of cytochrome c is not affected in sfxn3 KO mice. Data are represented as mean ± SEM, N=3, $p>0.05$ in unpaired two-tailed t-test.

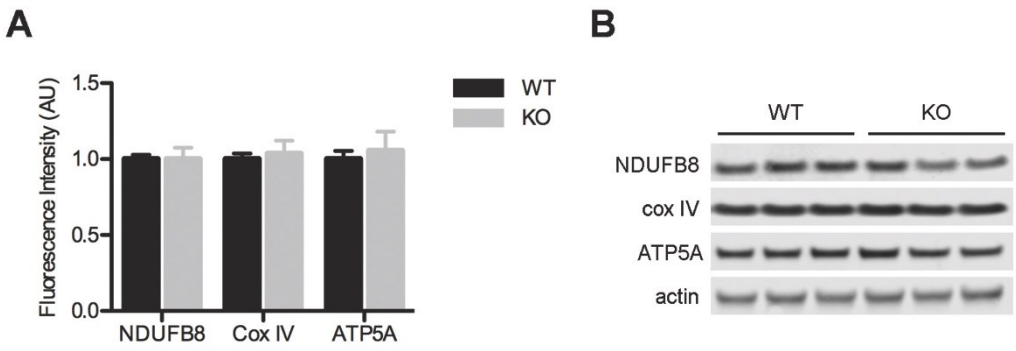


**Figure 5.15: Levels of key electron transport chain proteins are not altered in sfxn3 KO mice.** Quantitative Western blotting (A) and representative blots (B) of the levels of key ETC proteins indicate they are not altered in synaptosomes from WT and sfxn3 KO mice. Actin was used as a loading control. Data are represented as mean ± SEM, N=3, $p>0.05$ unpaired two-tailed t-test.

Taken together, the set of experiments performed in this section suggests that, although sfxn3 is not essential for oxidative phosphorylation pathways and does not impact on the enzymatic activity of mitochondrial complexes I and IV, it may play a modest role during sustained elevated activity of the ETC.

### 5.3.5. Sfxn3 influences synaptic morphology at the *Drosophila* neuromuscular junction

Given the close association between α-synuclein and sfxn3, we wanted to establish whether sfxn3 contributes to pathways regulating synaptic stability. We used the *Drosophila* UAS/Gal4 system to generate tissue-specific over-expression and knock-down of sfxn3 in third instar larval neurons using the pan-neuronal driver *elav-Gal4.*

High-dose overexpression of sfxn3 (Tg( +OE)) led to a significant reduction in the number of synaptic boutons, accompanied by an overall increase in mean bouton

diameter, at NMJs from muscle 6/7 and muscle 12 (Figure 5.16). The increase in bouton diameter was due to a preferential loss of small sized boutons. This fact was particularly striking at NMJs from muscle 12, in which there was a visible marked reduction in projections containing type II boutons (Figure 5.16). To confirm that these changes in synaptic morphology were occurring as a direct result of changes in sfxn3 levels, we repeated our analyses with a low dose overexpression of sfxn3 Tg(–OE). These experiments confirmed no alterations in any of the neuromuscular parameters analysed (Figure 5.16). Furthermore, analysis of eye morphology in Tg(+OE) flies showed no overt phenotype (Figure 5.17). The *Drosophila* eye is a robust and sensitive read-out for identifying neurodegeneration (Sanhueza et al., 2015), suggesting that over-expression of sfxn3 selectively influences synaptic morphology rather than initiating gross degenerative cascades.

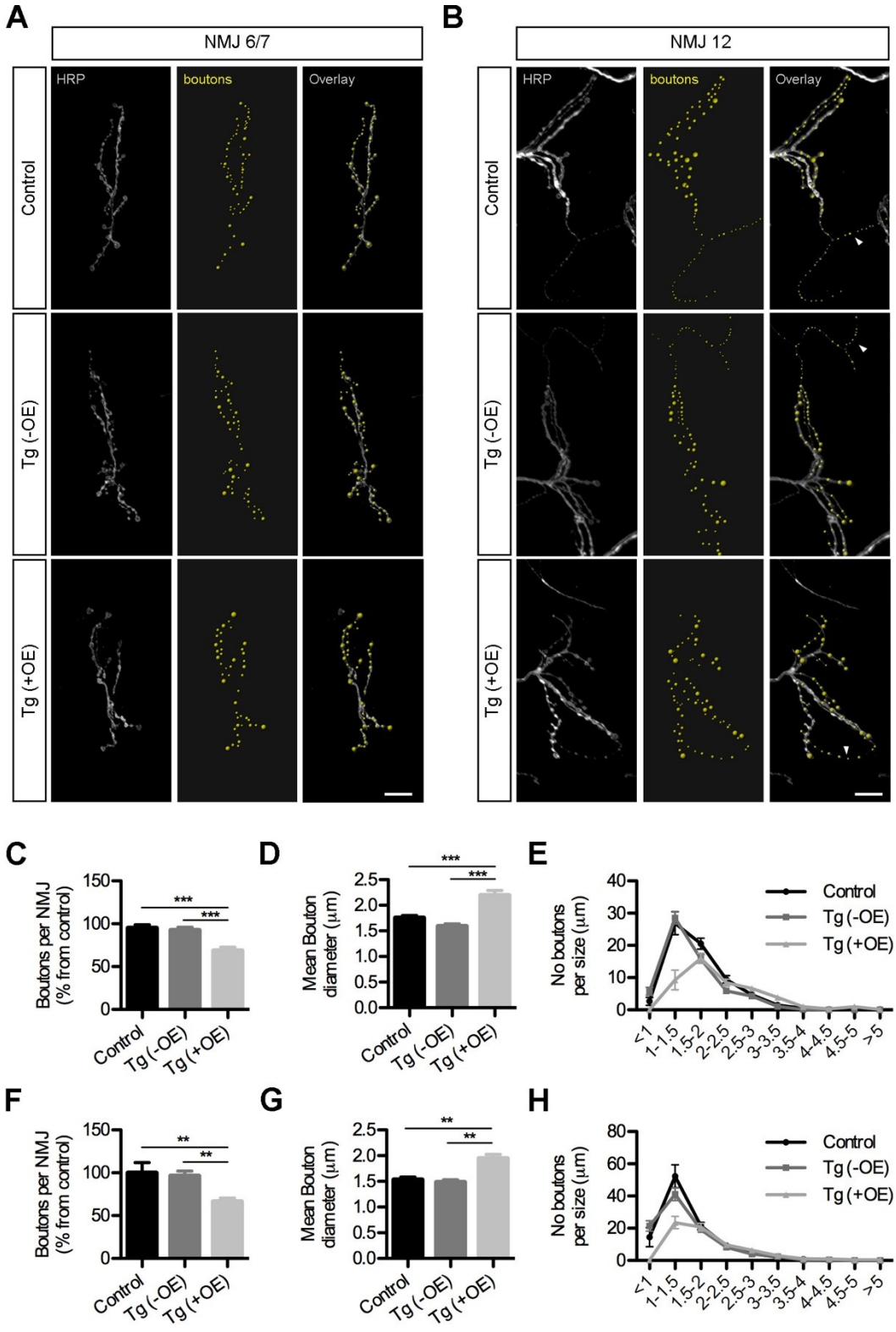


**Figure 5.16: Sfxn3 regulates synaptic morphology at the neuromuscular junction in *Drosophila* larvae. A, B)** Representative images from NMJs on muscle 6/7 (A) and muscle 12 (B) of control (Control)

and transgenic third instar larvae with low and high overexpression of sfxn3, Tg(-OE) and Tg(+OE) respectively. Note the reduction in small boutons in Tg(+OE) NMJs (arrow heads). Grey: HRP. Yellow: boutons. Scale bar = 10 μm. Reduction in the number of boutons and increase in mean bouton diameter on NMJs from muscle 6/7 (**C,D**) and muscle 12 (**F,G**) overexpressing sfxn3 (Tg(+OE)). Bars represent mean ± SEM, N=8-12, **p<0.01, ***p<0.001 in One-Way ANOVA with Tukey post-test. Distribution of the diameter of boutons from NMJs on muscle 6/7 (**E**) and muscle 12 (**H**) shows a specific reduction of small size (<1.5 μm) boutons in NMJs from Tg(+OE) larvae. Data are presented as mean ± SEM, N=8-12.

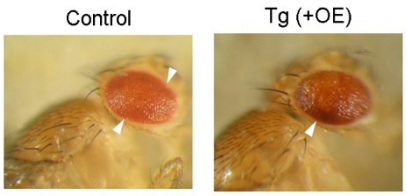


**Figure 5.17: *Drosophila* eye is not affect by overexpression of sfxn3.** Representative images of the eye from control and Tg(+OE) flies demonstrating no overt phenotype.

As expected, low-dose knock-down of sfxn3 (Tg(-KD)) did not produce overt defects in NMJ morphology (Figure 5.18 A-H). However, high-dose knock-down (Tg(+KD)) lead to highly variable phenotypes in nerve terminals from both muscles 6/7 and 12 (Figure 5.18 I). Knock-down induced either collapse and striking degeneration of NMJs, or considerable sprouting of small sized boutons. At muscle 12, it was particularly clear that many NMJs had an increase not only in satellite boutons but also in boutons with morphological characteristics of type II boutons. In some cases, NMJs from muscle 6/7 presented extremely small boutons, even though these are not characteristics from NMJ 6/7. The extreme variability of the phenotypes observed is incompatible with reliable quantification of any morphological parameters, thus no quantitative data are presented for Tg(+KD) experiments. Qualitative observations suggest, nonetheless, that

reduction of sfxn3 in *Drosophila* larvae destabilises the NMJ, leading to collapse of the synaptic structures or compensatory growth of satellite and small size boutons.

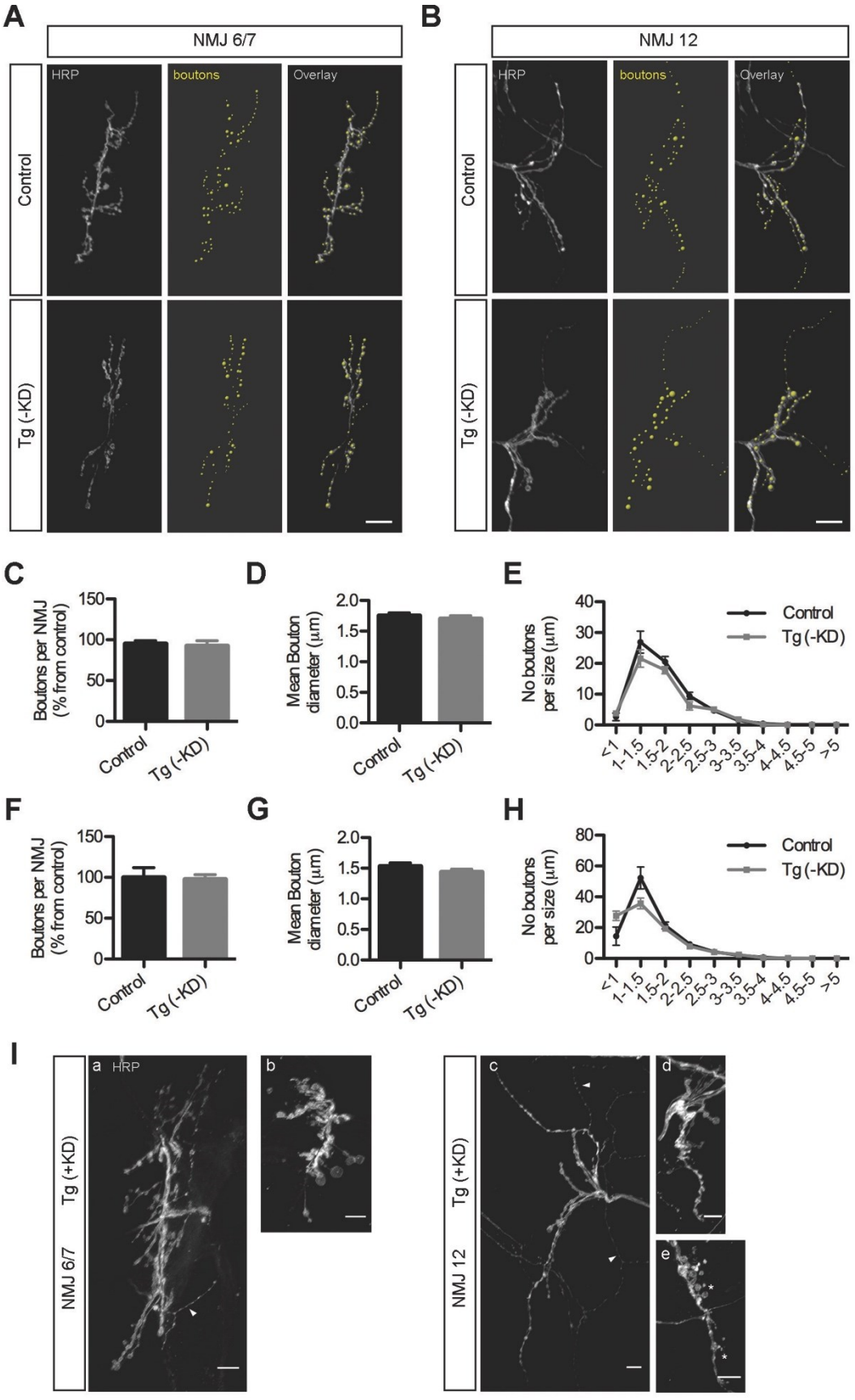
A
NMJ 6/7
HRP
boutons
Overlay
Control
Tg (-KD)
B
NMJ 12
HRP
boutons
Overlay
Control
Tg (-KD)
C
Boutons per NMJ (% from control)
150
100
50
0
Control
Tg (-KD)
D
Mean Bouton diameter (µm)
2.0
1.5
1.0
0.5
0.0
Control
Tg (-KD)
E
No boutons per size (µm)
40
30
20
10
0
Control
Tg (-KD)
<1
1-1.5
1.5-2
2-2.5
2.5-3
3-3.5
3.5-4
4-4.5
4.5-5
>5
F
Boutons per NMJ (% from control)
150
100
50
0
Control
Tg (-KD)
G
Mean Bouton diameter (µm)
2.0
1.5
1.0
0.5
0.0
Control
Tg (-KD)
H
No boutons per size (µm)
80
60
40
20
0
Control
Tg (-KD)
<1
1-1.5
1.5-2
2-2.5
2.5-3
3-3.5
3.5-4
4-4.5
4.5-5
>5
I
NMJ 6/7 Tg (+KD)
a HRP
b
NMJ 12 Tg (+KD)
c
d
e

**Figure 5.18: Sfxn3 down-regulation affects synaptic stability at the neuromuscular junction in *Drosophila* larvae. A, B)** Representative images from NMJs on muscle 6/7 (A) and muscle 12 (B) of control and transgenic third instar larvae with low knock-down of sfxn3, Tg(-KD). Grey: HRP. Yellow: boutons. Scale bar = 10 μm. C-H) Consistent number of boutons, mean bouton diameter and distribution of bouton diameter from control and Tg(-KD) NMJs from muscle 6/7 (**C, D, E**) and muscle 12 (**F, G, H**). Bars represent mean ± SEM, N=7-12, $p>0.05$ in One-Way ANOVA with Tukey post-test. **I)** Variable phenotypes observed in Tg(+KD) nerve terminals from muscles 6/7 and 12. Note the appearance of degenerating NMJs and collapsed structures (b, e) as well as highly ramified NMJs with abundant small size boutons (a, c, arrow heads) and satellite boutons (e, asterisc). Scale bars = 10 μm.

## 5.4. Discussion

### 5.4.1. Overview of results

α-synuclein plays a central role in Parkinson's disease, where it contributes to the vulnerability of synapses to degeneration. However, the mechanisms through which it controls synaptic stability and degeneration are not fully understood. First, we tested the possibility of using the PNS to study mechanisms downstream of α-synuclein that could contribute to the maintenance of synaptic stability, but the lack of any overt synaptic phenotypes in the PNS of mice lacking α-synuclein suggested that a focus on CNS phenotypes would be more biologically relevant. Therefore, we focused our research in the CNS, where a role for α-synuclein has been well established. Comparative proteomics on synapse enriched fractions from α-syn$^{+/+}$ and α-syn$^{-/-}$ mouse brain tissue identified robust perturbations of the synaptic proteome in the latter, with bioinformatics analysis revealing an enrichment of proteins contributing to mitochondrial pathways. One protein we identified in this screen was sideroflexin 3 (sfxn3). Biochemical characterization of sfxn3 confirmed that it is a mitochondrial protein preferentially localized to the inner mitochondrial membrane. Loss of sfxn3 did not overtly disturb the mitochondrial electron transport chain but experimental manipulation of sfxn3 levels in *Drosophila* larvae revealed a robust effect on synaptic stability at the level of the neuromuscular junction. Thus, our findings suggest that sfxn3 represents a novel α-synuclein-dependent mitochondrial regulator of synaptic stability *in vivo*.

### 5.4.2. α-synuclein does not overtly affect morphology and Wallerian degeneration of axons and nerve terminals in the peripheral nervous system

We found that deletion of α-synuclein did not impact on the morphological development or stability of axons and synapses in the PNS (Figure 5.3, Figure 5.4). In addition, when challenging these structures with a degeneration stimulus, via axotomy of the sciatic nerve, we found that endogenous levels of α-synuclein had no influence on the temporal or morphological characteristics of degenerating axons and neuromuscular synapses in the PNS (Figure 5.5 and Figure 5.6). These observations indicate that α-synuclein is not required for the basal stability of peripheral axons or neuromuscular synapses and that it does not overtly influence the process of Wallerian degeneration in the PNS in vivo.

Our finding that loss of α-synuclein had no influence on the progression of Wallerian degeneration in the PNS is in contrast to a previous similar study. Siebert and colleagues (Siebert et al., 2010) have suggested that α-synuclein may promote axonal degeneration in the PNS by looking at the preservation of axons and myelin sheaths in axotomized sciatic nerves from mice of several strains expressing varied levels of α-synuclein, including the strains we used in our study. However, their observations with respect to the progression of Wallerian degeneration were self-conflicting. Following nerve injury, they reported an increase in the number of preserved axons in α-synuclein null mice, which we identify as α-syn$^{-/-}$ in our study. However, this increase was accompanied by a higher density of axons in contralateral uninjured nerves when

compared to α-syn$^{+/+}$ mice, invalidating the comparison. Furthermore, they found a similar extent of axonal degeneration between transgenic mice overexpressing α-synuclein or genetically engineered α-synuclein knockout mice and their respective littermate controls, arguing against a significant influence of endogenous α-synuclein in the process of Wallerian degeneration in the PNS. By using electron microscopy we were able to perform a more thorough analysis of healthy and axotomized sciatic nerves of α-syn$^{+/+}$ and α-syn$^{-/-}$ mice. Both mouse strains were indistinguishable in all parameters assessed, including axon density and progression of Wallerian degeneration. In addition, we extended our study to include synapses, the neuronal compartment most affected by α-synuclein function, and found that neuromuscular terminals degenerated at the same rate regardless of the loss of α-synuclein.

Studies of transgenic mice over-expressing human full-length or mutant A53T α-synuclein have reported spontaneous nerve damage, denervation of NMJs or skeletal muscle atrophy (Martin et al., 2006, van der Putten et al., 2000). The difference in conclusions between these over-expression studies and our current loss-of-expression study could possibly be explained by α-synuclein toxicity in the PNS being caused by non-physiological effects associated with its excessive accumulation. In fact, the physiological and neuropathological characteristics of α-synuclein have been associated with different molecular mechanisms and distinct regions of the protein (Burre et al., 2012). The stability of PNS neurons could therefore possibly be affected by the formation of α-synuclein inclusions in transgenic mice without this being associated with a toxic gain-of-function of the protein. Accordingly, abnormal or aggregated α-synuclein disturbs axonal transport (Chu et al., 2012, Saha et al., 2004), which is a well-known

trigger of nerve damage and neurodegeneration (Coleman, 2005, De Vos et al., 2008). On the other hand, one of the few documented effects of physiological levels of α-synuclein on the PNS is the improvement of neuromuscular degeneration in CSP-α knock-out mice, which is mediated by α-synuclein's chaperone function (Chandra et al., 2005).

### 5.4.3. Mitochondrial pathways are affected by loss of α-synuclein

Comparative proteomics on synapses isolated from α-syn$^{-/-}$ mouse brain identified mitochondrial proteins as primary targets of α-synuclein deletion at CNS synapses. This is in agreement with a growing body of evidence suggesting that α-synuclein is an important regulator of mitochondrial function (Haelterman et al., 2014, Nakamura, 2013, Protter et al., 2012). In fact, a fraction of α-synuclein is associated with mitochondria (Li et al., 2007, Nakamura et al., 2008). Although believed to be primarily localized to the outer mitochondrial membrane, α-synuclein can be imported into mitochondria, via a process that is usually seen when variants of α-synuclein are expressed in transgenic animals or cell lines (Devi et al., 2008, Nakamura et al., 2011).

The role of α-synuclein in mitochondria function is still under investigation. Several groups have reported decreased complex I activity in PD patients and animal and cell models of α-synuclein pathology (Devi et al., 2008, Liu et al., 2009a, Parihar et al., 2008, Subramaniam et al., 2014). In addition, α-synuclein has also been found to increase oxidative stress and impair pathways involved in mitochondria fragmentation and mitophagy (Hsu et al., 2000, Kamp et al., 2010, Nakamura et al., 2011, Winslow et al., 2010). Deletion or knock-down of α-synuclein, on the other hand, partially decreases the susceptibility of some animal and cell models to Parkinson's toxin models, such as MPTP

and rotenone (Dauer et al., 2002, Klivenyi et al., 2006, Schluter et al., 2003, Zharikov et al., 2015).

Given the need to broaden our knowledge about how α-synuclein affects mitochondria, we extended our analysis of the proteomics data to reveal novel proteins not previously reported to broadly impact on neurodegenerative pathways or to interact with α-synuclein. We were able to identify 37 proteins with the greatest potential to be novel modulators of α-synuclein function in mitochondria. This list of proteins (Table 5.8) can be used to help interpret findings about α-synuclein and explore new mechanistic routes. We were particularly interested in sfxn3, as an extensive literature search revealed sfxn3 and proteins from the sideroflexin family are involved in neurodegenerative pathways (Charbonnier-Beaupel et al., 2015, Fowler et al., 2013, Fuller et al., 2014, Minjarez et al., 2016, Scifo et al., 2013, Simunovic et al., 2009).

### 5.4.4. Sfxn3 is a novel α-synuclein-dependent mitochondrial protein

We found sfxn3 levels were bi-directionally regulated by α-synuclein (Figure 5.9 and Figure 5.10). α-synuclein null mice have increased levels of sfxn3 in synapse enriched fractions, whereas SH-SY5Y cells overexpressing α-synuclein showed a decrease in the expression of sfxn3. The nature of the cooperation between α-synuclein and sfxn3 is not clear. On possibility is that α-synuclein interferes with the import of sfxn3 into mitochondria, since α-synuclein has been found to inhibit the import of nuclear encoded mitochondrial proteins through a pathological interaction with TOM20 (Di Maio et al., 2016). In support of this, we found several mitochondrial import proteins, such as TIM10B, TIM16, TOM40 and MIA40, to be upregulated in α-synuclein null mice

compared to WT controls (**Error! Reference source not found.**). Thus, it could be e xpected that levels of α-synuclein inversely correlate with the levels of some proteins of the inner mitochondrial membrane and mitochondrial matrix, of which sfxn3 might be one.

Nonetheless, at a functional level, it seems likely that sfxn3 acts downstream of α-synuclein. In support of this, α-synuclein overexpression has been found to affect the activity of mitochondria complex I (see above). We have reason to believe that reduced levels of sfxn3 could also modestly impair complex I activity under specific physiological conditions (Figure 5.13). Therefore, although still very speculative at this point, a relationship could exist in which the levels of α-synuclein indirectly regulate the availability of sfxn3. Reduction of sfxn3 could, in turn, be responsible for some of the negative effects of α-synuclein overexpression on complex I and/or other mitochondrial functions.

### 5.4.5. Function of sfxn3 in mitochondria

Loss of sfxn3 was not found to alter basal mitochondrial bioenergetics or the enzymatic activity of complex I and IV in young adult mice (Figure 5.13 B-D, Figure 5.14). However, sustained exposure to FCCP revealed subtle negative effects in oxidative phosphorylation, suggesting that sfxn3 deficiency could lead to impairments in the ability of the ETC to sustain prolonged high levels of activity (Figure 5.13 E-G). This is unlikely driven by defects in the oxidation of NADH, as the diaphorase activity of complex I was unaffected in enzymatic tests (Figure 5.14), but could be due to impairments in the electron flow machinery, such as in the integrity of iron-sulfur clusters (ISC). ISC are the

units responsible for the transfer of electrons along the ETC. Impairments in their assembly and altered levels of intracellular iron result in defects in ETC activity and oxidative stress (Rouault, 2012). Interestingly, elevated levels of iron are characteristic of PD and sideroflexins are proposed to be iron transporters (Fleming et al., 2001, Zecca et al., 2004). Furthermore, ISC assembly proteins and antioxidant proteins, such as peroxiredoxins, were upregulated, similarly to sfxn3, in α-syn$^{-/-}$ mice (Table 5.4), suggesting regulation of iron might be a common feature between these changes. In sfxn3$^{-/-}$ mice, a failure in iron import/export from mitochondria, due to loss of the proposed iron transport function of sxn3, could therefore potentially lead to impairments in the ETC. Specific experiments assessing the iron status of tissue from sfxn3$^{-/-}$ mice, as well as a better characterization of the influence of sfxn3 in oxidative phosphorylation, are nonetheless required before any theories can be drawn about the function of sfxn3.

### 5.4.6. Implications of sfxn3 for synaptic stability and Parkinson's Disease

Manipulation of sfxn3 levels in *Drosophila* larvae lead to robust negative effects on the stability of the neuromuscular junction (Figure 5.16, Figure 5.18). Increasing sfxn3 expression caused a consistent reduction in the number of boutons, whereas knock-down of the protein resulted in variable, striking defects in synaptic morphology. These experiments suggest that sfxn3 is important for synaptic development and/or maintenance of synaptic stability in *Drosophila*. The fact that both under and overexpression of sfxn3 destabilized synaptic morphology, indicates that a tight balance of the levels of sfxn3 is required to maintain synaptic form and function.

In contrast to what we saw in *Drosophila*, sfxn3$^{-/-}$ mice do show overt neuromuscular phenotypes. sfxn3$^{-/-}$ mice are viable and do not present observable motor deficits during the first months of life. In addition, neuromuscular junctions from their lumbrical muscles are morphologically very similar to those of young WT mice (data not shown). It will be important to formally assess motor function and synaptic morphology and function in young and aged sfxn3$^{-/-}$ mice. As with α-syn$^{-/-}$ mice, it is possible that effects of sfxn3 deletion are more prominent in aged animals or in specific regions of the nervous system. In addition, the contrast between the *Drosophila* experiments and the sfxn3$^{-/-}$ mice could be due to different compensatory mechanisms being triggered in the two species. It is well known that *Drosophila* do not express α-synuclein. If sfxn3 and α-synuclein cooperate to maintain synaptic function and stability it is conceivable that in a system where one is missing, manipulation of the other will result in more pronounced phenotypes.

Given the relationship between α-synuclein and sfxn3, increased levels of α-synuclein in PD are likely associated with decreased sfxn3. Indeed, microarray experiments performed on samples from the subtantia nigra of PD patients showed a decrease in sfxn3 transcripts compared to healthy controls (Simunovic et al., 2009). If proven useful, manipulation of sfxn3 could be used therapeutically to modulate some of the effects of α-synuclein that contribute to PD, instead of α-synuclein being targeted directly, a strategy that has not proven easy. First, however, we need to better understand the biology of sfxn3 and the nature of its relationship with α-synuclein.

# Chapter 6. General Discussion

## 6.1. Overview of results

The goal of the work developed in this thesis was to identify and explore novel proteins with potential to modulate synaptic stability in neurodegenerative conditions. In that regard, we performed three sets of experiments with the following main findings:

- Chapter 3: We demonstrated that synapses are affected in a large model of neurodegenerative disease, the CLN5 Batten sheep, and validated our initial targets for further study, calretinin and α-synuclein, as changed in this animal model. This provided useful novel information about the neuropathology of CLN5 Batten disease. In addition, gave us confidence that we were working with targets with potential to modulate neurodegeneration in large animals and, therefore, likely to be relevant to human conditions;
- Chapter 4: We explored the function of calretinin and its contribution to neurodegenerative pathways. We have shown calretinin is more widely expressed than reported in the literature and, particularly, that it is enriched in synapses. In addition, we showed calretinin presents activity-dependent properties and that loss of its expression in mice results in delayed Wallerian degeneration in the PNS and proteomic changes in brain synaptosomes consistent with impairments in cytoskeletal, synaptic and mitochondrial functions;
- Chapter 5: We explored downstream targets of α-synuclein and identified sfxn3 as an α-synuclein-dependent mitochondrial protein able to independently regulate synaptic morphology in *Drosophila*.

## 6.2. Implications for translational research

In Chapter 3 we explored synaptic pathology in a large animal model of neurodegenerative disease, the CLN5 Batten sheep. Not only we provided further insight into this disease model, which has not previously been characterized at the molecular level, but we also made a significant contribution to our ability to translate research from small animal models, such as *Drosophila*, through to rodents and large animal models of disease, such as sheep. The ability to work with tissue from large animals and to consistently identify changes at the protein level is extremely important when aiming to translate the abundant research performed in rodents to studies using human post-mortem or biopsy tissue. In addition, the confirmation that findings from mouse studies are applicable to studies in sheep is an important step for ensuring the applicability of the work performed in rodents or smaller animals to similar conditions in humans. Working with small animals is a valid option and continues to be preferable to most research groups from a time-frame and economic point of view. However, translational research would greatly benefit from confirmation studies performed in large animal models, such as the one performed in Chapter 3.

## 6.3. Novel targets contributing to synaptic function and stability

In Chapters 4 and 5 we presented work designed to explore novel molecular targets able to modulate synaptic stability *in vivo*. We have identified two candidates

(calretinin and sfxn3) which we show, for the first time, are directly involved in neurodegenerative pathways at the synapse.

In chapter 4, we established that calretinin is more widely expressed than previously believed and demonstrated that it is enriched at synapses, where it responds to synaptic activity and helps to regulate synaptic functions. In addition, we showed calretinin has the capacity to modulate neurodegenerative pathways. In particular, loss of calretinin was able to delay Wallerian degeneration but, on the other hand, aggravated cell death by oxidative stress. Thus, a compromise needs to be achieved when manipulating the levels of calretinin. Nonetheless, stabilizing the levels of this protein in conditions such as Batten disease, where calretinin is naturally upregulated during the course of disease, may help delay the loss of synapses characteristic of this condition without causing negative effects. Overall, our findings provide an important addition to the literature and place calretinin in the spotlight for future neurodegeneration research, where further *in vivo* and *in vitro* studies in models of neurodegenerative disease will help clarify the possibility of manipulating calretinin to obtain therapeutic benefits.

In chapter 5, we identified and characterized a novel mitochondrial protein (sfxn3) which functions downstream of α-synuclein at the synapse. Given the strong involvement of α-synuclein in the pathophysiology of Parkinson's disease and it's role in synaptic stability (Lashuel et al., 2013), our findings can help not only to further our understanding about the mechanisms involved in the initiation and progression of Parkinson's disease, but also to better understand the contribution of α-synuclein-dependent mechanisms to synaptic function and stability. Furthermore, sfxn3 was able to independently affect the

development/stability of neuromuscular synapses in *Drosophila*, indicating it could be an important modulator of synaptic stability across disease models. Therapies aimed at stabilizing the levels of sfxn3 may therefore prove beneficial for a range of neurodegenerative conditions, not limited to Parkinson's disease.

Taken together, this work identifies calretinin and sfxn3 as new modulators of synaptic stability and provides the basis for further studying their contributions to synaptic function and neurodegenerative mechanisms.

## 6.4. Conclusion

Taken together, the work in this thesis provides important new insights into underexplored molecular mechanisms involved in synaptic function and stability, and highlights the need and usefulness of continuing to explore new modulators of synaptic function and vulnerability. Moreover, it emphasizes the importance of synapses in the pathophysiology of neurodegenerative conditions across species and provides methods to study synaptic pathology in large animals, therefore supporting the translation of research across models of disease.

# References


ABELIOVICH, A., SCHMITZ, Y., FARINAS, I., CHOI-LUNDBERG, D., HO, W. H., CASTILLO, P. E., SHINSKY, N., VERDUGO, J. M., ARMANINI, M., RYAN, A., HYNES, M., PHILLIPS, H., SULZER, D. & ROSENTHAL, A. 2000. Mice lacking alpha-synuclein display functional deficits in the nigrostriatal dopamine system. *Neuron,* 25**,** 239-52.

ADI 2010. World Alzheimer Report 2010: The Global Economic Impact of Dementia. Alzheimer's Disease International.

AIGNER, B., RENNER, S., KESSLER, B., KLYMIUK, N., KUROME, M., WUNSCH, A. & WOLF, E. 2010. Transgenic pigs as models for translational biomedical research. *J Mol Med (Berl),* 88**,** 653-64.

AKHTAR, R. S., NESS, J. M. & ROTH, K. A. 2004. Bcl-2 family regulation of neuronal development and neurodegeneration. *Biochim Biophys Acta,* 1644**,** 189-203.

AL-WANDI, A., NINKINA, N., MILLERSHIP, S., WILLIAMSON, S. J., JONES, P. A. & BUCHMAN, V. L. 2010. Absence of alpha-synuclein affects dopamine metabolism and synaptic markers in the striatum of aging mice. *Neurobiol Aging,* 31**,** 796-804.

ALMEIDA, A., BROOKS, K. J., SAMMUT, I., KEELAN, J., DAVEY, G. P., CLARK, J. B. & BATES, T. E. 1995. Postnatal development of the complexes of the electron transport chain in synaptic mitochondria from rat brain. *Dev Neurosci,* 17**,** 212-8.

ALVES, C. J., DARIOLLI, R., JORGE, F. M., MONTEIRO, M. R., MAXIMINO, J. R., MARTINS, R. S., STRAUSS, B. E., KRIEGER, J. E., CALLEGARO, D. & CHADI, G. 2015. Gene expression profiling for human iPS-derived motor neurons from sporadic ALS patients reveals a strong association between mitochondrial functions and neurodegeneration. *Front Cell Neurosci,* 9**,** 289.

AMTUL, Z. 2016. Why therapies for Alzheimer's disease do not work: Do we have consensus over the path to follow? *Ageing Res Rev,* 25**,** 70-84.

ARENDT, O., SCHWALLER, B., BROWN, E. B., EILERS, J. & SCHMIDT, H. 2013. Restricted diffusion of calretinin in cerebellar granule cell dendrites implies Ca(2)(+)-dependent interactions via its EF-hand 5 domain. *J Physiol,* 591**,** 3887-99.

ARRASATE, M., MITRA, S., SCHWEITZER, E. S., SEGAL, M. R. & FINKBEINER, S. 2004. Inclusion body formation reduces levels of mutant huntingtin and the risk of neuronal death. *Nature,* 431**,** 805-10.

AS 2015. Drug treatments for Alzheimer's disease factsheet. Alzheimer's Society.

BABA, M., NAKAJO, S., TU, P. H., TOMITA, T., NAKAYA, K., LEE, V. M., TROJANOWSKI, J. Q. & IWATSUBO, T. 1998. Aggregation of alpha-synuclein in Lewy bodies of sporadic Parkinson's disease and dementia with Lewy bodies. *Am J Pathol,* 152**,** 879-84.

BAGLIETTO-VARGAS, D., MORENO-GONZALEZ, I., SANCHEZ-VARO, R., JIMENEZ, S., TRUJILLO-ESTRADA, L., SANCHEZ-MEJIAS, E., TORRES, M., ROMERO-ACEBAL, M., RUANO, D., VIZUETE, M., VITORICA, J. & GUTIERREZ, A. 2010. Calretinin interneurons are early targets of extracellular

amyloid-beta pathology in PS1/AbetaPP Alzheimer mice hippocampus. *J Alzheimers Dis,* 21**,** 119-32.

BAJIC, N., JENNER, P., BALLARD, C. G. & FRANCIS, P. T. 2012. Proteasome inhibition leads to early loss of synaptic proteins in neuronal culture. *J Neural Transm (Vienna),* 119**,** 1467-76.

BARABASI, A. L., GULBAHCE, N. & LOSCALZO, J. 2011. Network medicine: a network-based approach to human disease. *Nat Rev Genet,* 12**,** 56-68.

BARNHAM, K. J., MASTERS, C. L. & BUSH, A. I. 2004. Neurodegenerative diseases and oxidative stress. *Nat Rev Drug Discov,* 3**,** 205-14.

BARTELS, T., CHOI, J. G. & SELKOE, D. J. 2011. α-Synuclein occurs physiologically as a helically folded tetramer that resists aggregation. *Nature,* 477**,** 107-110.

BEARZATTO, B., SERVAIS, L., ROUSSEL, C., GALL, D., BABA-AISSA, F., SCHURMANS, S., DE KERCHOVE D'EXAERDE, A., CHERON, G. & SCHIFFMANN, S. N. 2006. Targeted calretinin expression in granule cells of calretinin-null mice restores normal cerebellar functions. *FASEB J,* 20**,** 380-2.

BECKER, R. E. & GREIG, N. H. 2012. Increasing the success rate for Alzheimer's disease drug discovery and development. *Expert Opin Drug Discov,* 7**,** 367-70.

BEIROWSKI, B., BEREK, L., ADALBERT, R., WAGNER, D., GRUMME, D. S., ADDICKS, K., RIBCHESTER, R. R. & COLEMAN, M. P. 2004. Quantitative and qualitative analysis of Wallerian degeneration using restricted axonal labelling in YFP-H mice. *J Neurosci Methods,* 134**,** 23-35.

BELLUCCI, A., ZALTIERI, M., NAVARRIA, L., GRIGOLETTO, J., MISSALE, C. & SPANO, P. 2012. From α-synuclein to synaptic dysfunctions: New insights into the pathophysiology of Parkinson's disease. *Brain Research*.

BENCE, N. F., SAMPAT, R. M. & KOPITO, R. R. 2001. Impairment of the ubiquitin-proteasome system by protein aggregation. *Science,* 292**,** 1552-5.

BENDER, A., DESPLATS, P., SPENCER, B., ROCKENSTEIN, E., ADAME, A., ELSTNER, M., LAUB, C., MUELLER, S., KOOB, A. O., MANTE, M., PHAM, E., KLOPSTOCK, T. & MASLIAH, E. 2013. TOM40 mediates mitochondrial dysfunction induced by alpha-synuclein accumulation in Parkinson's disease. *PLoS One,* 8**,** e62277.

BENITEZ, B. A., ALVARADO, D., CAI, Y., MAYO, K., CHAKRAVERTY, S., NORTON, J., MORRIS, J. C., SANDS, M. S., GOATE, A. & CRUCHAGA, C. 2011. Exome-sequencing confirms DNAJC5 mutations as cause of adult neuronal ceroid-lipofuscinosis. *PLoS One,* 6**,** e26741.

BENTHAM, P., GRAY, R., SELLWOOD, E. & RAFTERY, J. 1999. Effectiveness of rivastigmine in Alzheimer's disease. Improvements in functional ability remain unestablished. *Bmj,* 319**,** 640-1.

BERGER, Z., RAVIKUMAR, B., MENZIES, F. M., OROZ, L. G., UNDERWOOD, B. R., PANGALOS, M. N., SCHMITT, I., WULLNER, U., EVERT, B. O., O'KANE, C. J. & RUBINSZTEIN, D. C. 2006. Rapamycin alleviates toxicity of different aggregate-prone proteins. *Hum Mol Genet,* 15**,** 433-42.

BERGOFFEN, J., SCHERER, S. S., WANG, S., SCOTT, M. O., BONE, L. J., PAUL, D. L., CHEN, K., LENSCH, M. W., CHANCE, P. F. & FISCHBECK, K. H. 1993. Connexin mutations in X-linked Charcot-Marie-Tooth disease. *Science,* 262**,** 2039-42.

BINGOL, B. & SCHUMAN, E. M. 2005. Synaptic protein degradation by the ubiquitin proteasome system. *Curr Opin Neurobiol,* 15**,** 536-41.

BLOM, T., SCHMIEDT, M. L., WONG, A. M., KYTTALA, A., SORONEN, J., JAUHIAINEN, M., TYYNELA, J., COOPER, J. D. & JALANKO, A. 2013. Exacerbated neuronal ceroid lipofuscinosis phenotype in Cln1/5 double-knockout mice. *Dis Model Mech,* 6**,** 342-57.

BOFFOLI, D., SCACCO, S. C., VERGARI, R., SOLARINO, G., SANTACROCE, G. & PAPA, S. 1994. Decline with age of the respiratory chain activity in human skeletal muscle. *Biochim Biophys Acta,* 1226**,** 73-82.

BOWERMAN, M., MURRAY, L. M., BOYER, J. G., ANDERSON, C. L. & KOTHARY, R. 2012. Fasudil improves survival and promotes skeletal muscle development in a mouse model of spinal muscular atrophy. *BMC Med,* 10**,** 24.

BROOKMEYER, R., JOHNSON, E., ZIEGLER-GRAHAM, K. & ARRIGHI, H. M. 2007. Forecasting the global burden of Alzheimer's disease. *Alzheimers Dement,* 3**,** 186-91.

BROWN, M. R., SULLIVAN, P. G. & GEDDES, J. W. 2006. Synaptic mitochondria are more susceptible to Ca2+overload than nonsynaptic mitochondria. *J Biol Chem,* 281**,** 11658-68.

BURRE, J. 2015. The Synaptic Function of alpha-Synuclein. *J Parkinsons Dis,* 5**,** 699-713.

BURRE, J., SHARMA, M. & SUDHOF, T. C. 2012. Systematic mutagenesis of alpha-synuclein reveals distinct sequence requirements for physiological and pathological activities. *J Neurosci,* 32**,** 15227-42.

BURRE, J., SHARMA, M. & SUDHOF, T. C. 2014. alpha-Synuclein assembles into higher-order multimers upon membrane binding to promote SNARE complex formation. *Proc Natl Acad Sci U S A,* 111**,** E4274-83.

BURRE, J., SHARMA, M. & SUDHOF, T. C. 2015. Definition of a Molecular Pathway Mediating alpha-Synuclein Neurotoxicity. *J Neurosci,* 35**,** 5221-32.

BURRE, J., SHARMA, M., TSETSENIS, T., BUCHMAN, V., ETHERTON, M. R. & SUDHOF, T. C. 2010. Alpha-synuclein promotes SNARE-complex assembly in vivo and in vitro. *Science,* 329**,** 1663-7.

BURRE, J., VIVONA, S., DIAO, J., SHARMA, M., BRUNGER, A. T. & SUDHOF, T. C. 2013. Properties of native brain alpha-synuclein. *Nature,* 498**,** E4-6; discussion E6-7.

BURRONE, J., LI, Z. & MURTHY, V. N. 2006. Studying vesicle cycling in presynaptic terminals using the genetically encoded probe synaptopHluorin. *Nat Protoc,* 1**,** 2970-8.

BUTLER, B., SAHA, K., RANA, T., BECKER, J. P., SAMBO, D., DAVARI, P., GOODWIN, J. S. & KHOSHBOUEI, H. 2015. Dopamine Transporter Activity Is Modulated by alpha-Synuclein. *J Biol Chem,* 290**,** 29542-54.

CABIN, D. E., GISPERT-SANCHEZ, S., MURPHY, D., AUBURGER, G., MYERS, R. R. & NUSSBAUM, R. L. 2005. Exacerbated synucleinopathy in mice expressing A53T SNCA on a Snca null background. *Neurobiol Aging,* 26**,** 25-35.

CABIN, D. E., SHIMAZU, K., MURPHY, D., COLE, N. B., GOTTSCHALK, W., MCILWAIN, K. L., ORRISON, B., CHEN, A., ELLIS, C. E., PAYLOR, R., LU, B. & NUSSBAUM, R. L. 2002. Synaptic vesicle depletion correlates with

attenuated synaptic responses to prolonged repetitive stimulation in mice lacking alpha-synuclein. *J Neurosci,* 22**,** 8797-807.

CAMP, A. J. & WIJESINGHE, R. 2009. Calretinin: modulator of neuronal excitability. *Int J Biochem Cell Biol,* 41**,** 2118-21.

CAPUTI, A., ROZOV, A., BLATOW, M. & MONYER, H. 2009. Two calretinin-positive GABAergic cell types in layer 2/3 of the mouse neocortex provide different forms of inhibition. *Cereb Cortex,* 19**,** 1345-59.

CAULI, B., ZHOU, X., TRICOIRE, L., TOUSSAY, X. & STAIGER, J. F. 2014. Revisiting enigmatic cortical calretinin-expressing interneurons. *Front Neuroanat,* 8**,** 52.

CHANDRA, S., FORNAI, F., KWON, H.-B., YAZDANI, U., ATASOY, D., LIU, X., HAMMER, R. E., BATTAGLIA, G., GERMAN, D. C., CASTILLO, P. E. & SÜDHOF, T. C. 2004a. Double-knockout mice for α- and β-synucleins: Effect on synaptic functions. *Proc Natl Acad Sci U S A,* 101**,** 14966-14971.

CHANDRA, S., FORNAI, F., KWON, H. B., YAZDANI, U., ATASOY, D., LIU, X., HAMMER, R. E., BATTAGLIA, G., GERMAN, D. C., CASTILLO, P. E. & SUDHOF, T. C. 2004b. Double-knockout mice for alpha- and beta-synucleins: effect on synaptic functions. *Proc Natl Acad Sci U S A,* 101**,** 14966-71.

CHANDRA, S., GALLARDO, G., FERNANDEZ-CHACON, R., SCHLUTER, O. M. & SUDHOF, T. C. 2005. Alpha-synuclein cooperates with CSPalpha in preventing neurodegeneration. *Cell,* 123**,** 383-96.

CHANG, D. T. & REYNOLDS, I. J. 2006. Mitochondrial trafficking and morphology in healthy and injured neurons. *Prog Neurobiol,* 80**,** 241-68.

CHARBONNIER-BEAUPEL, F., MALERBI, M., ALCACER, C., TAHIRI, K., CARPENTIER, W., WANG, C., DURING, M., XU, D., WORLEY, P. F., GIRAULT, J. A., HERVE, D. & CORVOL, J. C. 2015. Gene expression analyses identify Narp contribution in the development of L-DOPA-induced dyskinesia. *J Neurosci,* 35**,** 96-111.

CHARTIER-HARLIN, M.-C., KACHERGUS, J., ROUMIER, C., MOUROUX, V., DOUAY, X., LINCOLN, S., LEVECQUE, C., LARVOR, L., ANDRIEUX, J., HULIHAN, M., WAUCQUIER, N., DEFEBVRE, L., AMOUYEL, P., FARRER, M. & DESTÉE, A. 2004. Alpha-synuclein locus duplication as a cause of familial Parkinson's disease. *Lancet,* 364**,** 1167-1169.

CHEN, Y., YANG, W., LI, X., LI, X., YANG, H., XU, Z. & YU, S. 2015. alpha-Synuclein-induced internalization of NMDA receptors in hippocampal neurons is associated with reduced inward current and Ca(2+) influx upon NMDA stimulation. *Neuroscience,* 300**,** 297-306.

CHENG, F., LI, X., LI, Y., WANG, C., WANG, T., LIU, G., BASKYS, A., UEDA, K., CHAN, P. & YU, S. 2011. alpha-Synuclein promotes clathrin-mediated NMDA receptor endocytosis and attenuates NMDA-induced dopaminergic cell death. *J Neurochem,* 119**,** 815-25.

CHI, P., GREENGARD, P. & RYAN, T. A. 2001. Synapsin dispersion and reclustering during synaptic activity. *Nat Neurosci,* 4**,** 1187-93.

CHOI, S. W., GERENCSER, A. A. & NICHOLLS, D. G. 2009. Bioenergetic analysis of isolated cerebrocortical nerve terminals on a microgram scale: spare respiratory capacity and stochastic mitochondrial failure. *J Neurochem,* 109**,** 1179-91.

CHOO, Y. S., JOHNSON, G. V., MACDONALD, M., DETLOFF, P. J. & LESORT, M. 2004. Mutant huntingtin directly increases susceptibility of mitochondria to the calcium-induced permeability transition and cytochrome c release. *Hum Mol Genet,* 13**,** 1407-20.

CHRISTEL, C. J., SCHAER, R., WANG, S., HENZI, T., KREINER, L., GRABS, D., SCHWALLER, B. & LEE, A. 2012. Calretinin regulates Ca2+-dependent inactivation and facilitation of Ca(v)2.1 Ca2+ channels through a direct interaction with the alpha12.1 subunit. *J Biol Chem,* 287**,** 39766-75.

CHU, Y., MORFINI, G. A., LANGHAMER, L. B., HE, Y., BRADY, S. T. & KORDOWER, J. H. 2012. Alterations in axonal transport motor proteins in sporadic and experimental Parkinson's disease. *Brain,* 135**,** 2058-73.

CHUNG, C. Y., KHURANA, V., AULUCK, P. K., TARDIFF, D. F., MAZZULLI, J. R., SOLDNER, F., BARU, V., LOU, Y., FREYZON, Y., CHO, S., MUNGENAST, A. E., MUFFAT, J., MITALIPOVA, M., PLUTH, M. D., JUI, N. T., SCHULE, B., LIPPARD, S. J., TSAI, L. H., KRAINC, D., BUCHWALD, S. L., JAENISCH, R. & LINDQUIST, S. 2013. Identification and rescue of alpha-synuclein toxicity in Parkinson patient-derived neurons. *Science,* 342**,** 983-7.

CICCHETTI, F. & PARENT, A. 1996. Striatal interneurons in Huntington's disease: selective increase in the density of calretinin-immunoreactive medium-sized neurons. *Mov Disord,* 11**,** 619-26.

CITRI, A. & MALENKA, R. C. 2008. Synaptic plasticity: multiple forms, functions, and mechanisms. *Neuropsychopharmacology,* 33**,** 18-41.

CLAYTON, E. L., EVANS, G. J. O. & COUSIN, M. A. 2007. Activity-dependent control of bulk endocytosis by protein dephosphorylation in central nerve terminals. *J Physiol,* 585**,** 687-691.

COLBRAN, R. J. & BROWN, A. M. 2004. Calcium/calmodulin-dependent protein kinase II and synaptic plasticity. *Curr Opin Neurobiol,* 14**,** 318-27.

COLEMAN, M. 2005. Axon degeneration mechanisms: commonality amid diversity. *Nat Rev Neurosci,* 6**,** 889-98.

CONNOR, B. & DRAGUNOW, M. 1998. The role of neuronal growth factors in neurodegenerative disorders of the human brain. *Brain Res Brain Res Rev,* 27**,** 1-39.

CULLEN, V., LINDFORS, M., NG, J., PAETAU, A., SWINTON, E., KOLODZIEJ, P., BOSTON, H., SAFTIG, P., WOULFE, J., FEANY, M. B., MYLLYKANGAS, L., SCHLOSSMACHER, M. G. & TYYNELA, J. 2009. Cathepsin D expression level affects alpha-synuclein processing, aggregation, and toxicity in vivo. *Mol Brain,* 2**,** 5.

CUMMINGS, D. M., MILNERWOOD, A. J., DALLERAC, G. M., WAIGHTS, V., BROWN, J. Y., VATSAVAYAI, S. C., HIRST, M. C. & MURPHY, K. P. 2006. Aberrant cortical synaptic plasticity and dopaminergic dysfunction in a mouse model of Huntington's disease. *Hum Mol Genet,* 15**,** 2856-68.

CUMMINGS, J. L., MORSTORF, T. & ZHONG, K. 2014. Alzheimer's disease drug-development pipeline: few candidates, frequent failures. *Alzheimers Res Ther,* 6**,** 37.

DANTUMA, N. P. & BOTT, L. C. 2014. The ubiquitin-proteasome system in neurodegenerative diseases: precipitating factor, yet part of the solution. *Front Mol Neurosci,* 7**,** 70.

DAUER, W., KHOLODILOV, N., VILA, M., TRILLAT, A. C., GOODCHILD, R., LARSEN, K. E., STAAL, R., TIEU, K., SCHMITZ, Y., YUAN, C. A., ROCHA, M., JACKSON-LEWIS, V., HERSCH, S., SULZER, D., PRZEDBORSKI, S., BURKE, R. & HEN, R. 2002. Resistance of alpha -synuclein null mice to the parkinsonian neurotoxin MPTP. *Proc Natl Acad Sci U S A,* 99**,** 14524-9.

DAVEY, G. P. & BOLANOS, J. P. 2013. Peroxiredoxin 5 links mitochondrial redox signalling with calcium dynamics: impact on Parkinson's disease. *J Neurochem,* 125**,** 332-3.

DAVEY, G. P., CANEVARI, L. & CLARK, J. B. 1997. Threshold effects in synaptosomal and nonsynaptic mitochondria from hippocampal CA1 and paramedian neocortex brain regions. *J Neurochem,* 69**,** 2564-70.

DAVEY, G. P. & CLARK, J. B. 1996. Threshold effects and control of oxidative phosphorylation in nonsynaptic rat brain mitochondria. *J Neurochem,* 66**,** 1617-24.

DAVIDSON, W. S., JONAS, A., CLAYTON, D. F. & GEORGE, J. M. 1998. Stabilization of alpha-synuclein secondary structure upon binding to synthetic membranes. *The Journal of Biological Chemistry,* 273**,** 9443-9449.

DAVIES, C. A., MANN, D. M., SUMPTER, P. Q. & YATES, P. O. 1987. A quantitative morphometric analysis of the neuronal and synaptic content of the frontal and temporal cortex in patients with Alzheimer's disease. *J Neurol Sci,* 78**,** 151-64.

DAY, M., WANG, Z., DING, J., AN, X., INGHAM, C. A., SHERING, A. F., WOKOSIN, D., ILIJIC, E., SUN, Z., SAMPSON, A. R., MUGNAINI, E., DEUTCH, A. Y., SESACK, S. R., ARBUTHNOTT, G. W. & SURMEIER, D. J. 2006. Selective elimination of glutamatergic synapses on striatopallidal neurons in Parkinson disease models. *Nat Neurosci,* 9**,** 251-9.

DE VOS, K. J., GRIERSON, A. J., ACKERLEY, S. & MILLER, C. C. 2008. Role of axonal transport in neurodegenerative diseases. *Annu Rev Neurosci,* 31**,** 151-73.

DECRESSAC, M., KADKHODAEI, B., MATTSSON, B., LAGUNA, A., PERLMANN, T. & BJORKLUND, A. 2012. alpha-Synuclein-induced down-regulation of Nurr1 disrupts GDNF signaling in nigral dopamine neurons. *Sci Transl Med,* 4**,** 163ra156.

DEHAY, B., BOURDENX, M., GORRY, P., PRZEDBORSKI, S., VILA, M., HUNOT, S., SINGLETON, A., OLANOW, C. W., MERCHANT, K. M., BEZARD, E., PETSKO, G. A. & MEISSNER, W. G. 2015. Targeting alpha-synuclein for treatment of Parkinson's disease: mechanistic and therapeutic considerations. *Lancet Neurol,* 14**,** 855-66.

DEKOSKY, S. T., CARRILLO, M. C., PHELPS, C., KNOPMAN, D., PETERSEN, R. C., FRANK, R., SCHENK, D., MASTERMAN, D., SIEMERS, E. R., CEDARBAUM, J. M., GOLD, M., MILLER, D. S., MORIMOTO, B. H., KHACHATURIAN, A. S. & MOHS, R. C. 2011. Revision of the criteria for Alzheimer's disease: A symposium. *Alzheimers Dement,* 7**,** e1-12.

DEKOSKY, S. T. & SCHEFF, S. W. 1990. Synapse loss in frontal cortex biopsies in Alzheimer's disease: correlation with cognitive severity. *Ann Neurol,* 27**,** 457-64.

DEVI, L., RAGHAVENDRAN, V., PRABHU, B. M., AVADHANI, N. G. & ANANDATHEERTHAVARADA, H. K. 2008. Mitochondrial import and accumulation of alpha-synuclein impair complex I in human dopaminergic neuronal cultures and Parkinson disease brain. *J Biol Chem,* 283**,** 9089-100.

DI MAIO, R., BARRETT, P. J., HOFFMAN, E. K., BARRETT, C. W., ZHARIKOV, A., BORAH, A., HU, X., MCCOY, J., CHU, C. T., BURTON, E. A., HASTINGS, T. G. & GREENAMYRE, J. T. 2016. alpha-Synuclein binds to TOM20 and inhibits mitochondrial protein import in Parkinson's disease. *Sci Transl Med,* 8**,** 342ra78.

DIMAURO, S. & SCHON, E. A. 2008. Mitochondrial disorders in the nervous system. *Annu Rev Neurosci,* 31**,** 91-123.

DIOGENES, M. J., DIAS, R. B., ROMBO, D. M., VICENTE MIRANDA, H., MAIOLINO, F., GUERREIRO, P., NASSTROM, T., FRANQUELIM, H. G., OLIVEIRA, L. M., CASTANHO, M. A., LANNFELT, L., BERGSTROM, J., INGELSSON, M., QUINTAS, A., SEBASTIAO, A. M., LOPES, L. V. & OUTEIRO, T. F. 2012. Extracellular alpha-synuclein oligomers modulate synaptic transmission and impair LTP via NMDA-receptor activation. *J Neurosci,* 32**,** 11750-62.

DOLEZALOVA, D., HRUSKA-PLOCHAN, M., BJARKAM, C. R., SORENSEN, J. C., CUNNINGHAM, M., WEINGARTEN, D., CIACCI, J. D., JUHAS, S., JUHASOVA, J., MOTLIK, J., HEFFERAN, M. P., HAZEL, T., JOHE, K., CARROMEU, C., MUOTRI, A., BUI, J., STRNADEL, J. & MARSALA, M. 2014. Pig models of neurodegenerative disorders: Utilization in cell replacement-based preclinical safety and efficacy studies. *J Comp Neurol,* 522**,** 2784-801.

DONG, G., GROSS, K., QIAO, F., FERGUSON, J., CALLEGARI, E. A., REZVANI, K., ZHANG, D., GLOECKNER, C. J., UEFFING, M. & WANG, H. 2012. Calretinin interacts with huntingtin and reduces mutant huntingtin-caused cytotoxicity. *J Neurochem,* 123**,** 437-46.

DONMEZ, G. & OUTEIRO, T. F. 2013. SIRT1 and SIRT2: emerging targets in neurodegeneration. *EMBO Mol Med,* 5**,** 344-52.

DONNELIER, J. & BRAUN, J. E. 2014. CSPalpha-chaperoning presynaptic proteins. *Front Cell Neurosci,* 8**,** 116.

DORSEY, E. R., CONSTANTINESCU, R., THOMPSON, J. P., BIGLAN, K. M., HOLLOWAY, R. G., KIEBURTZ, K., MARSHALL, F. J., RAVINA, B. M., SCHIFITTO, G., SIDEROWF, A. & TANNER, C. M. 2007. Projected number of people with Parkinson disease in the most populous nations, 2005 through 2030. *Neurology,* 68**,** 384-6.

DU, H., GUO, L., YAN, S., SOSUNOV, A. A., MCKHANN, G. M. & YAN, S. S. 2010. Early deficits in synaptic mitochondria in an Alzheimer's disease mouse model. *Proc Natl Acad Sci U S A,* 107**,** 18670-5.

DUNKLEY, P. R., JARVIE, P. E. & ROBINSON, P. J. 2008. A rapid Percoll gradient procedure for preparation of synaptosomes. *Nat Protoc,* 3**,** 1718-1728.

DZAJA, D., HLADNIK, A., BICANIC, I., BAKOVIC, M. & PETANJEK, Z. 2014. Neocortical calretinin neurons in primates: increase in proportion and microcircuitry structure. *Front Neuroanat,* 8**,** 103.

EATON, S. L., ROCHE, S. L., LLAVERO HURTADO, M., OLDKNOW, K. J., FARQUHARSON, C., GILLINGWATER, T. H. & WISHART, T. M. 2013. Total Protein Analysis as a Reliable Loading Control for Quantitative Fluorescent Western Blotting. *PLoS One,* 8**,** e72457.

FAAS, G. C., SCHWALLER, B., VERGARA, J. L. & MODY, I. 2007. Resolving the fast kinetics of cooperative binding: Ca2+ buffering by calretinin. *PLoS Biol,* 5**,** e311.

FAHANDEJSAADI, A., LEUNG, E., RAHAII, R., BU, J. & GEULA, C. 2004. Calbindin-D28K, parvalbumin and calretinin in primate lower motor neurons. *Neuroreport,* 15**,** 443-8.

FEARNLEY, J. M. & LEES, A. J. 1991. Ageing and Parkinson's disease: substantia nigra regional selectivity. *Brain: A Journal of Neurology,* 114 ( Pt 5)**,** 2283-2301.

FERNANDEZ-CHACON, R., WOLFEL, M., NISHIMUNE, H., TABARES, L., SCHMITZ, F., CASTELLANO-MUNOZ, M., ROSENMUND, C., MONTESINOS, M. L., SANES, J. R., SCHNEGGENBURGER, R. & SUDHOF, T. C. 2004. The synaptic vesicle protein CSP alpha prevents presynaptic degeneration. *Neuron,* 42**,** 237-51.

FERRANDIZ, M. L., MARTINEZ, M., DE JUAN, E., DIEZ, A., BUSTOS, G. & MIQUEL, J. 1994. Impairment of mitochondrial oxidative phosphorylation in the brain of aged mice. *Brain Res,* 644**,** 335-8.

FERRANTE, R. J., KOWALL, N. W. & RICHARDSON, E. P., JR. 1991. Proliferative and degenerative changes in striatal spiny neurons in Huntington's disease: a combined study using the section-Golgi method and calbindin D28k immunocytochemistry. *J Neurosci,* 11**,** 3877-87.

FLEMING, M. D., CAMPAGNA, D. R., HASLETT, J. N., TRENOR, C. C., 3RD & ANDREWS, N. C. 2001. A mutation in a mitochondrial transmembrane protein is responsible for the pleiotropic hematological and skeletal phenotype of flexed-tail (f/f) mice. *Genes Dev,* 15**,** 652-7.

FONSECA, M. & SORIANO, E. 1995. Calretinin-immunoreactive neurons in the normal human temporal cortex and in Alzheimer's disease. *Brain Res,* 691**,** 83-91.

FOWLER, S. L., AKINS, M., ZHOU, H., FIGEYS, D. & BENNETT, S. A. 2013. The liver connexin32 interactome is a novel plasma membrane-mitochondrial signaling nexus. *J Proteome Res,* 12**,** 2597-610.

FRANCIS, P. T., PALMER, A. M., SNAPE, M. & WILCOCK, G. K. 1999. The cholinergic hypothesis of Alzheimer's disease: a review of progress. *J Neurol Neurosurg Psychiatry,* 66**,** 137-47.

FREUND, T. F. & MAGLOCZKY, Z. 1993. Early degeneration of calretinin-containing neurons in the rat hippocampus after ischemia. *Neuroscience,* 56**,** 581-96.

FRUGIER, T., MITCHELL, N. L., TAMMEN, I., HOUWELING, P. J., ARTHUR, D. G., KAY, G. W., VAN DIGGELEN, O. P., JOLLY, R. D. & PALMER, D. N. 2008. A new large animal model of CLN5 neuronal ceroid lipofuscinosis in Borderdale sheep is caused by a nucleotide substitution at a consensus splice site (c.571+1G>A) leading to excision of exon 3. *Neurobiol Dis,* 29**,** 306-15.

FULLER, H. R., HURTADO, M. L., WISHART, T. M. & GATES, M. A. 2014. The rat striatum responds to nigro-striatal degeneration via the increased expression of proteins associated with growth and regeneration of neuronal circuitry. *Proteome Sci,* 12**,** 20.

GALL, D., ROUSSEL, C., SUSA, I., D'ANGELO, E., ROSSI, P., BEARZATTO, B., GALAS, M. C., BLUM, D., SCHURMANS, S. & SCHIFFMANN, S. N. 2003. Altered neuronal excitability in cerebellar granule cells of mice lacking calretinin. *J Neurosci,* 23**,** 9320-7.

GARCIA-JUNCO-CLEMENTE, P., CANTERO, G., GOMEZ-SANCHEZ, L., LINARES-CLEMENTE, P., MARTINEZ-LOPEZ, J. A., LUJAN, R. & FERNANDEZ-CHACON, R. 2010. Cysteine string protein-alpha prevents activity-dependent degeneration in GABAergic synapses. *J Neurosci,* 30**,** 7377-91.

GARCIA-REITBOCK, P., ANICHTCHIK, O., BELLUCCI, A., IOVINO, M., BALLINI, C., FINEBERG, E., GHETTI, B., DELLA CORTE, L., SPANO, P., TOFARIS, G. K., GOEDERT, M. & SPILLANTINI, M. G. 2010. SNARE protein redistribution and synaptic failure in a transgenic mouse model of Parkinson's disease. *Brain,* 133**,** 2032-44.

GILLINGWATER, T. H. & RIBCHESTER, R. R. 2001. Compartmental neurodegeneration and synaptic plasticity in the Wlds mutant mouse. *J Physiol,* 534**,** 627-639.

GILLINGWATER, T. H., THOMSON, D., MACK, T. G., SOFFIN, E. M., MATTISON, R. J., COLEMAN, M. P. & RIBCHESTER, R. R. 2002. Age-dependent synapse withdrawal at axotomised neuromuscular junctions in Wld(s) mutant and Ube4b/Nmnat transgenic mice. *J Physiol,* 543**,** 739-55.

GILLINGWATER, T. H. & WISHART, T. M. 2013. Mechanisms underlying synaptic vulnerability and degeneration in neurodegenerative disease. *Neuropathol Appl Neurobiol,* 39**,** 320-34.

GOMEZ, L. A., MONETTE, J. S., CHAVEZ, J. D., MAIER, C. S. & HAGEN, T. M. 2009. Supercomplexes of the mitochondrial electron transport chain decline in the aging rat heart. *Arch Biochem Biophys,* 490**,** 30-5.

GORBATYUK, O. S., LI, S., NASH, K., GORBATYUK, M., LEWIN, A. S., SULLIVAN, L. F., MANDEL, R. J., CHEN, W., MEYERS, C., MANFREDSSON, F. P. & MUZYCZKA, N. 2010. In vivo RNAi-mediated alpha-synuclein silencing induces nigrostriatal degeneration. *Mol Ther,* 18**,** 1450-7.

GORDON, S. L., HARPER, C. B., SMILLIE, K. J. & COUSIN, M. A. 2016. A Fine Balance of Synaptophysin Levels Underlies Efficient Retrieval of Synaptobrevin II to Synaptic Vesicles. *PLoS One,* 11**,** e0149457.

GORDON, S. L., LEUBE, R. E. & COUSIN, M. A. 2011. Synaptophysin is required for synaptobrevin retrieval during synaptic vesicle endocytosis. *The Journal of Neuroscience,* 31**,** 14032-14036.

GRAVELAND, G. A., WILLIAMS, R. S. & DIFIGLIA, M. 1985. Evidence for degenerative and regenerative changes in neostriatal spiny neurons in Huntington's disease. *Science,* 227**,** 770-3.

GRAY, D. A. 2001. Damage control--a possible non-proteolytic role for ubiquitin in limiting neurodegeneration. *Neuropathol Appl Neurobiol,* 27**,** 89-94.

GULYAS, A. I., MIETTINEN, R., JACOBOWITZ, D. M. & FREUND, T. F. 1992. Calretinin is present in non-pyramidal cells of the rat hippocampus--I. A new type of neuron specifically associated with the mossy fibre system. *Neuroscience,* 48**,** 1-27.

GUO, J. T., CHEN, A. Q., KONG, Q., ZHU, H., MA, C. M. & QIN, C. 2008. Inhibition of vesicular monoamine transporter-2 activity in alpha-synuclein stably transfected SH-SY5Y cells. *Cell Mol Neurobiol,* 28**,** 35-47.

GUSTAVSSON, A., SVENSSON, M., JACOBI, F., ALLGULANDER, C., ALONSO, J., BEGHI, E., DODEL, R., EKMAN, M., FARAVELLI, C., FRATIGLIONI, L., GANNON, B., JONES, D. H., JENNUM, P., JORDANOVA, A., JONSSON, L., KARAMPAMPA, K., KNAPP, M., KOBELT, G., KURTH, T., LIEB, R., LINDE, M., LJUNGCRANTZ, C., MAERCKER, A., MELIN, B., MOSCARELLI, M., MUSAYEV, A., NORWOOD, F., PREISIG, M., PUGLIATTI, M., REHM, J., SALVADOR-CARULLA, L., SCHLEHOFER, B., SIMON, R., STEINHAUSEN, H. C., STOVNER, L. J., VALLAT, J. M., VAN DEN BERGH, P., VAN OS, J., VOS, P., XU, W., WITTCHEN, H. U., JONSSON, B., OLESEN, J. & GROUP, C. D. 2011. Cost of disorders of the brain in Europe 2010. *Eur Neuropsychopharmacol,* 21**,** 718-79.

HAASS, C. & SELKOE, D. J. 2007. Soluble protein oligomers in neurodegeneration: lessons from the Alzheimer's amyloid beta-peptide. *Nat Rev Mol Cell Biol,* 8**,** 101-12.

HACK, N. J., WRIDE, M. C., CHARTERS, K. M., KATER, S. B. & PARKS, T. N. 2000. Developmental changes in the subcellular localization of calretinin. *J Neurosci,* 20**,** RC67.

HAELTERMAN, N. A., YOON, W. H., SANDOVAL, H., JAISWAL, M., SHULMAN, J. M. & BELLEN, H. J. 2014. A mitocentric view of Parkinson's disease. *Annu Rev Neurosci,* 37**,** 137-59.

HALLIDAY, G. M., MCRITCHIE, D. A., MACDONALD, V., DOUBLE, K. L., TRENT, R. J. & MCCUSKER, E. 1998. Regional specificity of brain atrophy in Huntington's disease. *Exp Neurol,* 154**,** 663-72.

HAMPEL, H., FRANK, R., BROICH, K., TEIPEL, S. J., KATZ, R. G., HARDY, J., HERHOLZ, K., BOKDE, A. L., JESSEN, F., HOESSLER, Y. C., SANHAI, W. R., ZETTERBERG, H., WOODCOCK, J. & BLENNOW, K. 2010. Biomarkers for Alzheimer's disease: academic, industry and regulatory perspectives. *Nat Rev Drug Discov,* 9**,** 560-74.

HARDINGHAM, G. E. & BADING, H. 2010. Synaptic versus extrasynaptic NMDA receptor signalling: implications for neurodegenerative disorders. *Nat Rev Neurosci,* 11**,** 682-96.

HARRIS, J. J., JOLIVET, R. & ATTWELL, D. 2012. Synaptic energy use and supply. *Neuron,* 75**,** 762-77.

HEINONEN, O., SOININEN, H., SORVARI, H., KOSUNEN, O., PALJARVI, L., KOIVISTO, E. & RIEKKINEN, P. J., SR. 1995. Loss of synaptophysin-like immunoreactivity in the hippocampal formation is an early phenomenon in Alzheimer's disease. *Neuroscience,* 64**,** 375-84.

HENSTRIDGE, C. M., PICKETT, E. & SPIRES-JONES, T. L. 2016. Synaptic pathology: a shared mechanism in neurological disease. *Ageing Res Rev*.

HERRMANN, N., CHAU, S. A., KIRCANSKI, I. & LANCTOT, K. L. 2011. Current and emerging drug treatment options for Alzheimer's disease: a systematic review. *Drugs,* 71**,** 2031-65.

HILFIKER, S., PIERIBONE, V. A., CZERNIK, A. J., KAO, H. T., AUGUSTINE, G. J. & GREENGARD, P. 1999. Synapsins as regulators of neurotransmitter release. *Philosophical Transactions of the Royal Society of London. Series B, Biological Sciences,* 354**,** 269-279.

HOLMBERG, V., JALANKO, A., ISOSOMPPI, J., FABRITIUS, A. L., PELTONEN, L. & KOPRA, O. 2004. The mouse ortholog of the neuronal ceroid lipofuscinosis CLN5 gene encodes a soluble lysosomal glycoprotein expressed in the developing brain. *Neurobiol Dis,* 16**,** 29-40.

HOOVER, B. R., REED, M. N., SU, J., PENROD, R. D., KOTILINEK, L. A., GRANT, M. K., PITSTICK, R., CARLSON, G. A., LANIER, L. M., YUAN, L. L., ASHE, K. H. & LIAO, D. 2010. Tau mislocalization to dendritic spines mediates synaptic dysfunction independently of neurodegeneration. *Neuron,* 68**,** 1067-81.

HSIEH, H., BOEHM, J., SATO, C., IWATSUBO, T., TOMITA, T., SISODIA, S. & MALINOW, R. 2006. AMPAR removal underlies Abeta-induced synaptic depression and dendritic spine loss. *Neuron,* 52**,** 831-43.

HSU, L. J., SAGARA, Y., ARROYO, A., ROCKENSTEIN, E., SISK, A., MALLORY, M., WONG, J., TAKENOUCHI, T., HASHIMOTO, M. & MASLIAH, E. 2000. alpha-synuclein promotes mitochondrial deficit and oxidative stress. *Am J Pathol,* 157**,** 401-10.

HSU, M., SIK, A., GALLYAS, F., HORVATH, Z. & BUZSAKI, G. 1994. Short-term and long-term changes in the postischemic hippocampus. *Ann N Y Acad Sci,* 743**,** 121-39; discussion 139-40.

HUANG, Q. & FIGUEIREDO-PEREIRA, M. E. 2010. Ubiquitin/proteasome pathway impairment in neurodegeneration: therapeutic implications. *Apoptosis,* 15**,** 1292-311.

HUGHES, S. M., HOPE, K. M., XU, J. B., MITCHELL, N. L. & PALMER, D. N. 2014. Inhibition of storage pathology in prenatal CLN5-deficient sheep neural cultures by lentiviral gene therapy. *Neurobiol Dis,* 62**,** 543-50.

HUGHES, S. M., KAY, G. W., JORDAN, T. W., RICKARDS, G. K. & PALMER, D. N. 1999. Disease-specific pathology in neurons cultured from sheep affected with ceroid lipofuscinosis. *Mol Genet Metab,* 66**,** 381-6.

HUNTER, G., AGHAMALEKY SARVESTANY, A., ROCHE, S. L., SYMES, R. C. & GILLINGWATER, T. H. 2014. SMN-dependent intrinsic defects in Schwann cells in mouse models of spinal muscular atrophy. *Hum Mol Genet,* 23**,** 2235-50.

INGELSSON, M., FUKUMOTO, H., NEWELL, K. L., GROWDON, J. H., HEDLEY-WHYTE, E. T., FROSCH, M. P., ALBERT, M. S., HYMAN, B. T. & IRIZARRY, M. C. 2004. Early Abeta accumulation and progressive synaptic loss, gliosis, and tangle formation in AD brain. *Neurology,* 62**,** 925-31.

ISOSOMPPI, J., VESA, J., JALANKO, A. & PELTONEN, L. 2002. Lysosomal localization of the neuronal ceroid lipofuscinosis CLN5 protein. *Hum Mol Genet,* 11**,** 885-91.

IWAI, A., MASLIAH, E., YOSHIMOTO, M., GE, N., FLANAGAN, L., DE SILVA, H. A., KITTEL, A. & SAITOH, T. 1995. The precursor protein of non-A beta component of Alzheimer's disease amyloid is a presynaptic protein of the central nervous system. *Neuron,* 14**,** 467-75.

IWATA, A., CHRISTIANSON, J. C., BUCCI, M., ELLERBY, L. M., NUKINA, N., FORNO, L. S. & KOPITO, R. R. 2005. Increased susceptibility of cytoplasmic over nuclear polyglutamine aggregates to autophagic degradation. *Proc Natl Acad Sci U S A,* 102**,** 13135-40.

JACOBOWITZ, D. M. & WINSKY, L. 1991. Immunocytochemical localization of calretinin in the forebrain of the rat. *J Comp Neurol,* 304**,** 198-218.

JALANKO, A. & BRAULKE, T. 2009. Neuronal ceroid lipofuscinoses. *Biochimica et Biophysica Acta (BBA) - Molecular Cell Research,* 1793**,** 697-709.

JANEZIC, S., THRELFELL, S., DODSON, P. D., DOWIE, M. J., TAYLOR, T. N., POTGIETER, D., PARKKINEN, L., SENIOR, S. L., ANWAR, S., RYAN, B., DELTHEIL, T., KOSILLO, P., CIOROCH, M., WAGNER, K., ANSORGE, O., BANNERMAN, D. M., BOLAM, J. P., MAGILL, P. J., CRAGG, S. J. & WADE-MARTINS, R. 2013. Deficits in dopaminergic transmission precede neuron loss and dysfunction in a new Parkinson model. *Proc Natl Acad Sci U S A,* 110**,** E4016-25.

JIN, J., DAVIS, J., ZHU, D., KASHIMA, D. T., LEROUEIL, M., PAN, C., MONTINE, K. S. & ZHANG, J. 2007. Identification of novel proteins affected by rotenone in mitochondria of dopaminergic cells. *BMC Neurosci,* 8**,** 67.

JOLLY, R. D., ARTHUR, D. G., KAY, G. W. & PALMER, D. N. 2002. Neuronal ceroid-lipofuscinosis in Borderdale sheep. *N Z Vet J,* 50**,** 199-202.

JOLLY, R. D., MARTINUS, R. D. & PALMER, D. N. 1992. Sheep and other animals with ceroid-lipofuscinoses: their relevance to Batten disease. *Am J Med Genet,* 42**,** 609-14.

JOLLY, R. D., SHIMADA, A., DOPFMER, I., SLACK, P. M., BIRTLES, M. J. & PALMER, D. N. 1989. Ceroid-lipofuscinosis (Batten's disease): pathogenesis and sequential neuropathological changes in the ovine model. *Neuropathol Appl Neurobiol,* 15**,** 371-83.

JOLLY, R. D., SUTTON, R. H., SMITH, R. I. & PALMER, D. N. 1997. Ceroid-lipofuscinosis in miniature Schnauzer dogs. *Aust Vet J,* 75**,** 67.

KAMP, F., EXNER, N., LUTZ, A. K., WENDER, N., HEGERMANN, J., BRUNNER, B., NUSCHER, B., BARTELS, T., GIESE, A., BEYER, K., EIMER, S., WINKLHOFER, K. F. & HAASS, C. 2010. Inhibition of mitochondrial fusion by alpha-synuclein is rescued by PINK1, Parkin and DJ-1. *EMBO J,* 29**,** 3571-89.

KANNINEN, K. M., GRUBMAN, A., MEYEROWITZ, J., DUNCAN, C., TAN, J. L., PARKER, S. J., CROUCH, P. J., PATERSON, B. M., HICKEY, J. L., DONNELLY, P. S., VOLITAKIS, I., TAMMEN, I., PALMER, D. N. & WHITE, A. R. 2013. Increased zinc and manganese in parallel with neurodegeneration, synaptic protein changes and activation of Akt/GSK3 signaling in ovine CLN6 neuronal ceroid lipofuscinosis. *PLoS One,* 8**,** e58644.

KAUR, S. J., MCKEOWN, S. R. & RASHID, S. 2016. Mutant SOD1 mediated pathogenesis of Amyotrophic Lateral Sclerosis. *Gene,* 577**,** 109-18.

KELLER, J. N., HANNI, K. B. & MARKESBERY, W. R. 2000. Impaired proteasome function in Alzheimer's disease. *J Neurochem,* 75**,** 436-9.

KIELAR, C., MADDOX, L., BIBLE, E., PONTIKIS, C. C., MACAULEY, S. L., GRIFFEY, M. A., WONG, M., SANDS, M. S. & COOPER, J. D. 2007. Successive neuron loss in the thalamus and cortex in a mouse model of infantile neuronal ceroid lipofuscinosis. *Neurobiol Dis,* 25**,** 150-62.

KIELAR, C., WISHART, T. M., PALMER, A., DIHANICH, S., WONG, A. M., MACAULEY, S. L., CHAN, C. H., SANDS, M. S., PEARCE, D. A., COOPER, J. D. & GILLINGWATER, T. H. 2009. Molecular correlates of axonal and synaptic pathology in mouse models of Batten disease. *Hum Mol Genet,* 18**,** 4066-80.

KIERNAN, M. C., VUCIC, S., CHEAH, B. C., TURNER, M. R., EISEN, A., HARDIMAN, O., BURRELL, J. R. & ZOING, M. C. 2011. Amyotrophic lateral sclerosis. *The Lancet,* 377**,** 942-955.

KIM, J., MOODY, J. P., EDGERLY, C. K., BORDIUK, O. L., CORMIER, K., SMITH, K., BEAL, M. F. & FERRANTE, R. J. 2010. Mitochondrial loss, dysfunction and altered dynamics in Huntington's disease. *Hum Mol Genet,* 19**,** 3919-35.

KIM, S. H., CAIRNS, N., FOUNTOULAKISC, M. & LUBEC, G. 2001. Decreased brain histamine-releasing factor protein in patients with Down syndrome and Alzheimer's disease. *Neurosci Lett,* 300**,** 41-4.

KIM, S. J., ZHANG, Z., SARKAR, C., TSAI, P. C., LEE, Y. C., DYE, L. & MUKHERJEE, A. B. 2008. Palmitoyl protein thioesterase-1 deficiency impairs synaptic vesicle recycling at nerve terminals, contributing to neuropathology in humans and mice. *J Clin Invest,* 118**,** 3075-86.

KLIVENYI, P., SIWEK, D., GARDIAN, G., YANG, L., STARKOV, A., CLEREN, C., FERRANTE, R. J., KOWALL, N. W., ABELIOVICH, A. & BEAL, M. F. 2006. Mice lacking alpha-synuclein are resistant to mitochondrial toxins. *Neurobiol Dis,* 21**,** 541-8.

KOCH, S., MOLCHANOVA, S. M., WRIGHT, A. K., EDWARDS, A., COOPER, J. D., TAIRA, T., GILLINGWATER, T. H. & TYYNELA, J. 2011. Morphologic and functional correlates of synaptic pathology in the cathepsin D knockout mouse model of congenital neuronal ceroid lipofuscinosis. *J Neuropathol Exp Neurol,* 70**,** 1089-96.

KOFFIE, R. M., MEYER-LUEHMANN, M., HASHIMOTO, T., ADAMS, K. W., MIELKE, M. L., GARCIA-ALLOZA, M., MICHEVA, K. D., SMITH, S. J., KIM, M. L., LEE, V. M., HYMAN, B. T. & SPIRES-JONES, T. L. 2009. Oligomeric amyloid beta associates with postsynaptic densities and correlates with excitatory synapse loss near senile plaques. *Proc Natl Acad Sci U S A,* 106**,** 4012-7.

KOHANSAL-NODEHI, M., CHUA, J. J., URLAUB, H., JAHN, R. & CZERNIK, D. 2016. Analysis of protein phosphorylation in nerve terminal reveals extensive changes in active zone proteins upon exocytosis. *Elife,* 5.

KOHDA, M., TOKUZAWA, Y., KISHITA, Y., NYUZUKI, H., MORIYAMA, Y., MIZUNO, Y., HIRATA, T., YATSUKA, Y., YAMASHITA-SUGAHARA, Y., NAKACHI, Y., KATO, H., OKUDA, A., TAMARU, S., BORNA, N. N., BANSHOYA, K., AIGAKI, T., SATO-MIYATA, Y., OHNUMA, K., SUZUKI, T., NAGAO, A., MAEHATA, H., MATSUDA, F., HIGASA, K., NAGASAKI, M., YASUDA, J., YAMAMOTO, M., FUSHIMI, T., SHIMURA, M., KAIHO-ICHIMOTO, K., HARASHIMA, H., YAMAZAKI, T., MORI, M., MURAYAMA, K., OHTAKE, A. & OKAZAKI, Y. 2016. A Comprehensive Genomic Analysis Reveals the Genetic Landscape of Mitochondrial Respiratory Chain Complex Deficiencies. *PLoS Genet,* 12**,** e1005679.

KOLLMANN, K., UUSI-RAUVA, K., SCIFO, E., TYYNELÄ, J., JALANKO, A. & BRAULKE, T. 2013. Cell biology and function of neuronal ceroid lipofuscinosis-related proteins. *Biochimica et Biophysica Acta (BBA) - Molecular Basis of Disease,* 1832**,** 1866-1881.

KOWAL, S. L., DALL, T. M., CHAKRABARTI, R., STORM, M. V. & JAIN, A. 2013. The current and projected economic burden of Parkinson's disease in the United States. *Mov Disord,* 28**,** 311-8.

KRAMER, M. L. & SCHULZ-SCHAEFFER, W. J. 2007. Presynaptic alpha-synuclein aggregates, not Lewy bodies, cause neurodegeneration in dementia with Lewy bodies. *J Neurosci,* 27**,** 1405-10.

KRÜGER, R., KUHN, W., MÜLLER, T., WOITALLA, D., GRAEBER, M., KÖSEL, S., PRZUNTEK, H., EPPLEN, J. T., SCHÖLS, L. & RIESS, O. 1998. Ala30Pro mutation in the gene encoding alpha-synuclein in Parkinson's disease. *Nat Genet,* 18**,** 106-108.

KUBO, T., YAMAGUCHI, A., IWATA, N. & YAMASHITA, T. 2008. The therapeutic effects of Rho-ROCK inhibitors on CNS disorders. *Ther Clin Risk Manag,* 4**,** 605-15.

KUZNICKI, J., WANG, T. L., MARTIN, B. M., WINSKY, L. & JACOBOWITZ, D. M. 1995. Localization of Ca(2+)-dependent conformational changes of calretinin by limited tryptic proteolysis. *Biochem J,* 308 ( Pt 2)**,** 607-12.

LAI, J. C., WALSH, J. M., DENNIS, S. C. & CLARK, J. B. 1977. Synaptic and non-synaptic mitochondria from rat brain: isolation and characterization. *J Neurochem,* 28**,** 625-31.

LAKE, N. J., COMPTON, A. G., RAHMAN, S. & THORBURN, D. R. 2016. Leigh syndrome: One disorder, more than 75 monogenic causes. *Ann Neurol,* 79**,** 190-203.

LAMONTE, B. H., WALLACE, K. E., HOLLOWAY, B. A., SHELLY, S. S., ASCANO, J., TOKITO, M., VAN WINKLE, T., HOWLAND, D. S. & HOLZBAUR, E. L. 2002. Disruption of dynein/dynactin inhibits axonal transport in motor neurons causing late-onset progressive degeneration. *Neuron,* 34**,** 715-27.

LASHUEL, H. A., OVERK, C. R., OUESLATI, A. & MASLIAH, E. 2013. The many faces of alpha-synuclein: from structure and toxicity to therapeutic target. *Nat Rev Neurosci,* 14**,** 38-48.

LEE, B. R. & KAMITANI, T. 2011. Improved immunodetection of endogenous alpha-synuclein. *PLoS One,* 6**,** e23939.

LEE, J. T., WHEELER, T. C., LI, L. & CHIN, L. S. 2008a. Ubiquitination of alpha-synuclein by Siah-1 promotes alpha-synuclein aggregation and apoptotic cell death. *Hum Mol Genet,* 17**,** 906-17.

LEE, Y. M., PARK, S. H., SHIN, D. I., HWANG, J. Y., PARK, B., PARK, Y. J., LEE, T. H., CHAE, H. Z., JIN, B. K., OH, T. H. & OH, Y. J. 2008b. Oxidative modification of peroxiredoxin is associated with drug-induced apoptotic signaling in experimental models of Parkinson disease. *J Biol Chem,* 283**,** 9986-98.

LEVY, Y. S., GILGUN-SHERKI, Y., MELAMED, E. & OFFEN, D. 2005. Therapeutic potential of neurotrophic factors in neurodegenerative diseases. *BioDrugs,* 19**,** 97-127.

LI, S., HONG, S., SHEPARDSON, N. E., WALSH, D. M., SHANKAR, G. M. & SELKOE, D. 2009. Soluble oligomers of amyloid Beta protein facilitate hippocampal long-term depression by disrupting neuronal glutamate uptake. *Neuron,* 62**,** 788-801.

LI, S., JIN, M., KOEGLSPERGER, T., SHEPARDSON, N. E., SHANKAR, G. M. & SELKOE, D. J. 2011. Soluble Abeta oligomers inhibit long-term potentiation

through a mechanism involving excessive activation of extrasynaptic NR2B-containing NMDA receptors. *J Neurosci,* 31**,** 6627-38.
LI, W. W., YANG, R., GUO, J. C., REN, H. M., ZHA, X. L., CHENG, J. S. & CAI, D. F. 2007. Localization of alpha-synuclein to mitochondria within midbrain of mice. *Neuroreport,* 18**,** 1543-6.
LI, X., HAN, D., KIN TING KAM, R., GUO, X., CHEN, M., YANG, Y., ZHAO, H. & CHEN, Y. 2010. Developmental expression of sideroflexin family genes in Xenopus embryos. *Dev Dyn,* 239**,** 2742-7.
LIM, J. A., KAKHLON, O., LI, L., MYEROWITZ, R. & RABEN, N. 2015. Pompe disease: Shared and unshared features of lysosomal storage disorders. *Rare Dis,* 3**,** e1068978.
LIN, M. T. & BEAL, M. F. 2006. Mitochondrial dysfunction and oxidative stress in neurodegenerative diseases. *Nature,* 443**,** 787-95.
LIU, D., JIN, L., WANG, H., ZHAO, H., ZHAO, C., DUAN, C., LU, L., WU, B., YU, S., CHAN, P., LI, Y. & YANG, H. 2008. Silencing alpha-synuclein gene expression enhances tyrosine hydroxylase activity in MN9D cells. *Neurochem Res,* 33**,** 1401-9.
LIU, G., ZHANG, C., YIN, J., LI, X., CHENG, F., LI, Y., YANG, H., UEDA, K., CHAN, P. & YU, S. 2009a. alpha-Synuclein is differentially expressed in mitochondria from different rat brain regions and dose-dependently down-regulates complex I activity. *Neurosci Lett,* 454**,** 187-92.
LIU, R., STROM, A. L., ZHAI, J., GAL, J., BAO, S., GONG, W. & ZHU, H. 2009b. Enzymatically inactive adenylate kinase 4 interacts with mitochondrial ADP/ATP translocase. *Int J Biochem Cell Biol,* 41**,** 1371-80.
LIU, Y., ZHOU, Q., TANG, M., FU, N., SHAO, W., ZHANG, S., YIN, Y., ZENG, R., WANG, X., HU, G. & ZHOU, J. 2015. Upregulation of alphaB-crystallin expression in the substantia nigra of patients with Parkinson's disease. *Neurobiol Aging,* 36**,** 1686-91.
LONG, J., PAN, G., IFEACHOR, E., BELSHAW, R. & LI, X. 2016. Discovery of Novel Biomarkers for Alzheimer's Disease from Blood. *Dis Markers,* 2016**,** 4250480.
LU, B., NAGAPPAN, G., GUAN, X., NATHAN, P. J. & WREN, P. 2013. BDNF-based synaptic repair as a disease-modifying strategy for neurodegenerative diseases. *Nat Rev Neurosci,* 14**,** 401-16.
LUCKING, C. B., DURR, A., BONIFATI, V., VAUGHAN, J., DE MICHELE, G., GASSER, T., HARHANGI, B. S., MECO, G., DENEFLE, P., WOOD, N. W., AGID, Y., BRICE, A., FRENCH PARKINSON'S DISEASE GENETICS STUDY, G. & EUROPEAN CONSORTIUM ON GENETIC SUSCEPTIBILITY IN PARKINSON'S, D. 2000. Association between early-onset Parkinson's disease and mutations in the parkin gene. *N Engl J Med,* 342**,** 1560-7.
LUE, L. F., KUO, Y. M., ROHER, A. E., BRACHOVA, L., SHEN, Y., SUE, L., BEACH, T., KURTH, J. H., RYDEL, R. E. & ROGERS, J. 1999. Soluble amyloid beta peptide concentration as a predictor of synaptic change in Alzheimer's disease. *Am J Pathol,* 155**,** 853-62.
LUIRO, K., KOPRA, O., BLOM, T., GENTILE, M., MITCHISON, H. M., HOVATTA, I., TORNQUIST, K. & JALANKO, A. 2006. Batten disease (JNCL) is linked to disturbances in mitochondrial, cytoskeletal, and synaptic compartments. *J Neurosci Res,* 84**,** 1124-38.

LUK, K. C., KEHM, V. M., ZHANG, B., O'BRIEN, P., TROJANOWSKI, J. Q. & LEE, V. M. 2012. Intracerebral inoculation of pathological alpha-synuclein initiates a rapidly progressive neurodegenerative alpha-synucleinopathy in mice. *J Exp Med,* 209**,** 975-86.

LUK, K. C., SONG, C., O'BRIEN, P., STIEBER, A., BRANCH, J. R., BRUNDEN, K. R., TROJANOWSKI, J. Q. & LEE, V. M. 2009. Exogenous alpha-synuclein fibrils seed the formation of Lewy body-like intracellular inclusions in cultured cells. *Proc Natl Acad Sci U S A,* 106**,** 20051-6.

LUTH, E. S., STAVROVSKAYA, I. G., BARTELS, T., KRISTAL, B. S. & SELKOE, D. J. 2014. Soluble, prefibrillar alpha-synuclein oligomers promote complex I-dependent, Ca2+-induced mitochondrial dysfunction. *J Biol Chem,* 289**,** 21490-507.

LUTHI-CARTER, R., TAYLOR, D. M., PALLOS, J., LAMBERT, E., AMORE, A., PARKER, A., MOFFITT, H., SMITH, D. L., RUNNE, H., GOKCE, O., KUHN, A., XIANG, Z., MAXWELL, M. M., REEVES, S. A., BATES, G. P., NERI, C., THOMPSON, L. M., MARSH, J. L. & KAZANTSEV, A. G. 2010. SIRT2 inhibition achieves neuroprotection by decreasing sterol biosynthesis. *Proc Natl Acad Sci U S A,* 107**,** 7927-32.

LY, C. V. & VERSTREKEN, P. 2006. Mitochondria at the synapse. *Neuroscientist,* 12**,** 291-9.

LYLY, A., VON SCHANTZ, C., HEINE, C., SCHMIEDT, M. L., SIPILA, T., JALANKO, A. & KYTTALA, A. 2009. Novel interactions of CLN5 support molecular networking between Neuronal Ceroid Lipofuscinosis proteins. *BMC Cell Biol,* 10**,** 83.

MACIAS, W., CARLSON, R., RAJADHYAKSHA, A., BARCZAK, A. & KONRADI, C. 2001. Potassium chloride depolarization mediates CREB phosphorylation in striatal neurons in an NMDA receptor-dependent manner. *Brain Res,* 890**,** 222-32.

MAGNONI, R., PALMFELDT, J., CHRISTENSEN, J. H., SAND, M., MALTECCA, F., CORYDON, T. J., WEST, M., CASARI, G. & BROSS, P. 2013. Late onset motoneuron disorder caused by mitochondrial Hsp60 chaperone deficiency in mice. *Neurobiol Dis,* 54**,** 12-23.

MAMO, A., JULES, F., DUMARESQ-DOIRON, K., COSTANTINO, S. & LEFRANCOIS, S. 2012. The role of ceroid lipofuscinosis neuronal protein 5 (CLN5) in endosomal sorting. *Mol Cell Biol,* 32**,** 1855-66.

MARAGAKIS, N. J. & ROTHSTEIN, J. D. 2006. Mechanisms of Disease: astrocytes in neurodegenerative disease. *Nat Clin Pract Neurol,* 2**,** 679-89.

MARKS, B. & MCMAHON, H. T. 1998. Calcium triggers calcineurin-dependent synaptic vesicle recycling in mammalian nerve terminals. *Curr Biol,* 8**,** 740-9.

MARLAND, J. R., HASEL, P., BONNYCASTLE, K. & COUSIN, M. A. 2016. Mitochondrial Calcium Uptake Modulates Synaptic Vesicle Endocytosis in Central Nerve Terminals. *J Biol Chem,* 291**,** 2080-6.

MARTIN, L. J., PAN, Y., PRICE, A. C., STERLING, W., COPELAND, N. G., JENKINS, N. A., PRICE, D. L. & LEE, M. K. 2006. Parkinson's disease alpha-synuclein transgenic mice develop neuronal mitochondrial degeneration and cell death. *J Neurosci,* 26**,** 41-50.

MARTINEZ, M., HERNANDEZ, A. I., MARTINEZ, N. & FERRANDIZ, M. L. 1996. Age-related increase in oxidized proteins in mouse synaptic mitochondria. *Brain Res,* 731**,** 246-8.

MATSUMOTO, M., YADA, M., HATAKEYAMA, S., ISHIMOTO, H., TANIMURA, T., TSUJI, S., KAKIZUKA, A., KITAGAWA, M. & NAKAYAMA, K. I. 2004. Molecular clearance of ataxin-3 is regulated by a mammalian E4. *EMBO J,* 23**,** 659-69.

MCFARLAND, M. A., ELLIS, C. E., MARKEY, S. P. & NUSSBAUM, R. L. 2008. Proteomics analysis identifies phosphorylation-dependent alpha-synuclein protein interactions. *Mol Cell Proteomics,* 7**,** 2123-37.

MEINRENKEN, C. J., BORST, J. G. & SAKMANN, B. 2003. Local routes revisited: the space and time dependence of the Ca2+ signal for phasic transmitter release at the rat calyx of Held. *J Physiol,* 547**,** 665-89.

MERKSAMER, P. I. & PAPA, F. R. 2010. The UPR and cell fate at a glance. *Journal of Cell Science,* 123**,** 1003-1006.

MEZEY, E., DEHEJIA, A. M., HARTA, G., TRESSER, N., SUCHY, S. F., NUSSBAUM, R. L., BROWNSTEIN, M. J. & POLYMEROPOULOS, M. H. 1998. Alpha synuclein is present in Lewy bodies in sporadic Parkinson's disease. *Molecular Psychiatry,* 3**,** 493-499.

MIETTINEN, R., GULYAS, A. I., BAIMBRIDGE, K. G., JACOBOWITZ, D. M. & FREUND, T. F. 1992. Calretinin is present in non-pyramidal cells of the rat hippocampus--II. Co-existence with other calcium binding proteins and GABA. *Neuroscience,* 48**,** 29-43.

MILAKOVIC, T. & JOHNSON, G. V. 2005. Mitochondrial respiration and ATP production are significantly impaired in striatal cells expressing mutant huntingtin. *J Biol Chem,* 280**,** 30773-82.

MILEDI, R. & SLATER, C. R. 1970. On the degeneration of rat neuromuscular junctions after nerve section. *J Physiol,* 207**,** 507-28.

MILLER, B. R., WALKER, A. G., SHAH, A. S., BARTON, S. J. & REBEC, G. V. 2008. Dysregulated information processing by medium spiny neurons in striatum of freely behaving mouse models of Huntington's disease. *J Neurophysiol,* 100**,** 2205-16.

MILNERWOOD, A. J., CUMMINGS, D. M., DALLERAC, G. M., BROWN, J. Y., VATSAVAYAI, S. C., HIRST, M. C., REZAIE, P. & MURPHY, K. P. 2006. Early development of aberrant synaptic plasticity in a mouse model of Huntington's disease. *Hum Mol Genet,* 15**,** 1690-703.

MILNERWOOD, A. J., GLADDING, C. M., POULADI, M. A., KAUFMAN, A. M., HINES, R. M., BOYD, J. D., KO, R. W., VASUTA, O. C., GRAHAM, R. K., HAYDEN, M. R., MURPHY, T. H. & RAYMOND, L. A. 2010. Early increase in extrasynaptic NMDA receptor signaling and expression contributes to phenotype onset in Huntington's disease mice. *Neuron,* 65**,** 178-90.

MILNERWOOD, A. J. & RAYMOND, L. A. 2010. Early synaptic pathophysiology in neurodegeneration: insights from Huntington's disease. *Trends Neurosci,* 33**,** 513-23.

MINJAREZ, B., CALDERON-GONZALEZ, K. G., RUSTARAZO, M. L., HERRERA-AGUIRRE, M. E., LABRA-BARRIOS, M. L., RINCON-LIMAS, D. E., DEL PINO, M. M., MENA, R. & LUNA-ARIAS, J. P. 2016. Identification of proteins

that are differentially expressed in brains with Alzheimer's disease using iTRAQ labeling and tandem mass spectrometry. *J Proteomics,* 139**,** 103-21.
MITCHISON, H. M., LIM, M. J. & COOPER, J. D. 2004. Selectivity and types of cell death in the neuronal ceroid lipofuscinoses. *Brain Pathol,* 14**,** 86-96.
MONTI, B., POLAZZI, E., BATTI, L., CROCHEMORE, C., VIRGILI, M. & CONTESTABILE, A. 2007. Alpha-synuclein protects cerebellar granule neurons against 6-hydroxydopamine-induced death. *J Neurochem,* 103**,** 518-30.
MOR, D. E., UGRAS, S. E., DANIELS, M. J. & ISCHIROPOULOS, H. 2016. Dynamic structural flexibility of alpha-synuclein. *Neurobiol Dis,* 88**,** 66-74.
MORONI-RAWSON, P., PALMER, D. N., JOLLY, R. D. & JORDAN, T. W. 1995. Variant proteins in ovine ceroid-lipofuscinosis. *Am J Med Genet,* 57**,** 279-84.
MORRISON, B. M., GORDON, J. W., RIPPS, M. E. & MORRISON, J. H. 1996. Quantitative immunocytochemical analysis of the spinal cord in G86R superoxide dismutase transgenic mice: neurochemical correlates of selective vulnerability. *J Comp Neurol,* 373**,** 619-31.
MORRISON, B. M., JANSSEN, W. G., GORDON, J. W. & MORRISON, J. H. 1998. Light and electron microscopic distribution of the AMPA receptor subunit, GluR2, in the spinal cord of control and G86R mutant superoxide dismutase transgenic mice. *J Comp Neurol,* 395**,** 523-34.
MORTON, A. J. & HOWLAND, D. S. 2013. Large genetic animal models of Huntington's Disease. *J Huntingtons Dis,* 2**,** 3-19.
MURPHY, D. D., RUETER, S. M., TROJANOWSKI, J. Q. & LEE, V. M. 2000. Synucleins are developmentally expressed, and alpha-synuclein regulates the size of the presynaptic vesicular pool in primary hippocampal neurons. *J Neurosci,* 20**,** 3214-20.
MURRAY, L. M., COMLEY, L. H., THOMSON, D., PARKINSON, N., TALBOT, K. & GILLINGWATER, T. H. 2008. Selective vulnerability of motor neurons and dissociation of pre- and post-synaptic pathology at the neuromuscular junction in mouse models of spinal muscular atrophy. *Hum Mol Genet,* 17**,** 949-62.
MUZERENGI, S. & CLARKE, C. E. 2015. Initial drug treatment in Parkinson's disease. *BMJ,* 351**,** h4669.
NAGAHARA, A. H., MATELING, M., KOVACS, I., WANG, L., EGGERT, S., ROCKENSTEIN, E., KOO, E. H., MASLIAH, E. & TUSZYNSKI, M. H. 2013. Early BDNF treatment ameliorates cell loss in the entorhinal cortex of APP transgenic mice. *J Neurosci,* 33**,** 15596-602.
NAGAHARA, A. H., MERRILL, D. A., COPPOLA, G., TSUKADA, S., SCHROEDER, B. E., SHAKED, G. M., WANG, L., BLESCH, A., KIM, A., CONNER, J. M., ROCKENSTEIN, E., CHAO, M. V., KOO, E. H., GESCHWIND, D., MASLIAH, E., CHIBA, A. A. & TUSZYNSKI, M. H. 2009. Neuroprotective effects of brain-derived neurotrophic factor in rodent and primate models of Alzheimer's disease. *Nat Med,* 15**,** 331-7.
NAKAMURA, K. 2013. alpha-Synuclein and mitochondria: partners in crime? *Neurotherapeutics,* 10**,** 391-9.
NAKAMURA, K., NEMANI, V. M., AZARBAL, F., SKIBINSKI, G., LEVY, J. M., EGAMI, K., MUNISHKINA, L., ZHANG, J., GARDNER, B., WAKABAYASHI, J., SESAKI, H., CHENG, Y., FINKBEINER, S., NUSSBAUM, R. L., MASLIAH, E. & EDWARDS, R. H. 2011. Direct membrane

association drives mitochondrial fission by the Parkinson disease-associated protein alpha-synuclein. *The Journal of Biological Chemistry,* 286**,** 20710-20726.
NAKAMURA, K., NEMANI, V. M., WALLENDER, E. K., KAEHLCKE, K., OTT, M. & EDWARDS, R. H. 2008. Optical reporters for the conformation of alpha-synuclein reveal a specific interaction with mitochondria. *J Neurosci,* 28**,** 12305-17.
NEMANI, V. M., LU, W., BERGE, V., NAKAMURA, K., ONOA, B., LEE, M. K., CHAUDHRY, F. A., NICOLL, R. A. & EDWARDS, R. H. 2010. Increased expression of alpha-synuclein reduces neurotransmitter release by inhibiting synaptic vesicle reclustering after endocytosis. *Neuron,* 65**,** 66-79.
NISHIMURA, N., GOTOH, T., OIKE, Y. & YANO, M. 2014. TMEM65 is a mitochondrial inner-membrane protein. *PeerJ,* 2**,** e349.
NISTICO, R., PIGNATELLI, M., PICCININ, S., MERCURI, N. B. & COLLINGRIDGE, G. 2012. Targeting synaptic dysfunction in Alzheimer's disease therapy. *Mol Neurobiol,* 46**,** 572-87.
NONAKA, T., WATANABE, S. T., IWATSUBO, T. & HASEGAWA, M. 2010. Seeded aggregation and toxicity of {alpha}-synuclein and tau: cellular models of neurodegenerative diseases. *J Biol Chem,* 285**,** 34885-98.
NOSKOVA, L., STRANECKY, V., HARTMANNOVA, H., PRISTOUPILOVA, A., BARESOVA, V., IVANEK, R., HULKOVA, H., JAHNOVA, H., VAN DER ZEE, J., STAROPOLI, J. F., SIMS, K. B., TYYNELA, J., VAN BROECKHOVEN, C., NIJSSEN, P. C., MOLE, S. E., ELLEDER, M. & KMOCH, S. 2011. Mutations in DNAJC5, encoding cysteine-string protein alpha, cause autosomal-dominant adult-onset neuronal ceroid lipofuscinosis. *Am J Hum Genet,* 89**,** 241-52.
OLAH, J. & OVADI, J. 2014. Dual life of TPPP/p25 evolved in physiological and pathological conditions. *Biochem Soc Trans,* 42**,** 1762-7.
ONO, K., IKEDA, T., TAKASAKI, J.-I. & YAMADA, M. 2011. Familial Parkinson disease mutations influence α-synuclein assembly. *Neurobiology of Disease,* 43**,** 715-724.
OSWALD, M. J., PALMER, D. N., KAY, G. W., BARWELL, K. J. & COOPER, J. D. 2008. Location and connectivity determine GABAergic interneuron survival in the brains of South Hampshire sheep with CLN6 neuronal ceroid lipofuscinosis. *Neurobiol Dis,* 32**,** 50-65.
OSWALD, M. J., PALMER, D. N., KAY, G. W., SHEMILT, S. J., REZAIE, P. & COOPER, J. D. 2005. Glial activation spreads from specific cerebral foci and precedes neurodegeneration in presymptomatic ovine neuronal ceroid lipofuscinosis (CLN6). *Neurobiol Dis,* 20**,** 49-63.
OUTEIRO, T. F., KONTOPOULOS, E., ALTMANN, S. M., KUFAREVA, I., STRATHEARN, K. E., AMORE, A. M., VOLK, C. B., MAXWELL, M. M., ROCHET, J. C., MCLEAN, P. J., YOUNG, A. B., ABAGYAN, R., FEANY, M. B., HYMAN, B. T. & KAZANTSEV, A. G. 2007. Sirtuin 2 inhibitors rescue alpha-synuclein-mediated toxicity in models of Parkinson's disease. *Science,* 317**,** 516-9.
PAGLIARINI, D. J., CALVO, S. E., CHANG, B., SHETH, S. A., VAFAI, S. B., ONG, S. E., WALFORD, G. A., SUGIANA, C., BONEH, A., CHEN, W. K., HILL, D. E., VIDAL, M., EVANS, J. G., THORBURN, D. R., CARR, S. A. & MOOTHA,

V. K. 2008. A mitochondrial protein compendium elucidates complex I disease biology. *Cell,* 134**,** 112-23.

PALEOLOGOU, K. E., OUESLATI, A., SHAKKED, G., ROSPIGLIOSI, C. C., KIM, H. Y., LAMBERTO, G. R., FERNANDEZ, C. O., SCHMID, A., CHEGINI, F., GAI, W. P., CHIAPPE, D., MONIATTE, M., SCHNEIDER, B. L., AEBISCHER, P., ELIEZER, D., ZWECKSTETTER, M., MASLIAH, E. & LASHUEL, H. A. 2010. Phosphorylation at S87 is enhanced in synucleinopathies, inhibits alpha-synuclein oligomerization, and influences synuclein-membrane interactions. *J Neurosci,* 30**,** 3184-98.

PALMER, D. N., BARRY, L. A., TYYNELA, J. & COOPER, J. D. 2013. NCL disease mechanisms. *Biochim Biophys Acta*.

PALMER, D. N., FEARNLEY, I. M., WALKER, J. E., HALL, N. A., LAKE, B. D., WOLFE, L. S., HALTIA, M., MARTINUS, R. D. & JOLLY, R. D. 1992. Mitochondrial ATP synthase subunit c storage in the ceroid-lipofuscinoses (Batten disease). *Am J Med Genet,* 42**,** 561-7.

PANELLI, D., LORUSSO, F. P., PAPA, F., PANELLI, P., STELLA, A., CAPUTI, M., SARDANELLI, A. M. & PAPA, S. 2013. The mechanism of alternative splicing of the X-linked NDUFB11 gene of the respiratory chain complex I, impact of rotenone treatment in neuroblastoma cells. *Biochim Biophys Acta,* 1829**,** 211-8.

PANGRSIC, T., GABRIELAITIS, M., MICHANSKI, S., SCHWALLER, B., WOLF, F., STRENZKE, N. & MOSER, T. 2015. EF-hand protein Ca2+ buffers regulate Ca2+ influx and exocytosis in sensory hair cells. *Proc Natl Acad Sci U S A*.

PANOV, A., DIKALOV, S., SHALBUYEVA, N., TAYLOR, G., SHERER, T. & GREENAMYRE, J. T. 2005. Rotenone model of Parkinson disease: multiple brain mitochondria dysfunctions after short term systemic rotenone intoxication. *J Biol Chem,* 280**,** 42026-35.

PANOV, A. V., GUTEKUNST, C. A., LEAVITT, B. R., HAYDEN, M. R., BURKE, J. R., STRITTMATTER, W. J. & GREENAMYRE, J. T. 2002. Early mitochondrial calcium defects in Huntington's disease are a direct effect of polyglutamines. *Nat Neurosci,* 5**,** 731-6.

PARIHAR, M. S., PARIHAR, A., FUJITA, M., HASHIMOTO, M. & GHAFOURIFAR, P. 2008. Mitochondrial association of alpha-synuclein causes oxidative stress. *Cell Mol Life Sci,* 65**,** 1272-84.

PARTANEN, S., HAAPANEN, A., KIELAR, C., PONTIKIS, C., ALEXANDER, N., INKINEN, T., SAFTIG, P., GILLINGWATER, T. H., COOPER, J. D. & TYYNELA, J. 2008. Synaptic changes in the thalamocortical system of cathepsin D-deficient mice: a model of human congenital neuronal ceroid-lipofuscinosis. *J Neuropathol Exp Neurol,* 67**,** 16-29.

PATHAK, D., SHIELDS, L. Y., MENDELSOHN, B. A., HADDAD, D., LIN, W., GERENCSER, A. A., KIM, H., BRAND, M. D., EDWARDS, R. H. & NAKAMURA, K. 2015. The role of mitochondrially derived ATP in synaptic vesicle recycling. *J Biol Chem,* 290**,** 22325-36.

PAULSEN, J. S., LANGBEHN, D. R., STOUT, J. C., AYLWARD, E., ROSS, C. A., NANCE, M., GUTTMAN, M., JOHNSON, S., MACDONALD, M., BEGLINGER, L. J., DUFF, K., KAYSON, E., BIGLAN, K., SHOULSON, I., OAKES, D. & HAYDEN, M. 2008. Detection of Huntington's disease decades

before diagnosis: the Predict-HD study. *J Neurol Neurosurg Psychiatry,* 79**,** 874-80.
PEARS, M. R., SALEK, R. M., PALMER, D. N., KAY, G. W., MORTISHIRE-SMITH, R. J. & GRIFFIN, J. L. 2007. Metabolomic investigation of CLN6 neuronal ceroid lipofuscinosis in affected South Hampshire sheep. *J Neurosci Res,* 85**,** 3494-504.
PELKONEN, A. & YAVICH, L. 2011. Neuromuscular pathology in mice lacking alpha-synuclein. *Neuroscience Letters,* 487**,** 350-353.
PEREZ, R. G., WAYMIRE, J. C., LIN, E., LIU, J. J., GUO, F. & ZIGMOND, M. J. 2002. A role for alpha-synuclein in the regulation of dopamine biosynthesis. *The Journal of Neuroscience: The Official Journal of the Society for Neuroscience,* 22**,** 3090-3099.
PERRIN, S. 2014. Preclinical research: Make mouse studies work. *Nature,* 507**,** 423-5.
PICCONI, B., PICCOLI, G. & CALABRESI, P. 2012. Synaptic Dysfunction in Parkinson's Disease. *In:* KREUTZ, M. R. & SALA, C. (eds.). Springer Vienna.
PIKE, C. J. & COTMAN, C. W. 1995. Calretinin-immunoreactive neurons are resistant to beta-amyloid toxicity in vitro. *Brain Res,* 671**,** 293-8.
PISANI, V., STEFANI, A., PIERANTOZZI, M., NATOLI, S., STANZIONE, P., FRANCIOTTA, D. & PISANI, A. 2012. Increased blood-cerebrospinal fluid transfer of albumin in advanced Parkinson's disease. *J Neuroinflammation,* 9**,** 188.
POCHE, R. A., ZHANG, M., RUEDA, E. M., TONG, X., MCELWEE, M. L., WONG, L., HSU, C. W., DEJOSEZ, M., BURNS, A. R., FOX, D. A., MARTIN, J. F., ZWAKA, T. P. & DICKINSON, M. E. 2016. RONIN Is an Essential Transcriptional Regulator of Genes Required for Mitochondrial Function in the Developing Retina. *Cell Rep,* 14**,** 1684-97.
POLLANEN, M. S., DICKSON, D. W. & BERGERON, C. 1993. Pathology and biology of the Lewy body. *J Neuropathol Exp Neurol,* 52**,** 183-91.
POLYMEROPOULOS, M. H., LAVEDAN, C., LEROY, E., IDE, S. E., DEHEJIA, A., DUTRA, A., PIKE, B., ROOT, H., RUBENSTEIN, J., BOYER, R., STENROOS, E. S., CHANDRASEKHARAPPA, S., ATHANASSIADOU, A., PAPAPETROPOULOS, T., JOHNSON, W. G., LAZZARINI, A. M., DUVOISIN, R. C., DI IORIO, G., GOLBE, L. I. & NUSSBAUM, R. L. 1997. Mutation in the alpha-synuclein gene identified in families with Parkinson's disease. *Science (New York, N.Y.),* 276**,** 2045-2047.
POULADI, M. A., MORTON, A. J. & HAYDEN, M. R. 2013. Choosing an animal model for the study of Huntington's disease. *Nat Rev Neurosci,* 14**,** 708-21.
PROTTER, D., LANG, C. & COOPER, A. A. 2012. alphaSynuclein and Mitochondrial Dysfunction: A Pathogenic Partnership in Parkinson's Disease? *Parkinsons Dis,* 2012**,** 829207.
PRZEDBORSKI, S., TIEU, K., PERIER, C. & VILA, M. 2004. MPTP as a mitochondrial neurotoxic model of Parkinson's disease. *J Bioenerg Biomembr,* 36**,** 375-9.
QIAO, L., HAMAMICHI, S., CALDWELL, K. A., CALDWELL, G. A., YACOUBIAN, T. A., WILSON, S., XIE, Z. L., SPEAKE, L. D., PARKS, R., CRABTREE, D., LIANG, Q., CRIMMINS, S., SCHNEIDER, L., UCHIYAMA, Y., IWATSUBO, T., ZHOU, Y., PENG, L., LU, Y., STANDAERT, D. G., WALLS, K. C., SHACKA, J. J., ROTH, K. A. & ZHANG, J. 2008. Lysosomal enzyme cathepsin D protects against alpha-synuclein aggregation and toxicity. *Mol Brain,* 1**,** 17.

QUILTY, M. C., KING, A. E., GAI, W. P., POUNTNEY, D. L., WEST, A. K., VICKERS, J. C. & DICKSON, T. C. 2006. Alpha-synuclein is upregulated in neurones in response to chronic oxidative stress and is associated with neuroprotection. *Exp Neurol,* 199**,** 249-256.

RAMSER, J., AHEARN, M. E., LENSKI, C., YARIZ, K. O., HELLEBRAND, H., VON RHEIN, M., CLARK, R. D., SCHMUTZLER, R. K., LICHTNER, P., HOFFMAN, E. P., MEINDL, A. & BAUMBACH-REARDON, L. 2008. Rare missense and synonymous variants in UBE1 are associated with X-linked infantile spinal muscular atrophy. *Am J Hum Genet,* 82**,** 188-93.

RAPPSILBER, J., MANN, M. & ISHIHAMA, Y. 2007. Protocol for micro-purification, enrichment, pre-fractionation and storage of peptides for proteomics using StageTips. *Nat Protoc,* 2**,** 1896-906.

REN, K., RUDA, M. A. & JACOBOWITZ, D. M. 1993. Immunohistochemical localization of calretinin in the dorsal root ganglion and spinal cord of the rat. *Brain Research Bulletin,* 31**,** 13-22.

RIENTO, K. & RIDLEY, A. J. 2003. Rocks: multifunctional kinases in cell behaviour. *Nat Rev Mol Cell Biol,* 4**,** 446-56.

ROCHE, S. L., SHERMAN, D. L., DISSANAYAKE, K., SOUCY, G., DESMAZIERES, A., LAMONT, D. J., PELES, E., JULIEN, J. P., WISHART, T. M., RIBCHESTER, R. R., BROPHY, P. J. & GILLINGWATER, T. H. 2014. Loss of glial neurofascin155 delays developmental synapse elimination at the neuromuscular junction. *J Neurosci,* 34**,** 12904-18.

ROSS, C. A. & POIRIER, M. A. 2004. Protein aggregation and neurodegenerative disease. *Nat Med,* 10 Suppl**,** S10-7.

ROSS, C. A. & POIRIER, M. A. 2005. Opinion: What is the role of protein aggregation in neurodegeneration? *Nat Rev Mol Cell Biol,* 6**,** 891-8.

ROSSETTO, O., PIRAZZINI, M. & MONTECUCCO, C. 2014. Botulinum neurotoxins: genetic, structural and mechanistic insights. *Nat Rev Microbiol,* 12**,** 535-49.

ROUAULT, T. A. 2012. Biogenesis of iron-sulfur clusters in mammalian cells: new insights and relevance to human disease. *Dis Model Mech,* 5**,** 155-64.

RUBINSZTEIN, D. C. 2006. The roles of intracellular protein-degradation pathways in neurodegeneration. *Nature,* 443**,** 780-6.

RUI, Y., TIWARI, P., XIE, Z. & ZHENG, J. Q. 2006. Acute impairment of mitochondrial trafficking by beta-amyloid peptides in hippocampal neurons. *J Neurosci,* 26**,** 10480-7.

SAHA, A. R., HILL, J., UTTON, M. A., ASUNI, A. A., ACKERLEY, S., GRIERSON, A. J., MILLER, C. C., DAVIES, A. M., BUCHMAN, V. L., ANDERTON, B. H. & HANGER, D. P. 2004. Parkinson's disease alpha-synuclein mutations exhibit defective axonal transport in cultured neurons. *J Cell Sci,* 117**,** 1017-24.

SANHUEZA, M., CHAI, A., SMITH, C., MCCRAY, B. A., SIMPSON, T. I., TAYLOR, J. P. & PENNETTA, G. 2015. Network analyses reveal novel aspects of ALS pathogenesis. *PLoS Genet,* 11**,** e1005107.

SANKARANARAYANAN, S., DE ANGELIS, D., ROTHMAN, J. E. & RYAN, T. A. 2000. The use of pHluorins for optical measurements of presynaptic activity. *Biophys J,* 79**,** 2199-208.

SANTAVUORI, P., LAURONEN, L., KIRVESKARI, E., ABERG, L., SAINIO, K. & AUTTI, T. 2000. Neuronal ceroid lipofuscinoses in childhood. *Neurol Sci,* 21**,** S35-41.

SAWIAK, S. J., WOOD, N. I., WILLIAMS, G. B., MORTON, A. J. & CARPENTER, T. A. 2013. Voxel-based morphometry with templates and validation in a mouse model of Huntington's disease. *Magn Reson Imaging,* 31**,** 1522-31.

SCHEFF, S. W. & PRICE, D. A. 1993. Synapse loss in the temporal lobe in Alzheimer's disease. *Ann Neurol,* 33**,** 190-9.

SCHEFF, S. W., PRICE, D. A., SCHMITT, F. A. & MUFSON, E. J. 2006. Hippocampal synaptic loss in early Alzheimer's disease and mild cognitive impairment. *Neurobiol Aging,* 27**,** 1372-84.

SCHEIBYE-KNUDSEN, M., FANG, E. F., CROTEAU, D. L., WILSON, D. M., 3RD & BOHR, V. A. 2015. Protecting the mitochondrial powerhouse. *Trends Cell Biol,* 25**,** 158-70.

SCHEPER, W. & HOOZEMANS, J. J. 2015. The unfolded protein response in neurodegenerative diseases: a neuropathological perspective. *Acta Neuropathol,* 130**,** 315-31.

SCHIFFMANN, S. N., CHERON, G., LOHOF, A., D'ALCANTARA, P., MEYER, M., PARMENTIER, M. & SCHURMANS, S. 1999. Impaired motor coordination and Purkinje cell excitability in mice lacking calretinin. *Proc Natl Acad Sci U S A,* 96**,** 5257-62.

SCHIPPLING, S., SCHNEIDER, S. A., BHATIA, K. P., MUNCHAU, A., ROTHWELL, J. C., TABRIZI, S. J. & ORTH, M. 2009. Abnormal motor cortex excitability in preclinical and very early Huntington's disease. *Biol Psychiatry,* 65**,** 959-65.

SCHLIEBS, R. & ARENDT, T. 2011. The cholinergic system in aging and neuronal degeneration. *Behav Brain Res,* 221**,** 555-63.

SCHLUTER, O. M., FORNAI, F., ALESSANDRI, M. G., TAKAMORI, S., GEPPERT, M., JAHN, R. & SUDHOF, T. C. 2003. Role of alpha-synuclein in 1-methyl-4-phenyl-1,2,3,6-tetrahydropyridine-induced parkinsonism in mice. *Neuroscience,* 118**,** 985-1002.

SCHMIDT, H., BRACHTENDORF, S., ARENDT, O., HALLERMANN, S., ISHIYAMA, S., BORNSCHEIN, G., GALL, D., SCHIFFMANN, S. N., HECKMANN, M. & EILERS, J. 2013. Nanodomain coupling at an excitatory cortical synapse. *Curr Biol,* 23**,** 244-9.

SCHMIEDT, M. L., BESSA, C., HEINE, C., RIBEIRO, M. G., JALANKO, A. & KYTTALA, A. 2010. The neuronal ceroid lipofuscinosis protein CLN5: new insights into cellular maturation, transport, and consequences of mutations. *Hum Mutat,* 31**,** 356-65.

SCHMITZ, F., TABARES, L., KHIMICH, D., STRENZKE, N., DE LA VILLA-POLO, P., CASTELLANO-MUNOZ, M., BULANKINA, A., MOSER, T., FERNANDEZ-CHACON, R. & SUDHOF, T. C. 2006. CSPalpha-deficiency causes massive and rapid photoreceptor degeneration. *Proc Natl Acad Sci U S A,* 103**,** 2926-31.

SCHOCH, S., DEAK, F., KONIGSTORFER, A., MOZHAYEVA, M., SARA, Y., SUDHOF, T. C. & KAVALALI, E. T. 2001. SNARE function analyzed in synaptobrevin/VAMP knockout mice. *Science,* 294**,** 1117-22.

SCHONHOFEN, P., DE MEDEIROS, L. M., CHATAIN, C. P., BRISTOT, I. J. & KLAMT, F. 2014. Cofilin/actin rod formation by dysregulation of cofilin-1 activity as a central initial step in neurodegeneration. *Mini Rev Med Chem,* 14**,** 393-400.

SCHULTHEIS, P. J., FLEMING, S. M., CLIPPINGER, A. K., LEWIS, J., TSUNEMI, T., GIASSON, B., DICKSON, D. W., MAZZULLI, J. R., BARDGETT, M. E., HAIK, K. L., EKHATOR, O., CHAVA, A. K., HOWARD, J., GANNON, M., HOFFMAN, E., CHEN, Y., PRASAD, V., LINN, S. C., TAMARGO, R. J., WESTBROEK, W., SIDRANSKY, E., KRAINC, D. & SHULL, G. E. 2013. Atp13a2-deficient mice exhibit neuronal ceroid lipofuscinosis, limited alpha-synuclein accumulation and age-dependent sensorimotor deficits. *Hum Mol Genet,* 22**,** 2067-82.

SCHURMANS, S., SCHIFFMANN, S. N., GURDEN, H., LEMAIRE, M., LIPP, H. P., SCHWAM, V., POCHET, R., IMPERATO, A., BOHME, G. A. & PARMENTIER, M. 1997. Impaired long-term potentiation induction in dentate gyrus of calretinin-deficient mice. *Proc Natl Acad Sci U S A,* 94**,** 10415-20.

SCHWALLER, B. 2014. Calretinin: from a "simple" Ca buffer to a multifunctional protein implicated in many biological processes. *Front Neuroanat,* 8**,** 3.

SCHWALLER, B., DURUSSEL, I., JERMANN, D., HERRMANN, B. & COX, J. A. 1997. Comparison of the Ca2+-binding properties of human recombinant calretinin-22k and calretinin. *J Biol Chem,* 272**,** 29663-71.

SCIFO, E., SZWAJDA, A., DEBSKI, J., UUSI-RAUVA, K., KESTI, T., DADLEZ, M., GINGRAS, A. C., TYYNELA, J., BAUMANN, M. H., JALANKO, A. & LALOWSKI, M. 2013. Drafting the CLN3 protein interactome in SH-SY5Y human neuroblastoma cells: a label-free quantitative proteomics approach. *J Proteome Res,* 12**,** 2101-15.

SCOTT, D. & ROY, S. 2012. alpha-Synuclein inhibits intersynaptic vesicle mobility and maintains recycling-pool homeostasis. *J Neurosci,* 32**,** 10129-35.

SCOTT, D. A., TABAREAN, I., TANG, Y., CARTIER, A., MASLIAH, E. & ROY, S. 2010. A pathologic cascade leading to synaptic dysfunction in alpha-synuclein-induced neurodegeneration. *J Neurosci,* 30**,** 8083-95.

SELKOE, D. J. 2013. The therapeutics of Alzheimer's disease: where we stand and where we are heading. *Ann Neurol,* 74**,** 328-36.

SELKOE, D. J. & HARDY, J. 2016. The amyloid hypothesis of Alzheimer's disease at 25 years. *EMBO Mol Med,* 8**,** 595-608.

SEVLEVER, D., ZOU, F., MA, L., CARRASQUILLO, S., CRUMP, M. G., CULLEY, O. J., HUNTER, T. A., BISCEGLIO, G. D., YOUNKIN, L., ALLEN, M., CARRASQUILLO, M. M., SANDO, S. B., AASLY, J. O., DICKSON, D. W., GRAFF-RADFORD, N. R., PETERSEN, R. C., DEAK, F. & BELBIN, O. 2015. Genetically-controlled Vesicle-Associated Membrane Protein 1 expression may contribute to Alzheimer's pathophysiology and susceptibility. *Mol Neurodegener,* 10**,** 18.

SHANKAR, G. M., BLOODGOOD, B. L., TOWNSEND, M., WALSH, D. M., SELKOE, D. J. & SABATINI, B. L. 2007. Natural oligomers of the Alzheimer amyloid-beta protein induce reversible synapse loss by modulating an NMDA-type glutamate receptor-dependent signaling pathway. *J Neurosci,* 27**,** 2866-75.

SHANKAR, G. M., LI, S., MEHTA, T. H., GARCIA-MUNOZ, A., SHEPARDSON, N. E., SMITH, I., BRETT, F. M., FARRELL, M. A., ROWAN, M. J., LEMERE, C. A., REGAN, C. M., WALSH, D. M., SABATINI, B. L. & SELKOE, D. J. 2008. Amyloid-beta protein dimers isolated directly from Alzheimer's brains impair synaptic plasticity and memory. *Nat Med,* 14**,** 837-42.

SHAO, J., WELCH, W. J. & DIAMOND, M. I. 2008. ROCK and PRK-2 mediate the inhibitory effect of Y-27632 on polyglutamine aggregation. *FEBS Letters,* 582**,** 1637-1642.

SHARMA, M., BURRE, J., BRONK, P., ZHANG, Y., XU, W. & SUDHOF, T. C. 2012. CSPalpha knockout causes neurodegeneration by impairing SNAP-25 function. *EMBO J,* 31**,** 829-41.

SHARMA, M., BURRE, J. & SUDHOF, T. C. 2011. CSPalpha promotes SNARE-complex assembly by chaperoning SNAP-25 during synaptic activity. *Nat Cell Biol,* 13**,** 30-9.

SHENG, M., SABATINI, B. L. & SUDHOF, T. C. 2012. Synapses and Alzheimer's disease. *Cold Spring Harb Perspect Biol,* 4.

SHENG, Z. H. 2014. Mitochondrial trafficking and anchoring in neurons: New insight and implications. *J Cell Biol,* 204**,** 1087-98.

SHERMAN, D. L., KROLS, M., WU, L. M., GROVE, M., NAVE, K. A., GANGLOFF, Y. G. & BROPHY, P. J. 2012. Arrest of myelination and reduced axon growth when Schwann cells lack mTOR. *J Neurosci,* 32**,** 1817-25.

SHIRENDEB, U. P., CALKINS, M. J., MANCZAK, M., ANEKONDA, V., DUFOUR, B., MCBRIDE, J. L., MAO, P. & REDDY, P. H. 2012. Mutant huntingtin's interaction with mitochondrial protein Drp1 impairs mitochondrial biogenesis and causes defective axonal transport and synaptic degeneration in Huntington's disease. *Hum Mol Genet,* 21**,** 406-20.

SIEBERT, H., KAHLE, P. J., KRAMER, M. L., ISIK, T., SCHLUTER, O. M., SCHULZ-SCHAEFFER, W. J. & BRUCK, W. 2010. Over-expression of alpha-synuclein in the nervous system enhances axonal degeneration after peripheral nerve lesion in a transgenic mouse strain. *J Neurochem,* 114**,** 1007-18.

SIMMONS, D. A., REX, C. S., PALMER, L., PANDYARAJAN, V., FEDULOV, V., GALL, C. M. & LYNCH, G. 2009. Up-regulating BDNF with an ampakine rescues synaptic plasticity and memory in Huntington's disease knockin mice. *Proc Natl Acad Sci U S A,* 106**,** 4906-11.

SIMUNOVIC, F., YI, M., WANG, Y., MACEY, L., BROWN, L. T., KRICHEVSKY, A. M., ANDERSEN, S. L., STEPHENS, R. M., BENES, F. M. & SONNTAG, K. C. 2009. Gene expression profiling of substantia nigra dopamine neurons: further insights into Parkinson's disease pathology. *Brain,* 132**,** 1795-809.

SINGLETON, A. B., FARRER, M., JOHNSON, J., SINGLETON, A., HAGUE, S., KACHERGUS, J., HULIHAN, M., PEURALINNA, T., DUTRA, A., NUSSBAUM, R., LINCOLN, S., CRAWLEY, A., HANSON, M., MARAGANORE, D., ADLER, C., COOKSON, M. R., MUENTER, M., BAPTISTA, M., MILLER, D., BLANCATO, J., HARDY, J. & GWINN-HARDY, K. 2003. alpha-Synuclein locus triplication causes Parkinson's disease. *Science (New York, N.Y.),* 302.

SMILLIE, K. J. & COUSIN, M. A. 2005. Dynamin I phosphorylation and the control of synaptic vesicle endocytosis. *Biochem Soc Symp***,** 87-97.

SMILLIE, K. J., PAWSON, J., PERKINS, E. M., JACKSON, M. & COUSIN, M. A. 2013. Control of synaptic vesicle endocytosis by an extracellular signalling molecule. *Nat Commun,* 4**,** 2394.

SNYDER, H., MENSAH, K., THEISLER, C., LEE, J., MATOUSCHEK, A. & WOLOZIN, B. 2003. Aggregated and monomeric alpha-synuclein bind to the S6' proteasomal protein and inhibit proteasomal function. *J Biol Chem,* 278**,** 11753-9.

SONG, Y., CHEN, X., WANG, L. Y., GAO, W. & ZHU, M. J. 2013. Rho Kinase Inhibitor Fasudil Protects against beta-Amyloid-Induced Hippocampal Neurodegeneration in Rats. *CNS Neurosci Ther*.

SONSALLA, P. K., COLEMAN, C., WONG, L. Y., HARRIS, S. L., RICHARDSON, J. R., GADAD, B. S., LI, W. & GERMAN, D. C. 2013. The angiotensin converting enzyme inhibitor captopril protects nigrostriatal dopamine neurons in animal models of parkinsonism. *Exp Neurol,* 250**,** 376-83.

SPECHT, C. G. & SCHOEPFER, R. 2001. Deletion of the alpha-synuclein locus in a subpopulation of C57BL/6J inbred mice. *BMC Neurosci,* 2**,** 11.

SPEESE, S. D., TROTTA, N., RODESCH, C. K., ARAVAMUDAN, B. & BROADIE, K. 2003. The ubiquitin proteasome system acutely regulates presynaptic protein turnover and synaptic efficacy. *Curr Biol,* 13**,** 899-910.

SPINELLI, K. J., TAYLOR, J. K., OSTERBERG, V. R., CHURCHILL, M. J., POLLOCK, E., MOORE, C., MESHUL, C. K. & UNNI, V. K. 2014. Presynaptic Alpha-Synuclein Aggregation in a Mouse Model of Parkinson's Disease. *The Journal of Neuroscience,* 34**,** 2037-2050.

SPIRES-JONES, T. L. & HYMAN, B. T. 2014. The intersection of amyloid beta and tau at synapses in Alzheimer's disease. *Neuron,* 82**,** 756-71.

SPIRES-JONES, T. L., STOOTHOFF, W. H., DE CALIGNON, A., JONES, P. B. & HYMAN, B. T. 2009. Tau pathophysiology in neurodegeneration: a tangled issue. *Trends Neurosci,* 32**,** 150-9.

SPIRES, T. L., GROTE, H. E., GARRY, S., CORDERY, P. M., VAN DELLEN, A., BLAKEMORE, C. & HANNAN, A. J. 2004. Dendritic spine pathology and deficits in experience-dependent dendritic plasticity in R6/1 Huntington's disease transgenic mice. *Eur J Neurosci,* 19**,** 2799-807.

STAUCH, K. L., PURNELL, P. R. & FOX, H. S. 2014a. Aging synaptic mitochondria exhibit dynamic proteomic changes while maintaining bioenergetic function. *Aging (Albany NY),* 6**,** 320-34.

STAUCH, K. L., PURNELL, P. R. & FOX, H. S. 2014b. Quantitative proteomics of synaptic and nonsynaptic mitochondria: insights for synaptic mitochondrial vulnerability. *J Proteome Res,* 13**,** 2620-36.

STEFANIS, L. 2012. α-Synuclein in Parkinson's Disease. *Cold Spring Harbor Perspectives in Medicine,* 2.

STEPHENS, B., MUELLER, A. J., SHERING, A. F., HOOD, S. H., TAGGART, P., ARBUTHNOTT, G. W., BELL, J. E., KILFORD, L., KINGSBURY, A. E., DANIEL, S. E. & INGHAM, C. A. 2005. Evidence of a breakdown of corticostriatal connections in Parkinson's disease. *Neuroscience,* 132**,** 741-54.

STOUT, J. C., WEAVER, M., SOLOMON, A. C., QUELLER, S., HUI, S., JOHNSON, S. A., GRAY, J., BERISTAIN, X., WOJCIESZEK, J. & FOROUD, T. 2007. Are

cognitive changes progressive in prediagnostic HD? *Cogn Behav Neurol,* 20**,** 212-8.

SUBRAMANIAM, S. R., VERGNES, L., FRANICH, N. R., REUE, K. & CHESSELET, M. F. 2014. Region specific mitochondrial impairment in mice with widespread overexpression of alpha-synuclein. *Neurobiol Dis*.

SUDHOF, T. C. 2004. The synaptic vesicle cycle. *Annu Rev Neurosci,* 27**,** 509-47.

SUDHOF, T. C. 2012. The presynaptic active zone. *Neuron,* 75**,** 11-25.

SWEET, E. S., SAUNIER-REBORI, B., YUE, Z. & BLITZER, R. D. 2015. The Parkinson's Disease-Associated Mutation LRRK2-G2019S Impairs Synaptic Plasticity in Mouse Hippocampus. *J Neurosci,* 35**,** 11190-5.

SZE, C. I., TRONCOSO, J. C., KAWAS, C., MOUTON, P., PRICE, D. L. & MARTIN, L. J. 1997. Loss of the presynaptic vesicle protein synaptophysin in hippocampus correlates with cognitive decline in Alzheimer disease. *J Neuropathol Exp Neurol,* 56**,** 933-44.

TAKAHASHI, R. H., ALMEIDA, C. G., KEARNEY, P. F., YU, F., LIN, M. T., MILNER, T. A. & GOURAS, G. K. 2004. Oligomerization of Alzheimer's beta-amyloid within processes and synapses of cultured neurons and brain. *J Neurosci,* 24**,** 3592-9.

TERRY, R. D., MASLIAH, E., SALMON, D. P., BUTTERS, N., DETERESA, R., HILL, R., HANSEN, L. A. & KATZMAN, R. 1991. Physical basis of cognitive alterations in Alzheimer's disease: synapse loss is the major correlate of cognitive impairment. *Ann Neurol,* 30**,** 572-80.

TIRANTI, V., D'ADAMO, P., BRIEM, E., FERRARI, G., MINERI, R., LAMANTEA, E., MANDEL, H., BALESTRI, P., GARCIA-SILVA, M. T., VOLLMER, B., RINALDO, P., HAHN, S. H., LEONARD, J., RAHMAN, S., DIONISI-VICI, C., GARAVAGLIA, B., GASPARINI, P. & ZEVIANI, M. 2004. Ethylmalonic encephalopathy is caused by mutations in ETHE1, a gene encoding a mitochondrial matrix protein. *Am J Hum Genet,* 74**,** 239-52.

TONG, J. J. 2007. Mitochondrial delivery is essential for synaptic potentiation. *Biol Bull,* 212**,** 169-75.

TONG, Y., PISANI, A., MARTELLA, G., KAROUANI, M., YAMAGUCHI, H., POTHOS, E. N. & SHEN, J. 2009. R1441C mutation in LRRK2 impairs dopaminergic neurotransmission in mice. *Proc Natl Acad Sci U S A,* 106**,** 14622-7.

TÖNGES, L., FRANK, T., TATENHORST, L., SAAL, K. A., KOCH, J. C., SZEGŐ, É. M., BÄHR, M., WEISHAUPT, J. H. & LINGOR, P. 2012. Inhibition of rho kinase enhances survival of dopaminergic neurons and attenuates axonal loss in a mouse model of Parkinson's disease. *Brain*.

TONGES, L., KOCH, J. C., BAHR, M. & LINGOR, P. 2011. ROCKing Regeneration: Rho Kinase Inhibition as Molecular Target for Neurorestoration. *Front Mol Neurosci,* 4**,** 39.

TRIFONOV, S., HOUTANI, T., KASE, M., TOIDA, K., MARUYAMA, M., YAMASHITA, Y., SHIMIZU, J. & SUGIMOTO, T. 2012. Lateral regions of the rodent striatum reveal elevated glutamate decarboxylase 1 mRNA expression in medium-sized projection neurons. *Eur J Neurosci,* 35**,** 711-22.

TRUSHINA, E., DYER, R. B., BADGER, J. D., 2ND, URE, D., EIDE, L., TRAN, D. D., VRIEZE, B. T., LEGENDRE-GUILLEMIN, V., MCPHERSON, P. S.,

MANDAVILLI, B. S., VAN HOUTEN, B., ZEITLIN, S., MCNIVEN, M., AEBERSOLD, R., HAYDEN, M., PARISI, J. E., SEEBERG, E., DRAGATSIS, I., DOYLE, K., BENDER, A., CHACKO, C. & MCMURRAY, C. T. 2004. Mutant huntingtin impairs axonal trafficking in mammalian neurons in vivo and in vitro. *Mol Cell Biol,* 24**,** 8195-209.

TSEVELEKI, V., RUBIO, R., VAMVAKAS, S. S., WHITE, J., TAOUFIK, E., PETIT, E., QUACKENBUSH, J. & PROBERT, L. 2010. Comparative gene expression analysis in mouse models for multiple sclerosis, Alzheimer's disease and stroke for identifying commonly regulated and disease-specific gene changes. *Genomics,* 96**,** 82-91.

TYYNELA, J., COOPER, J. D., KHAN, M. N., SHEMILTS, S. J. & HALTIA, M. 2004. Hippocampal pathology in the human neuronal ceroid-lipofuscinoses: distinct patterns of storage deposition, neurodegeneration and glial activation. *Brain Pathol,* 14**,** 349-57.

TYYNELA, J., SUOPANKI, J., SANTAVUORI, P., BAUMANN, M. & HALTIA, M. 1997. Variant late infantile neuronal ceroid-lipofuscinosis: pathology and biochemistry. *J Neuropathol Exp Neurol,* 56**,** 369-75.

UCL. 2015. *NCL Resource - A gateway for Batten disease* [Online]. Available: http://www.ucl.ac.uk/ncl/ [Accessed 2015].

UEDA, K., FUKUSHIMA, H., MASLIAH, E., XIA, Y., IWAI, A., YOSHIMOTO, M., OTERO, D. A., KONDO, J., IHARA, Y. & SAITOH, T. 1993. Molecular cloning of cDNA encoding an unrecognized component of amyloid in Alzheimer disease. *Proc Natl Acad Sci U S A,* 90**,** 11282-6.

UUSI-RAUVA, K., KYTTALA, A., VAN DER KANT, R., VESA, J., TANHUANPAA, K., NEEFJES, J., OLKKONEN, V. M. & JALANKO, A. 2012. Neuronal ceroid lipofuscinosis protein CLN3 interacts with motor proteins and modifies location of late endosomal compartments. *Cell Mol Life Sci,* 69**,** 2075-89.

VALERA, E. & MASLIAH, E. 2016. Therapeutic approaches in Parkinson's disease and related disorders. *J Neurochem*.

VAMVACA, K., VOLLES, M. J. & LANSBURY, P. T., JR. 2009. The first N-terminal amino acids of alpha-synuclein are essential for alpha-helical structure formation in vitro and membrane binding in yeast. *Journal of Molecular Biology,* 389**,** 413-424.

VAN DER PUTTEN, H., WIEDERHOLD, K. H., PROBST, A., BARBIERI, S., MISTL, C., DANNER, S., KAUFFMANN, S., HOFELE, K., SPOOREN, W. P., RUEGG, M. A., LIN, S., CARONI, P., SOMMER, B., TOLNAY, M. & BILBE, G. 2000. Neuropathology in mice expressing human alpha-synuclein. *J Neurosci,* 20**,** 6021-9.

VAN DER SCHYF, C. J. & GELDENHUYS, W. J. 2011. Multimodal drugs and their future for Alzheimer's and Parkinson's disease. *Int Rev Neurobiol,* 100**,** 107-25.

VESA, J., CHIN, M. H., OELGESCHLAGER, K., ISOSOMPPI, J., DELLANGELICA, E. C., JALANKO, A. & PELTONEN, L. 2002. Neuronal ceroid lipofuscinoses are connected at molecular level: interaction of CLN5 protein with CLN2 and CLN3. *Mol Biol Cell,* 13**,** 2410-20.

VILLALBA, R. M., MATHAI, A. & SMITH, Y. 2015. Morphological changes of glutamatergic synapses in animal models of Parkinson's disease. *Front Neuroanat,* 9**,** 117.

VILLEMAGNE, V. L., BURNHAM, S., BOURGEAT, P., BROWN, B., ELLIS, K. A., SALVADO, O., SZOEKE, C., MACAULAY, S. L., MARTINS, R., MARUFF, P., AMES, D., ROWE, C. C., MASTERS, C. L., AUSTRALIAN IMAGING, B. & LIFESTYLE RESEARCH, G. 2013. Amyloid beta deposition, neurodegeneration, and cognitive decline in sporadic Alzheimer's disease: a prospective cohort study. *Lancet Neurol,* 12**,** 357-67.

VOLPICELLI-DALEY, L. A., LUK, K. C., PATEL, T. P., TANIK, S. A., RIDDLE, D. M., STIEBER, A., MEANEY, D. F., TROJANOWSKI, J. Q. & LEE, V. M. 2011. Exogenous alpha-synuclein fibrils induce Lewy body pathology leading to synaptic dysfunction and neuron death. *Neuron,* 72**,** 57-71.

VON SCHANTZ, C., KIELAR, C., HANSEN, S. N., PONTIKIS, C. C., ALEXANDER, N. A., KOPRA, O., JALANKO, A. & COOPER, J. D. 2009. Progressive thalamocortical neuron loss in Cln5 deficient mice: Distinct effects in Finnish variant late infantile NCL. *Neurobiol Dis,* 34**,** 308-19.

WALKER, A. G., MILLER, B. R., FRITSCH, J. N., BARTON, S. J. & REBEC, G. V. 2008. Altered information processing in the prefrontal cortex of Huntington's disease mouse models. *J Neurosci,* 28**,** 8973-82.

WALSH, D. M., KLYUBIN, I., FADEEVA, J. V., CULLEN, W. K., ANWYL, R., WOLFE, M. S., ROWAN, M. J. & SELKOE, D. J. 2002. Naturally secreted oligomers of amyloid beta protein potently inhibit hippocampal long-term potentiation in vivo. *Nature,* 416**,** 535-9.

WALTER, P. & RON, D. 2011. The unfolded protein response: from stress pathway to homeostatic regulation. *Science,* 334**,** 1081-6.

WANG, J., WANG, C. E., ORR, A., TYDLACKA, S., LI, S. H. & LI, X. J. 2008a. Impaired ubiquitin-proteasome system activity in the synapses of Huntington's disease mice. *J Cell Biol,* 180**,** 1177-89.

WANG, W., PEROVIC, I., CHITTULURU, J., KAGANOVICH, A., NGUYEN, L. T. T., LIAO, J., AUCLAIR, J. R., JOHNSON, D., LANDERU, A., SIMORELLIS, A. K., JU, S., COOKSON, M. R., ASTURIAS, F. J., AGAR, J. N., WEBB, B. N., KANG, C., RINGE, D., PETSKO, G. A., POCHAPSKY, T. C. & HOANG, Q. Q. 2011. A soluble α-synuclein construct forms a dynamic tetramer. *Proceedings of the National Academy of Sciences*.

WANG, X., SU, B., LEE, H. G., LI, X., PERRY, G., SMITH, M. A. & ZHU, X. 2009. Impaired balance of mitochondrial fission and fusion in Alzheimer's disease. *J Neurosci,* 29**,** 9090-103.

WANG, X., SU, B., SIEDLAK, S. L., MOREIRA, P. I., FUJIOKA, H., WANG, Y., CASADESUS, G. & ZHU, X. 2008b. Amyloid-beta overproduction causes abnormal mitochondrial dynamics via differential modulation of mitochondrial fission/fusion proteins. *Proc Natl Acad Sci U S A,* 105**,** 19318-23.

WARNE, J., PRYCE, G., HILL, J. M., SHI, X., LENNERAS, F., PUENTES, F., KIP, M., HILDITCH, L., WALKER, P., SIMONE, M. I., CHAN, A. W., TOWERS, G. J., COKER, A. R., DUCHEN, M. R., SZABADKAI, G., BAKER, D. & SELWOOD, D. L. 2016. Selective Inhibition of the Mitochondrial Permeability Transition Pore Protects against Neurodegeneration in Experimental Multiple Sclerosis. *J Biol Chem,* 291**,** 4356-73.

WASHBOURNE, P., THOMPSON, P. M., CARTA, M., COSTA, E. T., MATHEWS, J. R., LOPEZ-BENDITO, G., MOLNAR, Z., BECHER, M. W., VALENZUELA,

C. F., PARTRIDGE, L. D. & WILSON, M. C. 2002. Genetic ablation of the t-SNARE SNAP-25 distinguishes mechanisms of neuroexocytosis. *Nat Neurosci,* 5**,** 19-26.

WEBB, J. L., RAVIKUMAR, B., ATKINS, J., SKEPPER, J. N. & RUBINSZTEIN, D. C. 2003. Alpha-Synuclein is degraded by both autophagy and the proteasome. *J Biol Chem,* 278**,** 25009-13.

WESTLAKE, V. J., JOLLY, R. D., BAYLISS, S. L. & PALMER, D. N. 1995. Immunocytochemical studies in the ceroid-lipofuscinoses (Batten disease) using antibodies to subunit c of mitochondrial ATP synthase. *Am J Med Genet,* 57**,** 177-81.

WHITTEMORE, E. R., LOO, D. T., WATT, J. A. & COTMAN, C. W. 1995. A detailed analysis of hydrogen peroxide-induced cell death in primary neuronal culture. *Neuroscience,* 67**,** 921-32.

WHO Neurological Disorders: Public Health Challenges. 2016. World Health Organization.

WINNER, B., JAPPELLI, R., MAJI, S. K., DESPLATS, P. A., BOYER, L., AIGNER, S., HETZER, C., LOHER, T., VILAR, M., CAMPIONI, S., TZITZILONIS, C., SORAGNI, A., JESSBERGER, S., MIRA, H., CONSIGLIO, A., PHAM, E., MASLIAH, E., GAGE, F. H. & RIEK, R. 2011. In vivo demonstration that alpha-synuclein oligomers are toxic. *Proc Natl Acad Sci U S A,* 108**,** 4194-9.

WINSKY, L. & KUZNICKI, J. 1995. Distribution of calretinin, calbindin D28k, and parvalbumin in subcellular fractions of rat cerebellum: effects of calcium. *J Neurochem,* 65**,** 381-8.

WINSLOW, A. R., CHEN, C. W., CORROCHANO, S., ACEVEDO-AROZENA, A., GORDON, D. E., PEDEN, A. A., LICHTENBERG, M., MENZIES, F. M., RAVIKUMAR, B., IMARISIO, S., BROWN, S., O'KANE, C. J. & RUBINSZTEIN, D. C. 2010. alpha-Synuclein impairs macroautophagy: implications for Parkinson's disease. *J Cell Biol,* 190**,** 1023-37.

WISHART, T. M., PATERSON, J. M., SHORT, D. M., MEREDITH, S., ROBERTSON, K. A., SUTHERLAND, C., COUSIN, M. A., DUTIA, M. B. & GILLINGWATER, T. H. 2007. Differential proteomics analysis of synaptic proteins identifies potential cellular targets and protein mediators of synaptic neuroprotection conferred by the slow Wallerian degeneration (Wlds) gene. *Mol Cell Proteomics,* 6**,** 1318-30.

WISHART, T. M., ROONEY, T. M., LAMONT, D. J., WRIGHT, A. K., MORTON, A. J., JACKSON, M., FREEMAN, M. R. & GILLINGWATER, T. H. 2012. Combining comparative proteomics and molecular genetics uncovers regulators of synaptic and axonal stability and degeneration in vivo. *PLoS Genet,* 8**,** e1002936.

WISNIEWSKI, J. R., ZOUGMAN, A., NAGARAJ, N. & MANN, M. 2009. Universal sample preparation method for proteome analysis. *Nat Methods,* 6**,** 359-62.

YARANA, C., SANIT, J., CHATTIPAKORN, N. & CHATTIPAKORN, S. 2012. Synaptic and nonsynaptic mitochondria demonstrate a different degree of calcium-induced mitochondrial dysfunction. *Life Sci,* 90**,** 808-14.

YAVICH, L., JAKALA, P. & TANILA, H. 2006. Abnormal compartmentalization of norepinephrine in mouse dentate gyrus in alpha-synuclein knockout and A30P transgenic mice. *J Neurochem,* 99**,** 724-32.

YAVICH, L., TANILA, H., VEPSALAINEN, S. & JAKALA, P. 2004. Role of alpha-synuclein in presynaptic dopamine recruitment. *J Neurosci,* 24**,** 11165-70.

YOUDIM, M. B. 2010a. Why do we need multifunctional neuroprotective and neurorestorative drugs for Parkinson's and Alzheimer's diseases as disease modifying agents. *Exp Neurobiol,* 19**,** 1-14.

YOUDIM, M. B. 2010b. Why do we need multifunctional neuroprotective and neurorestorative drugs for Parkinson's and Alzheimer's disorders? *Rambam Maimonides Med J,* 1**,** e0011.

ZARRANZ, J. J., ALEGRE, J., GÓMEZ-ESTEBAN, J. C., LEZCANO, E., ROS, R., AMPUERO, I., VIDAL, L., HOENICKA, J., RODRIGUEZ, O., ATARÉS, B., LLORENS, V., GOMEZ TORTOSA, E., DEL SER, T., MUÑOZ, D. G. & DE YEBENES, J. G. 2004. The new mutation, E46K, of alpha-synuclein causes Parkinson and Lewy body dementia. *Annals of Neurology,* 55**,** 164-173.

ZECCA, L., YOUDIM, M. B., RIEDERER, P., CONNOR, J. R. & CRICHTON, R. R. 2004. Iron, brain ageing and neurodegenerative disorders. *Nat Rev Neurosci,* 5**,** 863-73.

ZHARIKOV, A. D., CANNON, J. R., TAPIAS, V., BAI, Q., HOROWITZ, M. P., SHAH, V., EL AYADI, A., HASTINGS, T. G., GREENAMYRE, J. T. & BURTON, E. A. 2015. shRNA targeting alpha-synuclein prevents neurodegeneration in a Parkinson's disease model. *J Clin Invest,* 125**,** 2721-35.

ZHOU, Q., HOMMA, K. J. & POO, M. M. 2004. Shrinkage of dendritic spines associated with long-term depression of hippocampal synapses. *Neuron,* 44**,** 749-57.

ZHU, Y., ZHANG, J. & ZENG, Y. 2012. Overview of tyrosine hydroxylase in Parkinson's disease. *CNS Neurol Disord Drug Targets,* 11**,** 350-8.

# Appendix I – IPA results from $CR^{-/-}$ proteomics

Top 50 list of Functions and Diseases associated with the proteomic changes identified in $CR^{-/-}$ mice. Functions and Diseases output from IPA was divided into Functions and Diseases tables, Table 25 and Table 26 respectively.

**Table 25: Top functions associated with the proteomic changes in $CR^{-/-}$ mice, as identified by IPA.**

| IPA Functions Annotation | p-Value | Molecules |
|---|---|---|
| organization of cytoskeleton | 3.26E-18 | ACTB,ACTN1,ADD1,CAMK2A,CANX,CAPZB,CKB,CNP,CTNNA2,CTNND2,DNM1,DNM1L,DPYSL5,FASN,GDI1,GFAP,GNAO1,GPI,GRIN2B,HSP90AA1,INA,KRT10,LGI1,MAP2,MAPT,MBP,MYH10,NEFH,NEFL,NEFM,NPTN,PACSIN1,PAK3,PCLO,PDIA3,PKM,PLEC,PLXNA4,PRKACA,RTN3,SEPT9,SLC3A2,SPTBN1,STIP1,STMN1,SV2A,SYNGAP1,TRAPPC4,TUBB3,VAPA,YWHAH |
| neuritogenesis | 1.75E-16 | ACTB,CAMK2A,CAPZB,CKB,CNP,CTNNA2,CTNND2,DNM1L,DPYSL5,GDI1,LGI1,MAP2,MAPT,MBP,MYH10,NEFH,NEFL,NEFM,NPTN,PACSIN1,PAK3,PDIA3,PLXNA4,RTN3,SPTBN1,STIP1,STMN1,SV2A,SYNGAP1,TRAPPC4,VAPA,YWHAH |
| cell death | 6.20E-16 | ACAT1,ACLY,ACTB,ADD1,AK1,AP2A2,ATP2A2,CAMK2A,CANX,CCT4,CNP,COX5A,CS,CSHL1,CSNK2A1,CTNNA2,CYFIP2,DNM1,DNM1L,DYNC1H1,ENO1,FASN,GDAP1,GFAP,GNAO1,GPI,GRIA2,GRIN2B,GSTM5,GSTP1,HADHA,HSP90AA1,HSP90B1,HSPA1B,HSPA5,HSPA9,HSPH1,IMMT,MAPT,MBP,MIF,NDRG2,NEFH,NEFL,NEFM,NME2,PAK3,PDHA1,PDIA3,PKM,PLCB1,PLEC,PLXNA4,PPIA,PPP2R1A,PPP3R1,PRKACA,RPS27A,RTN1,SDHB,SEPT9,SH3GL2,SLC25A4,SLC3A2,SLC8A1,SPTBN1,STIP1,STMN1,STXBP1,SYNGAP1,TCP1,TSPAN2,TUBB3,UBA1,UCHL3,VAPA,YWHAG,YWHAH |
| formation of cellular protrusions | 1.62E-15 | ACTB,CAMK2A,CAPZB,CKB,CNP,CTNNA2,CTNND2,DNM1,DNM1L,DPYSL5,FASN,GDI1,GNAO1,HSP90AA1,LGI1,MAP2,MAPT,MBP,MYH10,NEFH,NEFL,NEFM,NPTN,PACSIN1,PAK3,PDIA3,PLEC,PLXNA4,PRKACA,RTN3,SPTBN1,STIP1,STMN1,SV2A,SYNGAP1,TRAPPC4,VAPA,YWHAH |
| necrosis | 3.37E-15 | ACAT1,ACLY,ACTB,AP2A2,ATP2A2,CCT4,CNP,COX5A,CS,CSHL1,CSNK2A1,CTNNA2,CYFIP2,DNM1,DNM1L,DYNC1H1,ENO1,FASN,GFAP,GNAO1,GPI,GRIA2,GRIN2B,GSTM5,GSTP1,HADHA,HSP90AA1,HSP90B1,HSPA5,HSPA9,HSPH1,IMMT,MAPT,MBP,MIF,NDRG2,NEFH,NEFL,PAK3,PDHA1,PDIA3,PKM,PLCB1,PLEC,PLXNA4,PPIA,PPP2R1A,PPP3R1,PRKACA,RPS27A,RTN1,SDHB,SH3GL2,SLC25A4,SLC3A2,SLC8A1,SPTBN1,STIP1,STMN1,STXBP1,SYNGAP1,TCP1,TUBB3,UBA1,VAPA,YWHAG,YWHAH |
| microtubule dynamics | 4.02E-15 | ACTB,CAMK2A,CANX,CAPZB,CKB,CNP,CTNNA2,CTNND2,DNM1,DNM1L,DPYSL5,FASN,GDI1,GNAO1,GRIN2B,HSP90AA1,LGI1,MAP2,MAPT,MBP,MYH10,NEFH,NEFL,NEFM,NPTN,PACSIN1,PAK3,PDIA3,PKM,PLEC,PLXNA4,PRKACA,RTN3,SEPT9,SPTBN1,STIP1,STMN1,SV2A,SYNGAP1,TRAPPC4,TUBB3,VAPA,YWHAH |

| | | |
|---|---|---|
| morphology of cells | 7.46E-14 | ACADVL,ACSBG1,ACTN1,ADD1,AK1,AP2M1,ATP2A2,CAMK2A,CAPZB,CKB,CNP,CSNK2A1,CTNNA2,CTNND2,DNM1,DNM1L,DPYSL5,FASN,GDAP1,GDI1,GFAP,GNAO1,GPI,HADHA,HSP90AA1,HSP90B1,KRT10,LGI1,MAP2,MAPT,MBP,MIF,MYH10,NDUFS6,NEFH,NEFL,NEFM,NPTN,PACSIN1,PAK3,PLCB1,PLEC,PLXNA4,SEPT9,SH3GL2,SLC25A4,SLC4A4,SLC8A1,SPTBN1,STMN1,STX1B,SYNGAP1,SYNPO,UCHL3,YWHAG |
| development of neurons | 2.39E-13 | ACTB,CAMK2A,CAPZB,CKB,CNP,CTNNA2,CTNND2,DNM1L,DPYSL5,GDI1,LGI1,MAP2,MAPT,MBP,MYH10,NEFH,NEFL,NEFM,NPTN,PACSIN1,PAK3,PDIA3,PLXNA4,RTN3,SPTBN1,STIP1,STMN1,SV2A,SYNGAP1,TRAPPC4,VAPA,YWHAG,YWHAH |
| morphology of nervous system | 7.93E-13 | CAMK2A,CANX,CAPZB,CKB,CSNK2A1,CTNNA2,CTNND2,DNM1,DPYSL5,GDAP1,GDI1,GFAP,GRIA2,GRIN2B,LGI1,MAP2,MAPT,MBP,MIF,MYH10,NEFH,NEFL,NEFM,NPTN,PACSIN1,PAK3,PLEC,PLXNA4,PRKACA,SH3GL2,STMN1,STX1B,SYNGAP1,UCHL3 |
| morphology of nervous tissue | 1.25E-12 | CAMK2A,CAPZB,CKB,CTNNA2,CTNND2,DNM1,DPYSL5,GDAP1,GDI1,GFAP,LGI1,MAP2,MAPT,MBP,MYH10,NEFH,NEFL,NEFM,NPTN,PACSIN1,PAK3,PLEC,PLXNA4,SH3GL2,STX1B,SYNGAP1 |
| transport of molecule | 2.76E-12 | ABAT,ACAT1,ACLY,AK1,AP2A2,AP2M1,ARF5,ATP1A3,ATP2A2,ATP5D,CA2,CAMK2A,CANX,CNP,DNM1L,ERP29,FABP5,GNAO1,GRIA2,GRIN2B,HSPA5,HSPA9,KRT10,MAPT,MBP,MIF,NDRG2,NME2,PDIA3,PKM,PPIA,PRKACA,SCG2,SEPT5,SLC25A11,SLC25A12,SLC25A4,SLC3A2,SLC4A4,SLC8A1,SPTBN1,STX1B,STXBP1,SV2A,TRAPPC4,VAPA,YWHAH |
| generation of cells | 3.18E-12 | ACTB,ACTN1,ATPIF1,CAMK2A,CAPZB,CKB,CNP,CTNNA2,CTNND2,DNM1L,DPYSL5,GDI1,GFAP,GNAO1,HSP90AA1,HSP90B1,HSPA5,KRT10,LGI1,MAP2,MAPT,MBP,MIF,MYH10,NDRG2,NEFH,NEFL,NEFM,NPTN,PACSIN1,PAK3,PDIA3,PKM,PLXNA4,PPIA,PPP3R1,RTN3,SCG2,SEPT9,SLC3A2,SLC8A1,SPTBN1,STIP1,STMN1,SV2A,SYNGAP1,TCP1,TRAPPC4,TSPAN2,VAPA,YWHAG,YWHAH |
| morphology of neurons | 4.52E-12 | CAMK2A,CAPZB,CKB,CTNNA2,CTNND2,DNM1,DPYSL5,GDAP1,GDI1,LGI1,MAP2,MAPT,MBP,MYH10,NEFH,NEFL,NEFM,NPTN,PACSIN1,PAK3,PLEC,PLXNA4,SH3GL2,STX1B,SYNGAP1 |
| organismal death | 5.20E-12 | ACADVL,ACLY,ACTB,ADD1,AP2M1,ARF5,ATP1A3,ATP2A2,CANX,CAPZB,CKB,CNP,CSHL1,CSNK2A1,CTNNA2,DNM1,DNM1L,DYNC1H1,FASN,GFAP,GNAO1,GRIA2,GRIN2B,GSTP1,HADHA,HSP90AA1,HSP90B1,HSPA1B,HSPA5,KRT10,LGI1,LRPPRC,MAP2,MIF,MYH10,NDRG2,PCLO,PDHA1,PDIA3,PKM,PLCB1,PLEC,PPIA,PPP2R1A,PPP3R1,PRKACA,SEPT9,SH3GL2,SLC3A2,SLC4A4,SLC8A1,SPTBN1,STIP1,STX1B,STXBP1,SV2A,SYNGAP1 |
| neurotransmission | 1.43E-11 | CAMK2A,CNP,DNM1,GDAP1,GNAO1,GRIA2,GRIN2B,LGI1,MAPT,MBP,MYH10,NEFH,NEFM,NPTN,PAK3,PPP3R1,PRKACA,SH3GL2,STX1B,STXBP1,SV2A,SYNGAP1 |
| morphology of plasma membrane projections | 3.49E-11 | CKB,CNP,DPYSL5,GDAP1,GDI1,LGI1,MAP2,MAPT,MYH10,NEFH,NEFL,NEFM,PLEC,PLXNA4,SH3GL2,SYNGAP1 |
| abnormal morphology of nervous system | 5.88E-11 | CAMK2A,CANX,CKB,CTNNA2,DNM1,GDAP1,GFAP,GRIA2,GRIN2B,LGI1,MAP2,MAPT,MBP,MIF,MYH10,NEFH,NEFL,NEFM,NPTN,PACSIN1,PLEC,PLXNA4,PRKACA,SH3GL2,STMN1,STX1B,SYNGAP1,UCHL3 |
| morphology of neurites | 1.70E-10 | CKB,DPYSL5,GDAP1,GDI1,LGI1,MAP2,MAPT,MYH10,NEFH,NEFL,NEFM,PLEC,PLXNA4,SH3GL2,SYNGAP1 |
| axonogenesis | 2.70E-10 | ACTB,CNP,CTNNA2,GDI1,MAP2,MAPT,MBP,MYH10,NEFH,NEFL,PACSIN1,PAK3,PDIA3,STMN1,SYNGAP1 |
| abnormal morphology of plasma membrane | 5.72E-10 | CKB,GDAP1,LGI1,MAPT,MYH10,NEFH,NEFL,NEFM,PACSIN1,PLEC,PLXNA4,SH3GL2,STX1B,SYNGAP1 |

| | | |
|---|---|---|
| abnormal morphology of cells | 9.62E-10 | ACADVL,ACSBG1,ADD1,ATP2A2,CAMK2A,CKB,CTNNA2,DNM1,DNM1L,GDAP1,GFAP,HADHA,HSP90B1,KRT10,LGI1,MAP2,MAPT,MBP,MIF,MYH10,NDUFS6,NEFH,NEFL,NEFM,NPTN,PACSIN1,PLEC,PLXNA4,SH3GL2,SLC4A4,SLC8A1,SPTBN1,STX1B,SYNGAP1,SYNPO,UCHL3 |
| abnormal morphology of neurons | 9.74E-10 | CAMK2A,CKB,CTNNA2,DNM1,GDAP1,LGI1,MAP2,MAPT,MYH10,NEFH,NEFL,NEFM,NPTN,PACSIN1,PLEC,PLXNA4,SH3GL2,STX1B,SYNGAP1 |
| abnormal morphology of neurites | 1.07E-09 | CKB,GDAP1,LGI1,MAPT,MYH10,NEFH,NEFL,NEFM,PLEC,PLXNA4,SH3GL2,SYNGAP1 |
| morphogenesis of neurites | 1.15E-09 | CAMK2A,CAPZB,CTNNA2,CTNND2,DNM1L,DPYSL5,LGI1,MAPT,MYH10,NEFH,NEFL,NEFM,NPTN,PACSIN1,PDIA3,PLXNA4,SV2A,SYNGAP1,VAPA,YWHAH |
| proliferation of cells | 2.58E-09 | ACAT1,ACLY,ACTB,ACTN1,ATP2A2,ATP6V0D1,ATPIF1,CALB2,CAMK2A,CNP,CSHL1,CSNK2A1,CTNND2,DNM1L,DPYSL5,DYNC1H1,ENO1,FABP5,FASN,GDAP1,GFAP,GNAO1,GPI,GSTP1,HADHA,HSP90AA1,HSP90B1,HSPA5,HSPA9,IMMT,LGI1,MAP2,MAPT,MBP,MIF,MYH10,NAP1L1,NDRG2,NDUFS3,NEFH,NEFM,NME2,PAK3,PDIA3,PKM,PLEC,PLXNA4,PPIA,PPP2R1A,PPP3R1,PRKACA,SCG2,SDHB,SEPT9,SH3GL2,SLC25A4,SLC3A2,SLC8A1,SPTBN1,STIP1,STMN1,SYNGAP1,TCP1,TUBB2A,TUBB3,UBA1,UCHL3,VAPA,YWHAG |
| branching of neurites | 4.26E-09 | CAMK2A,CAPZB,CTNNA2,CTNND2,DNM1L,DPYSL5,MAPT,NEFH,NEFL,NEFM,NPTN,PACSIN1,PDIA3,PLXNA4,SV2A,SYNGAP1 |
| proliferation of neuronal cells | 5.00E-09 | CAMK2A,CNP,CSHL1,CTNND2,DNM1L,DPYSL5,GDAP1,GFAP,GNAO1,LGI1,MAP2,MAPT,MYH10,NEFH,NEFM,PDIA3,PLXNA4,PRKACA,SEPT9,SPTBN1,SYNGAP1,VAPA |
| abnormal morphology of axons | 5.93E-09 | CKB,LGI1,MAPT,NEFH,NEFL,NEFM,PLEC,PLXNA4,SH3GL2 |
| synaptic transmission | 6.38E-09 | CAMK2A,CNP,GRIA2,GRIN2B,LGI1,MAPT,MBP,MYH10,NPTN,PAK3,PPP3R1,PRKACA,SH3GL2,STX1B,STXBP1,SV2A,SYNGAP1 |
| apoptosis | 7.31E-09 | ACLY,AP2A2,CAMK2A,CANX,CCT4,CNP,COX5A,CS,CSHL1,CSNK2A1,CYFIP2,DNM1,DNM1L,DYNC1H1,ENO1,FASN,GNAO1,GPI,GRIA2,GRIN2B,GSTM5,GSTP1,HSP90AA1,HSP90B1,HSPA1B,HSPA5,HSPA9,HSPH1,IMMT,MAPT,MIF,NDRG2,NEFL,NME2,PAK3,PDHA1,PDIA3,PKM,PLXNA4,PPIA,PPP2R1A,PPP3R1,PRKACA,RTN1,SEPT9,SLC25A4,SLC8A1,SPTBN1,STIP1,STMN1,STXBP1,SYNGAP1,TCP1,UBA1,UCHL3 |
| differentiation of cells | 8.07E-09 | ACLY,ACTR1B,ADD1,ATP2A2,ATPIF1,CA2,CAMK2A,CAPZB,CNP,CSHL1,CTNNA2,CTNND2,DNM1L,DPYSL5,ENO1,FABP5,FASN,GFAP,GNAO1,HSP90AA1,HSP90B1,HSPA5,HSPA9,KRT10,MAPT,MBP,MIF,NAP1L1,NDRG2,NEFH,NEFL,NEFM,NME2,NPTN,PACSIN1,PDIA3,PKM,PLCB1,PLXNA4,PPIA,PRKACA,SLC3A2,STMN1,SV2A,SYNGAP1,TSPAN2,TUBB3,UCHL3,YWHAG |
| formation of filaments | 9.45E-09 | ADD1,CAPZB,CNP,GFAP,GNAO1,GPI,HSPA5,INA,MAP2,MAPT,MBP,MIF,NEFH,NEFL,NEFM,PAK3,STMN1,SYNPO |
| dendritic growth/branching | 9.99E-09 | CAMK2A,CAPZB,CTNNA2,CTNND2,DNM1L,DPYSL5,MAPT,NEFH,NEFL,NEFM,NPTN,PACSIN1,SV2A,SYNGAP1 |
| organization of nervous tissue | 1.16E-08 | CTNND2,INA,MBP,NEFH,NEFL,NEFM,NPTN,PAK3 |
| accumulation of filaments | 1.22E-08 | ACAT1,MAP2,MAPT,NEFH,NEFL,PLEC |
| quantity of neurons | 1.85E-08 | CAMK2A,CANX,CAPZB,DNM1,DNM1L,GNAO1,GRIN2B,MAPT,MIF,NEFH,NEFL,NEFM,NPTN,PACSIN1,PAK3,PCLO,SH3GL2,STX1B |
| long-term potentiation of synapse | 2.04E-08 | CALB2,CAMK2A,GFAP,GRIA2,GRIN2B,MAPT,PAK3,PPP3R1,PRKACA,SYNGAP1,SYNPO |

**Table 26: Top diseases associated with the proteomic changes in $CR^{-/-}$ mice, as identified by IPA.**

| IPA Diseases Annotation | p-Value | Molecules |
|---|---|---|
| disorder of basal ganglia | 1.20E-23 | ACAT1,ACTB,AK1,ATP1A3,ATP2A2,ATP5J,ATP5O,BCAS1,CA2,CAMK2A,CAPZB,CKB,CNP,CYFIP2,GFAP,GNAO1,GPI,GRIN2B,GSTP1,HSP90AA1,HSPA5,MAP2,MAPT,MBP,NDRG2,NDUFS2,NDUFS3,NEFL,PKM,PLCB1,PPIA,PPP3R1,RTN1,SCG2,SDHB,SEPT5,SH3GL2,STMN1,SUCLA2,SV2A,TUBB2A,TUBB3,UQCRC1,VPS35 |
| neuromuscular disease | 5.70E-22 | ACAT1,ACTB,AK1,ATP2A2,ATP5J,ATP5O,BCAS1,CA2,CAMK2A,CANX,CAPZB,CKB,CNP,CYFIP2,GFAP,GNAO1,GPI,GRIN2B,GSTP1,HSP90AA1,HSP90B1,HSPA5,MAP2,MAPT,MBP,MIF,NDRG2,NDUFS2,NDUFS3,NEFL,PDIA3,PKM,PLCB1,PPIA,PPP3R1,RTN1,SCG2,SDHB,SEPT5,SH3GL2,STMN1,SUCLA2,SV2A,UQCRC1,VPS35 |
| Movement Disorders | 7.03E-22 | ACAT1,ACTB,AK1,ATP1A3,ATP2A2,ATP5J,ATP5O,BCAS1,CA2,CAMK2A,CANX,CAPZB,CKB,CNP,CYFIP2,GDAP1,GFAP,GNAO1,GPI,GRIA2,GRIN2B,GSTP1,HSP90AA1,Hspa1b,HSPA5,MAP2,MAPT,MBP,NDRG2,NDUFS2,NDUFS3,NEFL,PKM,PLCB1,PPIA,PPP3R1,RTN1,SCG2,SDHB,SEPT5,SH3GL2,STMN1,SUCLA2,SV2A,SYNGAP1,TUBB2A,TUBB3,UQCRC1,VPS35 |
| dyskinesia | 1.98E-15 | ACAT1,ACTB,AK1,ATP2A2,ATP5J,ATP5O,CA2,CAMK2A,CKB,CYFIP2,GFAP,GNAO1,GPI,GRIA2,GRIN2B,HSP90AA1,HSPA5,MAP2,NDUFS2,NDUFS3,NEFL,PKM,PLCB1,PPIA,PPP3R1,SCG2,SDHB,SEPT5,SUCLA2,SV2A,UQCRC1 |
| neurological signs | 2.21E-15 | ACAT1,ACTB,AK1,ATP2A2,ATP5J,ATP5O,CA2,CAMK2A,CKB,CYFIP2,GFAP,GNAO1,GPI,GRIA2,GRIN2B,HSP90AA1,HSPA5,MAP2,MAPT,NDUFS2,NDUFS3,NEFL,PKM,PLCB1,PPIA,PPP3R1,SCG2,SDHB,SEPT5,SUCLA2,SV2A,UQCRC1 |
| Huntington's Disease | 1.33E-14 | ACAT1,ACTB,AK1,ATP2A2,ATP5J,ATP5O,CA2,CAMK2A,CKB,CYFIP2,GFAP,GNAO1,GPI,GRIN2B,HSP90AA1,HSPA5,MAP2,NDUFS2,NDUFS3,NEFL,PKM,PLCB1,PPIA,PPP3R1,SCG2,SDHB,SEPT5,SUCLA2,UQCRC1 |
| tauopathy | 4.64E-11 | ABAT,ACLY,ACTB,CAMK2A,CANX,CNP,DNM1L,GFAP,GRIA2,GRIN2B,HSPA5,HSPA9,IGSF8,MAPT,NEFH,NEFL,PAK3,PRKACA,RTN3,SH3GL2,STIP1,SV2A,TUBB2A,TUBB3,VPS35 |
| progressive motor neuropathy | 2.93E-10 | ABAT,ACTB,BCAS1,CAPZB,CNP,FASN,GFAP,GRIN2B,GSTP1,HSPA5,INA,MAPT,MBP,MIF,NDRG2,NEFH,NEFL,PDIA3,RTN1,SH3GL2,STMN1,SV2A,VPS35 |
| Alzheimer's disease | 6.65E-10 | ABAT,ACLY,ACTB,CAMK2A,CANX,CNP,DNM1L,GFAP,GRIA2,GRIN2B,HSPA5,HSPA9,IGSF8,MAPT,NEFH,NEFL,PAK3,PRKACA,RTN3,SH3GL2,STIP1,SV2A,VPS35 |
| hereditary myopathy | 1.98E-09 | ACADVL,ACLY,CA2,CANX,DYNC1H1,GDAP1,HSP90B1,HSPA5,LRPPRC,NDUFA12,NDUFS3,NEFL,PLCB1,PLEC,SEPT9,SLC25A4,SUCLA2,TUBB2A,UBA1 |
| autosomal dominant disease | 3.30E-09 | ACLY,ACTB,ACTN1,ATP1A3,CA2,DNM1,DNM1L,DYNC1H1,GDAP1,GNAO1,GRIN2B,LGI1,MAPT,NEFH,NEFL,PLCB1,PPP2R1A,SDHB,SLC25A4,STX1B,SYNGAP1,TUBB2A,TUBB3,VPS35 |
| sporadic motor neuron disease | 9.45E-09 | ACTB,GFAP,GSTP1,INA,NEFH,NEFL |

# Appendix II – Mitochondrial dysfunction pathway

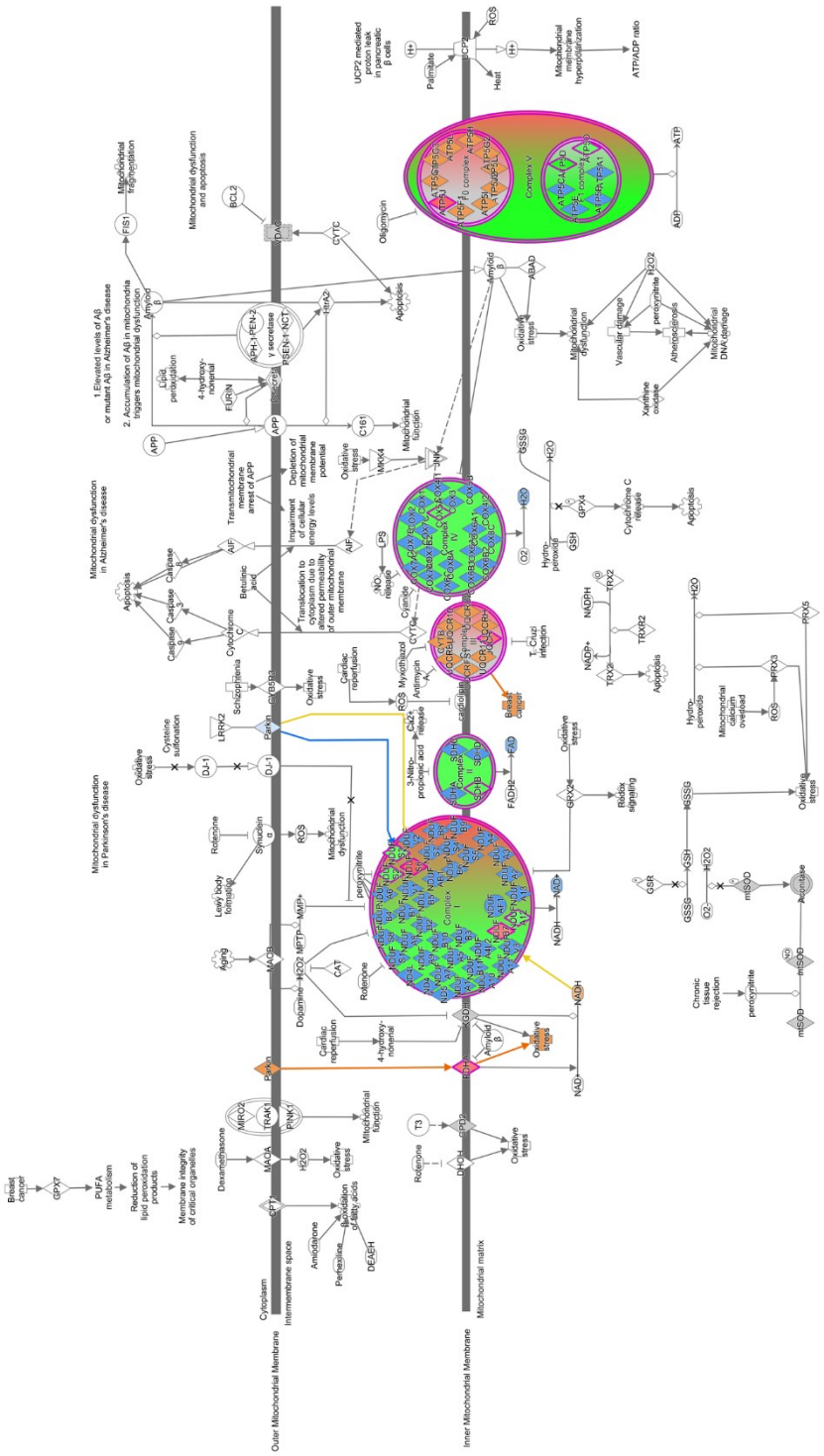

Mitochondria dysfunction pathway mapped by IPA highlighting the increased sensitivity of mitochondria from $CR^{-/-}$ mice to oxidative stress. Green coloured proteins are down-regulated in the proteomics data-set (Table 4.8), whereas red proteins are up-regulated and grey proteins were identified but their expression levels are not altered. Orange and blue lines or proteins indicate interactions that are predicted to be activated or inhibited, respectively. Yellow lines represent interactions that have not been consistently predicted. Overall, the mitochondria dysfunction map highlights changes in the oxidative phosphorylation chain in $CR^{-/-}$ mice and predicts that oxidative stress pathways should be activated by loss of CR.